

~~CONFIDENTIAL~~

SECURITY INFORMATION

Copy 204

RM A53A30

6405  
NACA RM A53A30



# RESEARCH MEMORANDUM

LIFT, DRAG, AND PITCHING MOMENT OF LOW-ASPECT-RATIO  
WINGS AT SUBSONIC AND SUPERSONIC SPEEDS

By Charles F. Hall

Ames Aeronautical Laboratory  
Moffett Field, Calif.

Classification cancelled (or changed to UNCLASSIFIED)  
By authority of NASA Tech Pub Announcement 27-24  
OFFICER AUTHORIZED TO CHANGE

By 10 FEB 58

NAME AND

ANB

GRADE OF OFFICER MAKING CHANGE

8 Mar 61

DATE

400324

Information affecting the National Defense of the United States will not be transmitted by radio. Article 18, U.S.C., Secs. 753 and 754, the transmission of which to unauthorized persons is prohibited by law.

NATIONAL ADVISORY COMMITTEE  
FOR AERONAUTICS

WASHINGTON

April 14, 1953

319.98/13

~~CONFIDENTIAL~~

1056



1Q

NACA RM A53A30

CONFIDENTIAL

0143579

## NATIONAL ADVISORY COMMITTEE FOR AERONAUTICS

RESEARCH MEMORANDUMLIFT, DRAG, AND PITCHING MOMENT OF LOW-ASPECT-RATIO  
WINGS AT SUBSONIC AND SUPERSONIC SPEEDS

By Charles F. Hall

## SUMMARY

Results are presented of a coordinated investigation to evaluate the lift, drag, and pitching-moment characteristics of thin, low-aspect-ratio wings in combination with a body. Wind-tunnel data were obtained in the Mach number range from 0.25 to as high as 1.9.

The investigation of a series of 3-percent-thick triangular wings of 2, 3, and 4 aspect ratio showed that the lift-curve slope was predicted satisfactorily by linearized theory except near a Mach number of unity and over portions of the supersonic speed range. As predicted by linearized theory, the aerodynamic center moved aft with increasing Mach number at subsonic speeds, the over-all travel increasing with aspect ratio. The data indicated that, in general, it would be more accurate to calculate the drag due to lift at supersonic speeds, assuming that the net force due to angle of attack was normal to the wing chord than to use available theoretical methods which consider leading-edge thrust.

The investigation of a series of 3-percent-thick wings having sweep-back, unswept, and triangular plan forms of aspect ratios 2 and 3 showed that, as predicted by theory, the lift-curve slope decreased with increasing sweepback, but with increasing Mach number the effects of plan form and aspect ratio on the lift-curve slope diminished and essentially vanished at the highest supersonic Mach number of the investigation. The over-all travel of the aerodynamic center decreased with increasing sweep.

The investigation of a series of triangular wings of aspect ratio 2 and thicknesses of 3, 5, and 8 percent showed that the wave drag was proportional to the thickness ratio squared. The drag due to lift decreased with increase in thickness ratio from 3 percent to 5 percent, the effect being most pronounced at Mach numbers of 0.9 and below.

A series of wings was investigated to determine the effects of thickness distribution. The results showed that, in general, wings with sharp leading edges had a lower value of minimum drag at supersonic

CONFIDENTIAL

110-24186

speeds above those estimated for attachment of the bow wave, and a higher value at subsonic speeds than wings with round leading edges. The effects of airfoil section on the drag due to lift were small, however.

The results showed that twisting and cambering a triangular wing of aspect ratio 2 reduced the drag coefficient at a lift coefficient above 0.1. Such benefits of camber and twist did not occur, however, if the component of the free-stream Mach number perpendicular to the leading edge exceeded a value of approximately 0.7.

#### INTRODUCTION

In selecting a wing for a high-speed interceptor airplane, the designer has the choice of a large variety of possible shapes. Since an intelligent selection requires a knowledge of the effects of the various shape parameters on the aerodynamic characteristics of the wings, a program to provide information was formulated at the Ames Laboratory in the latter part of 1950. The purpose of this program was twofold:

1. To investigate at Mach numbers from 0.25 to 1.9 the effects of type of plan form, aspect ratio, thickness, thickness distribution, and wing camber and twist for wing-body combinations. Such combinations would be selected to minimize the effects of other differences generally present in a comparison of data obtained from several facilities, such as body shape, body size, and Reynolds number.
2. To provide data at supersonic speeds to fill the gap existing between tests made at low Reynolds number over a range of angle of attack in small wind tunnels and tests with rocket-powered models made at high Reynolds number, but generally at zero lift.

When the program at the Ames Laboratory was first formulated, it was realized that a considerable period of time would elapse before its completion because of the time required to construct and test the models. Furthermore, it was desired to maintain a certain amount of fluidity in the program so that parts might be added to the program as it progressed. Because of the time involved, it was decided to expedite publication of the results by reporting the data obtained for each wing-body combination immediately after testing. These reports (refs. 1 to 17) were brief and no analysis of the data was attempted. The purpose of the present report is therefore to compare and to analyze these data. The data will also be used to ascertain the adequacy of existing theoretical solutions in predicting the lift, drag, and pitching-moment characteristics of low-aspect-ratio wing and body combinations.

The large amount of data obtained during this program prevents a presentation in graphical form of all the results. However, for the interested reader, all the data are presented in tables I through XIX.

## SYMBOLS

A	aspect ratio
b	wing span, in.
$C_D$	drag coefficient, $\frac{\text{drag}}{qS}$
$C_{D\min}$	minimum drag coefficient
$C_L$	lift coefficient, $\frac{\text{lift}}{qS}$
$C_{L\text{des}}$	design lift coefficient
$C_{L\text{opt}}$	lift coefficient at maximum lift-drag ratio
$C_m$	pitching-moment coefficient, $\frac{\text{pitching moment}}{qS\bar{c}}$
	(The pitching moment is referred to the quarter point of the wing mean aerodynamic chord.)
c	local wing chord, in.
$\bar{c}$	mean aerodynamic chord of wing, $\frac{\int_0^{b/2} c^2 dy}{\int_0^{b/2} c dy}$ , in.
$c_l$	section lift coefficient, $\frac{\text{section lift}}{q_c}$
$c_r$	root chord, in.
$dc_L/d\alpha$	rate of change of lift coefficient with angle of attack at zero lift, per deg
$d\epsilon/d\alpha$	rate of change of downwash angle with angle of attack
$dz/dx$	slope of the theoretical lifting surface, with respect to a horizontal plane

F	force on wing due to angle of attack, lb
G(m)	$\frac{\sqrt{1 - m^2}}{m} \left( \cosh^{-1} \frac{x - m\beta y}{ \beta y - mx } + \cosh^{-1} \frac{x + m\beta y}{ \beta y + mx } \right)$
L	lift, lb
L/D	lift-drag ratio
(L/D) <sub>max</sub>	maximum lift-drag ratio
l	length of body including portion removed to accommodate sting, in.
M	free-stream Mach number
m	cotangent of sweepback angle of leading edge of uniformly loaded wing surface or sector
$m_0$	$\cot \Lambda$
n	arbitrary positive integer
$\Delta p$	pressure difference between upper and lower surface of sector, lb/sq ft
q	free-stream dynamic pressure, lb/sq ft
R	Reynolds number based on the mean aerodynamic chord of the wing
r	radius of body, in.
$r_0$	maximum radius of body, in.
S	wing area, sq ft (The area is formed by extending the leading and trailing edges to the plane of symmetry.)
s	spanwise distance from wing plane of symmetry to edge of wing, in.
t/c	ratio of maximum wing thickness to wing chord
u	perturbation velocity in the x direction, ft/sec
w	perturbation velocity in the z direction, ft/sec

x, y, z    Cartesian coordinates in streamwise, spanwise, and vertical directions, respectively  
(The origin is at the wing apex for dimensions referring to wing and at nose of body for dimensions referring to body.)

$\alpha$     angle of attack of body axis, deg

$\beta$      $\sqrt{|1-M^2|}$

$\theta$     angle between the resultant force vector and the normal to the wing chord, deg

$\Lambda$     angle of sweepback of wing leading edge, deg

#### Subscripts

a    constant-load solution for superimposed sector

u    constant-load solution for entire wing surface

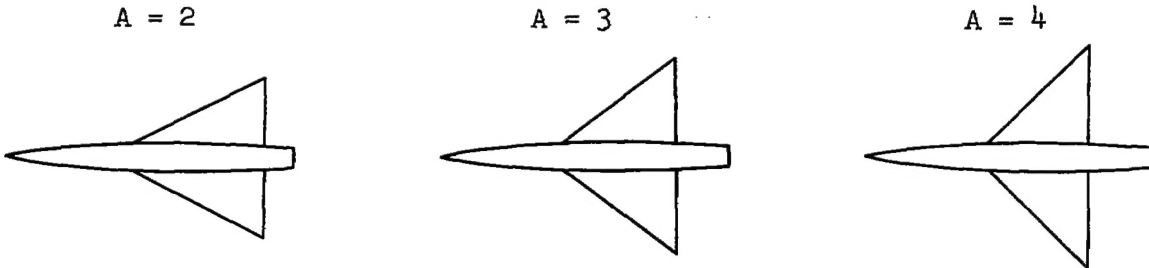
#### SELECTION OF MODELS

The geometric parameters which determine the aerodynamic characteristics of a wing are many and, in order to keep a research program within reasonable limits, it is necessary to select carefully the range of variables to be investigated. As a guide in planning the present program, which was directed primarily to the investigation of wings for high-speed fighters, a study of current design trends and anticipated developments for such airplanes was made. In the following paragraphs, a discussion of the various factors influencing the selection of the models will be given.

#### Wings

Aspect ratio.- For the unswept wings at supersonic speeds and, to a lesser extent, for sweptback wings at Mach numbers above that at which the component of the free-stream Mach number perpendicular to the leading edge becomes sonic, the flow field over most of the wing is essentially two-dimensional. In the region enclosed by the tip Mach cone, the effects of tip shape are predominant. Variation of aspect ratio for such wings merely alters the extent of the wing subjected to the two-dimensional flow, and it is possible to estimate with sufficient accuracy the effects

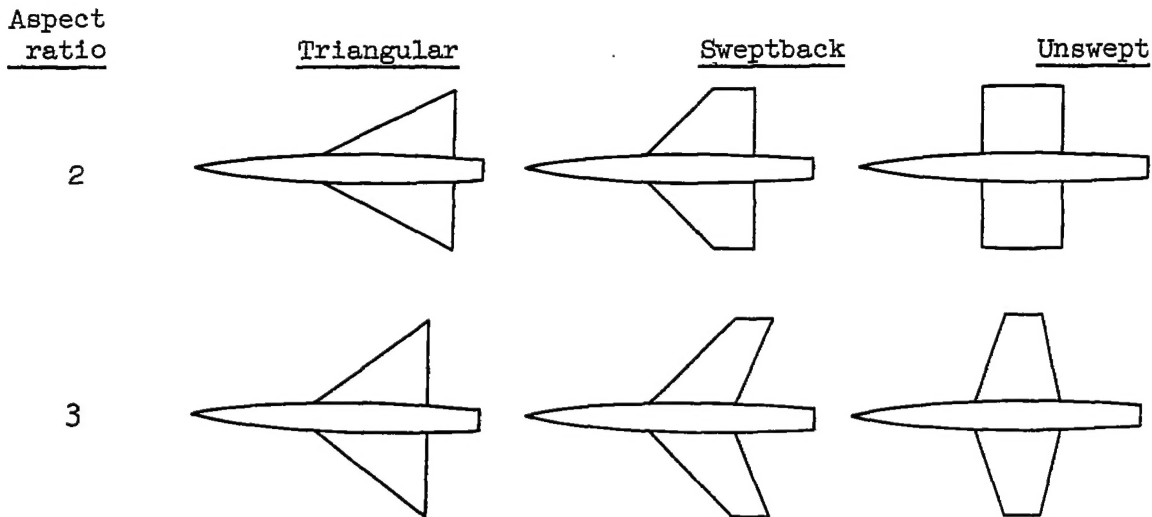
of aspect ratio from two-dimensional data when tip effects are known. For triangular wings, however, the flow field over the entire wing surface is affected by variation of aspect ratio. Hence, in this program, it was appropriate to investigate the effects of aspect ratio on wings of triangular plan form. Triangular wings of aspect ratios 2, 3, and 4 were investigated, therefore, in combination with a body and are illustrated in sketch (a) for comparison. For this portion of the pro-



Sketch (a)

gram, the thickness of the wings was 3 percent, a thickness structurally feasible and yet sufficiently small that thickness effects would not obscure the effects of aspect ratio.

Type of plan form.— In the transonic speed range and at landing conditions, plan form is an important parameter, particularly in regard to its effect on the lift and pitching-moment characteristics. It was therefore necessary to include a series of wings of varying plan form to investigate these effects. Again the wings were 3 percent thick and were investigated in combination with a body as shown in sketch (b).



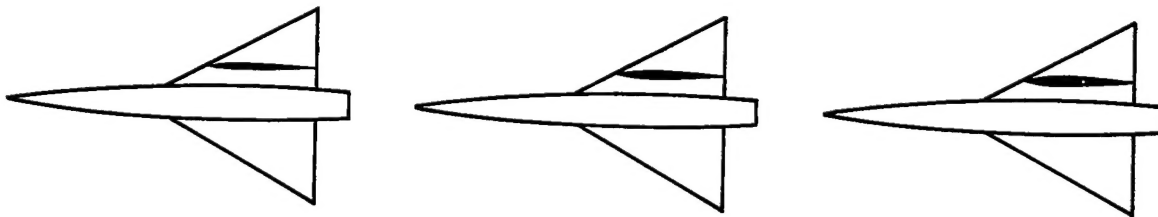
The sweptback and unswept wings of aspect ratio 3 had the same taper ratio in order to eliminate such effects from the comparison, and a value of 0.4 was selected as representative of current design trends. A value of unity was selected as the taper ratio for the unswept wing of aspect ratio 2 since theoretical studies showed that such a wing had the highest lift-curve slope at a given aspect ratio at supersonic speeds.

Thickness.- An investigation of the effects of wing thickness in the present program is of greatest interest for wings of small aspect ratio since, as the aspect ratio increases, such effects can be more easily estimated from the extensive theoretical and two-dimensional experimental results. Such results are more applicable for unswept wings, however, whereas the effects of thickness on triangular wings are not as well known. It was decided, therefore, to investigate the effects of thickness using a wing with a triangular plan form of aspect ratio 2. The models for this portion of the investigation are shown in sketch (c).

$t/c = 0.03$

$t/c = 0.05$

$t/c = 0.08$



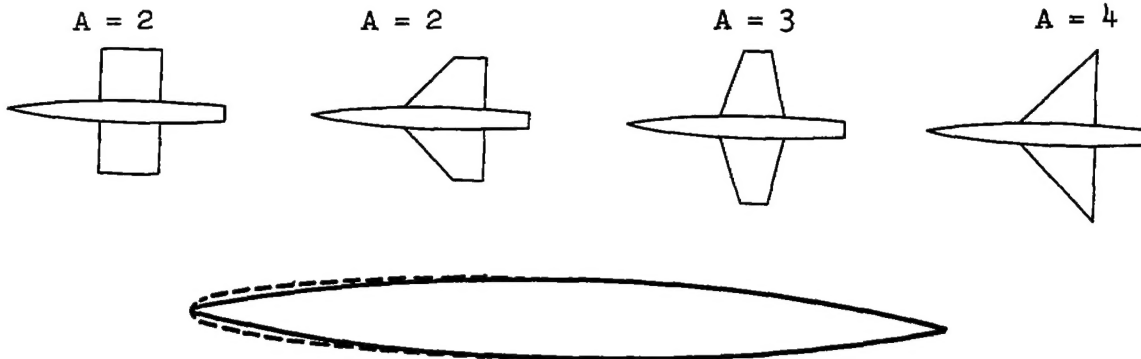
Sketch (c)

Type of profile.- The criteria for selecting the type of profile were that it should cause the minimum wave drag and should be conducive to a small value of drag due to lift. Available data indicated that small wave drag at high supersonic speeds was generally associated with sharp leading edges and a small value of drag due to lift with rounded leading edges. Hence, wings having leading edges supersonic<sup>1</sup> over much of the supersonic speed range of the tests and for which the wave drag might be sizable were designed with sharp leading edges. A 3-percent-thick biconvex section was used. However, in order to ascertain the penalty in wave drag due to round leading edges on such wings, the wings

---

<sup>1</sup>An edge is defined as subsonic or supersonic according to whether the edge lies behind or ahead of the free-stream Mach cone from the most forward point on the edge.

shown in sketch (d) were also investigated with an elliptically shaped section forward of the midchord. The coordinates for this latter section are given in table XX.



Sketch (d)

Camber and twist. - In supersonic thin-airfoil theory for wings having leading edges subsonic, an infinite suction associated with the lift on the wing occurs along the leading edge which results in a force in the thrust direction and a reduction in the drag due to lift. In general, experimental data have indicated that the full amount of leading-edge thrust predicted theoretically is not realized with wings having subsonic leading edges. A theoretical study by Jones in reference 18 showed, however, that an effective leading-edge thrust could be obtained in the case of a sweptback wing by cambering and twisting the wing. A theoretical study was made, therefore, of various types of camber and twist for triangular wings, using as a basis that required for a uniform load distribution as given in reference 18.

The shape of the surface for a uniform load distribution requires a large twist at the root section. The study showed that because of the larger root chord of the triangular wing in comparison to those of the sweptback wings treated in reference 18, the twist at the root resulted in a drag due to lift considerably greater than that indicated by theory for a plane wing. The large twist was associated with the last term in the theoretical solution for the shape of the surface to produce a uniform load distribution, as given by

$$\left( \frac{dz}{dx} \right)_u = \frac{\beta \left( \frac{\Delta p}{q} \right)_u}{4\pi m_u} \left[ G(m_u) - 2 \cosh^{-1} \frac{x}{|\beta y|} \right] \quad (1)$$

whereas the camber near the leading edge which resulted in the effective leading-edge thrust was more closely associated with the first term. Since the above expression was obtained from a linearized-lifting-

surface theory and, hence, the principal of superposition of solutions was applicable, it was reasoned that it should be possible to derive another camber and twist from the above expression by writing

$$\frac{dz}{dx} = \left( \frac{dz}{dx} \right)_u + \left( \frac{dz}{dx} \right)_a \quad (2)$$

The additional solution,  $\left( \frac{dz}{dx} \right)_a$ , must be of such a form as to cancel the

last term in equation (1) in order to eliminate the large twist at the root and at the same time have little effect on the first term. The two following solutions obtained from equation (1) and which met the requirement were studied:

$$\left( \frac{dz}{dx} \right)_a = - \frac{\beta \left( \frac{\Delta p}{q} \right)_a}{4\pi m_a} \left[ G(m_a) - 2 \cosh^{-1} \frac{x}{|\beta y|} \right] \quad (3)$$

where

$$\frac{\left( \frac{\Delta p}{q} \right)_a}{m_a} = \frac{\left( \frac{\Delta p}{q} \right)_u}{m_u} \quad (4)$$

and

$$\frac{dz}{dx} = - \frac{\beta}{4\pi} \int_0^{m_0} \frac{d \left( \frac{\Delta p}{q} \right)_a}{dm} \left[ G(m) - 2 \cosh^{-1} \frac{x}{|\beta y|} \right] dm \quad (5)$$

where

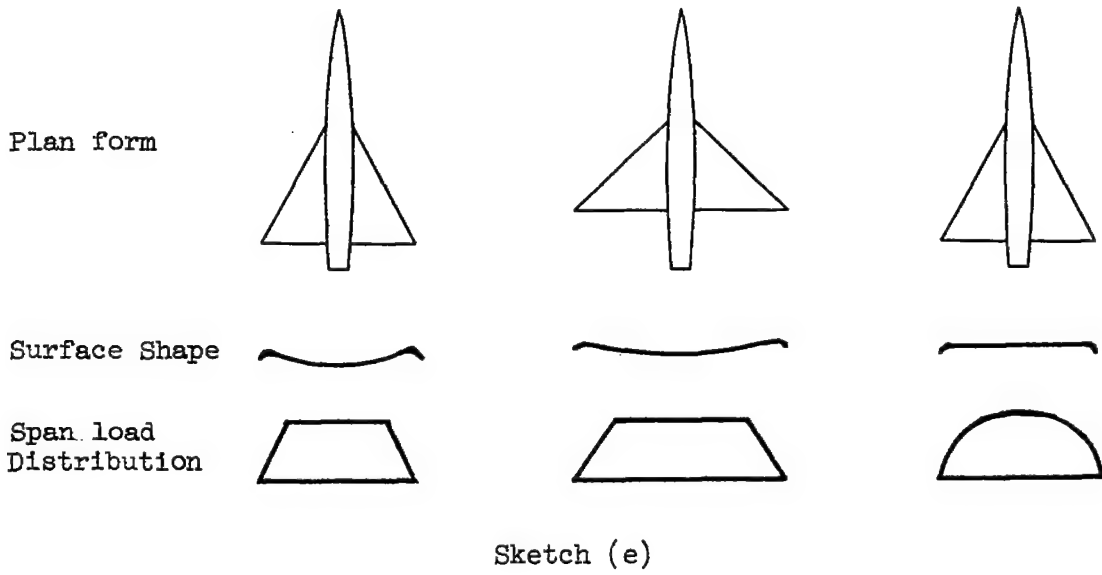
$$\frac{d \left( \frac{\Delta p}{q} \right)_a}{dm} = \frac{n \left( \frac{\Delta p}{q} \right)_u}{m_0^{n+1}} m^n \quad (6)$$

A study of the load distribution resulting from the camber and twist derived from equations (1), (2), and (3) showed that the minimum value of drag due to lift was obtained for  $m_a = 5/8 m_u$ , a value approximately equal to that given by the theory for the plane wing. Hence, two triangular wings, 5 percent thick, incorporating this camber and twist and having aspect ratios of 2 and 4 were constructed. The wing of aspect ratio 2 was designed for  $C_L = 0.25$  at  $M = 1.53$ ; the wing of aspect ratio 4 was designed for  $C_L = 0.35$  at  $M = 1.15$ . The theoretical span load distribution and the trace of the surface and projection of the wing leading edge in a plane perpendicular to the flight direction are shown for the wing of aspect ratio 2 at the design conditions in figure 1. Since the surface is conical with respect to the wing apex, the surface trace and leading-edge projection will be similar irrespective of the location

of the plane along the  $x$  axis so that the entire surface is represented by this one plot.

Analysis of the span load distribution resulting from the camber and twist derived from equations (1), (2), and (5) showed that, for a value of  $n = 3$ , the distribution was nearly elliptical (see fig.2). Thus, the drag due to lift would be expected to approach that of a wing with elliptical span load distribution, believed to be the optimum. Furthermore, it was indicated from the trace of the surface in a plane perpendicular to the flight direction that with minor modifications, the surface would be planar over most of the wing and therefore simple to construct. These modifications, wherein the trace was first made linear from the root to the 80-percent-semispan station and then sheared downward in order to have the trace straight across the inboard 80 percent of the semispan, are shown in figure 3. The effects of these modifications on the span load distribution cannot be determined from the linear theory, but it is believed that they would be small for the wing in combination with a fuselage in view of the fact that the principal modification of the curved trace occurs in the region enclosed by the fuselage. Two triangular wings of aspect ratio 2 with 3- and 5-percent thickness were built incorporating the latter type of twist and camber. Both wings were designed for  $C_L = 0.25$  at  $M = 1.53$ .

For reference, sketches of the several cambered wings together with the span load distribution and shape of the cambered surface are shown in sketch (e).



## Body

The body used in conjunction with the various wings was that shown by the theoretical study of reference 19 to have the minimum wave drag for a given length and volume of body. Its shape can be expressed by the equation for the radius of the body as

$$r = r_0 \left[ 1 - \left( 1 - \frac{2x}{l} \right)^2 \right]^{3/2} \quad (7)$$

In the equation, the symbol  $l$  represents the length of the body for complete closure at the aft end. The necessity for providing an opening at the aft end of the body to accommodate the sting support required that the actual body length be less. With the exception of the bodies for the triangular wings of aspect ratio 4 with 5-percent thickness (tables XV and XVI), the actual body length was 79 percent of the length for complete closure. In the cases of the two exceptions, the actual length was 84 percent of the length for complete closure.

For each wing-body combination investigated, the ratio of the maximum cross-sectional area of the body to the wing area was the same. The value of this ratio was 0.0509. Also, the location of the intersection of the wing leading edge with the body was nearly the same for all models. The intersection was between 34 and 38 percent of the length  $l$ .

Further information pertaining to the body, as well as a tabulation of experimental data for the body alone, obtained during the investigation is given in table XIX.

## Summary of Models

The various wing and body combinations investigated in the program, together with the number of the table in which the geometric and aerodynamic characteristics can be found, are summarized as follows:

Table No.	Type of plan form	Aspect ratio	Taper ratio	Airfoil section	Mean-surface shape
I	Triangular	2	0	0003-63	Plane
II	Triangular	3	0	0003-63	Plane
III	Triangular	4	0	3% round nose	Plane
IV	Unswept	3.08	0.388	3% biconvex	Plane
V	Sweptback	3	0.4	3% biconvex	Plane
VI	Rectangular	2	1	3% biconvex	Plane
VII	Sweptback	2	0.33	3% biconvex	Plane
VIII	Triangular	2	0	0005-63	Plane
IX	Triangular	2	0	0008-63	Plane
X	Triangular	4	0	3% biconvex	Plane
XI	Rectangular	2	1	3% round nose	Plane
XII	Sweptback	2	0.33	3% round nose	Plane
XIII	Unswept	3.08	0.388	3% round nose	Plane
XIV	Triangular	2	0	0005-63	Twisted and cambered
XV	Triangular	4	0	0005-63	Twisted and cambered
XVI	Triangular	4	0	0005-63	Plane
XVII	Triangular	2	0	0003-63	Twisted and cambered
XVIII	Triangular	2	0	0005-63	Twisted and cambered
XIX	Body alone				

## THEORETICAL METHODS

The experimental results of the present report will be compared with available theoretical solutions. It is pertinent, therefore, to devote a portion of this report to a discussion of the various methods considered and their manner of application.

## Lift-Curve Slope

Wing at subsonic speeds.— Three theoretical methods were considered for estimating the lift-curve slope of low-aspect-ratio wings at subsonic speeds; those of Weissinger (ref. 20), Lawrence (ref. 21), and Lomax and Sluder (ref. 22). These three methods may be considered as simplified lifting-surface theories, the differences in the various solutions resulting from the varying approximations and assumptions made in simplifying the integral equation relating the value of  $w$  in the  $z = 0$  plane to the value of the jump in  $u$  across the wing surface in the  $z = 0$  plane. The Weissinger method can be derived by assuming that the distribution of

the perturbation velocity in the chordwise direction is the same as that for a wing of infinite aspect ratio, and that the square of chordwise distances may be approximated by the semichord squared when comparing with the spanwise distances squared. The method of Lawrence assumes that the distribution of the perturbation velocity in the spanwise direction is the same as that given by slender-wing theory, and that the square of spanwise distances may be approximated by the semispan squared when compared with chordwise distances squared. In both cases, these simplifications reduce the lifting-surface integral equation from one of two variables to one of a single variable. The method of Lomax and Sluder also assumes that the spanwise velocity distribution is the same as that given by slender-wing theory. No approximations are made for distances on the wing. The equation is solved, in the case of the triangular wing, by finding the average value of  $w$  along the span at a given chord station and, in the case of the rectangular wing, by finding the value of  $w$  along the  $x$  axis only.

Because of the assumptions made with regard to the perturbation velocity distribution, it would seem that the Weissinger method is better suited for high-aspect-ratio wings; whereas the other two methods are better suited for low-aspect-ratio wings. However, Lawrence (ref. 21) has shown that in the limiting case of low aspect ratio, the Weissinger method agrees with the slender-wing theory of Jones (ref. 23) and the Lawrence method was designed to agree with two-dimensional results in the limiting case of infinite aspect ratio. It also can be shown that the Lomax and Sluder method agrees with two-dimensional results at infinite aspect ratio. It is observed therefore that because of the similarity of the three methods, it is not possible to assess readily their relative merits for estimating the lift-curve slope of low-aspect-ratio wings at subsonic speeds by a study of the methods alone.

Results for the three methods just described are shown in figure 4. It will be noted that the Weissinger and Lawrence methods give the same result in the range of aspect ratios of interest in this report. The Lomax and Sluder method predicts a higher lift-curve slope, however. Since the Weissinger method has been reduced to design-chart form for a wide range of plan forms by DeYoung and Harper (ref. 24), this method has been selected to compare and to correlate the experimental results in the subsonic speed range.

Wing at supersonic speeds.—Exact solutions of the linearized equation for inviscid compressible flow can be found for determining the load distribution of thin wings at supersonic speeds. These solutions can be obtained from many sources, for example reference 25 for the triangular wing, reference 26 for the sweptback wing, and reference 27 for the rectangular wing. However, for the rectangular and sweptback wings, the solutions at supersonic speeds entail extensive computations when the Mach lines from one tip intersect the opposite tip. In this

~~CONFIDENTIAL~~

speed range, approximate solutions are more satisfactory. For rectangular wings, the Lomax and Sluder method may be used. As shown in figure 4, this method gives results in satisfactory agreement with the Weissinger results at sonic speed and with the exact solutions at Mach numbers above those for which the tip Mach lines intersect the opposite tip. This condition occurs when  $\beta A$  is greater than unity. With reference to swept-back wings, a method for estimating lift and lift distribution for the supersonic speed regime near a Mach number of 1.0 is given by Lomax and Heaslet (ref. 28). It can therefore be seen that no difficulty arises in the selection of theoretical solutions for use at supersonic speeds. The sources of the solutions used in this report are those previously listed and, in addition, the graphs of reference 29.

Wing-body interference.— The experimental results presented herein are principally for wing and body combinations. For a valid comparison between such results and theoretical solutions, account must be made in the theoretical calculations of the interference effects of the wing and body. The method of Nielsen and Kaattari (ref. 30) for estimating lift interference of wing-body combinations at supersonic speeds was used. In this method, the lift of the combination is obtained by finding the lift on the body in the presence of the wing and the lift of the wing in the presence of the body. The lift on the wing, as well as the lift on the body for wings of small aspect ratio, is found to be determined best by the slender-body theory. For bodies in combination with wings of higher aspect ratio, a procedure is developed which is based on the assumption that the influence of the wing lift on the body pressure field occurs only in that region enclosed by the Mach lines originating at the leading and trailing edges of the wing-body juncture. Tip effects are not considered. For the aspect ratios for which these solutions are applicable, however, the tip effects on the lift interference are either small or may vanish if the body does not extend any considerable distance downstream of the wing trailing edge.

It should be mentioned that for the wing-body combinations discussed herein, the net effect of the wing-body interference, as given by reference 30, is small. The effects range from approximately a 4-percent reduction in lift for the triangular wing of aspect ratio 2 to an 8-percent increase in lift for the rectangular wing of aspect ratio 2.

#### Aerodynamic Center

Wing alone.— In the case of the triangular wing, the position of the aerodynamic center for the wing alone is quite easily obtained. At supersonic speeds, exact methods show the aerodynamic center to be fixed at the midpoint of the mean aerodynamic chord. At subsonic speeds, the three theoretical methods previously considered in connection with the lift

of low-aspect-ratio wings also present methods for predicting the location of the aerodynamic center of the wing. It is therefore necessary again to consider the approximations used in the several methods in order to select the method believed to be the best suited for the estimation of this characteristic.

In the Weissinger method, the chordwise distribution of load is approximated by assuming it to have the same shape as that for a wing of infinite aspect ratio in order to solve the integral equation obtained from the lifting-surface theory. This approximation automatically restricts the location of the aerodynamic center to a point on the quarter-chord line of the wing. The aerodynamic center with respect to the mean aerodynamic chord is then obtained by calculating the chordwise projection of the distance along the quarter-chord line from the mean aerodynamic chord to the spanwise location of the aerodynamic center. It can be seen, therefore, that such a procedure cannot account for the important effects of Mach number on the chordwise position of the aerodynamic center of low-aspect-ratio wings. Because of this restriction, the method is not considered suitable for the estimation of the aerodynamic center of low-aspect-ratio wings at high subsonic Mach numbers.

In contrast to the Weissinger method, the methods of Lawrence and of Lomax and Sluder determine the chordwise distribution of load from their solutions of the integral equation obtained from the lifting-surface theory. These methods may be in error because of the approximation made that the spanwise load distribution is elliptical. However, possible differences in the span load distribution from the assumed elliptical load will have only a small effect on the chordwise location of the aerodynamic center. Thus, in these two methods, the aerodynamic center is based primarily on the solution of the lifting-surface theory and only to a minor extent on the assumptions used in obtaining the solutions. This circumstance leads to the conclusion that either of these methods is better suited to the estimation of the aerodynamic center of low-aspect-ratio wings than the Weissinger method.

A comparison of the location of the aerodynamic center for triangular and rectangular wings, as determined by the three methods, is shown in figure 5. The curves show, as might be expected from the previous discussions, that the methods of Lawrence and of Lomax and Sluder give similar results and that these results are considerably different from those determined by the Weissinger method. In the present report the Lomax and Sluder method has been selected because it has been extended to include the characteristics of the triangular and rectangular wings at supersonic speeds also.

For wings having plan forms other than triangular or rectangular, the aerodynamic center at supersonic speeds can be calculated by applying the results given in any of the references previously mentioned in

connection with the lift-curve slope in this speed range. Such results have been obtained from exact solutions of the linearized equation for inviscid compressible flow and are therefore correct within the limitations of the theory. For the theoretical results presented herein, the methods of reference 31 have been used.

The methods of Lawrence and Lomax and Sluder have not been extended, as yet, to permit the calculation of the aerodynamic center at subsonic speeds for wings having plan forms other than triangular and rectangular. Also, in view of the previous discussion concerning the Weissinger method, there is some question as to its applicability for wings of small aspect ratio near a Mach number of unity. Hence, no theoretical results were computed for the aerodynamic center for wings having other than triangular or rectangular plan forms at subsonic speeds.

Wing-body interference.- As in the case of lift-curve slope, it is necessary to consider the effects of wing-body interference in calculating the aerodynamic center. Such effects have been treated in reference 32, which is an extension of the aforementioned Nielsen and Kaattari method (ref. 30) to the case of wing-body interference on the aerodynamic center.

In reference 32, it was shown that, in general, the aerodynamic center determined theoretically was behind that determined experimentally for a wide range of missile-type wing and body combinations. It was recommended, therefore, that an empirical factor be used to adjust the theoretical results. This recommendation, however, is based mainly on results for wing and body combinations in which the wing was small with respect to the body. There is some doubt as to whether the empirical factor would also apply to the cases treated herein, in which the wing is large with respect to the body, and therefore has not been used in the calculated results presented herein.

#### Drag

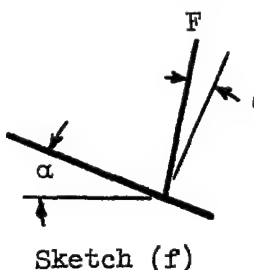
It is customary generally to divide the drag of a wing-body combination into two parts. One part is considered to be independent of the lift on the wing and is the result of viscous forces on the wing and body and, in addition, at supersonic speeds, the result of pressure or thickness drag. The second part of the drag is associated with the lift on the wing and body.

The estimation of that portion of the drag independent of lift is difficult and the methods available are not entirely satisfactory. To determine the viscous forces, it is necessary to ascertain the characteristics of the boundary layer on the surface. Often, it is assumed that the boundary layer on the wing is the same as on a flat plate of identical

plan form, and an estimation is made of the location of the region of transition from laminar to turbulent boundary-layer flow in order to calculate the viscous forces. For the purposes of this report, such a method would be unsatisfactory since it is dependent to such a great extent on an initial assumption. The comparison would offer no means of assessing the accuracy of the method. Furthermore, at supersonic speeds, the theory for determining the wave drag has been concerned mainly with sharp-nose airfoils. A method has been developed for round-nose wings (ref. 33) but is unsuited for wings having arbitrary profiles. Because of these limitations, no theoretical results for the drag at zero lift have been included herein.

The drag due to lift can be treated by thin-airfoil theory if it is considered independent of viscous forces and wing profile. In the theory, the drag due to lift can be subdivided into a force in the thrust direction associated with an infinite suction pressure acting along the leading edge of the wing and a force in the drag direction associated with the streamwise component of the normal force on the wing. A discussion of the concept of leading-edge thrust, in the case of incompressible flow, is given in reference 34 and it is shown that for a flat plate of infinite aspect ratio, the thrust is exactly equal to the streamwise component of the normal force and is determined wholly by the velocity distribution in the immediate neighborhood of the leading edge. Similarly, for a wing of finite aspect ratio, the leading-edge thrust at each section of the wing can be related to the velocity distribution near the leading edge of the section. If the velocity distribution near the leading edge of the wing of finite aspect ratio is the same as that for the wing of infinite aspect ratio, an assumption used in the Weissinger method, the leading-edge suction at each section of the wing will be the same as that for the wing of infinite aspect ratio having the same lift as the section. The streamwise component of the normal force is greater for the wing of finite aspect ratio than that for the wing of infinite aspect ratio, however, since the angle of attack must be larger to counterbalance the loss of lift associated with the finite span. There results, therefore, a net force in the drag direction generally called induced drag. It can be seen, however, that the drag due to lift may not only be composed of this induced drag but also a drag resulting from a loss of leading-edge thrust as well. The preceding concepts are based on subsonic thin-airfoil theory. However, in a similar manner, the supersonic thin-airfoil theory shows that a suction force along the leading edge is possible if the distribution of velocity near the leading edge is similar to that at subsonic speeds. Such a distribution occurs when the leading edge is swept behind the free-stream Mach lines originating at the wing apex. As at subsonic speeds, the streamwise component of the normal force is greater than the suction force, resulting in a net force in the drag direction.

In the present report, the drag due to lift for the plane wings will be considered in terms of the inclination of the force due to angle of attack<sup>2</sup> with respect to the normal to the chord as shown in sketch (f).



This approach was selected because of its close association with the manner in which the drag forces arise on the wing, as discussed previously. Thus, the basic concepts underlying the method are of equal applicability at both subsonic and supersonic speeds. The method has an advantage in that the results can be obtained with accuracy and ease from the normal and chord force measurements taken during the investigation.

The angle of inclination of the force  $F$  is dependent on both the normal force and the leading-edge thrust and, for small values, is equal to the ratio of the leading-edge thrust to the normal force. Since in the thin airfoil theory for plane wings these quantities are proportional to the second and first powers of the angle of attack, respectively,  $\theta$  is also proportional to the angle of attack. Thus the rate of change of  $\theta$  with  $\alpha$  is constant. Experimental results, in general, also show that for plane wings at small angles of attack, the rate of change of  $\theta$  with  $\alpha$  is constant. For such results, the normal force usually agrees satisfactorily with theoretical results. Thus a comparison of the experimental and theoretical values of the ratio,  $\theta/\alpha$ ,<sup>3</sup> will show, principally, the extent to which the chordwise force on the wing approaches the theoretical value for full leading-edge thrust.

In figure 6, the values of the ratio are shown for triangular and rectangular wings at both subsonic and supersonic speeds. These results are for the wings having the full leading-edge thrust predicted by the theory. Furthermore, in order to simplify the calculations for subsonic speeds, it has been assumed that the span load distribution is elliptical since the value of the drag due to lift for a wing with such a distribution and having full leading-edge thrust is well known. Since the effect of the deviation from such a distribution on the drag due to lift for most wings is small, this assumption will have little effect on the significance of  $\theta/\alpha$ . At supersonic speeds, the ratio was determined using the expression given in reference 25 for the drag due to lift.

---

<sup>2</sup>The force due to angle of attack is the force on the wing at angle of attack less the force at zero lift.

<sup>3</sup>The ratio  $\theta/\alpha$  can replace the rate of change of  $\theta$  with  $\alpha$  because for plane wings,  $\theta = 0$  at  $\alpha = 0$ .

## EXPERIMENTAL PROCEDURE

## Facilities

Most of the experimental results presented herein were obtained in three facilities at the Ames Aeronautical Laboratory. At Mach numbers of 0.6 and less, the wings were investigated in the Ames 12-foot wind tunnel only. At Mach numbers of 1.2 and above, data were obtained in the Ames 6- by 6-foot wind tunnel only. Between these two ranges of Mach numbers, some of the wings were tested in both of these facilities and on the 16-foot wind-tunnel bump as well. In addition, during the calibration period of a 2- by 2-foot transonic wind tunnel, the unswept wing of aspect ratio 3 was investigated in the Mach number range from 0.6 to 1.35 and these data are included herein.

## Reduction of Data

A complete discussion of the methods used in reducing the wind-tunnel data to coefficient form and the various corrections applied to the results will be found in any of references 1 to 17. Therefore, only a brief summary of the methods will be presented herein.

The data obtained in both the Ames 12-foot wind tunnel and the 6- by 6-foot supersonic wind tunnel have been corrected for the following factors:

1. Induced effects of the tunnel walls at subsonic speed resulting from lift on the model.
2. The change in the airspeed in the vicinity of the model at subsonic speed resulting from the constriction of the flow by the walls.
3. The pressure at the base of the model being different from that for a full-scale airplane as the result of support interference as well as other unknown effects on the base pressure. To partially account for these effects, the drag coefficient was adjusted to correspond to that in which the base pressure would be equal to the free-stream static pressure.

Data obtained in the 6- by 6-foot wind tunnel and presented herein were corrected for the longitudinal force on the model due to streamwise variation of the static pressure as measured in the empty test section. This correction was not applied to the subsonic data as presented in references 1 to 16 because of the lack of a complete static-pressure

~~CONFIDENTIAL~~

survey of the tunnel at the time of publication. The correction amounts to as much as 0.0010 at a Mach number of 0.93. The data obtained in the 6- by 6-foot wind tunnel also indicated nonuniformities of the airstream in the plane of pitch equivalent to a stream angle of as much as  $0.10^{\circ}$  for some of the models. The data presented herein have not been corrected for this effect.

Data presented herein which were obtained on the 16-foot wind-tunnel bump and in the 2- by 2-foot transonic wind tunnel have had no corrections applied.

#### RESULTS AND DISCUSSION

In portions of the Mach number range of the program discussed herein, some of the wings were tested in several facilities so that a choice of data for graphical presentation was possible. The general procedure has been to show the lift-curve slope and aerodynamic-center characteristics as determined in all facilities. However, in showing the variation of lift with angle of attack or of pitching moment with lift, results from only one facility have been used in order to avoid congestion of the figure, the facility being chosen wherein the most complete investigation for the particular series of wings under discussion was made. The drag characteristics shown for the various wings at high subsonic speeds were obtained from tests in the 6- by 6-foot wind tunnel only, because the Reynolds number of the tests in that facility was considerably larger than for corresponding tests in the 12-foot wind tunnel, and because the wings investigated in the 16-foot wind tunnel did not have a body in combination.

With regard to the Reynolds number for the data presented graphically herein, the general procedure has been to present data at the highest Reynolds numbers for which complete data were obtained throughout the Mach number range presented. However, for the lift and pitching-moment characteristics at high angle of attack, it has been necessary to use results obtained at the lowest Reynolds number in order that a large range of angles of attack could be presented. This condition arises since the lift on the models was restricted because of strength limitations.

All data obtained in the 6- by 6-foot and 12-foot wind tunnels and discussed herein are presented in tables I to XIX.

#### Effects of Aspect Ratio

The effects of aspect ratio on triangular wings were studied through experiments on three wings of aspect ratios 2, 3, and 4. All wings were

3-percent-thick, NACA 0003-63 sections (streamwise) being used for the wings of aspect ratios 2 and 3. The section profile of the wing of aspect ratio 4 was obtained by joining a semiellipse forward of the 50-percent-chord station with a semibiconvex section aft. Further information pertaining to the geometric characteristics of these wing-body combinations, as well as a tabulation of the experimental data obtained during the investigation can be found in tables I, II, and III.

Lift-curve slope. - The discussion of the lift characteristics of these wings will be directed first to the angle-of-attack range near zero lift, wherein the variation of lift with angle of attack was linear. A later section will present the characteristics at high angles of attack. In figure 7, experimental lift-curve slopes as influenced by aspect ratio for triangular wings are shown for Mach numbers between 0.25 and 1.7, and the results are compared with theoretical estimates.

The experimental results of figure 7 show a sizable effect of aspect ratio on the lift-curve slope of triangular wings, an increase in aspect ratio causing an increase in lift-curve slope through the Mach number range of these tests. Although the effect of aspect ratio as determined in each facility was nearly identical, the lift-curve slopes measured in the 6- by 6-foot wind tunnel between Mach numbers of 0.60 and 0.93 were somewhat larger than those obtained in the other two facilities. The cause of this difference is not known. A possible explanation is the fact that the effective Reynolds number for the data obtained in the 6- by 6-foot wind tunnel was considerably higher than that in the other two wind tunnels because of the greater turbulence in the air stream.<sup>4</sup>

The results of figure 7 indicate that the linearized theory predicted satisfactorily the effects of aspect ratio and Mach number on the lift-curve slopes over much of the subsonic speed range. However, at Mach numbers ranging about 1.0, the extent of the range depending on the aspect ratio, the agreement was less satisfactory. At a Mach number

<sup>4</sup>A similar difference in lift-curve slope occurred for all wings investigated during this program in the 12-foot and 6- by 6-foot wind tunnels at a Mach number of 0.6, even when the nominal Reynolds numbers were the same. In general, the difference was greater for wings with round leading edges than for those with sharp leading edges. The difference also decreased with increasing Mach number in the two cases where the same model was tested up to a Mach number of approximately 0.9 in each facility. These two facts are in agreement with the possible explanation of the difference. A sharp leading edge would promote premature transition and increased turbulence in the boundary layer, thus causing the results for such wings to be less influenced by change in effective Reynolds number, and with increasing Mach number the effects of Reynolds number would become secondary to the effects of compressibility.

near 1.0, the agreement became progressively worse with increasing aspect ratio. Results obtained from the investigation of the triangular wing of aspect ratio 4 with the NACA 0005-63 section up to Mach numbers of 0.96 have further established this trend (ref. 3 and table XVI). The disagreement between theory and experiment is believed attributable to second-order effects of the velocities induced by the wing thickness and lift and the possibility of shock formation in the transonic speed range.

The lack of agreement between theory and experiment in the supersonic speed range may also be considered a transonic-flow effect in that the poor agreement occurred when the component of the free-stream Mach number perpendicular to the leading edge,  $M \cos \Lambda$ , became sonic. For the triangular wings of aspect ratios 2, 3, and 4, the values of the free-stream Mach numbers at  $M \cos \Lambda = 1.0$  are 2.25, 1.67, and 1.41, respectively. At the latter two Mach numbers, for which results are shown in figure 7, the lift-curve slopes for the corresponding triangular wings were approximately 10 percent below those predicted by the theoretical methods. A similar effect has been observed in other investigations of triangular wings. In reference 35, the lift-curve slopes for a series of flat-plate triangular wings tested at a Mach number of 1.92 were also approximately 10 percent less than predicted by theory when  $M \cos \Lambda$  was equal to 1.0. This lack of agreement between experimental and theoretical results in the Mach number range near  $M \cos \Lambda = 1.0$  is not surprising in view of the pressure measurements made on a triangular wing of aspect ratio 4 at supersonic speeds (ref. 36). These results showed that in this apparent transonic range for the triangular wing, the pressure distributions along transverse sections of the wing resembled closely those occurring on two-dimensional airfoils at transonic speeds, in that shock waves oblique to the free stream and pressure discontinuities occurred in a fashion similar to the two-dimensional transonic results. Furthermore, the results indicated that the presence of a detached bow wave caused significant differences between the experimental and theoretical pressure distributions near the leading edge at Mach numbers corresponding to values of  $M \cos \Lambda$  greater than 1.0, and it was surmised that the agreement between experimental and theoretical results would improve as the Mach number increased and the bow wave approached attachment. Such an effect was evident in the results for the triangular wing of aspect ratio 4 in figure 7.

The results of figure 7 were obtained at the highest Reynolds number possible in each facility for the Mach number range tested. For the wings of aspect ratios 2, 3, and 4, results obtained in the 6- by 6-foot wind tunnel are at Reynolds numbers of 7.5, 4.8, and 4.2 millions, respectively, and results from the 12-foot wind tunnel are at Reynolds numbers of 4.9, 3.1, and 2.7 millions, respectively. The Reynolds numbers for results obtained on the 16-foot wind-tunnel bump were not constant but increased with Mach number from approximately 2.1 to 2.8 millions. The effects of Reynolds number were investigated in the 6- by 6-foot wind

tunnel through the Mach number range of that facility and for a range of Reynolds numbers commencing at approximately one third of that for the results of figure 7. In the 12-foot wind tunnel the effect of Reynolds number was investigated at a Mach number of 0.25 only, and the range extends from that for the results of figure 7 to approximately 3-1/2 times that value. In these ranges of Reynolds and Mach numbers, no significant effect of change in Reynolds number was evident in the slope of the lift curve through zero lift. (See tabulated data.)

Lift at angle of attack. - The experimental and theoretical values of the lift-curve slope previously discussed may not be applicable over wide ranges of lift coefficient if the variation of lift with angle of attack is nonlinear. It is therefore necessary to examine the lift curve, and in figure 8 a comparison of lift at angle of attack for the three triangular wings is shown. Results are shown at two subsonic and one supersonic Mach number to indicate typical effects of aspect ratio. The results of figure 8 are for a lower Reynolds number than those of figure 7. However, in the ranges of Reynolds numbers and Mach numbers investigated in each facility, no significant effect of change in Reynolds number was evident in the lift characteristics up to lift coefficients of approximately 0.5, the limit for which a comparison could be made.

The results of figure 8 show a nonlinear variation of lift with angle of attack for the triangular wings of aspect ratios 2, 3, and 4, throughout the Mach number range. Thus there was a limit in lift coefficient to which the theoretical lift-curve slope at zero lift could be used to estimate the lift characteristics at angle of attack.

The results of figure 8 show that the departure from linearity of the variation of lift with angle of attack was different at subsonic and supersonic speeds. For example, at a Mach number of 0.25 the variation of lift with angle of attack increased with angle of attack for the wing of aspect ratio 2, whereas the opposite effect was noted for the wing of aspect ratio 4. In fact, at a high angle of attack the lift of the aspect ratio 2 wing was greater than that of the wing of aspect ratio 4, although at zero lift the variation of lift with angle of attack of the former wing was only about 65 percent as great as that for the latter wing. At a Mach number of 0.9, trends similar to those at a Mach number of 0.25 are noted. However, the data are limited in lift coefficient so that the characteristics near maximum lift are not known. On the other hand, at supersonic Mach numbers the nonlinear behavior of lift with angle of attack was essentially the same for the three wings.

Aerodynamic center. - The aerodynamic centers for the three triangular wings are compared with the theoretical solutions over the Mach number range of the program in figure 9. The Reynolds numbers of these data are the same as those for figure 7 and listed previously in the discussion

of lift-curve slope. The experimental aerodynamic center was determined from the change in pitching moment with lift near zero lift.

The results shown in figure 9 have been obtained from three different facilities at the Ames Laboratory and, as with lift-curve slope, small discrepancies existed among the several sets of results. The largest discrepancy occurred between results obtained in the Ames 16-foot wind tunnel and those obtained in the 12-foot and 6- by 6-foot wind tunnels. This discrepancy was probably the result of wing-body interference, since the data obtained in the 16-foot wind tunnel were for a wing alone, whereas the other data were for a wing and body combination.

The results of figure 9 show satisfactory agreement between the experimental and theoretical results at supersonic speeds. The forward movement of the aerodynamic center with increasing aspect ratio and Mach number was caused by wing-body interference. Such effects are seen to be very small for the triangular wing and body combinations under discussion. The theoretical results were adjusted for these effects of wing-body interference by the methods of reference 32.

At subsonic speeds, the agreement between the experimental and theoretical results is also seen to be quite good. It will be recalled that the effects of wing-body interference have not been accounted for in the theoretical results at subsonic speeds. The net effects of wing-body interference are probably small for these triangular wing and body combinations, as judged by the small differences between the experimental results for wing and body combinations and those for the wing alone, so that the theoretical results would probably not be affected significantly by the inclusion of such effects.

The results of figure 9 show that the rearward movement of the aerodynamic center with increasing Mach number in the subsonic range became considerably larger as the aspect ratio was increased. It is interesting to note, however, that these data are based on the length of the wing mean aerodynamic chord, a length which decreases with increasing aspect ratio. If the wing area were the same for these triangular wings, the actual rearward travel of the aerodynamic center would have been nearly the same in each case. Thus the aerodynamic-center travel for the triangular wing of aspect ratio 4 would be only 14 percent greater than that for the wing of aspect ratio 2, in contrast to a figure of 61 percent when the aerodynamic-center travel is expressed in terms of the mean aerodynamic chord. This fact would have significance, for example, in comparing the effect of change in wing aspect ratio on the stability characteristics of an airplane in which the tail length might be fixed from other considerations. Other factors remaining equal, such a comparison would show little effect of aspect ratio on the change in stability of the airplane with increasing Mach number.

Pitching moment at angle of attack. - The aerodynamic center, as determined near zero lift and discussed previously, has significance only if the variation of pitching moment with lift is nearly linear. It is therefore necessary to examine the pitching-moment characteristics at angle of attack for the triangular wings, and such data are presented in figure 10.

These data show that at a Mach number of 1.53, the variation of pitching moment with lift was nearly linear throughout the range of lift coefficients investigated. This characteristic was typical of the data obtained at Mach numbers from 1.2 to 1.7, the supersonic portion of the range investigated in this program. Thus the aerodynamic center determined near zero lift, and hence the results obtained from the theory, may be used satisfactorily for the stability characteristics of the triangular wings over a wide range of lift coefficient at supersonic speeds.

Similar characteristics did not occur at subsonic speeds, the results at a Mach number of 0.25 being extremely nonlinear, particularly in the case of the triangular wing of aspect ratio 4. Thus the aerodynamic center determined near zero lift and, hence, the results obtained from the theory are not usable as a measure of the stability of these triangular wing and body combinations above a lift coefficient of approximately 0.2 at subsonic speeds. The cause of this nonlinear variation of pitching moment with lift has been shown in references 37 and 38 to be flow separation which occurs first near the tip of the wing and moves inboard with increasing angle of attack.

From an inspection of the data in figure 10 at a Mach number of 0.25, it would appear that the stability characteristics of the triangular wing of aspect ratio 4 were considerably inferior to those of the wing of aspect ratio 2. For the former wing, there was a sizable decrease in stability with increasing lift coefficient to approximately 0.6 and an extreme increase in stability at higher lift coefficients. However, it was shown in reference 39 that a triangular wing of aspect ratio 4 required a horizontal tail to provide satisfactory damping-in-pitch characteristics at transonic speeds, whereas the characteristics of the triangular wing of aspect ratio 2 alone were satisfactory. This fact must be considered, therefore, in evaluating the effects of aspect ratio on the stability characteristics at low speeds. In reference 38 it was shown that proper location of a horizontal tail behind a triangular wing of aspect ratio 4 eliminated the decrease in stability at low lift coefficients and reduced the increase in stability at high lift coefficients exhibited by the wing alone. The resultant characteristics compared favorably then with the triangular wing of aspect ratio 2 alone or in combination with a tail (ref. 40).

Minimum drag coefficient. - The effects of aspect ratio on the minimum drag coefficient of triangular wings are shown in figure 11. Only data

at the highest Reynolds number obtained for each wing during the investigation have been included in this figure because of the sizable effects of Reynolds number on the minimum drag coefficient. Also at the highest Reynolds number, the drag force is largest so that the balance is working at more nearly the design load, resulting in greatest accuracy. The Reynolds numbers for the triangular wings of aspect ratios 2, 3, and 4 were 16.6, 10.6, and 9.1 millions, respectively, at a Mach number of 0.25 and 7.5, 4.8 and 4.2 millions, respectively, at Mach numbers of 0.6 and above.

For the triangular wings of aspect ratios 2 and 3, the significant effects of Reynolds number were confined principally to the range of lift coefficients between -0.05 and +0.05. In this range of lift coefficients at Reynolds numbers less than those of figure 11, the variation of drag with lift resembled that for the NACA 6-series airfoil in the region of low drag. (See ref. 41.) However, the data at the Reynolds numbers shown in figure 11 did not exhibit this characteristic. Thus the minimum drag coefficient at a Reynolds number of approximately one third that of figure 11 was as much as 0.0015 less than that at the highest Reynolds number, whereas at lift coefficients outside the low drag range, the effects of Reynolds number on the drag coefficient were negligible.

For the triangular wing of aspect ratio 4, the effects of Reynolds number on the drag at low lift were also significant. However, in contrast to the results for the lower-aspect-ratio wings, the drag coefficient showed no abrupt increase with lift coefficient at the lower Reynolds number but increased gradually and became contiguous with the results for the highest Reynolds number at lift coefficients which varied irregularly with the Mach number but were less than 0.4. The largest increase in minimum drag coefficient with increasing Reynolds number from  $1.6 \times 10^6$  to  $4.2 \times 10^6$  occurred at a Mach number of 1.6 and was approximately 0.0015. These effects of Reynolds number on the minimum drag coefficient varied irregularly with Mach number; the general trend, however, was as described.

The variation with Mach number of the wave drag of a sharp-nose triangular wing, as determined by linear theory (ref.42), shows large discontinuities in slope as the Mach number is varied in the range where the leading edge becomes supersonic. To the extent of the data shown in figure 11, there are no indications of these discontinuities. For the triangular wings of aspect ratios 3 and 4, the leading edges become supersonic at Mach numbers of 1.67 and 1.41, respectively. Although the results of figure 11 are for round-nose triangular wings, results from tests of a sharp-nose airfoil to be discussed in a subsequent section have indicated a similar characteristic. Also, in reference 35 the results from tests of a series of 11 sharp-nose triangular wings of aspect ratios from 0.70 to 4.023 and 8 percent thick have shown essentially a linear variation of minimum drag coefficient with Mach number

in this range. These results therefore indicate that the existing linearized theory is inadequate for predicting the wave drag of triangular wings. This deficiency of the linearized theory is believed to be due to the fact that the effect of the detached bow wave at Mach numbers in the region where the leading edge becomes supersonic is not considered by the theory.

The results of figure 11 show that in the subsonic speed range the minimum drag coefficient for the triangular wings varied with aspect ratio. At a Mach number of 0.25, the minimum drag coefficient increased with aspect ratio. This characteristic is believed to be due to the fact that with increasing aspect ratio a smaller portion of the wing was enclosed within the body, resulting in an increase in the exposed surface area and the skin-friction drag. At subsonic Mach numbers above 0.6, the variation of minimum drag coefficient with aspect ratio was irregular, that for the triangular wing of aspect ratio 3 being roughly 0.001 less than those for the wings of aspect ratios 2 and 4. The cause of this variation is not known but may possibly be due to differences in the skin-friction drag.

The variation of minimum drag coefficient with aspect ratio at supersonic speeds was due primarily to the effect of aspect ratio on the wave drag of these triangular wings. The results indicate that this effect was largest as the aspect ratio increased from 3 to 4. It should be pointed out, however, that possible differences in the surface condition of the wings previously mentioned in connection with the variation of minimum drag coefficient at high subsonic speeds may also affect the drag coefficient at supersonic speeds. Thus, if the data were adjusted so that the minimum drag coefficient for the three wings would be approximately the same between Mach numbers of 0.6 and 0.9, the results would indicate a nearly linear increase in minimum drag coefficient with increasing aspect ratio. Such a characteristic is in agreement with the results shown in references 35 and 43. It would appear, therefore, that the increment of minimum drag coefficient between that at Mach numbers up to 0.9 and that at Mach numbers above 1.2 shown in figure 11 was correct for the triangular wings investigated. The skin-friction drag coefficient for the wing of aspect ratio 3 at Mach numbers of 0.6 and above, however, may be as much as 0.001 less than that for the wings of aspect ratios 2 and 4, due to differences in the surface conditions of the wings.

Drag due to lift.— The drag due to lift is a function of the lift of the wing, the lift-curve slope, and the relative inclination of the force

vector, as indicated in the following expression<sup>5</sup> for the drag coefficient due to lift:

$$C_D - C_{D_{\min}} = \frac{1 - (\theta/\alpha)}{dC_L/d\alpha} C_L^2 \quad (8)$$

Since the lift characteristics of these triangular wings have been presented previously, the present sections will be concerned primarily with the inclination of the force vector.

The effects of aspect ratio on the ratio of the angle between the force vector and the normal to the wing chord,  $\theta$ , to the angle of attack,  $\alpha$ , are shown in figure 12. The experimental data presented are for the highest Reynolds number obtained for each wing during the investigation. The Reynolds numbers for these data are the same as those of figure 11. In general, an increase in Reynolds number within the limits of the present test caused a small increase in the value of  $\theta/\alpha$ . Also, at supersonic speeds, the values  $\theta/\alpha$  shown are applicable up to lift coefficients of the order of 0.5, the limit of the tests. At subsonic speeds, however, values of  $\theta/\alpha$  presented are applicable only to approximately the lift coefficient for maximum lift-drag ratio. At higher lift coefficients, the values of  $\theta/\alpha$  showed an abrupt decrease, becoming approximately equal to the value at supersonic speed. This decrease is probably associated with the onset of the vortex-separation type of flow characteristic of triangular wings.

Included in figure 12 are values of  $\theta/\alpha$  as determined from thin-airfoil theory. As indicated, the experimental results show little resemblance to the theoretical results. It will be recalled, however, that the results at subsonic speeds were obtained under the assumption that the span load distribution was elliptical in order to simplify the calculations. Hence, a small part of the discrepancy may be the result of a difference in the span load distribution. At supersonic speeds, no assumptions beyond those implicit in linear theory were required in making the calculations. The discrepancy between experimental and theoretical results must be attributed entirely, therefore, to a deficiency in the thin-airfoil theory as applied to the calculation of drag due to lift. Hence, it must be concluded that for thin triangular wings the drag due to lift cannot be predicted accurately by available theoretical methods. In general, it appears that for supersonic speeds, it is more accurate to base calculations on the assumption that the net force on the airfoil due to angle of attack is normal to the chord line than to use available theoretical methods.

---

<sup>5</sup>The expression is restricted to plane wings having a linear variation of lift with angle of attack. The units of lift-curve slope are per radian in this expression.

Although somewhat irregular at the high subsonic speeds, the general trend of the results indicates that  $\theta/\alpha$  decreased with increasing aspect ratio. The value of  $\theta/\alpha$ , in effect, represents the decrease in the drag due to lift from that experienced by the wing if the force vector were normal to the chord. Hence, the drag due to lift for thin triangular wings is not influenced predominantly by these effects of aspect ratio. Rather, the primary influence of aspect ratio on the drag due to lift is felt through its effect on the variation of lift with angle of attack.

Maximum lift-drag ratio. - When the variation of drag with lift is parabolic, as shown by the results for these triangular wings at low lift coefficients, the maximum lift-drag ratio and the lift coefficient at maximum lift-drag ratio can be expressed as follows:

$$\left(\frac{L}{D}\right)_{\max} = \frac{1}{2} \sqrt{\frac{dC_L/d\alpha}{C_{D\min} [1 - (\theta/\alpha)]}} \quad (9)$$

$$C_{L\text{opt}} = \sqrt{\frac{C_{D\min} (dC_L/d\alpha)}{1 - (\theta/\alpha)}} \quad (10)$$

Such expressions are helpful in the discussion of the maximum lift-drag ratios and corresponding lift coefficients for the triangular wings shown in figure 13. As with previous data concerned with the drag of the wing-body combinations, the results shown in figure 13 are for the highest Reynolds number obtained for each wing during the investigation.

The results of figure 13 indicate no consistent trend of maximum lift-drag ratio with increasing aspect ratio in the Mach number range of the investigation. At subsonic speeds, the maximum lift-drag ratio increased with aspect ratio. This characteristic could be expected in light of equation (9) from the fact that the variation of minimum drag coefficient and  $\theta/\alpha$  with aspect ratio was small, whereas the increase in lift-curve slope with increasing aspect ratio was large. As previously mentioned, however, the minimum drag coefficient was smallest for the wing of aspect ratio 3 between Mach numbers of 0.6 and 0.93, which would account for the maximum lift-drag ratio of this wing being nearly as large as that of the wing of aspect ratio 4 in this range. In the supersonic speed range of these investigations, the triangular wing of aspect ratio 3 exhibited the highest maximum lift-drag ratio. This characteristic indicated that the increase in lift-curve slope had a greater effect on maximum lift-drag ratio than the increase in minimum drag coefficient as the aspect ratio was increased to 3. However, for aspect ratio greater than 3, the opposite effect occurred. It should be mentioned that had the variation of minimum drag coefficient with aspect ratio been more linear,

as discussed previously in connection with the drag of these triangular wings, the maximum lift-drag ratio of the wing of aspect ratio 3 would be less than shown in figure 13 and would be approximately that of the wing of aspect ratio 4.

It was previously shown that at supersonic speeds, the increase of lift-curve slope with aspect ratio decreased with increasing Mach number, and it might be expected from theoretical considerations that the lift-curve slopes of these triangular wings at Mach numbers above approximately 2.3 would be the same. However, the variation of minimum drag coefficient with aspect ratio did not change significantly with Mach number. These facts would indicate that the wing having the lowest minimum drag coefficient, the wing of aspect ratio 2, would tend to have the highest maximum lift-drag ratio as the Mach number increased. Such a tendency is evident from figure 13, although the Mach number at which it would be expected that the highest maximum lift-drag ratio was obtained by the wing of smallest aspect ratio is outside the range of the investigation.

The lift coefficient for maximum lift-drag ratio showed a consistent increase with increasing aspect ratio throughout the Mach number range of the investigation. As can be seen from equation (10), this variation is consistent with the previously noted behavior of lift-curve slope, minimum drag coefficient, and  $\theta/a$ .

#### Effects of Type of Plan Form

The effects of type of wing plan form were investigated with two groups of wings, one of aspect ratio 2 and the other of aspect ratio 3. Plane wings, 3 percent thick, were used for both series of wings. An NACA 0003-63 airfoil section was used for the triangular wings. The unswept and sweptback plan forms in each aspect-ratio group had a biconvex section. Further information pertaining to the geometry of the wings of aspect ratio 3 as well as tabulated data obtained during the investigation can be found in tables II, IV, and V. Similar information for the wings of aspect ratio 2 is contained in tables I, VI, and VII. In addition, a more complete discussion of the characteristics of the wings of aspect ratio 2 is given in reference 44.

Several of the wings having the biconvex section were also investigated with round-nose sections and will be discussed in a subsequent section of this report. It is sufficient at this time to say that the effect of such differences in section on the lift and pitching-moment characteristics was not significant. In general, however, the drag characteristics of the wings with biconvex sections were better than those with round-nose sections at high supersonic speed, indicating that such a section would be preferable for airplanes with wings having small leading-edge sweep and for which the attainment of high speeds of the order of  $M = 2$

was desired. It was for this reason that the type of profile, that is, round or sharp nose, was not the same for all wings in the present grouping, and the wings of  $45^{\circ}$  sweepback or less have the biconvex section.

Lift-curve slope. - The lift-curve slope for the wings under discussion is shown in figure 14. Again, the results shown are for the highest Reynolds number obtained in each facility for the Mach number range tested. For the triangular, sweptback, and unswept wings of aspect ratio 3, the results obtained in the 6- by 6-foot wind tunnel are at Reynolds numbers of 4.8, 3.8, and 2.4 millions, respectively, and results from the 12-foot wind tunnel are at Reynolds numbers of 3.1, 2.5, and 2.4 millions, respectively. Results obtained in the 2- by 2-foot wind tunnel are at a Reynolds number of 1.5 million. The Reynolds number of the data obtained on the 16-foot wind-tunnel bump increased from 2.1 to 2.8 millions with increasing Mach number for the triangular wing of aspect ratio 3, and from 1.9 to 2.5 millions for the unswept wing of aspect ratio 3. For the triangular, sweptback, and unswept wings of aspect ratio 2, results obtained in the 6- by 6-foot wind tunnel are at Reynolds numbers of 7.5, 4.8, and 4.4 millions, respectively. Data obtained for the triangular wing of aspect ratio 2 in the 12-foot wind tunnel are at a Reynolds number of 4.9 million and those obtained on the 16-foot wind-tunnel bump are at Reynolds numbers between 2.1 million and 2.8 million. The Reynolds number of the data for the unswept wing of aspect ratio 2 obtained on the 16-foot wind-tunnel bump varied with Mach number from 1.8 to 2.0 millions.

A comparison of the theoretical and measured lift-curve slopes for the wings under discussion (fig. 14) indicates satisfactory agreement over much of the Mach number range of the investigation. In general, in the Mach number range near unity, the trend of the experimental results was different from that predicted by the theory. However, these differences may be due, in part, to deficiencies in the experimental results since it will be noted that for the unswept wing of aspect ratio 3, as yet unpublished results obtained in the 2- by 2-foot transonic wind tunnel were in better agreement with the theoretical trends at Mach numbers near unity than those obtained on the 16-foot wind-tunnel bump.

Considering the effects on lift-curve slope of the sweepback of the leading edge at constant aspect ratio and taper ratio, the results for the wings of aspect ratio 3 at subsonic speeds indicated a decrease in lift-curve slope with increasing sweepback. This trend conforms with the predictions of reference 24, although in that reference the angle of sweep for maximum lift-curve slope was shown not to be zero, but varied from a small angle of forward sweep to a small angle of sweepback as the aspect ratio and taper ratio were decreased. The same trend was evident at low supersonic speeds. However, with increasing Mach number, the effect of sweep diminished until at a Mach number of 1.7, the limit of the data, the lift-curve slopes for the sweptback and unswept wings were the

same. At higher Mach numbers, it would be expected that the lift-curve slope of the sweptback wing would be slightly higher because of the smaller portion of the wing influenced by the tip Mach cone.

The same general effects of sweepback on the lift-curve slope were also evident in the results for the sweptback and unswept wings of aspect ratio 2. These effects are altered to a small extent, however, by the fact that the taper ratio was not the same for both wings.

The theoretical results indicate that at a Mach number of 1.0, the lift-curve slope for these wings of aspect ratios 2 and 3 is a function only of aspect ratio, the small differences shown in figure 14 being the result of differences in wing-body interferences. As previously indicated, the experimental results did not confirm this prediction. The theoretical results also indicate that in the supersonic speed range, the effects of plan form and aspect ratio decrease with increasing Mach number, and that at sufficiently high Mach number, the lift-curve slopes of the wings will be nearly the same. The trend of the experimental results tended to confirm this latter prediction.

Lift at angle of attack. - The effects of wing plan form on the lift at angle of attack are shown in figure 15 for the wings of aspect ratio 3 at two subsonic and one supersonic Mach number. Lack of data at a Mach number of 0.25 prevented making a comparable plot for the wings of aspect ratio 2.

The variation of lift with angle of attack was somewhat nonlinear for the wings of aspect ratio 3, and thus there is a limit to which the experimental or theoretical lift-curve slope at zero lift may be used to estimate the lift characteristics at angle of attack.

In the subsonic speed range, the most pronounced effect of wing plan form on the lift characteristics occurred at high angles of attack. A comparison of the results for the sweptback and unswept plan forms, in which the primary plan-form difference is sweepback of the leading edge, shows that the variation of lift with angle of attack became less abrupt as the sweepback was increased. The results for the triangular wing, the wing having the greatest sweepback of the leading edge, further established this trend, although in this case the taper ratio of the wing is different from that of the other wings. Further evidence that the sweep of the leading edge was the primary factor affecting the lift characteristics at high angle of attack is offered by a comparison between the data for the sweptback plan form in figure 15 and those for the triangular wing of aspect ratio 4 in figure 8. For both wings, the sweep of the leading edge is the same. The data indicate that the lift characteristics at high angles of attack were very similar for both wings at a Mach number of 0.25.

In the case of the unswept wing, the abrupt change in lift variation with angle of attack can be delayed to a higher angle by use of a leading-edge flap (ref. 45). Cambering the wing near the leading edge should offer similar improvements, although such a modification may cause an increase in the minimum drag coefficient, particularly at supersonic speeds.

Aerodynamic center. - The aerodynamic center in percent of the mean aerodynamic chord is shown for the wings of aspect ratios 2 and 3 in figure 16. The Reynolds numbers for these data are the same as previously listed in connection with the lift-curve slope of these wings. In general, these results have been obtained from the variation of the pitching-moment coefficient with lift coefficient through zero lift. However, in the Mach number range from 0.7 to 0.9, the variation of pitching-moment coefficient with lift coefficient through zero lift was somewhat nonlinear for the sweptback and unswept wings. The nonlinear variation of pitching-moment coefficient was influenced significantly by Reynolds number, but was smallest at the highest Reynolds number of the investigation. In this range of Mach numbers, the aerodynamic center for the sweptback and unswept wings was determined, therefore, from the variation of pitching-moment coefficient with lift coefficient outside the region of the nonlinearity. Because of the decrease in the nonlinearity with increasing Reynolds number, it is believed that the results so obtained are representative of full-scale wings.

The results shown in figure 16 are compared with theoretical predictions except at subsonic speeds in the cases of the sweptback wings of aspect ratios 2 and 3 and the unswept wing of aspect ratio 3 since, as previously mentioned, there is some question as to the applicability of the methods of reference 24 to the prediction of aerodynamic-center position for low-aspect-ratio wings at high subsonic speeds. At supersonic speeds, the theoretical predictions have been corrected for the effects of wing-body interference. The data indicate that at supersonic speeds, the agreement between theoretical and experimental results was good when the wing leading edge was swept behind the Mach cone from the wing apex (subsonic leading edge). This condition existed throughout the test range for the triangular wing of aspect ratio 2, up to a Mach number of 1.67 for the triangular wing of aspect ratio 3, and up to a Mach number of 1.41 for the sweptback wings of aspect ratios 2 and 3. For the wings having leading edges supersonic, the agreement between the theoretical and experimental results was not good.

The cause of this discrepancy between experimental and theoretical values of the aerodynamic center has been discussed in reference 46. In that reference it was shown that for wings with supersonic leading edges, both the higher-order pressure effects neglected in the linearized theory and fluid viscosity caused the aerodynamic center to be farther forward than indicated by the linear theory. For wings with subsonic

leading edges, the results of reference 46 showed that the aerodynamic center determined experimentally was aft of that determined from linear theory. In such cases, it is probable that the neglected higher-order effects tend to move the aerodynamic center aft, whereas viscous effects again tend to move the aerodynamic center forward of that determined from linear theory. Such compensating effects would result in the better agreement between theory and experiment for wings with subsonic leading edges shown in figure 16.

The results presented herein also indicate that a possible factor contributing to the poor agreement between experimental and theoretical values of the aerodynamic center is the inability of the theory to predict accurately the lift distribution in the vicinity of the tips. It was shown in figure 9 that the agreement between theory and experiment was good in the case of the triangular wing of aspect ratio 4 throughout the supersonic Mach number range of the test. For this wing, the leading edges are supersonic above a Mach number of 1.4. Furthermore, the taper ratio of the wing is zero. In contrast, the wings of figure 16 have taper ratios of 0.33 or greater and, as previously stated, show poor agreement between theory and experiment when the leading edges were supersonic.

Another possible factor contributing to the discrepancy between theory and experiment shown in figure 16 may be an incomplete accounting for wing-body interference effects. The methods of reference 32 do not account entirely for such effects, as evidenced by the recommendation in that reference that an empirical factor be used in the theoretical computations which moves the aerodynamic center determined theoretically forward. Although, in general, such a factor would bring the results of figure 16 into better agreement, it has not been used because the results from which it was determined were obtained with wing-body combinations having wings small with respect to the body. Further evidence that wing-body interference effects tend to move the aerodynamic center forward is shown in figure 16 by a comparison between results from the 6- by 6-foot and 12-foot wind tunnels and those from the 16-foot wind-tunnel bump. A body was used in conjunction with the wings tested in the former facilities, whereas the wing alone was investigated in the latter facility. The data of figure 16 show that the aerodynamic center of the wing and body combinations is consistently forward of that for the wing alone.

The results of figure 16 show that the over-all travel of the aerodynamic center with variation in Mach number was reduced by increase in leading-edge sweep. If the wing areas were the same, the aerodynamic-center travel expressed in feet would also indicate the same characteristic. Furthermore, the aerodynamic center for the unswept wings moved forward with increasing Mach number at subsonic speeds, whereas for the sweptback and triangular wings it moved continuously rearward. This latter effect has increased significance when the contribution of a

horizontal tail to the stability characteristics is considered. All the wing plan forms shown in figure 16 with the possible exception of the triangular wing of aspect ratio 2 will probably be used in combination with a horizontal tail to provide control as well as damping in pitch at transonic speeds. The results of references 47 to 50 indicate that for both triangular and unswept plan forms, the stability contribution of the tail will be a minimum at a Mach number near 0.9 because of the variation of the parameter  $d\epsilon/d\alpha$  with Mach number. Thus, the effect of the horizontal tail on the aerodynamic center would be to cause a forward movement with increasing Mach number to approximately 0.9 and then a rearward movement with further increase in Mach number. Such an effect would increase the over-all aerodynamic-center travel with variation in Mach number for the unswept wings but would have little or no influence in the cases of the sweptback and triangular wings. An estimation of the magnitude of this effect was made for the unswept and triangular wings of aspect ratio 3 having the same wing area, a tail area equal to 20 percent of the wing area, and a tail length in each case equal to twice the mean aerodynamic chord of the unswept wing. The results showed that the actual travel of the aerodynamic center for the unswept wing and body was approximately 16 percent greater than that for the triangular wing and body, whereas a corresponding value for the wing-body-tail combinations was approximately 31 percent.

Pitching moment at angle of attack. - The variation of pitching-moment coefficient with lift coefficient for the wings of aspect ratio 3 is shown in figure 17 at two subsonic Mach numbers and at a Mach number of 1.5. For the wings of aspect ratio 2, no data were obtained at a Mach number of 0.25 so that a comparable figure is not shown for these wings.

The results show that the variation of pitching-moment coefficient with lift coefficient was nearly linear over the lift-coefficient range of these investigations at a Mach number of 1.5. This characteristic was evident throughout the range of supersonic Mach numbers investigated for these wings of aspect ratio 3 as well as the wings of aspect ratio 2. Furthermore, in the range of Reynolds numbers between those for the results in figure 17 at a Mach number of 1.5 and approximately 2-1/2 times those values, no appreciable change in the characteristics was evident up to lift coefficients of approximately 0.4, the limit of the data.

At a Mach number of 0.25, the results show that the variation of pitching-moment coefficient with lift coefficient was linear only to a lift coefficient of approximately 0.3. At higher lift coefficients, the data show that increase in leading-edge sweep increased the lift coefficient at which the stability of the wing suddenly increased. That leading-edge sweep is the primary factor affecting these characteristics at high angles of attack is again indicated by a comparison between the

results for the sweptback wing and those for the triangular wing of aspect ratio 4 (fig. 10). The sweepback of the leading edge is  $45^\circ$  in both cases, and the results show that the region of extreme stability occurred at a lift coefficient of approximately 0.85 in both cases.

These wings of aspect ratio 3 were investigated at a Mach number of 0.25 over a range of Reynolds numbers to approximately 3-1/2 times the values for the results in figure 17. None of these wings showed any significant effect of Reynolds number up to a lift coefficient of approximately 0.8, the limit of the comparison.

The results presented for a Mach number of 0.91 show the slight discontinuity or nonlinearity in the variation of pitching-moment coefficient with lift coefficient at zero lift for the unswept wing and, to a lesser extent, for the sweptback wing. This characteristic was referred to previously in connection with the aerodynamic center for the sweptback and unswept wings and it will be noted, as mentioned then, that the effect is confined to a small range of lift coefficients. Furthermore, the severity of the discontinuity or nonlinearity reduced with increasing Reynolds number, suggesting that the characteristic may not be present at full-scale Reynolds number.

Drag coefficient at zero lift.—Because of the previously mentioned effects of Reynolds number on the drag at zero lift for triangular wings, a comparison of such data for these wings of various plan forms will be made at the highest Reynolds number obtained during the investigation. The Reynolds numbers for the triangular, sweptback, and unswept wings of aspect ratio 3 were 10.6, 8.4, and 8.3 millions, respectively, at a Mach number of 0.25, and 4.8, 3.8, and 2.4 millions, respectively, at Mach numbers of 0.6 and above. For the triangular wing of aspect ratio 2, the Reynolds number was 16.6 million at a Mach number of 0.25. At Mach numbers of 0.6 and above, the Reynolds numbers for the triangular, sweptback and unswept wings of aspect ratio 2 were 7.5, 4.8, and 4.4 millions, respectively. During the program, the effects of Reynolds number on the characteristics of the sweptback and unswept wings were investigated also. These effects on the drag at zero lift were not as consistent with variation of Mach number as were those for the triangular wings. In general, however, the drag at zero lift increased slightly with Reynolds number.

A comparison of the drag coefficient at zero lift for the wings of various plan forms is shown in figure 18. It should be emphasized that the airfoil sections are not the same for each plan form shown, the triangular wings having the NACA 0003-63 section and the remaining wings having biconvex sections. In a subsequent section, the effects of modifying the biconvex sections forward of the midchord to have a round leading edge will be discussed. It will be shown that, at a Mach number of 1.2, the effect of modifying the biconvex sections on the minimum drag

coefficient was small. Hence, the differences in minimum drag coefficient at a Mach number of 1.2 shown in figure 18 are due primarily to plan-form effects. The results show that increase in leading-edge sweep caused a decrease in minimum drag coefficient for wings of aspect ratios 2 and 3. With increase in Mach number, the effects of airfoil section became of greater importance. Thus, the wings of lesser sweep indicated a greater reduction in minimum drag coefficient with increasing Mach number, an effect probably due to the attachment of the bow wave to the sharp leading edges of the wings of lesser sweepback with a consequent reduction in wave drag. It is of interest to note that because of the attachment of the bow wave, the minimum drag coefficient for the unswept wing of aspect ratio 3 was the smallest of those presented in figure 18 above a Mach number of 1.6.

The results of figure 18 give indications that the minimum drag coefficient may decrease with increasing taper. A comparison of the results for the unswept wings of aspect ratios 2 and 3 shows that although the variation of drag coefficient at zero lift with Mach number was similar for both wings and was characteristic of wings having sharp leading edges with little or no sweepback, the drag coefficient for the wing of aspect ratio 2 was approximately 0.0020 larger than that for the wing of aspect ratio 3 throughout the Mach number range. This difference in drag coefficient is believed not to be due to the difference in aspect ratio, since the results of reference 51 have shown a slight increase in drag coefficient with aspect ratio for rectangular wings. The greater sweep of the leading edge, in the case of the wing of aspect ratio 3, is also believed not to be the cause, since that effect would not explain the drag difference at subsonic speeds. Another indication of the detrimental effect of small taper is provided by a comparison between the minimum drag coefficient for the triangular wing of aspect ratio 4 (fig. 11) and the sweepback wing of aspect ratio 2. The minimum drag coefficient was less for the triangular wing than for the sweepback wing up to a Mach number of 1.5, an effect particularly noticeable at a Mach number of 1.2 where the difference was approximately 0.0020.

Drag due to lift.— The effects of plan form on the value of the criterion of drag due to lift for wings of aspect ratios 2 and 3 are shown in figure 19. These data were obtained at the highest Reynolds numbers of the investigations. The Reynolds numbers were given previously in connection with the minimum drag coefficient of these wings. The effects of Reynolds number were small, however, a slight increase in  $\theta/a$  resulting from an increase in Reynolds number over the range investigated. As for the triangular wings discussed previously, the values of  $\theta/a$  in figure 19 are applicable at supersonic speeds up to lift coefficients of approximately 0.5, the limit of the data. At subsonic speeds, the values of  $\theta/a$  presented are applicable only to lift coefficients near those for maximum lift-drag ratio. At higher lift coefficients  $\theta/a$ , in general, showed an abrupt decrease.

The data of figure 19 show, as in the comparison previously made for the triangular wings, that the experimental values of  $\theta/\alpha$  had little resemblance to results obtained from the thin-airfoil theory at supersonic speeds or to those obtained assuming an elliptical span load distribution at subsonic speeds. Hence, it must be concluded that for thin wings of low aspect ratio, the drag due to lift cannot be predicted accurately by available theoretical methods.

A comparison of the results for the sweptback and unswept wings in figure 19 indicate that for wings having the same taper ratio, an increase in sweepback of the leading edge increased the value of  $\theta/\alpha$  at supersonic speeds. Such a characteristic is affected considerably by factors other than leading-edge sweepback, however, as shown by a comparison of the results for the sweptback wing with those for the triangular wing of aspect ratio 4 in figure 12 (both wings having leading edges swept back  $45^\circ$ ). The sweptback wing had a value of  $\theta/\alpha$  of roughly twice that for the triangular wing. Although the former wing had a sharp leading edge and the latter wing had a round leading edge, data discussed in a subsequent section will show that such a difference in profile had no effect on the results for the triangular wing.

Maximum lift-drag ratio.— A comparison of the maximum lift-drag ratio for the wings of different plan form (fig. 20) shows that no single plan form was superior throughout the Mach number range of the investigation. For the wings of aspect ratio 2, the triangular plan form was superior over the major portion of the test range, a result associated with the minimum drag coefficient. For the wings of aspect ratio 3, the maximum lift-drag ratios of the triangular and sweptback wings were nearly the same throughout the Mach number range of the investigation and were superior to the unswept wing except at Mach numbers above 1.6 and near 0.9. Thus, in spite of the fact that the minimum drag coefficient for the sweptback wing was considerably greater than that for the unswept and triangular plan forms through most of the supersonic range, the larger value of lift-curve slope for the swept wing, in comparison with that for the triangular wing, and larger value of  $\theta/\alpha$ , in comparison with that for the unswept wing, resulted in the sweptback wing comparing quite favorably with the other plan forms in regard to maximum lift-drag ratio and drag coefficient at higher lift coefficients.

The Reynolds numbers for the data presented in figure 20 were the same as those for the data in figures 18 and 19.

#### Effects of Thickness

The effects of wing thickness on the lift, drag, and pitching-moment characteristics were investigated with three triangular wings of aspect

ratio 2 with thicknesses of 3, 5, and 8 percent of the streamwise chord. These wings employed the NACA 000X-63 airfoil sections. Further information pertaining to the geometric characteristics of these wings of 3-, 5-, and 8-percent thicknesses and a tabulation of wind-tunnel data obtained during the investigation can be found in tables I, VIII, and IX, respectively.

Lift and pitching moment. - No data are presented showing the lift-curve slope and aerodynamic-center position near zero lift for the three triangular wings since a comparison of the data showed almost no effects of wing thickness on these characteristics. Hence, the previous discussion of such characteristics for the 3-percent-thick wing applies to the thicker wings as well.

The variation of pitching moment with lift and, to a lesser extent, the variation of lift with angle of attack were influenced at lift coefficients above approximately 0.4 by the thickness of the wing. A comparison of such characteristics is shown in figures 21 and 22 presenting the variation of lift coefficient with angle of attack and of pitching-moment coefficient with lift coefficient at three subsonic Mach numbers and at a Mach number of 1.53. It will be noted that the main differences in the pitching-moment characteristics due to wing thickness are confined to the subsonic speed range. The results shown for a Mach number of 1.53 are typical of those obtained in the supersonic speed range and indicate nearly identical characteristics for the three wings throughout the lift-coefficient range.

At a Mach number of 0.25, the effects of thickness on the pitching-moment characteristics were very pronounced. The results for the 3-percent-thick wing show a large decrease in slope of the pitching-moment curve between lift coefficients from 0.4 to 0.5 and then a slight increase at higher lift coefficient. For the 5-percent-thick wing, the stability decreased only to that of the 3-percent-thick wing at the high lift coefficients. For both wings, the lift-curve slope increased in these regions of reduced stability. However, the results for the 8-percent-thick wing show neither the increase in lift-curve slope nor the decrease in stability indicated by the thinner wings.

Of equal importance, were the effects of thickness at Mach numbers above 0.25. At those speeds, the results for the 5-percent-thick wing show a sudden decrease in stability between lift coefficients of approximately 0.45 and 0.55 at a Mach number of 0.60 and between 0.6 and 0.7 at a Mach number of 0.9. For the 3-percent-thick wing, data at high lift coefficients were available only at a Mach number of 0.6, and these data showed that the region of reduced stability occurred between lift coefficients of 0.9 and 1.0. In contrast to the effect at a Mach number of 0.25, the lift-curve slope decreased in the region of reduced stability at the higher Mach numbers. Furthermore, the data indicate that the

lift coefficient at which the region of reduced stability occurred increased with Mach number.

Neither the flow phenomena associated with the region of reduced stability nor the reasons for the large effects of wing thickness on such phenomena are understood at present. It is believed that these stability characteristics are associated with the vortex-separation type of flow existing near the leading edge of low-aspect-ratio triangular wings which is influenced more by the shape of the airfoil section near the leading edge rather than by merely the leading-edge radius or thickness of the section (see ref. 37).

The regions of reduced stability occurring at subsonic speeds, because of the nonlinear character of the pitching-moment curves, are of considerable importance since the results show the minimum static margin for these wings was determined thereby. Some research has been devoted to eliminating this region of reduced stability. Unpublished data from tests of a triangular wing of aspect ratio 2 in the Ames 6- by 6-foot supersonic wind tunnel have shown that leading-edge-chord extensions tend to eliminate the nonlinear pitching moments at high subsonic speed.

The data of figure 22 indicate an apparent effect of thickness on the stability characteristics at a Mach number of 0.9. Above a lift coefficient of approximately 0.2, the stability of the 3-percent-thick wing was greater than that of the thicker wings. The results shown for the 3-percent-thick wing at a Mach number of 0.9 in figures 21 and 22 were obtained in the 6- by 6-foot supersonic wind tunnel, however, whereas the remainder of the data at subsonic speeds was obtained in the 12-foot wind tunnel. It is possible that because of the large size of the triangular wings of aspect ratio 2, in comparison with the size of the 6- by 6-foot wind tunnel, the characteristics of the wings were influenced by unknown constriction effects of the tunnel wall at the high lift coefficients and a Mach number of 0.9. Such an effect would explain the large differences in the stability of these wings above a lift coefficient of approximately 0.2 at a Mach number of 0.9.

The data presented in figures 21 and 22 were obtained at a low Reynolds number. At Mach numbers above 0.25, the effects of Reynolds number on the stability characteristics of these wings in the region of reduced stability could not be determined in this investigation because of the restricted range of lift coefficient at high Reynolds number. At a Mach number of 0.25, it was possible to test these wings at a Reynolds number approximately 3-1/2 times greater than that for the data presented. The stability characteristics of the wings at the higher Reynolds number were essentially the same as shown in figure 22.

Minimum drag coefficient.- A primary purpose for investigating a series of wings differing only in thickness was to ascertain the effects of thickness on the drag characteristics of the wings. The drag data for these wings are therefore presented in figure 23. Results for the 8-percent-thick wing at Mach numbers between 0.6 and 0.9 were obtained only at a low Reynolds number and, therefore, are not shown since the data presented were obtained at a Reynolds number of 6 million or greater.

As expected, the results indicate a large increase in minimum drag coefficient at supersonic speeds with increasing thickness. Furthermore, as indicated by the linearized theory, the increase in minimum drag coefficient was proportional to the square of the thickness ratio. The constant of proportionality was less, however, than indicated by the theoretical results of reference 42 for a triangular wing of aspect ratio 2 and having a double-wedge section with maximum thickness at 30 percent of the chord. The experimental results showed a decrease in the constant from 2.0 to 1.6 between Mach numbers of 1.3 to 1.7, whereas the theoretical results show an increase from 2.1 to 3.3 in the same range of Mach numbers.

It is interesting to note that, if the data at supersonic speeds are extrapolated to a wing of zero thickness, the resultant minimum drag coefficient is approximately 0.0010 greater than the results at subsonic speeds. This drag increment can be accounted for by the wave drag of the body. With these data as a guide, it would appear that the viscous drag for the wings in this program was essentially independent of Mach number and that the variation of drag with Mach number was caused entirely by wave drag.

Drag due to lift.- The results of figure 23 presenting the quantity,  $\theta/a$ , indicate that increasing the section thickness and, hence, the leading-edge radius reduced the drag due to lift. Between Mach numbers of 0.6 and 0.9, an increase in thickness from 3 to 5 percent of the chord approximately doubled the value of  $\theta/a$ . Since the lift-curve slope and minimum drag coefficient were approximately the same for these wings in this range of Mach numbers, the large effect of thickness on the quantity  $\theta/a$  resulted in the maximum lift-drag ratio of the 5-percent-thick wing being as much as 15 percent greater than that for the 3-percent-thick wing.

At supersonic speeds, the effects of thickness on the drag due to lift were small. The data show that the 5-percent-thick wing had the highest value of  $\theta/a$  in the supersonic Mach number range. The large increase in minimum drag coefficient with thickness more than offset this small advantage of thickness in reducing the drag due to lift, so that the drag coefficient for the 3-percent-thick wing was less than that for the 5-percent-thick wing throughout the range of lift coefficients investigated at supersonic speeds.

## Effects of Type of Profile

It was mentioned previously in the section entitled "Selection of Models" that several of the wings would be investigated with both sharp and round leading edges. The effect of such a section modification was investigated on wings of both aspect ratios 2 and 3 and of unswept, sweptback, and triangular plan forms. The airfoil sections investigated with each plan form were:

1. Biconvex sections 3 percent thick with maximum ordinate at 50 percent of the wing chord
2. Round-nose sections obtained by substituting a semiellipse for the forward 50 percent of the wing chord of the biconvex section noted above

Further information pertaining to the geometric characteristics and a tabulation of the data for the wings with sharp leading edges will be found in tables IV, VI, VII, and X. Similar information is presented in tables III, XI, XII, and XIII for the wings with round leading edges.

The aerodynamic characteristics of the unswept wing of aspect ratio 3 and with round leading edge were previously published in reference 15. After publication of those results, it was discovered that the bent sting used in those tests to obtain a high angle of attack caused the minimum drag coefficient to be approximately 0.0006 less than that obtained with the straight sting used for other portions of this program. The unswept wing was tested again with the straight sting, therefore, and it is these later results which are given in table XIII.

Lift and pitching-moment characteristics.- A comparison of the data for the wings investigated in this portion of the program showed that the change in section profile had almost no effect on the variation of lift coefficient with angle of attack throughout the test range. Also in the case of variation of pitching-moment coefficient with lift coefficient, no significant effects were noted at high Reynolds number, due to change in section profile. However, at the low Reynolds number, the data for the unswept wings with round leading edges did not exhibit the abrupt change in pitching-moment coefficient near zero lift at high subsonic Mach numbers which was discussed previously in the section on plan-form effects.

Drag coefficient.- As pointed out previously, the shape of the airfoil section may have a significant effect on the drag characteristics of the wing. For wings having little sweep of the leading edges, it is generally recognized that at Mach numbers well above unity sharp leading edges are required for a small wave drag. However, a low value of drag

due to lift is generally associated with a wing having round leading edges. The investigation of such effects was the primary purpose of this portion of the program.

The results of figure 24 show that the effect of the section profile on the minimum drag coefficient was affected considerably by Mach number, a characteristic in agreement with that determined on a large-scale unswept wing between Mach numbers of 0.8 and 1.6 by the rocket-model technique. (See ref. 52.) At Mach numbers less than 1.3, the minimum drag coefficient was greater for the wings having sharp leading edges, whereas with the exception of the sweptback wing of aspect ratio 2, the opposite effect was obtained at higher Mach numbers. Based upon theoretical results for wedge-shaped profiles, it is estimated that a Mach number of 1.3 is approximately that for attachment of the bow wave to the sharp leading edges for the unswept wings. This fact would explain the smaller value of minimum drag coefficient for the unswept wings with sharp leading edges above a Mach number of approximately 1.3, since the wave drag would be smaller after attachment of the bow wave. At Mach numbers below 1.3, it is believed that the larger minimum drag coefficient for the wings with sharp leading edges was due to such edges causing the transition point to be considerably ahead of that for the wings with round leading edges. It should be noted, however, that the Reynolds number for these investigations is considerably less than would be obtained on the full-scale wing. For the rectangular and sweptback wings of aspect ratio 2, the Reynolds numbers were 4.4 and 4.8 millions, respectively. For the unswept wings of aspect ratio 3 and the triangular wings of aspect ratio 4, the Reynolds numbers were 8.3 and 9.1 millions, respectively, at a Mach number of 0.25, and 2.4 and 4.2 millions at Mach numbers of 0.6 and above. Since these values of Reynolds number are considerably less than would be obtained on the full-scale wing, the possibility exists that the extent of laminar boundary layer on the wing having a round leading edge was greater than on a comparable full-scale wing; whereas the small extent of the laminar boundary layer in the cases of the wings with sharp leading edges would be more nearly the same on both model and full-scale wing. Hence, the improvement in minimum drag coefficient due to rounding the leading edge may not be as great for a full-scale wing as indicated by the results shown herein.

One point of inconsistency occurred in the data for the sweptback wing of aspect ratio 2 and the triangular wing of aspect ratio 4 which is not understood at present. The angle of sweepback is the same for both wings. By use of simple sweep theory, it is estimated that the bow wave would attach to the sharp leading edges of these wings at a Mach number of approximately 1.7. Based upon the results for the rectangular and unswept wings, it would be expected that at Mach numbers less than 1.7, the minimum drag coefficient would be less for the wing with a round leading edge than for the wing with a sharp leading edge. At higher Mach numbers, the opposite characteristic would be expected. The results for the sweptback

wing of aspect ratio 2 are in agreement with this reasoning; whereas those for the triangular wing of aspect ratio 4 show the wing with sharp leading edges to have a smaller minimum drag coefficient than that for the wing with round leading edges at Mach numbers above approximately 1.3.

Included in figure 24 are values of  $\theta/\alpha$  for the various wings to indicate the effects of section profile on the drag due to lift. In general, the data show little difference between the values of  $\theta/\alpha$  for the wings with either sharp or round leading edges. It should be mentioned that at subsonic speeds the values of  $\theta/\alpha$  generally are applicable only to a lift coefficient of approximately 0.2 and, with increase in lift coefficient, decrease abruptly. The drag data of figure 24 indicate that at subsonic speeds, the difference in drag due to lift between that for wings with sharp leading edges and that for wings with round leading edges was not the same for all plan forms. Thus for the triangular wing of aspect ratio 4 above a lift coefficient of 0.2, the drag due to lift for the wing with a round leading edge was less than that for the wing with a sharp leading edge; for the unswept wing of aspect ratio 3 and the sweptback wing of aspect ratio 2, the drag due to lift was essentially the same for the wing with either section; for the unswept wing of aspect ratio 2, the drag due to lift for the wing with a round leading edge was greater than that for the wing with a sharp leading edge.

#### Effects of Camber and Twist

In the section on Selection of Models, it was stated that a theoretical study in reference 18 had shown that camber and twist could be employed on a sweptback wing to obtain a low value of drag due to lift. Further study, based upon the results of reference 18, indicated a similar effect for triangular wings. The theoretical study showed that a low value of drag due to lift could be obtained with two types of camber, one designed to produce a trapezoidal span load distribution and the other, a nearly elliptical span load distribution. Several wings incorporating these types of camber were investigated, therefore, in order to evaluate experimentally the effects of camber and twist for triangular wings. Two of the wings were cambered and twisted to produce the trapezoidal span load distribution and had aspect ratios of 2 and 4 and NACA 0005-63 thickness distributions. The design lift coefficients for these wings were 0.25 at a Mach number of 1.53 and 0.35 at a Mach number of 1.15, respectively. Tabulated data obtained during the investigation of these wings are presented in tables XIV and XV; results for the corresponding plane wings are presented in tables VIII and XVI. Two wings of aspect ratio 2 and having NACA 0003-63 and 0005-63 thickness distributions were also cambered and twisted for the nearly elliptical span load distribution. The design lift coefficient for both wings was 0.25 at a Mach number of

1.53. Tabulated data obtained during the investigation of these wings are presented in tables XVII and XVIII; results for the corresponding plane wings are given in tables I and VIII.

Analysis of the results for these cambered and twisted wings showed that the drag due to lift and the minimum drag coefficient was considerably higher for the wing having the trapezoidal span load distribution than for the wing having a nearly elliptical span load distribution. This characteristic was attributed to the differences in the pressure distributions occurring on these wings at the design conditions. For the wing having the trapezoidal span load distribution, there is an abrupt adverse gradient in the pressure distribution determined theoretically. The abrupt gradient occurs along a straight line passing through the wing apex and a point on the trailing edge five eighths of the semispan from the plane of symmetry. In contrast, the wing having a nearly elliptical span load distribution has a smooth adverse pressure gradient from the leading to trailing edge of the wing. The abrupt gradient will cause premature separation of the boundary layer, thereby resulting in a higher drag coefficient for the wing with the trapezoidal span load distribution than for the wing with the elliptical span load distribution. For this reason, as well as the fact that the wing having a nearly elliptical span load distribution is plane over a considerable portion of the wing area, it was believed that the results for this latter wing would be of greater interest and, hence, only those data will be discussed hereinafter.

Lift and pitching moment. - Since the lift-curve slope and aerodynamic center near zero lift are influenced primarily by the wing plan form, it would be expected that such characteristics for the cambered wing would be essentially the same as for the plane wing of corresponding plan form. Such was the case as indicated by the results shown in figures 25 and 26. In these figures, the variation of lift coefficient with angle of attack and pitching-moment coefficient with lift coefficient are shown for the plane and cambered wings of 3- and 5-percent thickness at three subsonic Mach numbers and a Mach number of 1.53. In all cases shown, the curves of the lift and pitching-moment characteristics of the cambered wings are parallel, although displaced, to those of the plane wings near zero lift. In the case of the variation of lift with angle of attack, the displacement of the curve is of little importance.<sup>6</sup> However, in the case of the variation of pitching-moment coefficient with lift coefficient, the cambered wing showed a positive pitching moment at zero lift for the Mach numbers included in the figure. Such a characteristic would result in a decrease in the increment of pitching moment required

<sup>6</sup>For the cambered wings discussed herein, the wing chord at the plane of symmetry was coincident with the axis of the body. The angle of attack for the cambered wings is measured, therefore, with respect to the chord at the plane of symmetry.

to trim the airplane under flight conditions and therefore a slight reduction in trim drag. Unfortunately, this effect of camber on the pitching moment at zero lift reduced with increasing Mach number, becoming almost insignificant at a Mach number of 1.7.

At the higher lift coefficients, the effects of camber on the lift and pitching-moment characteristics were generally small. However, the results for the 5-percent-thick wing at a Mach number of 0.60 did show a significant effect. It will be noticed that the region of reduced stability, previously discussed in connection with the effects of thickness on the triangular wings of aspect ratio 2, occurred at a considerably higher lift coefficient in the case of the cambered wing ( $C_L = 0.75$ ) than in the case of the plane wing ( $C_L = 0.45$ ). This comparison adds further support to the belief that the reduced-stability region is associated with the vortex-separation type of flow near the wing leading edge. Since the camber is obtained by drooping the wing leading edge, the angle of attack and, hence, the lift coefficient for the cambered wing may be increased over that of the plane wing before separation occurs near the leading edge. These results indicate the possibility, therefore, that correctly drooping the leading edge of an aspect ratio 2 triangular wing may delay to a lift coefficient beyond the flight range the undesirable reduced-stability region.

The results shown in figures 25 and 26 have been obtained at low Reynolds numbers in order not to restrict the lift-coefficient range. Within the range of lift coefficients for which data were available, up to a lift coefficient of roughly 0.5, increase in Reynolds number to  $16.6 \times 10^6$  at a Mach number of 0.25 and to  $7.5 \times 10^6$  at other speeds caused no appreciable changes in the lift and pitching-moment characteristics of the cambered wings.

Drag coefficient.— The primary purpose for investigating the various cambered wings was to determine the effects of camber on the drag coefficient. Such effects are shown in figure 27, wherein the drag coefficient at constant lift coefficient is shown in relation to Mach number for the cambered and plane wings of 3- and 5-percent thickness. The results show that throughout the Mach number range, the drag coefficient at zero lift was lower for the plane wings than for the comparable cambered wings. For lift coefficients above approximately 0.1, however, the drag coefficient for the cambered wing was lower. The results indicate, therefore, that the potentialities for reducing the drag due to lift indicated by the theory were more fully realized in the case of a cambered wing having subsonic leading edges than in the case of a plane wing with subsonic leading edges.

These benefits of camber arose from the fact that, at the design lift coefficient, the lifting force vector was inclined farther forward in the case of the cambered wing than for the plane wing. The more

forward inclination of the force vector in the case of the cambered wing at the design lift coefficient was due to the fact that, as indicated by theory, lifting pressures occurred on those portions of the wing which were drooped. Thus there resulted a component of this force in the thrust direction which caused the vector to be inclined forward. In the case of the plane wing, the analogous effect, which theoretical considerations indicate will cause a forward inclination of the force vector, that is, high lifting pressures acting near the leading edge, was considerably less than predicted.

In the off-design condition the lift distribution on a cambered and twisted wing can be considered as that due to camber and twist and that due to change in angle of attack. The drag of the cambered and twisted wing results from both types of lift distribution. The effect of change in angle of attack on the drag characteristics of the cambered and twisted wings was very similar to that for the plane wings. For the 3-percent-thick wings, the curvature of the drag polar was approximately the same for both the plane and cambered and twisted wing in the lift-coefficient range wherein the shape of the polar was parabolic. For the 5-percent-thick cambered and twisted wing, the curvature of the drag polar was greater than that of the 5-percent-thick plane wing and more closely resembled that of the 3-percent plane wing.

It will be noticed that reduction in drag coefficient due to camber was not as great for the 5-percent-thick wing as for the 3-percent-thick wing. This effect resulted from the fact that, as discussed previously for the uncambered wings, the inclination of the force vector for the 5-percent-thick wing was farther forward than that for the 3-percent-thick wing and, thus, a greater portion of the reduction in drag due to lift indicated by the theory was realized by the thicker wing. In the case of cambered wings of both thicknesses, however, the variation of drag due to lift at Mach numbers where shock waves were not present was nearly the same. It appears, therefore, that the beneficial effects of thickness or camber in reducing the drag coefficient are not additive and that the reduction in drag in each case stems from the same cause; that is, the surface area of the wing near the leading edge inclined forward has been increased either by drooping the leading edge or increasing the section thickness so that the lifting pressure acting on these surfaces results in a greater component of force in the thrust direction and, therefore, a more forward inclination of the force vector.

The beneficial effect of camber in reducing the drag coefficient is seen to be greatest at the subsonic Mach numbers and decreases with increasing Mach number. At a Mach number of 1.7, the effect was negligible. This characteristic was also evident in a comparison of the data for the wings with the other type of camber investigated in this program. The results showed that when the Mach number exceeded that at which the component of the free-stream Mach number perpendicular to the leading

edge was approximately 0.7, no further benefits of camber were realized. In fact, in the case of the triangular wing of aspect ratio 4 where appropriate data were available, further increase in Mach number resulted in a detrimental effect on the drag coefficient due to the use of camber.

### CONCLUSIONS

The present report presents results of a coordinated program to investigate the effects of aspect ratio, plan form, thickness, thickness distribution, and camber and twist on the lift, drag, and pitching-moment characteristics of low-aspect-ratio wings in combination with a body at Mach numbers from 0.25 to as high as 1.9.

1. The investigation of a series of 3-percent-thick triangular wings of aspect ratios 2, 3, and 4 showed that:

(a) The lift-curve slope was predicted satisfactorily by linearized theory over much of the subsonic speed range but, at Mach numbers near unity and over portions of the supersonic speed range, the extent depending on aspect ratio, the lift-curve slopes predicted by theory were not in close agreement with experimental results.

(b) Linearized theory satisfactorily indicated the effects of Mach number and aspect ratio on the position of the aerodynamic center, which moved rearward with increasing Mach number at subsonic speeds. The over-all travel of the aerodynamic center increased with aspect ratio.

(c) The minimum drag coefficient increased with aspect ratio at supersonic speeds.

(d) The drag due to lift was not predicted accurately by available theoretical methods. In general, it appeared to be more accurate to calculate the drag due to lift at supersonic speeds, assuming that the net force on the airfoil due to angle of attack is normal to the chord line, than to use the available theoretical methods which include leading-edge thrust.

2. The investigation of a series of 3-percent-thick wings having sweptback, unswept, and triangular plan forms of aspect ratios 2 and 3 showed that:

(a) As predicted by linearized theory, the lift-curve slope near zero lift decreased with increasing sweepback of the leading edge; with increasing Mach number the effects of plan form and aspect ratio on lift-curve slope diminished and essentially vanished at the highest supersonic Mach number.

(b) Linearized theory satisfactorily predicted the location of the aerodynamic center at supersonic speeds for wings with subsonic leading edges, but predicted a location behind that determined experimentally for wings with supersonic leading edges.

(c) The over-all travel of the aerodynamic center with variation in Mach number decreased with increasing sweepback of the leading edge.

(d) At low supersonic Mach numbers, the minimum drag coefficient decreased with increasing sweepback. However, the wings of lesser sweep and with sharp leading edges showed a greater decrease in minimum drag coefficient with increasing Mach number, so that above a Mach number of 1.6, the minimum drag coefficient was lowest for an unswept tapered wing of aspect ratio 3 with sharp leading edges.

3. The investigation of a series of triangular wings of aspect ratio 2 with NACA 000X-63 series airfoil section and thicknesses of 3, 5, and 8 percent showed that:

(a) Lift-curve slope and aerodynamic center near zero lift were almost unaffected by thickness.

(b) Thickness affected the stability characteristics at moderate lift coefficients at high subsonic Mach numbers, the 3-percent- and 5-percent-thick wings having an abrupt decrease in stability over a small range of lift coefficients.

(c) The wave drag was proportional to the thickness ratio squared, as predicted by linear theory.

(d) The drag due to lift decreased with increase in thickness from 3 percent to 5 percent, the effect being most pronounced at Mach numbers of 0.9 and below.

4. The investigation of a series of wings having sharp and round leading edges showed that:

(a) The shape of the airfoil section had almost no effect on the lift and pitching-moment characteristics.

(b) The airfoil section affected the minimum drag coefficient, in general; the wings with sharp leading edges had a lower value at supersonic speeds (above those estimated for attachment of the bow wave) and a higher value at subsonic speeds.

(c) In general, the effects of airfoil section on the drag due to lift were small.

5. An investigation to determine the effects of twist and camber on triangular wings of aspect ratio 2 and having 3- and 5-percent thicknesses showed that:

(a) The lift-curve slope and aerodynamic center were unaffected by the camber and twist. The camber and twist caused a small positive pitching moment at zero lift up to a Mach number of 1.7.

(b) The drag coefficient for the cambered and twisted wing was less than that for the plane wing at lift coefficients above approximately 0.1 up to Mach numbers at which the component of the free-stream Mach number perpendicular to the leading edge exceeded approximately 0.7.

Ames Aeronautical Laboratory  
National Advisory Committee for Aeronautics  
Moffett Field, Calif.

#### REFERENCES

1. Smith, Donald W., and Heitmeyer, John C.: Lift, Drag, and Pitching Moment of Low-Aspect-Ratio Wings at Subsonic and Supersonic Speeds - Plane Triangular Wing of Aspect Ratio 2 With NACA 0008-63 Section. NACA RM A50K20, 1951.
2. Smith, Donald W., and Heitmeyer, John C.: Lift, Drag, and Pitching Moment of Low-Aspect-Ratio Wings at Subsonic and Supersonic Speeds - Plane Triangular Wing of Aspect Ratio 2 With NACA 0005-63 Section. NACA RM A50K21, 1951.
3. Heitmeyer, John C., and Stephenson, Jack D.: Lift, Drag, and Pitching Moment of Low-Aspect-Ratio Wings at Subsonic and Supersonic Speeds - Plane Triangular Wing of Aspect Ratio 4 With NACA 0005-63 Section. NACA RM A50K24, 1951.
4. Phelps, E. Ray, and Smith, Willard G.: Lift, Drag, and Pitching Moment of Low-Aspect-Ratio Wings at Subsonic and Supersonic Speeds - Triangular Wing of Aspect Ratio 4 With NACA 0005-63 Thickness Distribution, Cambered and Twisted for Trapezoidal Span Load Distribution. NACA RM A50K24b, 1951.
5. Heitmeyer, John C., and Smith, Willard G.: Lift, Drag, and Pitching Moment of Low-Aspect-Ratio Wings at Subsonic and Supersonic Speeds - Plane Triangular Wing of Aspect Ratio 2 With NACA 0003-63 Section. NACA RM A50K24a, 1951.

6. Smith, Willard G., and Phelps, E. Ray: Lift, Drag, and Pitching Moment of Low-Aspect-Ratio Wings at Subsonic and Supersonic Speeds - Triangular Wing of Aspect Ratio 2 With NACA 0005-63 Thickness Distribution, Cambered and Twisted for a Trapezoidal Span Load Distribution. NACA RM A50K27a, 1951.
7. Reese, David E., and Phelps, E. Ray: Lift, Drag, and Pitching Moment of Low-Aspect-Ratio Wings at Subsonic and Supersonic Speeds - Plane Tapered Wing of Aspect Ratio 3.1 With 3-Percent-Thick, Biconvex Section. NACA RM A50K28, 1951.
8. Hall, Charles, F., and Heitmeyer, John C.: Lift, Drag, and Pitching Moment of Low-Aspect-Ratio Wings at Subsonic and Supersonic Speeds - Twisted and Cambered Triangular Wing of Aspect Ratio 2 With NACA 0003-63 Thickness Distribution. NACA RM A51E01, 1951.
9. Heitmeyer, John C.: Lift, Drag, and Pitching Moment of Low-Aspect-Ratio Wings at Subsonic and Supersonic Speeds - Plane Triangular Wing of Aspect Ratio 4 With 3-Percent-Thick, Biconvex Section. NACA RM A51D30, 1951.
10. Heitmeyer, John C., and Hightower, Ronald C.: Lift, Drag, and Pitching Moments of Low-Aspect-Ratio Wings at Subsonic and Supersonic Speeds - Plane Triangular Wing of Aspect Ratio 4 With 3-Percent-Thick Rounded Nose Section. NACA RM A51F21, 1951.
11. Heitmeyer, John C.: Lift, Drag, and Pitching Moment of Low-Aspect-Ratio Wings at Subsonic and Supersonic Speeds - Plane Triangular Wing of Aspect Ratio 3 With NACA 0003-63 Section. NACA RM A51H02, 1951.
12. Heitmeyer, John C.: Lift, Drag, and Pitching Moment of Low-Aspect-Ratio Wings at Subsonic and Supersonic Speeds - Plane  $45^\circ$  Swept-Back Wing of Aspect Ratio 3, Taper Ratio 0.4 With 3-Percent-Thick Biconvex Section. NACA RM A51H10, 1951.
13. Heitmeyer, John C.: Lift, Drag, and Pitching Moment of Low-Aspect-Ratio Wings at Subsonic and Supersonic Speeds - Body of Revolution. NACA RM A51H22, 1951.
14. Heitmeyer, John C. and Petersen, Robert B.: Lift, Drag, and Pitching Moment of Low-Aspect-Ratio Wings at Subsonic and Supersonic Speeds - Twisted and Cambered Triangular Wing of Aspect Ratio 2 With NACA 0005-63 Thickness Distribution. NACA RM A52B08, 1952.
15. Heitmeyer, John C.: Lift, Drag, and Pitching Moment of Low-Aspect-Ratio Wings at Subsonic and Supersonic Speeds - Plane Tapered Wing of Aspect Ratio 3.1 With 3-Percent-Thick Rounded-Nose Section. NACA RM A52D23, 1952.

~~CONFIDENTIAL~~

16. Smith, Donald W., Shibata, Harry H., and Selan, Ralph: Lift, Drag, and Pitching Moment of Low-Aspect-Ratio Wings at Subsonic and Supersonic Speeds - An Investigation at Large Reynolds Numbers of the Low-Speed Characteristics of Several Wing-Body Combinations. NACA RM A51K28, 1952.
17. Emerson, Horace F., and Gale, Bernard M.: Transonic Aerodynamic Characteristics of Three Thin Triangular Wings and A Trapezoidal Wing, All of Low Aspect Ratio. NACA RM A52D21, 1952.
18. Jones, Robert T.: Estimated Lift-Drag Ratios at Supersonic Speed. NACA TN 1350, 1947.
19. Haack, W.: Geschossformen Kleinsten Wellenwiderstandes. Lilienthal-Gesellschaft für Luftfahrtforschung, Bericht 139, Teil 1, 1941.
20. Weissinger, J.: The Lift Distribution of Swept-Back Wings. NACA TM 1120, 1947.
21. Lawrence, H. R.: The Lift Distribution on Low Aspect Ratio Wings at Subsonic Speeds. Jour. Aero. Sci., vol. 18, no. 10, Oct. 1951, pp. 683-695.
22. Lomax, Harvard, and Sluder, Loma: Chordwise and Compressibility Corrections to Slender-Wing Theory. NACA Rep. 1105, 1952. (Supersedes NACA TN 2295)
23. Jones, Robert T.: Properties of Low-Aspect-Ratio Pointed Wings at Speeds Below and Above the Speed of Sound. NACA Rep. 835, 1946.
24. DeYoung, John, and Harper, Charles W.: Theoretical Symmetric Span Loading at Subsonic Speeds for Wings Having Arbitrary Plan Form. NACA Rep. 921, 1948.
25. Brown, Clinton E.: Theoretical Lift and Drag of Thin Triangular Wings at Supersonic Speeds. NACA Rep. 839, 1946.
26. Cohen, Doris: Formulas and Charts for the Supersonic Lift and Drag of Flat Swept-Back Wings With Interacting Leading and Trailing Edges. NACA TN 2093, 1950.
27. Bonney, E. Arthur: Engineering Supersonic Aerodynamics. McGraw-Hill Book Co., N. Y., 1950, pp. 136-141.
28. Lomax, Harvard, and Heaslet, Max. A.: Linearized Lifting-Surface Theory for Swept-Back Wings With Slender Plan Forms. NACA TN 1992, 1949.

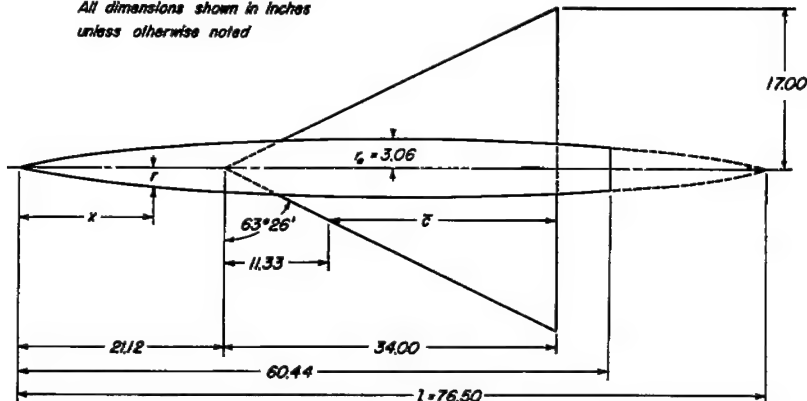
29. Lapin, Ellis: Charts for the Computation of Lift and Drag of Finite Wings at Supersonic Speeds. Douglas Aircraft Co. Rep. SM-13480, Oct. 1949.
30. Nielsen, Jack N., and Kaattari, George E.: Method for Estimating Lift Interference of Wing-Body Combinations at Supersonic Speeds. NACA RM A51J04, 1951.
31. Cohen, Doris: The Theoretical Lift of Flat Swept-Back Wings at Supersonic Speeds. NACA TN 1555, 1948.
32. Kaattari, George E., Nielsen, Jack N., and Pitts, William C.: Method for Estimating Pitching-Moment Interference of Wing-Body Combinations at Supersonic Speed. NACA RM A52B06, 1952.
33. Squire, H. B.: Theory of the Flow Over a Particular Wing in a Supersonic Stream. Rep. No. Aero. 2184, R.A.E. (British), Feb. 1947.
34. von Kármán, Th., and Burgers, J. M.: General Aerodynamic Theory - Perfect Fluids. Vol. II, Div. E, Sec. 10, Ch. II of Aerodynamic Theory, W. F. Durand, ed., Julius Springer (Berlin) 1935, pp. 51-52.
35. Love, Eugene S.: Investigations at Supersonic Speeds of 22 Triangular Wings Representing Two Airfoil Sections for Each of 11 Apex Angles. NACA RM L9D07, 1949.
36. Boyd, John W., and Phelps, E. Ray: A comparison of the Experimental and Theoretical Loading Over Triangular Wings at Supersonic Speeds. NACA RM A50J17, 1951.
37. Anderson, Adrien E.: Chordwise and Spanwise Loadings Measured at Low Speed on Large Triangular Wings. NACA RM A9B17, 1949.
38. Graham, David, and Koenig, David G.: Tests in the Ames 40- by 80-Foot Wind Tunnel of an Airplane Configuration With an Aspect Ratio 4 Triangular Wing and an All-Movable Horizontal Tail - Longitudinal Characteristics. NACA RM A51H10a, 1951.
39. Tobak, Murray: Damping in Pitch of Low-Aspect-Ratio Wings at Subsonic and Supersonic Speeds. NACA RM A52L04a, 1953.
40. Graham, David, and Koenig, David G.: Tests in the Ames 40- by 80-Foot Wind Tunnel of an Airplane Configuration with an Aspect Ratio 2 Triangular Wing and an All-Movable Horizontal Tail - Longitudinal Characteristics. NACA RM A51B21, 1951.

41. Abbott, Ira H., von Doenhoff, Albert E., and Stivers, Louis S., Jr.: Summary of Airfoil Data. NACA Rep. 824, 1945.
42. Puckett, A. E., and Stewart, H. J.: Aerodynamic Performance of Delta Wings at Supersonic Speeds. Jour. Aero. Sci., vol. 14, no. 10, Oct. 1947, pp. 567-578.
43. Katzen, Elliott D., and Kaattari, George E.: Drag Interference Between a Pointed Cylindrical Body and Triangular Wings of Various Aspect Ratios at Mach Numbers of 1.50 and 2.02. NACA RM A51C27, 1951.
44. Hightower, Ronald C.: Lift, Drag, and Pitching Moment of Low-Aspect-Ratio Wings at Subsonic and Supersonic Speeds - Comparison of Three Wings of Aspect Ratio 2 of Rectangular, Swept-Back and Triangular Plan Form, Including the Effects of Thickness Distribution. NACA RM A52L02, 1953.
45. Johnson, Ben H., and Bandettini, Angelo: Investigation of a Thin Wing of Aspect Ratio 4 in the Ames 12-Foot Pressure Wind Tunnel. II - The Effect of Constant-Chord Leading- and Trailing-Edge Flaps on the Low-Speed Characteristics of the Wing. NACA RM A8F15, 1948.
46. Vincenti, Walter G.: Comparison Between Theory and Experiment for Wings at Supersonic Speeds. NACA Rep. 1033, 1951. (Supersedes NACA TN 2100)
47. Johnson, Ben H., and Rollins, Francis W.: Investigation of a Thin Wing of Aspect Ratio 4 in the Ames 12-Foot Pressure Wind Tunnel. V - Static Longitudinal Stability and Control Throughout the Subsonic Speed Range of a Semispan Model of a Supersonic Airplane. NACA RM A9I01, 1949.
48. Perkins, Edward W., and Canning, Thomas N.: Investigation of Downwash and Wake Characteristics at a Mach Number of 1.53. I - Rectangular Wing. NACA RM A8L16, 1949.
49. Allen, Edwin C.: Investigation of a Triangular Wing in Conjunction With a Fuselage and Horizontal Tail to Determine Downwash and Longitudinal-Stability Characteristics - Transonic Bump Method. NACA RM A51F12a, 1951.
50. Perkins, Edward W., and Canning, Thomas N.: Investigation of Downwash and Wake Characteristics at a Mach Number of 1.53. II - Triangular Wing. NACA RM A9D20, 1949.

51. McDevitt, John B.: A Correlation by Means of the Transonic Similarity Rules of the Experimentally Determined Characteristics of 22 Rectangular Wings of Symmetrical Profile. NACA RM A51L17b, 1952.
52. Morrow, John D., and Nelson, Robert L.: Large-Scale Flight Measurements of Zero-Lift Drag of 10 Wing-Body Combinations at Mach Numbers From 0.8 to 1.6. NACA RM L52D18a, 1952.

TABLE I.- GEOMETRIC CHARACTERISTICS AND WIND-TUNNEL DATA FOR A PLANE  
 TRIANGULAR WING OF ASPECT RATIO 2 WITH NACA 0003-63 SECTION  
 (a) Geometric characteristics

*All dimensions shown in inches  
unless otherwise noted*



Aspect ratio . . . . .	2
Taper ratio . . . . .	0
Airfoil section (streamwise) . . . . .	NACA 0003-63
Total area, square feet . . . . .	4.014
Mean aerodynamic chord, $\bar{c}$ , feet . . . . .	1.889
Dihedral, degrees . . . . .	0
Twist, degrees . . . . .	0
Incidence, degrees . . . . .	0
Camber . . . . .	None
Distance, wing reference plane to body axis, feet . . . . .	0

(b) Data obtained in Ames 12-foot pressure wind tunnel

$\alpha$	$C_L$	$C_D$	$C_m$	$\alpha$	$C_L$	$C_D$	$C_m$	$\alpha$	$C_L$	$C_D$	$C_m$	$\alpha$	$C_L$	$C_D$	$C_m$
$M=0.25$		$R=4.9 \times 10^6$		$M=0.60$		$R=4.9 \times 10^6$		$M=0.25$		$R=9.3 \times 10^6$		$M=0.25$		$R=16.6 \times 10^6$	
0	-0.006	0.0051	0	0	-0.005	0.0064	-0.001	0	-0.005	0.0067	-0.001	0	-0.009	0.0069	0
-7.71	-0.031	0.0061	.003	-7.71	-0.034	0.0060	.003	-7.71	-0.033	0.0072	.003	-7.76	-0.037	0.0073	.003
0	-.006	.0051	0	0	-.005	.0062	-.001	0	-.005	.0067	-.001	0	-.008	.0070	-.001
1.01	.031	.0056	-.005	1.01	.030	.0067	-.006	1.01	.035	.0072	-.006	1.01	.030	.0074	-.005
2.02	.063	.0064	-.009	2.02	.075	.0092	-.012	2.02	.077	.0088	-.011	2.02	.068	.0085	-.010
3.03	.116	.0109	-.017	3.03	.116	.0118	-.019	3.03	.108	.0099	-.016	3.03	.105	.0102	-.016
4.04	.152	.0138	-.022	4.04	.156	.0157	-.025	4.04	.145	.0127	-.021	4.04	.142	.0129	-.021
5.05	.192	.0188	-.028	5.05	.197	.0214	-.031	5.05	.196	.0179	-.029	5.05	.183	.0162	-.027
6.06	.234	.0242	-.033	6.07	.252	.0299	-.039	6.06	.227	.0222	-.034	6.06	.227	.0216	-.034
8.09	.332	.0454	-.046	8.09	.352	.0515	-.052	8.08	.313	.0400	-.045	8.08	.316	.0382	-.047
10.11	.423	.0710	-.055	10.12	.440	.0775	-.063	10.11	.406	.0649	-.055	10.11	.413	.0637	-.057
12.14	.506	.1010	-.061	12.15	.550	.1150	-.075	12.13	.497	.0968	-.062	12.14	.508	.0962	-.065
14.16	.590	.1372	-.069	14.17	.653	.1586	-.088	14.16	.596	.1370	-.071	14.16	.603	.1363	-.074
16.18	.694	.1859	-.080	16.20	.761	.2117	-.102	16.18	.692	.1834	-.081	16.19	.700	.1833	-.084
18.21	.793	.2418	-.090	18.23	.861	.2713	-.112	18.21	.800	.2413	-.092	18.21	.799	.2391	-.094
20.23	.880	.2998	-.099	20.24	.914	.3238	-.121	20.24	.894	.3032	-.103	19.23	.853	.2717	-.099
22.25	.963	.3681	-.109	22.26	.994	.3914	-.126	22.26	.975	.3676	-.112	0	-.007	.0080	-.001
24.28	1.050	.4423	-.119	24.28	1.100	.4782	-.144	24.28	1.066	.4463	-.122				
26.31	1.162	.5382	-.132	0	-.004	.0067	-.001	26.31	1.160	.5358	-.130				
28.32	1.206	.6101	-.136					28.32	1.213	.6193	-.141				
0	-.006	.0057	0					0	-.008	.0064	0				

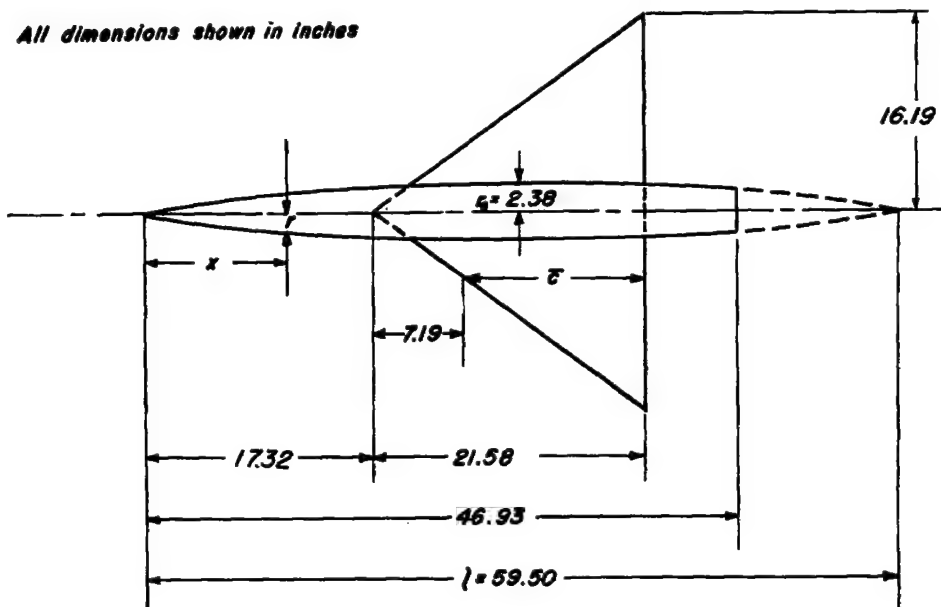
NACA

TABLE I. - GEOMETRIC CHARACTERISTICS AND WIND-TUNNEL DATA FOR  
A PLANE TRIANGULAR WING OF ASPECT RATIO 2 WITH  
NACA 0003-63 SECTION - Concluded  
(c) Data obtained in Ames 6- by 6-foot supersonic wind tunnel

$\alpha$	$C_L$	$C_D$	$C_M$	$\alpha$	$C_L$	$C_D$	$C_M$	$\alpha$	$C_L$	$C_D$	$C_M$	$\alpha$	$C_L$	$C_D$	$C_M$	$\alpha$	$C_L$	$C_D$	$C_M$	$\alpha$	$C_L$	$C_D$	$C_M$	
$M=0.61 \quad B=3.0 \times 10^{-6}$																								
0	0	0.0070	-0.003	0	-0.003	0.0067	-0.003	0	0.001	0.0074	-0.004	0	-0.003	0.0092	-0.001	0	-0.002	0.0104	-0.001	-0.01	-0.006	0.0103	0	
-5.43	-286	0.0361	-0.051	-6.51	-385	0.0418	-0.051	-6.57	-356	0.0457	-0.051	-6.59	-290	0.0392	-0.053	-6.19	-262	0.0395	-0.051	-6.18	-260	0.0375	-0.051	0.65
-5.36	-280	0.0270	-0.051	-5.42	-263	0.0397	-0.051	-5.49	-261	0.0322	-0.051	-5.56	-243	0.0300	-0.051	-5.16	-236	0.0305	-0.051	-5.15	-219	0.0293	-0.051	0.65
-1.28	-187	0.0190	-0.051	-4.38	-203	0.0203	-0.051	-4.35	-221	0.0269	-0.051	-4.13	-193	0.0227	-0.051	-4.14	-186	0.0235	-0.051	-4.12	-176	0.0225	-0.051	0.64
-3.20	-137	0.0132	-0.051	-3.23	-150	0.0182	-0.051	-3.26	-162	0.0156	-0.051	-3.09	-142	0.0168	-0.051	-3.09	-139	0.0178	-0.051	-3.09	-130	0.0171	-0.051	0.62
-2.14	-0.91	0.0097	-0.051	-2.16	-107	0.0101	-0.051	-2.18	-102	0.0106	-0.051	-2.06	-97	0.0125	-0.051	-2.06	-93	0.0138	-0.051	-2.06	-87	0.0133	-0.051	0.61
-1.05	-0.48	0.0078	-0.051	-1.08	-90	0.0079	-0.051	-1.05	-92	0.0083	-0.051	-1.03	-97	0.0102	-0.051	-1.03	-93	0.0113	-0.051	-1.03	-85	0.0107	-0.051	0.61
0	-0.04	0.0067	-0.051	-0.04	-94	0.0068	-0.051	0	-0.004	0.0073	-0.003	0	-0.003	0.0094	-0.001	0	-0.002	0.0104	-0.001	0	-0.005	0.0096	0	
1.06	0.04	0.0084	-0.051	1.07	0.048	0.0092	-0.051	1.08	0.051	0.0097	-0.051	1.03	0.041	0.0105	-0.051	1.03	0.044	0.0110	-0.051	1.03	0.044	0.0110	-0.051	0.61
2.12	0.088	0.0105	-0.051	2.15	0.100	0.0110	-0.051	2.17	0.103	0.0115	-0.051	2.06	0.067	0.0131	-0.051	2.06	0.069	0.0140	-0.051	2.06	0.067	0.0138	-0.051	0.61
3.19	134	0.0137	-0.051	3.23	149	0.0157	-0.051	3.25	164	0.0165	-0.051	3.09	155	0.0170	-0.051	3.09	152	0.0178	-0.051	3.09	152	0.0177	-0.051	0.61
4.28	193	0.0202	-0.051	4.31	206	0.0211	-0.051	4.35	223	0.0239	-0.051	4.12	187	0.0227	-0.051	4.12	182	0.0235	-0.051	4.12	173	0.0228	-0.051	0.61
5.25	242	0.0274	-0.051	5.41	229	0.0301	-0.051	5.45	265	0.0346	-0.051	5.16	238	0.0304	-0.051	5.16	233	0.0310	-0.051	5.16	221	0.0293	-0.051	0.61
6.43	292	0.0368	-0.051	6.51	314	0.0324	-0.051	6.56	367	0.0456	-0.051	6.19	319	0.0395	-0.051	6.18	318	0.0411	-0.051	6.18	318	0.0396	-0.051	0.61
8.61	409	0.0633	-0.051	8.71	457	0.0674	-0.051	8.80	519	0.0747	-0.051	8.26	485	0.0633	-0.051	8.25	473	0.0735	-0.051	8.24	454	0.0658	-0.051	0.61
10.77	516	0.0966	-0.051	10.81	559	0.113	-0.051	10.85	606	0.125	-0.051	9.35	570	0.1297	-0.051	9.31	557	0.1327	-0.051	9.30	530	0.1313	-0.051	0.61
12.96	643	1460	-0.051	13.11	706	1288	-0.051	13.15	744	1446	-0.051	12.05	780	1277	-0.051	12.10	744	1300	-0.051	12.09	724	1298	-0.051	0.61
13.18	764	2023	-0.051	13.25	837	2260	-0.051	13.29	905	1454	-0.051	12.05	877	1297	-0.051	12.10	837	1300	-0.051	12.09	817	1298	-0.051	0.61
17.33	874	2641	-0.125	17.45	985	2593	-0.125	17.48	1071	1454	-0.125	16.47	1071	1454	-0.125	16.50	987	1454	-0.125	16.48	1054	1454	-0.125	0.61
$M=1.60 \quad B=3.0 \times 10^{-6}$																								
$M=1.70 \quad B=3.0 \times 10^{-6}$																								
$M=0.61 \quad B=5.0 \times 10^{-6}$																								
0	-0.003	0.0068	-0.001	0	-0.001	0.0097	-0.001	-6.53	-296	0.0368	0.041	-6.59	-328	0.0400	0.041	-6.51	-303	0.0382	0.040	-6.51	-335	0.0368	0.040	0
-6.18	-291	0.0375	-0.051	-6.17	-239	0.0349	-0.051	-5.34	-240	0.0270	0.033	-5.24	-269	0.0307	0.033	-5.71	-321	0.0368	0.036	-5.33	-385	0.0313	0.046	0.61
-5.25	-210	0.0276	-0.051	-5.14	-202	0.0274	-0.051	-4.50	-235	0.0292	0.032	-4.22	-227	0.0337	0.033	-5.98	-287	0.0336	0.032	-5.28	-327	0.0310	0.046	0.61
-4.11	-167	0.0210	-0.051	-4.18	-182	0.0203	-0.051	-3.85	-157	0.0211	0.033	-3.31	-192	0.0250	0.033	-4.45	-223	0.0257	0.030	-4.22	-287	0.0237	0.046	0.61
-3.08	-124	0.0150	-0.051	-3.05	-180	0.0153	-0.051	-2.85	-157	0.0171	0.032	-2.31	-192	0.0207	0.033	-3.34	-257	0.0227	0.030	-3.14	-327	0.0207	0.046	0.61
-2.05	-0.94	0.0129	-0.051	-2.08	-180	0.0160	-0.051	-1.95	-166	0.0165	0.032	-1.45	-206	0.0170	0.033	-2.22	-222	0.0173	0.030	-2.11	-296	0.0179	0.046	0.61
-1.03	-0.043	0.0098	0	-0.043	0.0102	0.0098	0	-0.003	0.0101	0.0098	0	-0.002	0.0102	0	-0.003	0.0103	0	-0.002	0.0103	0	-0.005	0.0095	0	0
0	-0.003	0.0091	-0.001	0	-0.003	0.0095	-0.001	-0.01	-0.002	0.0080	-0.003	-0.01	-0.002	0.0073	-0.003	-0.01	-0.002	0.0072	-0.003	-0.01	-0.006	0.0095	0	0
-6.30	-261	0.0378	-0.051	-236	-0.0359	0.051	-0.051	-239	-0.0299	0.0376	-0.042	-238	-0.0324	0.042	-0.041	-271	-0.0311	0.0348	-0.053	-350	0.0319	0.046	0.61	
-5.25	-222	0.0296	-0.051	-5.28	-207	0.0280	-0.051	-5.56	-245	0.0273	0.031	-5.70	-271	0.0311	0.033	-5.77	-297	0.0346	0.031	-5.43	-350	0.0319	0.046	0.61
-4.21	-177	0.0227	-0.051	-4.19	-165	0.0217	-0.051	-4.43	-192	0.0189	0.031	-4.15	-219	0.0219	0.034	-4.61	-231	0.0243	0.041	-4.36	-326	0.0236	0.046	0.61
-3.15	-134	0.0176	-0.051	-3.13	-115	0.0170	-0.051	-3.34	-144	0.0181	0.031	-3.10	-157	0.0151	0.028	-3.45	-172	0.0169	0.030	-3.12	-210	0.0179	0.046	0.61
-2.10	-107	0.0139	-0.051	-2.09	-93	0.0134	-0.051	-1.84	-105	0.0107	0.031	-1.62	-111	0.0111	0.025	-2.31	-122	0.0118	0.028	-2.18	-190	0.0138	0.046	0.61
-1.05	-0.043	0.0111	0	-0.043	0.0110	0.0093	0	-0.003	0.0111	0.0093	0	-0.002	0.0111	0	-0.003	0.0111	0	-0.002	0.0111	0	-0.005	0.0093	0	0
-0.01	-0.004	0.0098	0	-0.004	0.0098	0.0098	0	-0.003	0.0098	0.0098	0	-0.002	0.0098	0	-0.003	0.0098	0	-0.002	0.0098	0	-0.006	0.0080	0	0
2.09	0.04	0.0140	-0.051	2.09	0.063	0.0126	-0.051	2.11	0.058	0.0118	-0.051	2.08	0.26	0.026	-0.051	2.11	0.055	0.022	-0.051	2.11	0.050	0.026	-0.051	0
3.15	138	0.0179	-0.051	3.18	125	0.0174	-0.051	3.32	116	0.0174	-0.051	3.05	129	0.0174	-0.051	3.39	137	0.0174	-0.051	3.28	150	0.0182	-0.051	0
4.20	177	0.0231	-0.051	4.19	167	0.0223	-0.051	4.44	195	0.0200	-0.051	4.24	220	0.0225	-0.051	4.49	238	0.0250	-0.051	4.34	199	0.0261	-0.051	0
5.20	221	0.0296	-0.051	5.23	207	0.0285	-0.051	5.56	232	0.0280	-0.051	5.29	258	0.0316	-0.051	5.77	277	0.0322	-0.051	5.44	249	0.0321	-0.051	0
6.30	260	0.0379	-0.051	6.28	248	0.0364	-0.051	6.68	305	0.0379	-0.051	6.05	285	0.0349	-0.051	6.22	335	0.0413	-0.051	6.34	300	0.0421	-0.051	0
8.40	343	0.0590	-0.051	8.37	319	0.0593	-0.051	8.96	326	0.0563	-0.051	7.98	356	0.0461	-0.051	-	-	-	-	-	-	-	-	-
10.50	422	0.0652	-0.105	10.46	392	0.0799	-0.100	-	-	-	-	-	-	-	-	-	-	-	-	-	-	-	-	-
$M=1.53 \quad B=5.0 \times 10^{-6}$																								

TABLE II.- GEOMETRIC CHARACTERISTICS AND WIND-TUNNEL DATA FOR A PLANE  
TRIANGULAR WING OF ASPECT RATIO 3 WITH NACA 0003-63 SECTION  
(a) Geometric characteristics

All dimensions shown in inches



Aspect ratio . . . . .	3
Taper ratio . . . . .	0
Airfoil section (streamwise) . . . . .	NACA 0003-63
Total area, square feet . . . . .	2.425
Mean aerodynamic chord, $c$ , feet . . . . .	1.199
Dihedral, degrees . . . . .	0
Twist, degrees . . . . .	0
Incidence, degrees . . . . .	0
Camber . . . . .	None
Distance, wing reference plane to body axis, feet . . . . .	0

(b) Data obtained in Ames 12-foot pressure wind tunnel

$\alpha$	$c_L$	$c_D$	$c_m$	$\alpha$	$c_L$	$c_D$	$c_m$	$\alpha$	$c_L$	$c_D$	$c_m$	$\alpha$	$c_L$	$c_D$	$c_m$
M=0.25 R=3.1x10 <sup>6</sup>				M=0.60 R=3.1x10 <sup>6</sup>				M=0.25 R=5.9x10 <sup>6</sup>				M=0.25 R=10.6x10 <sup>6</sup>			
0	-0.010	0.0054	0	0	-0.010	0.0074	0.001	0	-0.009	0.0070	0.002	0	-0.010	0.0078	0.001
-.71	-.044	.0056	.004	-.71	-.046	.0083	.005	-.76	-.046	.0073	.005	-.76	-.046	.0081	.005
0	-.007	-.0048	0	0	-.008	-.0076	0.001	0	-.010	-.0070	0.002	0	-.011	-.0078	.001
1.00	.034	.0064	-.002	1.01	.046	.0088	-.005	1.01	.043	.0082	-.004	1.01	.044	.0082	-.004
2.01	.080	.0067	-.007	2.02	.095	.0101	-.011	2.02	.091	.0100	-.009	2.01	.091	.0094	-.009
3.02	.143	.0114	-.014	3.02	.148	.0134	-.016	3.02	.146	.0132	-.014	3.02	.125	.0112	-.012
4.03	.193	.0156	-.017	4.03	.204	.0189	-.023	4.03	.190	.0171	-.018	4.03	.178	.0147	-.018
5.04	.249	.0231	-.022	5.04	.265	.0273	-.028	5.04	.241	.0234	-.023	5.04	.234	.0197	-.023
6.05	.304	.0325	-.026	6.05	.320	.0365	-.033	6.05	.298	.0326	-.027	6.04	.283	.0266	-.028
8.06	.395	.0519	-.031	8.07	.428	.0609	-.039	8.06	.393	.0528	-.033	8.06	.392	.0486	-.035
10.08	.494	.0806	-.033	10.08	.521	.0913	-.042	10.08	.502	.0839	-.035	10.08	.493	.0771	-.039
12.09	.594	.1170	-.039	12.10	.636	.1327	-.052	12.10	.607	.1214	-.042	12.10	.613	.1184	-.044
14.11	.687	.1587	-.044	14.12	.721	.1737	-.056	14.11	.702	.1640	-.046	14.11	.708	.1612	-.049
16.12	.776	.2073	-.048	16.13	.817	.2297	-.065	16.13	.789	.2127	-.051	0	-.007	.0076	0
18.14	.857	.2616	-.053	18.14	.888	.2842	-.072	18.14	.860	.2640	-.054				
20.15	.917	.3161	-.057	20.15	.923	.3332	-.084	20.15	.937	.3243	-.059				
22.16	.974	.3771	-.070	22.15	.946	.3852	-.124	22.16	.991	.3846	-.071				
24.16	1.021	.4411	-.088	0	-.005	.0078	-.002	24.16	1.024	.4470	-.099				
26.17	1.052	.5011	-.102					26.16	1.023	.4899	-.108				
28.17	1.088	.5410	-.113					28.17	1.043	.5457	-.115				
0	-.010	.0041	.018					0	-.010	.0072	.001				

CONFIDENTIAL

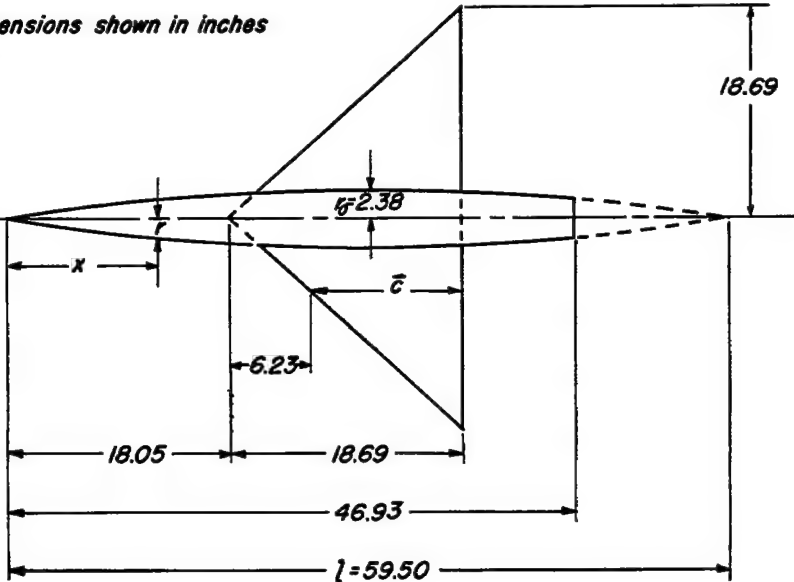


TABLE II.-- GEOMETRIC CHARACTERISTICS AND WIND-TUNNEL DATA FOR  
A PLANE TRIANGULAR WING OF ASPECT RATIO 3 WITH  
NACA 0003-63 SECTION - Concluded  
(c) Data obtained in Ames 6- by 6-foot supersonic wind tunnel

$c$	$c_L$	$c_D$	$c_a$	$c$	$c_L$	$c_D$	$c_a$	$c$	$c_L$	$c_D$	$c_a$													
M=0.61	R=1.9x10 <sup>6</sup>	M=0.91	R=1.9x10 <sup>6</sup>	M=0.92	R=1.9x10 <sup>6</sup>	M=1.20	R=1.9x10 <sup>6</sup>	M=1.40	R=1.9x10 <sup>6</sup>	M=1.53	R=1.9x10 <sup>6</sup>													
-0.55	-0.047	0.0072	0.006	-0.57	-0.063	0.0073	0.010	-0.57	-0.054	0.0067	0.011	-0.53	-0.053	0.0099	0.013	-0.52	-0.042	0.0113	0.010	-0.52	-0.033	0.0110	0.006	
-1.07	-0.075	0.0059	0.008	-1.10	-0.100	0.0069	0.016	-1.10	-0.101	0.0084	0.017	-1.03	-0.068	0.0114	0.017	-1.03	-0.070	0.0123	0.017	-1.03	-0.061	0.0118	0.015	
-2.12	-0.135	0.0109	0.016	-2.16	-0.159	0.0122	0.027	-2.12	-0.124	0.0107	0.022	-2.06	-0.150	0.0156	0.037	-2.06	-0.126	0.0162	0.030	-2.05	-0.119	0.0150	0.028	
-3.18	-0.196	0.0156	0.028	-3.23	-0.209	0.0180	0.048	-3.18	-0.186	0.0185	0.045	-3.09	-0.217	0.0214	0.054	-3.07	-0.181	0.0212	0.047	-3.06	-0.165	0.0201	0.040	
-4.23	-0.256	0.0235	0.037	-4.31	-0.252	0.0264	0.074	-4.23	-0.234	0.0286	0.060	-4.12	-0.267	0.0296	0.072	-4.10	-0.237	0.0293	0.064	-4.09	-0.214	0.0264	0.052	
-5.29	-0.326	0.0336	0.052	-5.39	-0.343	0.0347	0.094	-5.29	-0.307	0.0415	0.072	-5.14	-0.352	0.0401	0.086	-5.12	-0.292	0.0371	0.072	-5.12	-0.263	0.0345	0.064	
-6.34	-0.391	0.0433	0.063	-6.43	-0.408	0.0447	0.105	-6.34	-0.370	0.0475	0.086	-5.91	-0.417	0.0428	0.103	-5.91	-0.317	0.0420	0.095	-5.91	-0.219	0.0316	0.065	
-7.41	-0.456	0.0532	0.074	-7.51	-0.471	0.0559	0.116	-7.41	-0.427	0.0572	0.093	-7.03	-0.448	0.0515	0.113	-7.02	-0.347	0.0513	0.102	-7.02	-0.243	0.0321	0.062	
-8.46	-0.521	0.0632	0.084	-8.56	-0.536	0.067	0.126	-8.46	-0.487	0.0696	0.098	-8.08	-0.515	0.0636	0.113	-8.07	-0.404	0.0631	0.102	-8.07	-0.298	0.0328	0.069	
-9.51	-0.586	0.0732	0.094	-9.61	-0.598	0.078	0.136	-9.51	-0.547	0.0816	0.104	-9.13	-0.575	0.0756	0.119	-9.12	-0.474	0.0751	0.107	-9.12	-0.369	0.0335	0.076	
-10.56	-0.651	0.0832	0.104	-10.66	-0.662	0.082	0.146	-10.56	-0.610	0.0846	0.116	-10.18	-0.638	0.0796	0.130	-10.17	-0.536	0.0791	0.121	-10.17	-0.430	0.0342	0.078	
-11.61	-0.716	0.0932	0.124	-11.71	-0.727	0.093	0.156	-11.61	-0.675	0.0966	0.126	-11.23	-0.703	0.0916	0.140	-11.22	-0.599	0.0906	0.132	-11.22	-0.495	0.0352	0.082	
-12.66	-0.781	0.1032	0.144	-12.76	-0.792	0.097	0.166	-12.66	-0.740	0.1001	0.136	-12.28	-0.764	0.0950	0.150	-12.26	-0.659	0.0940	0.142	-12.26	-0.555	0.0361	0.089	
-13.71	-0.846	0.1132	0.164	-13.81	-0.856	0.101	0.176	-13.71	-0.804	0.1036	0.146	-13.33	-0.832	0.0986	0.160	-13.32	-0.728	0.0976	0.150	-13.32	-0.624	0.0371	0.096	
-14.76	-0.911	0.1232	0.184	-14.86	-0.921	0.092	0.186	-14.76	-0.869	0.1066	0.156	-14.38	-0.897	0.1016	0.170	-14.37	-0.792	0.1005	0.159	-14.37	-0.688	0.0379	0.103	
-15.81	-0.976	0.1332	0.204	-15.91	-0.986	0.083	0.196	-15.81	-0.934	0.1086	0.166	-15.43	-0.962	0.1036	0.180	-15.42	-0.857	0.1025	0.169	-15.42	-0.753	0.0387	0.112	
-16.86	-0.031	0.2071	-0.071					-16.96	-0.031	0.2081	-0.071	-16.58	-0.031	0.2091	-0.071	-16.57	-0.021	0.2080	-0.071	-16.57	-0.011	0.2079	-0.071	
-17.81	-0.880	0.2750	-0.073					-17.91	-0.880	0.2760	-0.073	-17.53	-0.880	0.2770	-0.073	-17.52	-0.770	0.2760	-0.073	-17.52	-0.660	0.2759	-0.072	
M=1.70	R=1.9x10 <sup>6</sup>	M=0.61	R=3.1x10 <sup>6</sup>	M=0.91	R=3.1x10 <sup>6</sup>	M=0.93	R=3.1x10 <sup>6</sup>	M=1.20	R=3.1x10 <sup>6</sup>	M=1.40	R=3.1x10 <sup>6</sup>	M=1.53	R=3.1x10 <sup>6</sup>											
-0.56	-0.030	0.0129	0.007	-0.57	-0.046	0.008	0.004	-0.57	-0.032	0.0077	0.006	-0.57	-0.056	0.0079	0.007	-0.53	-0.049	0.0115	0.012	-0.53	-0.035	0.0121	0.010	
-1.03	-0.093	0.0310	0.012	-1.05	-0.089	0.031	-0.07	-1.01	-0.092	0.089	0.013	-1.11	-0.092	0.089	-0.14	-1.05	-0.078	0.123	0.019	-1.05	-0.066	0.132	0.016	
-2.04	-0.099	0.0354	0.024	-2.15	-0.101	0.0315	-0.21	-1.68	-0.115	0.095	0.025	-2.10	-0.170	0.026	-0.20	-2.10	-0.189	0.067	0.036	-2.09	-0.124	0.069	0.011	
-3.07	-0.142	0.0494	0.034	-3.11	-0.146	0.0201	-0.30	-2.47	-0.169	0.058	-0.23	-3.11	-0.253	0.0201	-0.3	-3.11	-0.216	0.0222	0.077	-3.13	-0.183	0.0222	0.046	
-4.08	-0.188	0.0526	0.045	-4.18	-0.186	0.0261	-0.46	-3.19	-0.289	0.047	-0.40	-3.33	-0.308	0.026	-0.49	-4.19	-0.266	0.0307	0.072	-4.17	-0.230	0.0251	0.060	
-5.11	-0.239	0.0587	0.057	-5.35	-0.232	0.0332	-0.57	-4.01	-0.324	0.060	-0.50	-5.11	-0.413	0.024	-0.74	-5.24	-0.375	0.0416	0.089	-5.22	-0.329	0.0382	0.073	
-5.51	-0.288	0.0613	0.064	-5.56	-0.297	0.0372	-0.64	-4.07	-0.324	0.065	-0.54	-5.56	-0.472	0.024	-0.74	-5.67	-0.372	0.0422	0.087	-5.66	-0.322	0.0384	0.075	
1.08	0.042	0.017	0.011	1.05	0.049	0.0082	-0.07	1.07	0.027	0.073	-0.10	1.07	0.056	0.007	-0.07	1.07	0.027	0.019	0.13	1.07	0.053	0.0121	0.013	
2.04	0.089	0.037	0.022	2.11	0.087	0.0314	-0.16	1.95	0.029	0.073	-0.21	2.11	0.101	0.025	-0.21	2.11	0.059	0.030	0.208	2.10	0.146	0.027		
3.06	-0.135	0.1080	0.033	3.19	0.170	0.0411	-0.21	3.26	0.105	0.037	-0.26	3.26	0.229	0.027	-0.27	3.26	0.194	0.0203	0.048	3.26	0.169	0.0202	0.042	
4.06	0.161	0.1237	0.044	4.23	0.232	0.0406	-0.27	4.35	0.201	0.027	-0.34	4.36	0.305	0.0273	-0.34	4.36	0.26	0.0279	0.066	4.37	0.227	0.0273	0.056	
5.10	0.224	0.1309	0.053	5.32	0.294	0.0429	-0.38	5.44	0.260	0.0271	-0.45	5.45	0.362	0.0400	-0.45	5.45	0.323	0.0383	0.084	5.45	0.284	0.0379	0.070	
6.12	0.267	0.0888	0.063	6.38	0.366	0.0407	-0.57	6.53	0.333	0.0271	-0.65	6.55	0.447	0.053	-0.77	6.57	0.405	0.0502	0.100	6.55	0.360	0.0484	0.068	
6.18	0.213	0.0809	0.068	6.34	0.371	0.0403	-0.57	6.50	0.331	0.0284	-0.65	6.52	0.447	0.053	-0.77	6.54	0.405	0.0502	0.100	6.52	0.367	0.0484	0.068	
15.20	-0.042	0.0783	-0.08	10.54	-0.042	0.0783	-0.07	10.83	-0.075	0.1310	-0.099					10.48	-0.087	0.1261	-0.099	10.40	-0.047	0.1060	-0.134	
16.25	-0.087	0.1277	-0.126	12.77	-0.084	0.1322	-0.06	10.83	-0.075	0.1310	-0.099					11.39	-0.750	0.1512	-0.179	12.47	-0.039	0.1449	-0.155	
17.30	-0.050	0.1483	-0.146	14.59	-0.055	0.1403	-0.05	10.83	-0.075	0.1309	-0.099					15.12	-0.698	0.1911	-0.168	15.12	-0.028	0.1449	-0.168	
17.35	-0.146	0.1483	-0.146	14.59	-0.145	0.1403	-0.05	10.83	-0.075	0.1309	-0.099					15.12	-0.698	0.1911	-0.168	15.12	-0.028	0.1449	-0.168	
M=1.73	R=3.1x10 <sup>6</sup>	M=1.70	R=3.1x10 <sup>6</sup>	M=0.61	R=4.8x10 <sup>6</sup>	M=0.91	R=4.8x10 <sup>6</sup>	M=0.93	R=4.8x10 <sup>6</sup>	M=1.20	R=4.8x10 <sup>6</sup>	M=1.40	R=4.8x10 <sup>6</sup>	M=1.53	R=4.8x10 <sup>6</sup>									
-0.55	-0.040	0.0128	0.010	-0.56	-0.036	0.0121	0.009	-0.55	-0.034	0.0123	0.010	-0.53	-0.034	0.0119	0.009	-0.52	-0.034	0.0112	0.010	-0.52	-0.034	0.0110	0.006	
-1.07	-0.069	0.0136	0.017	-1.07	-0.068	0.0131	0.017	-1.06	-0.066	0.0114	0.017	-1.03	-0.066	0.0112	0.017	-1.03	-0.066	0.0113	0.016	-1.03	-0.066	0.0113	0.016	
-2.14	-0.126	0.0173	0.022	-2.14	-0.124	0.0151	0.022	-2.14	-0.126	0.0111	0.022	-2.11	-0.126	0.0127	0.022	-2.11	-0.126	0.0128	0.022	-2.11	-0.126	0.0127	0.022	
-3.21	-0.186	0.0226	0.046	-3.21	-0.184	0.0176	0.046	-3.21	-0.186	0.0111	0.046	-3.17	-0.186	0.0212	0.046	-3.17	-0.186	0.0212	0.046	-3.17	-0.186	0.0212	0.046	
-4.28	-0.246	0.0288	0.061	-4.28	-0.245	0.0221	0.061	-4.28	-0.246	0.0176	0.061	-4.24	-0.246	0.0278	0.064	-4.24	-0.246	0.0278	0.064	-4.24	-0.246	0.0278	0.064	
-5.34	-0.303	0.0329	0.074	-5.34	-0.302	0.0254	0.074	-5.34	-0.303	0.0174	0.074	-5.29	-0.303	0.0354	0.075	-5.29	-0.303	0.0354	0.075	-5.29	-0.303	0.0354	0.075	

TABLE III.- GEOMETRIC CHARACTERISTICS AND WIND-TUNNEL  
DATA FOR A PLANE TRIANGULAR WING OF ASPECT RATIO 4  
WITH 3-PERCENT-THICK ROUNDED-NOSE SECTION  
(a) Geometric characteristics

*All dimensions shown in inches*



Aspect ratio . . . . .	4
Taper ratio . . . . .	0
Airfoil section (streamwise) . . . . .	3-percent-thick biconvex with elliptical nose
Total area, square feet . . . . .	2.425
Mean aerodynamic chord, $\bar{c}$ , feet . . . . .	1.038
Dihedral, degrees . . . . .	0
Twist, degrees . . . . .	0
Incidence, degrees . . . . .	0
Camber . . . . .	None
Distance, wing reference plane to body axis, feet . . . . .	0

(b) Data obtained in Ames 12-foot pressure wind tunnel

$\alpha$	$C_L$	$C_D$	$C_m$	$\alpha$	$C_L$	$C_D$	$C_m$	$\alpha$	$C_L$	$C_D$	$C_m$	$\alpha$	$C_L$	$C_D$	$C_m$
M=0.25 R=2.7x10 <sup>6</sup>				M=0.60 R=2.7x10 <sup>6</sup>				M=0.25 R=5.01x10 <sup>6</sup>				M=0.25 R=9.1x10 <sup>6</sup>			
0	-0.010	0.0066	0	0	-0.010	0.0072	0	0	-0.009	0.0074	-0.001	0	-0.008	0.0079	-0.001
-0.75	-0.047	0.0103	.002	-0.71	-0.052	0.0086	.001	-0.71	-0.050	0.0080	0.002	-0.76	-0.050	0.0081	.003
0	-.010	0.0072	0	0	-.010	0.0074	-.001	0	-.010	0.0074	-.001	0	-.006	0.0084	-.001
1.00	.047	.0084	-.004	1.01	.054	.0089	-.007	1.00	.046	.0088	-.004	1.01	.054	.0085	-.005
2.00	.107	.0104	-.009	2.02	.096	.0102	-.010	2.02	.111	.0105	-.009	2.02	.110	.0099	-.009
3.00	.174	.0148	-.012	3.03	.173	.0149	-.016	3.03	.179	.0149	-.013	3.03	.166	.0128	-.013
4.00	.231	.0211	-.015	4.04	.231	.0213	-.018	4.04	.228	.0203	-.014	4.04	.225	.0182	-.016
5.00	.290	.0266	-.015	5.05	.310	.0307	-.021	5.05	.290	.0273	-.017	5.05	.285	.0253	-.018
6.01	.345	.0395	-.016	6.06	.371	.0426	-.023	6.06	.352	.0395	-.017	6.05	.344	.0365	-.019
8.01	.460	.0663	-.016	8.08	.477	.0685	-.023	8.07	.454	.0643	-.016	8.07	.450	.0620	-.017
10.02	.545	.0956	-.013	10.09	.584	.1040	-.022	10.09	.561	.0978	-.013	10.09	.559	.0947	-.015
12.02	.633	.1317	-.012	12.11	.670	.1434	-.026	12.10	.647	.1351	-.014	12.10	.643	.1306	-.016
14.03	.714	.1749	-.014	14.12	.746	.1868	-.034	14.12	.729	.1780	-.016	14.12	.743	.1784	-.019
16.04	.782	.2200	-.020	16.13	.796	.2324	-.053	16.13	.798	.2256	-.022	0	-.008	.0083	-.002
18.04	.839	.2743	-.048	18.13	.815	.2721	-.080	18.13	.839	.2755	-.053				
20.05	.874	.3217	-.072	20.14	.847	.3179	-.093	20.14	.872	.3220	-.075				
22.06	.896	.3653	-.079	22.14	.874	.3658	-.103	22.14	.887	.3643	-.080				
24.07	.911	.4096	-.087	24.14	.882	.4049	-.111	24.15	.911	.4121	-.087				
26.07	.919	.4559	-.096	0	-.005	.0078	-.004	26.15	.944	.4651	-.085				
28.08	.928	.5008	-.101	0				28.15	.958	.5150	-.095				
0	-.010	.0058	-.002					0	-.012	.0074	-.001				

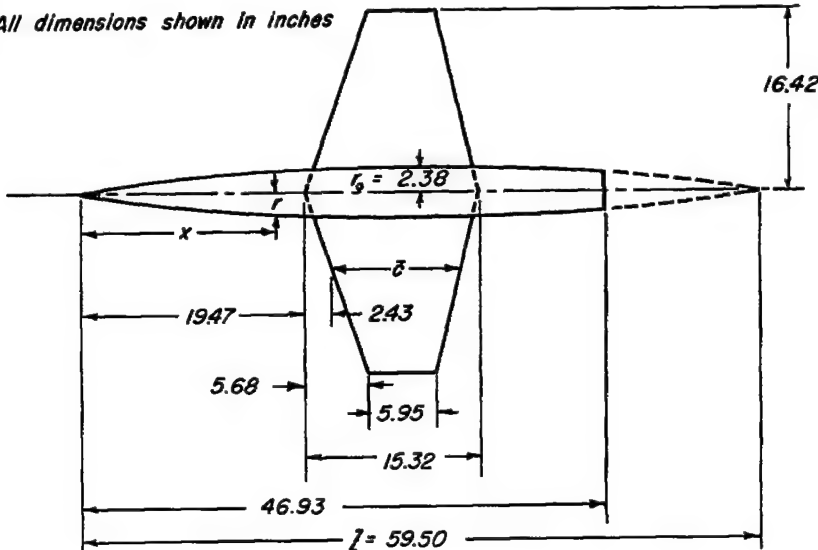
TABLE III.- GEOMETRIC CHARACTERISTICS AND WIND-TUNNEL DATA FOR  
A PLANE TRIANGULAR WING OF ASPECT RATIO 4 WITH 3-PERCENT-THICK  
ROUNDED-NOSE SECTION - Concluded

(c) Data obtained in Ames 6- by 6-foot supersonic wind tunnel

$c$	$c_L$	$c_D$	$c_m$	$a$	$c_L$	$c_D$	$c_m$	$a$	$c_L$	$c_D$	$c_m$	$a$	$c_L$	$c_D$	$c_m$	$a$	$c_L$	$c_D$	$c_m$	$a$	$c_L$	$c_D$	$c_m$	
$M=0.61 \quad R=1.7 \times 10^6$																								
-0.58	-0.047	0.0068	0	-0.59	-0.079	0.0080	0.004	-0.57	-0.065	0.0088	0.008	-0.56	-0.062	0.0095	0.011	-0.56	-0.044	0.0135	0.009	-0.54	-0.037	0.0143	0.009	
-1.07	-0.062	-0.099	-0.04	-1.09	-0.099	-0.018	-0.12	-1.03	-0.111	-0.19	-1.12	-0.123	-0.152	-0.21	-1.04	-0.086	-0.153	-0.19	-1.04	-0.075	-0.155	-0.16	-1.04	
-2.14	-1.13	-0.127	-0.04	-2.18	-1.18	-0.136	-0.19	-2.21	-0.220	-0.195	-2.26	-0.220	-0.174	-0.142	-2.08	-0.165	-0.265	-0.198	-2.07	-0.147	-0.280	-0.24	-2.07	
-3.21	-2.26	-0.180	-0.06	-3.16	-2.61	-0.201	-0.27	-3.30	-0.300	-0.228	-3.33	-0.315	-0.261	-0.225	-3.11	-0.247	-0.369	-0.285	-3.12	-0.212	-0.363	-0.29	-3.12	
-4.28	-2.97	-0.270	-0.09	-4.33	-3.39	-0.303	-0.38	-4.41	-0.418	-0.369	-4.48	-0.421	-0.361	-0.328	-4.19	-0.389	-0.508	-0.442	-4.20	-0.356	-0.505	-0.446	-4.20	
-5.33	-3.63	-0.380	-0.08	-5.41	-4.10	-0.434	-0.50	-5.49	-0.508	-0.429	-5.57	-0.517	-0.434	-0.371	-5.29	-0.499	-0.606	-0.539	-5.30	-0.468	-0.606	-0.548	-5.30	
-5.52	-3.96	-0.681	-0.08	-5.79	-4.94	-0.704	-0.77	-5.87	-0.787	-0.683	-5.95	-0.794	-0.700	-0.650	-5.52	-0.741	-0.858	-0.796	-5.53	-0.702	-0.854	-0.797	-5.53	
1.06	-0.04	-0.104	-0.010	1.08	-0.06	-0.097	-0.01	1.10	-0.103	-0.098	1.12	-0.102	-0.096	-0.046	1.04	-0.074	-0.147	-0.117	1.04	-0.071	-0.155	-0.117	1.04	
2.13	-0.14	-0.127	-0.017	2.16	-0.168	-0.024	-0.04	2.18	-0.203	-0.044	2.22	-0.204	-0.050	-0.095	2.10	-0.157	-0.245	-0.177	2.10	-0.154	-0.248	-0.174	2.10	
3.20	-0.26	-0.219	-0.026	3.25	-0.295	-0.034	-0.06	3.28	-0.328	-0.049	3.31	-0.331	-0.055	-0.146	3.10	-0.237	-0.328	-0.210	3.10	-0.236	-0.328	-0.210	3.10	
4.26	-0.39	-0.327	-0.027	4.32	-0.393	-0.044	-0.08	4.37	-0.416	-0.050	4.41	-0.421	-0.056	-0.205	4.15	-0.317	-0.413	-0.285	4.15	-0.315	-0.413	-0.287	4.15	
5.33	-0.50	-0.561	-0.027	5.39	-0.607	-0.056	-0.10	5.47	-0.641	-0.060	5.57	-0.671	-0.063	-0.305	5.19	-0.539	-0.645	-0.517	5.19	-0.537	-0.645	-0.519	5.19	
6.39	-0.61	-0.684	-0.027	6.46	-0.690	-0.057	-0.10	6.57	-0.711	-0.063	6.70	-0.748	-0.066	-0.328	6.23	-0.648	-0.750	-0.620	6.23	-0.646	-0.750	-0.622	6.23	
8.49	-0.71	-0.823	-0.026	8.59	-0.900	-0.067	-0.10	8.70	-0.998	-0.073	8.70	-1.000	-0.075	-0.350	8.19	-0.848	-0.949	-0.827	8.19	-0.846	-0.949	-0.829	8.19	
10.60	-0.76	-1.190	-0.026	10.72	-0.715	-0.067	-0.10	10.88	-0.867	-0.073	10.98	-0.998	-0.075	-0.350	10.32	-0.749	-0.867	-0.727	10.32	-0.747	-0.867	-0.729	10.32	
12.69	-0.77	-1.638	-0.026	12.78	-0.784	-0.069	-0.10	12.88	-0.926	-0.073	12.98	-1.000	-0.075	-0.350	12.40	-0.859	-0.967	-0.838	12.40	-0.857	-0.967	-0.839	12.40	
14.74	-0.81	-2.129	-0.026	14.86	-0.874	-0.070	-0.10	14.98	-0.998	-0.073	15.08	-1.000	-0.075	-0.350	14.50	-0.906	-1.020	-0.885	14.50	-0.904	-1.020	-0.887	14.50	
17.81	-0.87	-2.556	-0.026	17.92	-0.923	-0.070	-0.10	18.00	-1.000	-0.073	18.10	-1.000	-0.075	-0.350	17.62	-0.939	-1.020	-0.918	17.62	-0.937	-1.020	-0.920	17.62	
$M=1.10 \quad R=1.7 \times 10^6$																								
$M=1.33 \quad R=1.7 \times 10^6$																								
-0.58	-0.013	0.0184	0.007	-0.51	-0.026	0.0133	0.006	-0.50	-0.086	0.0146	0.006	-0.51	-0.104	0.0140	0.005	-0.50	-0.041	0.0086	0.001	-0.57	-0.045	0.0089	0.001	
-1.13	-0.066	-0.152	-0.030	-1.03	-0.099	-0.135	-0.01	-1.03	-0.109	-0.135	-1.03	-0.112	-0.136	-0.011	-1.11	-0.090	-0.109	-0.011	-1.12	-0.089	-0.109	-0.011	-1.12	
-2.07	-1.13	-0.200	-0.030	-2.06	-1.18	-0.217	-0.036	-2.06	-1.13	-0.167	-2.07	-1.12	-0.167	-0.022	-2.19	-1.071	-0.222	-0.022	-2.23	-1.074	-0.225	-0.023	-2.23	
-3.10	-1.99	-0.352	-0.035	-3.09	-1.79	-0.327	-0.039	-3.08	-1.68	-0.218	-3.08	-1.65	-0.214	-0.021	-3.30	-1.29	-0.229	-0.020	-3.37	-1.29	-0.237	-0.021	-3.37	
-4.12	-2.86	-0.524	-0.035	-4.11	-2.92	-0.302	-0.033	-4.11	-2.22	-0.290	-4.10	-2.08	-0.285	-0.026	-4.36	-1.36	-0.286	-0.026	-4.36	-1.36	-0.294	-0.026	-4.36	
-5.15	-3.21	-0.632	-0.037	-5.13	-2.86	-0.377	-0.047	-5.13	-2.71	-0.355	-5.13	-2.57	-0.344	-0.034	-5.45	-1.51	-0.372	-0.036	-5.45	-1.51	-0.380	-0.036	-5.45	
-5.52	-3.61	-0.811	-0.037	-5.79	-3.13	-0.356	-0.050	-5.79	-2.71	-0.346	-5.79	-2.34	-0.336	-0.047	-5.98	-1.71	-0.362	-0.047	-5.98	-1.71	-0.370	-0.047	-5.98	
1.03	-0.06	-0.147	-0.015	1.03	-0.09	-0.139	-0.013	1.03	-0.10	-0.132	1.02	-0.102	-0.129	-0.011	1.08	-0.070	-0.109	-0.006	1.11	-0.060	-0.109	-0.011	1.11	
2.07	-1.03	-0.184	-0.011	2.06	-0.119	-0.168	-0.027	2.06	-0.111	-0.165	2.05	-0.111	-0.165	-0.012	2.16	-0.089	-0.128	-0.023	2.23	-0.080	-0.128	-0.023	2.23	
3.09	-1.97	-0.284	-0.043	3.09	-1.76	-0.226	-0.041	3.08	-1.65	-0.204	3.08	-1.54	-0.207	-0.033	3.26	-1.29	-0.208	-0.037	3.34	-1.29	-0.210	-0.038	3.34	
4.12	-2.61	-0.312	-0.061	4.10	-2.13	-0.227	-0.049	4.10	-1.29	-0.217	4.09	-1.29	-0.217	-0.037	4.37	-1.29	-0.261	-0.047	4.46	-1.29	-0.263	-0.048	4.46	
5.16	-3.22	-0.407	-0.073	5.13	-2.89	-0.377	-0.067	5.13	-2.71	-0.355	5.12	-2.53	-0.345	-0.057	5.43	-1.53	-0.373	-0.067	5.52	-1.53	-0.381	-0.068	5.52	
6.19	-3.83	-0.525	-0.090	6.16	-3.43	-0.482	-0.079	6.16	-3.14	-0.458	6.14	-3.04	-0.458	-0.069	6.49	-1.94	-0.520	-0.089	6.58	-1.94	-0.526	-0.090	6.58	
8.23	-5.04	-0.845	-0.118	8.22	-4.71	-0.750	-0.104	8.21	-4.51	-0.728	8.19	-4.31	-0.728	-0.104	8.56	-2.94	-0.859	-0.120	8.65	-2.94	-0.869	-0.121	8.65	
10.30	-6.16	-1.199	-0.144	10.28	-5.54	-0.981	-0.121	10.27	-5.34	-0.958	10.25	-5.14	-0.958	-0.121	10.62	-3.94	-1.026	-0.139	10.71	-3.94	-1.032	-0.140	10.71	
12.36	-7.18	-1.657	-0.168	12.33	-5.90	-1.046	-0.146	12.31	-5.69	-1.024	12.29	-5.49	-1.024	-0.146	12.70	-4.26	-1.072	-0.153	12.79	-4.26	-1.078	-0.155	12.79	
14.41	-8.17	-2.140	-0.190	14.38	-7.44	-1.463	-0.169	14.36	-7.24	-1.443	14.34	-7.04	-1.443	-0.169	14.74	-5.74	-1.500	-0.180	14.83	-5.74	-1.506	-0.182	14.83	
17.48	-9.36	-2.966	-0.211	17.46	-8.79	-2.079	-0.201	17.44	-8.57	-2.054	17.42	-8.35	-2.054	-0.201	17.82	-6.78	-2.107	-0.218	17.91	-6.78	-2.112	-0.220	17.91	
$M=0.91 \quad R=2.9 \times 10^6$																								
$M=0.93 \quad R=2.9 \times 10^6$																								
-0.58	-0.009	-0.048	0.009	-0.58	-0.073	0.010	0.007	-0.58	-0.065	0.011	-0.58	-0.071	0.010	0.005	-0.58	-0.048	0.011	0.009	-0.58	-0.043	0.011	0.009	-0.58	
-1.15	-1.02	-0.178	-0.009	-1.15	-1.18	-0.176	-0.023	-1.15	-1.09	-0.157	-1.15	-1.02	-0.157	-0.016	-1.15	-0.095	-0.157	-0.016	-1.16	-0.090	-0.157	-0.016	-1.16	
-2.30	-2.13	-0.317	-0.027	-2.31	-2.21	-0.227	-0.037	-2.31	-2.13	-0.199	-2.30	-2.05	-0.199	-0.028	-2.31	-1.51	-0.227	-0.028	-2.32	-1.51	-0.232	-0.028	-2.32	
-3.38	-3.18	-0.520	-0.043	-3.36	-3.36	-0.426	-0.053	-3.36	-3.28	-0.395	-3.35	-3.18	-0.395	-0.043	-3.38	-2.78	-0.426	-0.043	-3.39	-2.78	-0.434	-0.043	-3.39	
-4.36	-3.86	-0.839	-0.059	-4.34	-3.86	-0.735	-0.068	-4.34	-3.76	-0.704	-4.33	-3.66	-0.704	-0.059	-4.36	-3.16	-0.							

TABLE IV.- GEOMETRIC CHARACTERISTICS AND WIND-TUNNEL DATA FOR A PLANE TAPERED WING OF ASPECT RATIO 3.1 WITH 3-PERCENT-THICK BICONVEX SECTION  
 (a) Geometric characteristics

*All dimensions shown in inches*



Aspect ratio . . . . .	3.08
Taper ratio . . . . .	.388
Airfoil section (streamwise) . . . . .	3-percent-thick biconvex
Total area, square feet . . . . .	2.425
Mean aerodynamic chord, $\bar{c}$ , feet . . . . .	.944
Biplane, degrees . . . . .	0
Twist, degrees . . . . .	0
Incidence, degrees . . . . .	0
Camber . . . . .	None
Distance, wing reference plane to body axis, feet . . . . .	0

(b) Data obtained in Ames 12-foot pressure wind tunnel

$\alpha$	$C_L$	$C_D$	$C_m$	$\alpha$	$C_L$	$C_D$	$C_m$	$\alpha$	$C_L$	$C_D$	$C_m$	$\alpha$	$C_L$	$C_D$	$C_m$
M=0.25		R=2.4x10 <sup>6</sup>		M=0.60		R=2.4x10 <sup>6</sup>		M=0.25		R=4.6x10 <sup>6</sup>		M=0.25		R=8.3x10 <sup>6</sup>	
0	-0.008	0.0158	-0.002	0	-0.009	0.0094	-0.001	0	-0.011	0.0093	0	0	-0.013	0.0086	-0.002
-.76	-0.052	0.0092	-0.003	-.71	-.054	0.0087	-.005	-.76	-.055	0.0092	-.003	-.76	-.058	0.0087	-.004
0	-0.013	0.0088	.001	0	-.010	0.0093	-.001	0	-.012	0.0094	0	0	-.012	0.0085	-.001
1.01	.042	0.0089	.006	1.01	.053	0.0095	.005	1.01	.042	0.0092	.005	1.01	.055	0.0089	.005
2.02	.110	0.0111	.012	2.02	.110	0.0116	.010	2.02	.103	0.0111	.010	2.02	.105	0.0104	.009
3.03	.168	0.0157	.023	3.03	.172	0.0154	.015	3.03	.169	0.0154	.015	3.03	.162	0.0139	.014
4.04	.226	0.0213	.021	4.04	.247	0.0224	.020	4.04	.223	0.0206	.022	4.04	.220	0.0194	.017
5.04	.277	0.0280	.026	5.05	.312	0.0309	.029	5.05	.285	0.0282	.026	5.05	.287	0.0276	.023
6.05	.338	0.0378	.031	6.06	.384	0.0425	.027	6.06	.351	0.0386	.028	6.06	.348	0.0377	.027
8.08	.478	0.0681	.029	8.08	.519	0.0747	.016	8.08	.479	0.0669	.027	8.08	.485	0.0769	.021
10.10	.615	1.095	.004	10.10	.639	1.171	-.015	10.10	.613	1.084	-.004	10.10	.630	1.105	-.002
12.11	.697	1.566	-.046	12.11	.682	1.552	-.054	12.11	.704	1.563	-.048	11.11	.686	1.347	-.024
14.11	.714	1.888	-.068	14.11	.695	1.883	-.074	14.11	.712	1.892	-.073	0	-.014	0.0087	-.003
16.11	.712	2.186	-.077	16.11	.702	2.183	-.078	16.11	.700	2.156	-.079				
18.11	.704	2.452	-.074	18.12	.726	2.545	-.081	18.11	.706	2.454	-.078				
20.12	.725	2.802	-.078	20.12	.732	2.870	-.078	20.12	.748	2.880	-.083				
22.12	.771	3.283	-.081	22.13	.781	3.367	-.089	22.13	.796	3.368	-.083				
24.13	.817	3.796	-.086	24.13	.841	3.958	-.099	24.13	.825	3.725	-.086				
26.14	.845	4.302	-.094	26.14	.880	4.578	-.106	26.14	.854	4.327	-.091				
28.14	.855	4.727	-.100	28.14	.901	5.014	-.110	28.14	.861	4.768	-.099				
0	-.010	0.0094	-.001	0	-.005	0.0103	-.005	0	-.007	0.0100	-.003				

CONTINENTAL.

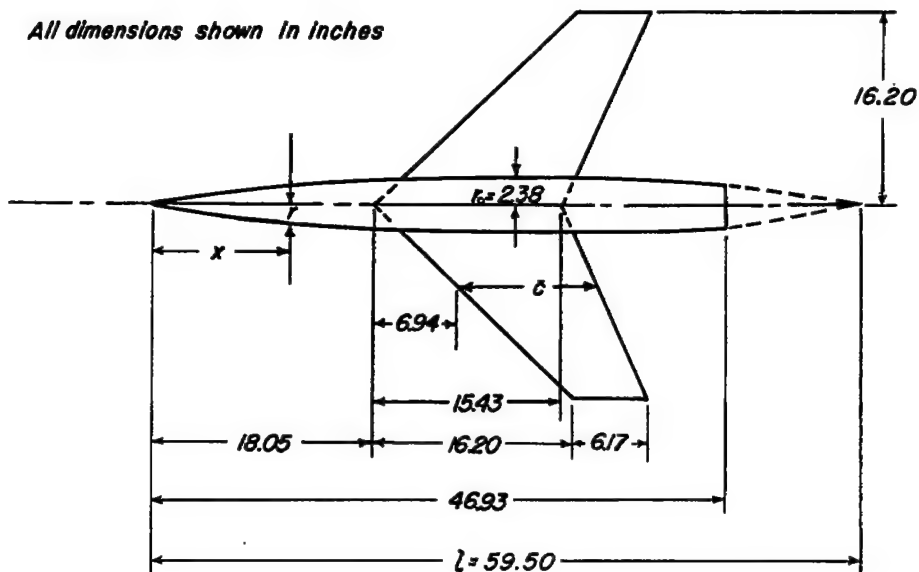
TABLE IV. - GEOMETRIC CHARACTERISTICS AND WIND-TUNNEL DATA  
FOR A PLANE TAPERED WING OF ASPECT RATIO 3.1 WITH  
3-PERCENT-THICK  $\delta$ -CONVEX SECTION - Concluded

(c) Data obtained in Ames 6- by 6-foot supersonic wind tunnel



TABLE V.- GEOMETRIC CHARACTERISTICS AND WIND-TUNNEL DATA FOR A  
 PLANE 45° SWEPTBACK WING OF ASPECT RATIO 3  
 WITH 3-PERCENT-THICK BICONVEX SECTION  
 (a) Geometric characteristics

*All dimensions shown in inches*



Aspect ratio . . . . .	3
Taper ratio . . . . .	.4
Airfoil section (streamwise) . . . . .	3-percent-thick biconvex
Total area, square feet . . . . .	2.430
Mean aerodynamic chord, $\bar{c}$ , feet . . . . .	.956
Dihedral, degrees. . . . .	0
Twist, degrees . . . . .	0
Incidence, degrees . . . . .	0
Camber . . . . .	None
Distance, wing reference plane to body axis, feet . . . . .	0

(b) Data obtained in Ames 12-foot pressure wind tunnel

$\alpha$	$C_L$	$C_D$	$C_m$	$\alpha$	$C_L$	$C_D$	$C_m$	$\alpha$	$C_L$	$C_D$	$C_m$	$\alpha$	$C_L$	$C_D$	$C_m$
M=0.25 R=2.5x10 <sup>-5</sup>				M=0.50 R=2.5x10 <sup>-5</sup>				M=0.25 R=4.7x10 <sup>-5</sup>				M=0.25 R=8.4x10 <sup>-5</sup>			
0	-0.007	0.0062	0	0	-0.006	0.0082	-0.002	0	-0.010	0.0083	0	0	-0.016	0.0080	-0.001
-7.1	-0.047	0.0070	.001	-7.6	-0.047	0.0089	-0.002	-7.1	-0.040	0.0085	0	-7.4	-0.053	.0085	0
0	-0.007	0.0062	0	0	-0.006	0.0085	-.002	0	-0.010	0.0081	0	0	-0.014	.0081	0
1.01	.027	0.0060	.001	1.01	.041	0.0081	0	1.00	.026	0.0077	.002	1.00	.032	.0084	0
2.01	.094	0.0085	0	2.02	.098	0.0103	-.002	2.01	.080	0.0100	.001	2.01	.089	.0106	0
3.03	.158	0.0138	0	3.03	.173	0.0154	-.003	3.02	.139	0.0140	.001	3.02	.149	.0145	0
4.03	.214	0.0187	-.001	4.04	.229	0.0209	-.005	4.03	.209	0.0199	0	4.03	.213	.0199	0
5.04	.278	0.0269	-.003	5.03	.312	0.0313	-.010	5.05	.283	0.0287	-.004	5.03	.270	.0270	-.004
6.05	.344	0.0377	-.007	6.06	.374	0.0421	-.014	6.05	.330	0.0370	-.005	6.05	.324	.0361	-.006
8.08	.469	0.060	-.008	8.08	.493	0.0709	-.017	8.07	.467	0.0662	-.008	8.07	.457	.0641	-.009
10.09	.564	0.0979	-.002	10.10	.598	0.1061	-.013	10.09	.569	0.0990	-.003	10.09	.571	.0985	-.006
12.11	.660	0.1387	.001	12.11	.684	0.1465	-.013	12.11	.659	0.1378	.001	12.11	.659	.1366	-.003
14.12	.742	0.1827	.001	14.12	.769	0.1935	-.019	14.12	.750	0.1842	-.001	13.62	.728	.1641	-.003
16.13	.814	0.2315	-.005	16.13	.807	0.2364	-.038	16.13	.832	0.2359	-.006	0	.011	.0084	-.001
18.14	.847	0.2787	-.044	18.13	.826	0.2756	-.057	18.14	.865	0.2819	-.036				
20.14	.867	.3206	-.055	20.14	.853	0.3200	-.068	20.14	.894	0.3287	-.055				
22.14	.891	.3660	-.056	22.14	.873	0.3636	-.074	22.15	.913	0.3739	-.058				
24.14	.910	.4117	-.063	24.14	.891	0.4087	-.080	24.15	.931	0.4188	-.060				
26.15	.944	.4663	-.069	26.15	.907	0.4552	-.084	26.15	.942	0.4642	-.063				
28.15	.948	.5119	-.078	0	-.003	0.0093	-.005	28.15	.941	0.5070	-.072				
0	-.007	.0054	0					0	-.009	0.0084	-.002				

### COMPUTER INTEGRATION

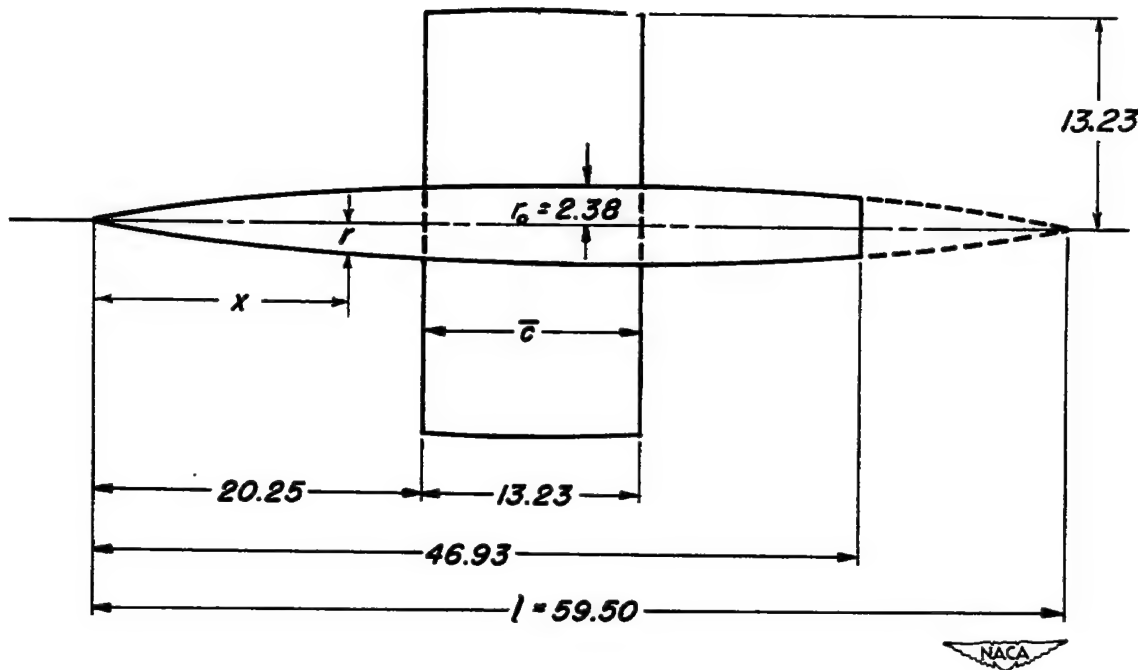


TABLE V. -- GEOMETRIC CHARACTERISTICS AND WIND-TUNNEL DATA FOR A PLANE 45° SWEEPBACK WING OF ASPECT RATIO 3 WITH 3-PERCENT-THICK BICONVEX SECTION - Concluded  
(c) Data obtained in Ames 6- by 6-foot supersonic wind tunnel

$a$	$c_L$	$c_D$	$c_m$	$\alpha$	$c_L$	$c_D$	$c_m$	$\alpha$	$c_L$	$c_D$	$c_m$													
$M=0.61 \quad R=1.5 \times 10^6$																								
-0.75	-0.047	0.0082	0.003	-0.56	-0.026	0.0083	0.005	-0.59	-0.061	0.0082	0.005	-0.59	-0.069	0.0083	0.006	-0.52	-0.021	0.0133	0.010	-0.32	0.006	0.0133	0.007	
-1.05	-0.063	0.0066	0.004	-1.10	-0.092	0.0086	0.007	-1.12	-0.109	0.0087	0.011	-1.11	-0.111	0.0098	0.014	-1.04	-0.086	0.014	0.016	-1.04	-0.079	0.0143	0.013	
-2.15	-1.17	-0.113	0.004	-2.20	-1.06	-0.019	0.007	-2.20	-1.07	-0.019	0.012	-2.20	-1.08	-0.018	0.023	-2.08	-0.95	-0.108	0.030	-2.07	-1.04	-0.179	0.026	
-3.21	-2.02	-0.104	0.005	-3.28	-1.04	-0.017	0.011	-3.21	-0.93	-0.019	0.013	-3.20	-0.92	-0.020	0.023	-3.12	-0.89	-0.018	0.030	-3.11	-0.88	-0.026	0.020	
-5.31	-3.89	-0.092	0.010	-5.36	-3.82	-0.089	0.020	-5.31	-3.97	-0.074	0.014	-5.42	-3.91	-0.074	0.020	-5.15	-3.18	-0.036	0.029	-5.14	-2.85	-0.032	0.029	
-5.37	-3.69	-0.097	0.014	-5.46	-3.31	-0.084	0.027	-5.41	-4.77	-0.074	0.023	-5.39	-0.76	-0.076	0.027	-5.19	-3.96	-0.070	0.027	-5.17	-3.32	-0.047	0.021	
-5.52	-3.05	-0.072	0.006	-5.53	-0.92	-0.067	0.006	-5.59	-0.76	-0.076	0.007	-5.51	-0.67	-0.076	0.006	-5.31	-0.23	-0.030	0.004	-5.30	-0.23	-0.030	0.004	
1.07	-0.094	0.0072	0.007	1.09	-0.073	0.0086	0.010	1.09	-0.079	0.0085	0.011	2.21	-0.120	0.013	0.014	2.03	-0.063	0.014	0.016	1.03	-0.056	0.014	0.011	
2.13	-1.30	-0.077	0.007	2.17	-1.32	-0.018	0.013	2.17	-1.70	-0.022	0.019	3.30	-0.275	0.0203	0.034	2.07	-1.36	-0.065	0.026	2.07	-1.27	-0.074	0.024	
3.21	-1.95	-0.074	0.008	3.26	-2.26	-0.016	0.013	3.26	-1.76	-0.026	0.017	4.40	-0.368	0.0203	0.034	3.12	-2.39	-0.064	0.026	3.11	-2.18	-0.026	0.026	
4.29	-2.78	-0.076	0.013	4.33	-3.06	-0.024	0.019	4.36	-3.58	-0.027	0.039	5.40	-0.470	0.0203	0.034	4.14	-2.13	-0.024	0.026	4.12	-2.07	-0.032	0.024	
5.35	-3.96	-0.075	0.017	5.43	-4.08	-0.024	0.025	5.48	-4.70	-0.047	0.065	6.51	-0.59	0.0203	0.034	5.17	-3.17	-0.045	0.027	5.16	-2.16	-0.037	0.026	
6.43	-4.33	-0.073	0.022	6.50	-4.72	-0.024	0.021	6.52	-5.23	-0.022	0.052	7.58	-0.63	0.0203	0.034	6.21	-1.90	-0.052	0.029	6.19	-1.96	-0.035	0.029	
8.54	-7.25	-0.072	0.020	8.62	-7.96	-0.020	0.014	8.68	-0.68	-0.047	0.070	10.36	-0.88	0.0203	0.034	8.86	-2.05	-0.057	0.029	8.84	-1.90	-0.037	0.029	
10.62	-8.73	-0.070	0.020	10.74	-7.34	-0.020	0.014	10.74	-1.81	-0.020	0.014	12.41	-0.84	0.0203	0.034	10.31	-1.61	-0.061	0.029	10.30	-1.74	-0.037	0.029	
12.72	-7.82	-0.068	0.022	12.81	-7.96	-0.020	0.014	12.81	-1.81	-0.020	0.014	14.43	-0.84	0.0203	0.034	12.43	-1.51	-0.061	0.029	12.42	-1.64	-0.037	0.029	
14.79	-10.24	-0.068	0.022	14.87	-8.86	-0.020	0.014	14.87	-1.81	-0.020	0.014	16.43	-0.84	0.0203	0.034	14.47	-1.43	-0.061	0.029	14.46	-1.56	-0.037	0.029	
16.88	-10.70	-0.068	0.022	16.92	-9.00	-0.020	0.014	16.92	-1.81	-0.020	0.014	18.49	-0.84	0.0203	0.034	16.47	-1.43	-0.061	0.029	16.46	-1.56	-0.037	0.029	
17.88	-10.73	-0.069	0.021	17.92	-9.02	-0.020	0.014	17.92	-1.81	-0.020	0.014	19.49	-0.84	0.0203	0.034	17.47	-1.43	-0.061	0.029	17.46	-1.56	-0.037	0.029	
$M=1.40 \quad R=1.5 \times 10^6$																								
-0.58	-0.041	0.0125	0.006	-0.58	-0.036	0.0122	0.007	-0.58	-0.036	0.0105	0.006	-0.58	-0.032	0.0118	0.004	-0.56	-0.049	0.0085	-0.003	-0.52	-0.050	0.0085	-0.002	
-1.04	-0.072	0.0133	0.007	-1.03	-0.067	0.0111	0.013	-1.03	-0.067	0.0112	0.010	-1.03	-0.071	0.0123	0.010	-1.02	-0.082	0.0094	-0.003	-1.01	-0.087	0.0095	-0.002	
-2.07	-1.37	-0.172	0.008	-2.06	-1.25	-0.024	0.025	-2.06	-1.16	-0.021	0.026	-2.06	-1.11	-0.020	0.026	-2.06	-1.21	-0.021	0.026	-2.06	-1.17	-0.027	0.025	
-3.10	-2.01	-0.227	0.018	-3.09	-1.88	-0.022	0.035	-3.09	-1.78	-0.020	0.031	-3.08	-1.62	-0.020	0.032	-3.08	-2.31	-0.028	0.027	-3.08	-1.81	-0.029	0.027	
-4.12	-2.61	-0.305	0.023	-4.11	-2.43	-0.028	0.045	-4.11	-2.27	-0.027	0.046	-4.10	-2.14	-0.026	0.044	-4.10	-3.08	-0.028	0.028	-4.10	-2.35	-0.032	0.028	
-5.16	-3.35	-0.306	0.023	-5.14	-2.98	-0.028	0.045	-5.14	-2.89	-0.027	0.046	-5.13	-2.74	-0.026	0.045	-5.13	-3.58	-0.036	0.031	-5.13	-2.43	-0.040	0.032	
-5.51	-3.22	-0.18	0.008	-5.51	-0.93	-0.014	0.014	-5.51	-0.82	-0.014	0.014	-5.51	-0.67	-0.014	0.014	-5.51	-1.08	-0.016	0.008	-5.50	-0.77	-0.017	0.008	
-1.03	-0.95	0.012	0.007	-1.03	-0.95	-0.014	0.013	-1.03	-0.85	-0.014	0.013	-1.03	-0.74	-0.014	0.014	-1.03	-1.12	-0.018	0.009	-1.02	-1.15	-0.017	0.009	
2.06	-1.68	-0.169	0.023	2.06	-1.09	-0.017	0.020	2.06	-1.07	-0.017	0.020	2.06	-0.92	-0.017	0.020	2.06	-1.28	-0.020	0.014	2.05	-1.37	-0.021	0.014	
3.09	-2.68	-0.214	0.026	3.09	-1.67	-0.019	0.026	3.09	-1.56	-0.019	0.026	3.09	-1.45	-0.019	0.026	3.09	-2.32	-0.024	0.014	3.08	-2.63	-0.025	0.014	
4.12	-2.49	-0.280	0.026	4.11	-2.26	-0.027	0.047	4.11	-2.15	-0.027	0.047	4.11	-2.07	-0.027	0.047	4.11	-2.96	-0.028	0.026	4.10	-2.65	-0.028	0.026	
5.15	-3.10	-0.303	0.027	5.14	-2.83	-0.027	0.047	5.14	-2.69	-0.027	0.046	5.14	-2.58	-0.027	0.046	5.14	-3.58	-0.028	0.026	5.13	-3.17	-0.028	0.026	
6.18	-3.71	-0.304	0.027	6.22	-3.73	-0.028	0.047	6.22	-3.63	-0.028	0.047	6.22	-3.53	-0.028	0.047	6.22	-4.26	-0.028	0.027	6.21	-3.86	-0.028	0.027	
8.83	-1.64	-0.794	0.112	8.83	-1.43	-0.027	0.047	8.83	-1.32	-0.027	0.047	8.83	-1.21	-0.027	0.047	8.83	-2.05	-0.028	0.027	8.82	-1.70	-0.028	0.027	
10.29	-1.21	-1.23	0.112	10.29	-1.26	-0.027	0.047	10.29	-1.16	-0.027	0.047	10.29	-1.05	-0.027	0.047	10.29	-1.90	-0.028	0.027	10.28	-1.55	-0.028	0.027	
12.35	-1.62	-1.62	0.112	12.35	-1.62	-0.027	0.047	12.35	-1.52	-0.027	0.047	12.35	-1.41	-0.027	0.047	12.35	-2.26	-0.028	0.027	12.34	-1.86	-0.028	0.027	
14.41	-2.12	-2.12	0.112	14.41	-2.12	-0.027	0.047	14.41	-2.02	-0.027	0.047	14.41	-1.91	-0.027	0.047	14.41	-2.76	-0.028	0.027	14.40	-2.36	-0.028	0.027	
16.47	-2.66	-2.66	0.112	16.47	-2.66	-0.027	0.047	16.47	-2.56	-0.027	0.047	16.47	-2.45	-0.027	0.047	16.47	-3.48	-0.028	0.027	16.46	-3.08	-0.028	0.027	
17.47	-2.66	-2.66	0.112	17.47	-2.66	-0.027	0.047	17.47	-2.56	-0.027	0.047	17.47	-2.45	-0.027	0.047	17.47	-3.48	-0.028	0.027	17.46	-3.08	-0.028	0.027	
$M=1.70 \quad R=1.5 \times 10^6$																								
$M=1.70 \quad R=1.5 \times 10^6$																								
-0.53	-0.048	0.0127	0.007	-0.53	-0.036	0.0128	0.007	-0.53	-0.036	0.0105	0.006	-0.53	-0.049	0.0114	0.006	-0.53	-0.049	0.0095	0.001	-0.52	-0.038	0.0132	0.006	
-1.06	-0.065	0.0133	0.012	-1.05	-0.062	0.0130	0.012	-1.05	-0.062	0.0137	0.011	-1.05	-0.072	0.0123	0.011	-1.04	-0.072	0.0124	0.001	-1.03	-0.063	0.0143	0.011	
-2.11	-1.22	-0.163	0.004	-2.10	-1.14	-0.023	0.024	-2.10	-1.05	-0.023	0.024	-2.10	-0.95	-0.023	0.024	-2.10	-2.36	-0.028	0.024	-2.09</td				

TABLE VI.- GEOMETRIC CHARACTERISTICS AND WIND-TUNNEL DATA FOR A PLANE  
 RECTANGULAR WING OF ASPECT RATIO 2 WITH 3-PERCENT-  
 THICK BICONVEX SECTION  
 (a) Geometric characteristics

*All dimensions shown in inches  
 unless otherwise noted*



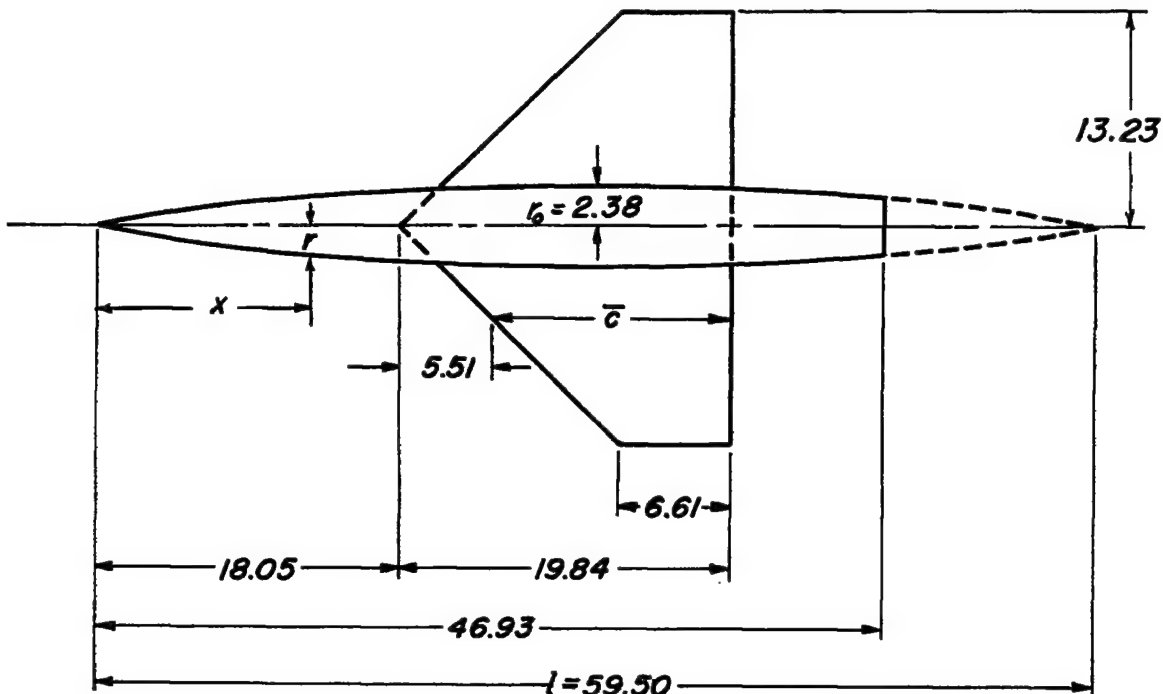
Aspect ratio . . . . .	2
Taper ratio . . . . .	1
Airfoil section (streamwise) . . . . .	3-percent-thick biconvex
Total area, square feet . . . . .	2.430
Mean aerodynamic chord, $\bar{c}$ , feet . . . . .	1.102
Dihedral, degrees . . . . .	0
Twist, degrees . . . . .	0
Incidence, degrees . . . . .	0
Camber . . . . .	0
Distance, wing reference plane to body axis, feet . . . . .	0

TABLE VI.- GEOMETRIC CHARACTERISTICS AND WIND-TUNNEL DATA  
FOR A PLANE RECTANGULAR WING OF ASPECT RATIO 2 WITH  
3-PERCENT-THICK BICONVEX SECTION - Concluded  
(b) Data obtained in Ames 6- by 6-foot supersonic wind tunnel

$c$	$c_L$	$c_D$	$c_m$	$\alpha$	$c_L$	$c_D$	$c_m$	$\alpha$	$c_L$	$c_D$	$c_m$	$\alpha$	$c_L$	$c_D$	
$M=0.61 \quad R=1.8 \times 10^6$								$M=0.71 \quad R=1.8 \times 10^6$							
-0.27	-0.024	0.009	0	-0.28	-0.022	0.0107	-0.001	-0.28	-0.020	0.0105	-0.003	-0.28	-0.016	0.0100	-0.006
-0.25	-0.034	0.006	-0.002	-0.25	-0.033	0.0100	-0.003	-0.25	-0.031	0.0100	-0.006	-0.25	-0.027	0.0100	-0.011
-0.22	-0.048	0.006	-0.004	-0.22	-0.046	0.0097	-0.005	-0.22	-0.045	0.0099	-0.006	-0.22	-0.042	0.0100	-0.012
-1.07	-0.042	0.006	-1.06	-0.041	0.006	-0.007	-1.06	-0.061	0.0102	-0.009	-1.06	-0.056	0.0102	-0.014	-1.06
-2.15	-0.117	0.023	-0.09	-2.17	-0.118	0.026	-0.012	-2.19	-0.120	0.026	-0.016	-2.19	-0.123	0.026	-0.020
-3.23	-0.174	0.017	-0.13	-3.27	-0.181	0.022	-0.016	-3.26	-0.187	0.022	-0.017	-3.21	-0.197	0.021	-0.025
-4.30	-0.238	0.020	-0.16	-3.33	-0.246	0.023	-0.020	-3.35	-0.257	0.026	-0.020	-4.40	-0.278	0.024	-0.029
-5.38	-0.272	0.006	-0.21	-5.39	-0.282	0.016	-0.021	-5.37	-0.294	0.016	-0.021	-5.42	-0.307	0.011	-0.025
-6.45	-0.313	0.003	-0.24	-6.45	-0.315	0.018	-0.023	-6.45	-0.317	0.018	-0.023	-6.45	-0.324	0.012	-0.027
-7.52	-0.353	0.001	-0.28	-7.52	-0.358	0.016	-0.028	-7.52	-0.360	0.016	-0.028	-7.52	-0.363	0.011	-0.030
-8.59	-0.39	-0.004	-0.35	-8.59	-0.396	0.004	-0.035	-8.59	-0.396	0.005	-0.035	-8.59	-0.397	0.013	-0.036
-9.66	-0.43	-0.020	-0.40	-9.66	-0.436	0.006	-0.044	-9.66	-0.436	0.007	-0.044	-9.66	-0.437	0.011	-0.045
-10.73	-0.47	-0.046	-0.45	-10.73	-0.476	0.008	-0.054	-10.73	-0.476	0.009	-0.054	-10.73	-0.477	0.012	-0.055
-11.80	-0.51	-0.073	-0.53	-11.80	-0.512	0.012	-0.074	-11.80	-0.512	0.012	-0.074	-11.80	-0.512	0.013	-0.075
-12.87	-0.55	-0.103	-0.57	-12.87	-0.542	0.016	-0.084	-12.87	-0.542	0.016	-0.084	-12.87	-0.542	0.016	-0.085
-13.94	-0.59	-0.133	-0.60	-13.94	-0.582	0.019	-0.094	-13.94	-0.582	0.019	-0.094	-13.94	-0.582	0.019	-0.095
-14.00	-0.63	-0.171	-0.63	-14.00	-0.620	0.024	-0.103	-14.00	-0.620	0.024	-0.103	-14.00	-0.620	0.024	-0.104
-14.06	-0.67	-0.211	-0.67	-14.06	-0.658	0.028	-0.113	-14.06	-0.658	0.028	-0.113	-14.06	-0.658	0.028	-0.115
$M=1.30 \quad R=1.8 \times 10^6$								$M=0.71 \quad R=1.8 \times 10^6$							
-0.26	-0.036	0.016	0.003	-0.27	-0.022	0.0136	-0.005	-0.27	-0.017	0.0149	-0.001	-0.27	-0.012	0.0129	-0.003
-0.24	-0.042	0.016	0.004	-0.24	-0.036	0.0135	-0.004	-0.24	-0.031	0.0151	-0.003	-0.24	-0.033	0.0132	-0.004
-0.21	-0.058	0.012	0.005	-0.21	-0.056	0.0160	-0.005	-0.21	-0.056	0.0159	-0.004	-0.21	-0.047	0.0135	-0.006
-1.06	-0.075	0.017	-1.08	-0.069	0.016	-0.007	-1.06	-0.074	0.0161	-0.007	-1.06	-0.060	0.0161	-0.008	-1.05
-2.14	-0.141	0.022	-0.12	-2.14	-0.127	0.020	-0.023	-2.13	-0.115	0.0191	-0.022	-2.12	-0.112	0.0175	-0.021
-3.19	-0.207	0.018	-0.18	-3.18	-0.189	0.026	-0.023	-3.17	-0.171	0.0188	-0.019	-3.17	-0.165	0.0234	-0.023
-4.24	-0.272	0.011	-0.23	-4.24	-0.256	0.030	-0.021	-4.23	-0.257	0.037	-0.019	-4.21	-0.219	0.037	-0.017
-5.29	-0.336	0.006	-0.29	-5.29	-0.321	0.035	-0.018	-5.28	-0.321	0.037	-0.018	-5.27	-0.295	0.039	-0.018
-6.35	-0.394	0.002	-0.35	-6.35	-0.376	0.039	-0.015	-6.34	-0.376	0.039	-0.015	-6.33	-0.349	0.039	-0.015
-7.40	-0.452	0.001	-0.41	-7.40	-0.436	0.043	-0.012	-7.39	-0.436	0.043	-0.012	-7.38	-0.406	0.043	-0.012
-8.45	-0.511	-0.034	-0.47	-8.45	-0.492	0.051	-0.009	-8.38	-0.492	0.051	-0.009	-8.37	-0.462	0.051	-0.009
-9.51	-0.569	-0.074	-0.52	-9.51	-0.586	0.058	-0.006	-9.46	-0.586	0.058	-0.006	-9.45	-0.556	0.058	-0.006
-10.57	-0.615	-0.125	-0.58	-10.57	-0.600	0.065	-0.003	-10.52	-0.600	0.065	-0.003	-10.49	-0.570	0.065	-0.003
-11.63	-0.659	-0.175	-0.64	-11.63	-0.674	0.072	-0.001	-11.58	-0.674	0.072	-0.001	-11.55	-0.644	0.072	-0.001
-12.69	-0.709	-0.221	-0.70	-12.69	-0.720	0.078	-0.000	-12.64	-0.720	0.078	-0.000	-12.61	-0.690	0.078	-0.000
$M=0.61 \quad R=4.4 \times 10^6$								$M=0.71 \quad R=4.4 \times 10^6$							
-0.30	-0.020	0.010	-0.001	-0.31	-0.023	0.0102	-0.004	-0.31	-0.026	0.0104	-0.004	-0.35	-0.031	0.0103	-0.005
-0.29	-0.034	0.013	-0.007	-0.30	-0.037	0.0101	-0.005	-0.30	-0.037	0.0103	-0.005	-0.35	-0.049	0.0104	-0.006
-0.27	-0.048	0.011	-0.007	-0.29	-0.050	0.0100	-0.006	-0.29	-0.050	0.0103	-0.006	-0.35	-0.069	0.0105	-0.006
-1.15	-0.061	0.012	-0.029	-1.19	-0.064	0.0102	-0.009	-1.20	-0.066	0.0106	-0.011	-1.17	-0.074	0.0105	-0.012
-2.27	-0.125	0.018	-0.114	-2.30	-0.120	0.0129	-0.012	-2.28	-0.126	0.0129	-0.012	-2.16	-0.126	0.0128	-0.013
-3.36	-0.174	0.017	-0.133	-3.36	-0.181	0.0171	-0.013	-3.30	-0.192	0.0190	-0.013	-3.20	-0.221	0.0186	-0.014
-4.45	-0.235	0.018	-0.202	-4.45	-0.247	0.0229	-0.015	-4.46	-0.265	0.0277	-0.015	-4.33	-0.283	0.0234	-0.015
-5.53	-0.293	0.019	-0.274	-5.53	-0.312	0.0281	-0.016	-5.53	-0.312	0.0281	-0.016	-5.40	-0.329	0.0281	-0.016
-6.61	-0.351	0.024	-0.323	-6.61	-0.376	0.0321	-0.017	-6.61	-0.376	0.0321	-0.017	-6.48	-0.393	0.0321	-0.017
-7.69	-0.409	0.024	-0.392	-7.69	-0.432	0.0361	-0.018	-7.69	-0.432	0.0361	-0.018	-7.56	-0.452	0.0361	-0.018
-8.76	-0.467	0.022	-0.452	-8.76	-0.492	0.0401	-0.019	-8.76	-0.492	0.0401	-0.019	-8.63	-0.512	0.0401	-0.019
-9.84	-0.524	0.024	-0.509	-9.84	-0.556	0.0441	-0.020	-9.84	-0.556	0.0441	-0.020	-9.71	-0.576	0.0441	-0.020
-1.12	-0.47	0.023	-0.06	-1.12	-0.517	0.0507	-0.021	-1.12	-0.517	0.0507	-0.021	-1.09	-0.537	0.0507	-0.021
-2.24	-1.01	0.025	-0.12	-2.24	-1.07	0.0513	-0.021	-2.21	-1.13	0.0518	-0.021	-2.18	-1.14	0.0518	-0.021
-3.36	-1.61	0.029	-0.16	-3.36	-1.70	0.0566	-0.021	-3.37	-1.70	0.0573	-0.021	-3.33	-1.75	0.0566	-0.021
-4.47	-2.21	0.030	-0.21	-4.47	-2.34	0.0626	-0.023	-4.43	-2.34	0.0626	-0.023	-4.37	-2.38	0.0626	-0.023
-5.58	-2.80	0.045	-0.27	-5.58	-3.04	0.0711	-0.025	-5.58	-3.04	0.0711	-0.025	-5.53	-3.09	0.0711	-0.025
-6.74	-3.36	0.061	-0.33	-6.74	-3.64	0.0751	-0.025	-6.74	-3.64	0.0751	-0.025	-6.70	-3.77	0.0751	-0.025
-8.82	-4.00	0.061	-0.06	-8.82	-4.34	0.0781	-0.025	-8.82	-4.34	0.0781	-0.025	-8.78	-4.49	0.0781	-0.025
$M=1.40 \quad R=4.4 \times 10^6$								$M=1.50 \quad R=4.4 \times 10^6$							
-0.31	-0.026	0.016	0.003	-0.31	-0.020	0.0154	0.002	-0.31	-0.018	0.0142	0.003	-0.39	-0.037	0.0137	0.003
-0.60	-0.040	0.016	0.004	-0.60	-0.033	0.0157	0.004	-0.60	-0.032	0.0157	0.004	-0.60	-0.040	0.0157	0.004
-0.91	-0.057	0.017	0.006	-0.91	-0.050	0.0161	0.006	-0.91	-0.047	0.0159	0.006	-0.91	-0.059	0.0158	0.006
-1.19	-0.074	0.018	0.008	-1.19	-0.067	0.0167	0.007	-1.19	-0.066	0.0158	0.006	-1.19	-0.077	0.0158	0.006
-2.30	-0.135	0.022	0.015	-2.30	-0.124	0.0207	0.015	-2.30	-0.123	0.0201	0.015	-2.29	-0.137	0.0201	0.015
-3.43	-0.199	0.028	0.022	-3.43	-0.184	0.0271	0.023	-3.43	-0.177	0.0270	0.023	-3.43	-0.198	0.0270	0.023
-4.51	-0.276	0.036	0.033	-4.51	-0.255	0.0365	0.032	-4.51	-0.248	0.0363	0.033	-4.44	-0.272	0.0364	0.033
-5.58	-0.331	0.047	0.039	-5.58	-0.313	0.0413	0.036	-5.58	-0.305	0.0413	0.036	-5.53	-0.337	0.0413	0.036
-6.66	-0.406	0.047	0.045	-6.66	-0.384	0.0461	0.040	-6.66	-0.377	0.0461	0.040	-6.61	-0.406	0.0461	0.040
-7.74	-0.472	0.047	0.047	-7.74	-0.452	0.0482	0.040	-7.74	-0.445	0.0482	0.040	-7.70	-0.472	0.0482	0.040
-1.17	-0.62	0.047	-0.007	-1.17	-0.60	0.0488	-0.006	-1.17	-0.59	0.0481	-0.007	-1.14	-0.64	0.0483	-0.0

TABLE VII.- GEOMETRIC CHARACTERISTICS AND WIND-TUNNEL DATA  
 FOR A PLANE 45° SWEPTBACK WING OF ASPECT RATIO 2  
 WITH 3-PERCENT-THICK BICONVEX SECTION  
 (a) Geometric characteristics

*All dimensions shown in inches  
 unless otherwise noted*



Aspect ratio . . . . .	2
Taper ratio . . . . .	.333
Airfoil section (streamwise) . . . . .	3-percent-thick biconvex
Total area, square feet. . . . .	2.430
Mean aerodynamic chord, $\bar{c}$ , feet . . . . .	1.194
Dihedral, degrees . . . . .	0
Twist, degrees . . . . .	0
Incidence, degrees . . . . .	0
Camber . . . . .	None
Distance, wing reference plane to body axis, feet . . . . .	0

CONFIDENTIAL

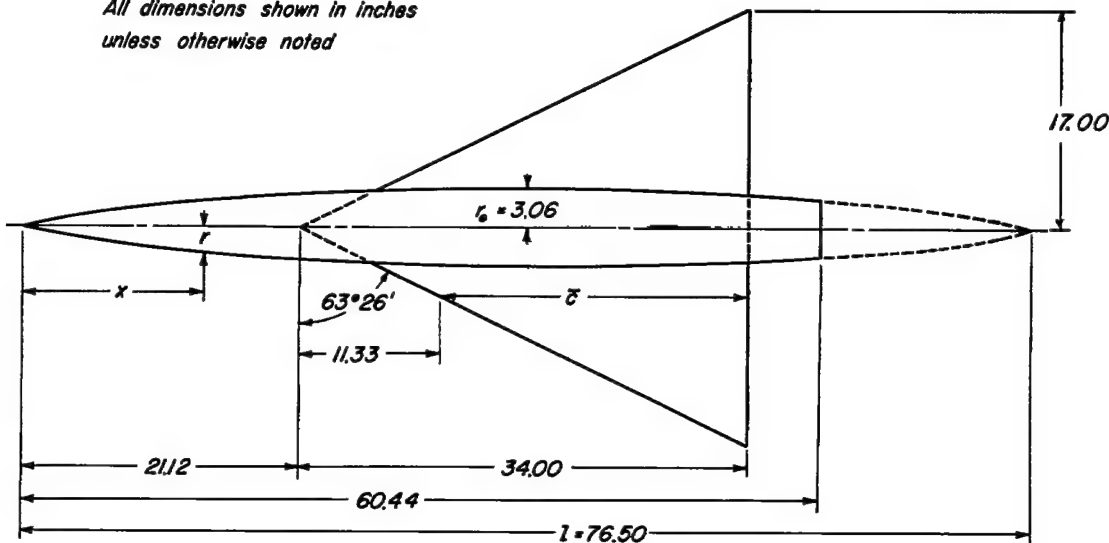


TABLE VII.- GEOMETRIC CHARACTERISTICS AND WIND-TUNNEL DATA FOR  
 A PLANE 45° SWEPTBACK WING OF ASPECT RATIO 2 WITH  
 3-PERCENT-THICK BICONVEX SECTION - Concluded  
 (b) Data obtained in Ames 6- by 6-foot supersonic wind tunnel

$\alpha$	$C_L$	$C_D$	$C_M$	$\alpha$	$C_L$	$C_D$	$C_M$	$\alpha$	$C_L$	$C_D$	$C_M$	$\alpha$	$C_L$	$C_D$	$C_M$	$\alpha$	$C_L$	$C_D$	$C_M$	$\alpha$	$C_L$	$C_D$	
$\text{N=0.61}$ $\text{R=1.9x10}^{-6}$																							
-0.27	-0.020	0.071	-0.001	-0.27	-0.019	0.077	-0.002	-0.27	-0.019	0.076	-0.003	-0.27	-0.012	0.068	-0.007	-0.29	-0.009	0.068	-0.007	-0.27	-0.028	0.019	
-5.5	-0.031	0.072	-0.001	-5.5	-0.030	0.074	-0.002	-5.5	-0.029	0.077	-0.003	-5.5	-0.026	0.072	-0.007	-5.5	-0.026	0.081	-0.005	-5.5	-0.045	0.033	
-7.9	-0.043	0.072	-0.001	-8.1	-0.045	0.076	-0.002	-8.1	-0.045	0.080	-0.003	-8.1	-0.040	0.080	-0.007	-7.9	-0.037	0.083	-0.008	-8.0	-0.060	0.034	
-1.06	-0.056	0.079	-0.001	-1.07	-0.056	0.083	-0.003	-1.07	-0.056	0.088	-0.002	-1.07	-0.056	0.087	-0.007	-1.04	-0.054	0.086	-0.007	-1.06	-0.076	0.040	
-2.13	-0.111	0.103	-0.001	-2.13	-0.116	0.110	-0.001	-2.16	-0.119	0.100	-0.002	-2.17	-0.121	0.115	-0.005	-2.11	-0.118	0.113	-0.007	-2.11	-0.140	0.116	
-3.19	-0.163	0.146	-0.001	-3.22	-0.177	0.157	-0.001	-3.23	-0.183	0.158	-0.001	-3.25	-0.193	0.173	-0.002	-3.15	-0.189	0.165	-0.002	-3.15	-0.207	0.168	
-4.27	-0.230	0.222	-0.001	-4.29	-0.240	0.232	-0.001	-4.22	-0.250	0.236	-0.002	-4.34	-0.271	0.260	-0.004	-4.20	-0.262	0.284	-0.005	-4.19	-0.275	0.324	
-5.3	-0.001	0.079	-0.001	-5.3	-0.001	0.075	-0.001	-5.1	-0.001	0.077	-0.001	-5.1	-0.001	0.080	-0.002	-5.1	-0.001	0.082	-0.002	-4.7	-0.023	0.037	
-5.1	-0.012	0.075	-0.001	-5.1	-0.013	0.076	-0.001	-5.2	-0.013	0.077	-0.001	-5.1	-0.012	0.080	-0.002	-5.1	-0.012	0.082	-0.002	-4.7	-0.015	0.036	
-7.6	-0.023	0.077	-0.001	-7.8	-0.023	0.081	-0.001	-7.8	-0.027	0.080	-0.001	-7.8	-0.024	0.085	-0.003	-7.7	-0.024	0.084	-0.003	-7.8	-0.032	0.035	
1.04	-0.036	0.080	-0.001	1.04	-0.039	0.081	-0.001	1.05	-0.040	0.080	-0.001	1.06	-0.039	0.088	-0.004	1.04	-0.040	0.089	-0.004	1.03	-0.048	0.037	
2.11	-0.091	0.097	-0.001	2.12	-0.097	0.108	-0.001	2.13	-0.100	0.103	-0.001	2.15	-0.104	0.112	-0.003	2.10	-0.106	0.110	-0.002	2.09	-0.112	0.113	
3.17	-0.149	0.140	-0.001	3.19	-0.157	0.147	-0.002	3.21	-0.165	0.151	-0.002	3.24	-0.177	0.150	-0.006	3.18	-0.179	0.160	-0.002	3.13	-0.186	0.161	
4.25	-0.209	0.202	-0.001	4.26	-0.227	0.205	-0.001	4.28	-0.230	0.222	-0.001	4.31	-0.247	0.238	-0.007	4.18	-0.248	0.239	-0.009	4.16	-0.247	0.238	
6.35	-0.323	0.393	-0.007	6.40	-0.350	0.428	-0.009	6.42	-0.366	0.447	-0.012	6.48	-0.418	0.533	-0.012	6.27	-0.417	0.503	-0.008	6.23	-0.422	0.523	
8.47	-0.437	0.663	-0.013	8.48	-0.474	0.737	-0.011	8.55	-0.490	0.770	-0.012	8.61	-0.548	0.894	-0.015	8.34	-0.548	0.863	-0.004	8.24	-0.540	0.865	
10.56	-0.562	1.063	-0.017	10.63	-0.583	1.115	-0.023	10.69	-0.624	1.101	-0.036	10.76	-0.674	1.147	-0.045	10.38	-0.684	1.132	-0.045	10.38	-0.704	1.132	
12.67	-0.665	1.497	-0.025	12.73	-0.693	1.580	-0.037	12.76	-0.699	1.629	-0.045	12.80	-0.748	1.774	-0.055	12.44	-0.754	1.824	-0.055	12.44	-0.775	1.824	
14.77	-0.763	2.013	-0.040	14.80	-0.774	2.078	-0.057	14.87	-0.807	2.085	-0.059	14.92	-0.857	2.188	-0.065	14.59	-0.864	2.248	-0.065	14.59	-0.885	2.248	
16.80	-0.813	2.479	-0.071	16.84	-0.823	2.599	-0.083	16.87	-0.87	2.856	-0.095	16.92	-0.927	3.174	-0.105	16.59	-0.934	3.324	-0.105	16.59	-0.954	3.324	
17.82	-0.836	2.736	-0.095	17.87	-0.87	2.856	-0.095	17.92	-0.927	3.174	-0.105	17.97	-0.977	3.504	-0.115	17.64	-0.984	3.654	-0.115	17.64	-0.994	3.654	
$\text{N=1.30}$ $\text{R=1.9x10}^{-6}$																							
$\text{N=1.40}$ $\text{R=1.9x10}^{-6}$																							
$\text{N=1.50}$ $\text{R=1.9x10}^{-6}$																							
$\text{N=1.60}$ $\text{R=1.9x10}^{-6}$																							
$\text{N=1.70}$ $\text{R=1.9x10}^{-6}$																							
$\text{N=1.90}$ $\text{R=1.9x10}^{-6}$																							
-0.27	-0.023	0.0130	0.002	-0.27	-0.020	0.0135	0.006	-0.27	-0.016	0.0131	0.002	-0.27	-0.018	0.0118	0.006	-0.27	-0.016	0.0118	0.006	-0.27	-0.017	0.0126	
-5.5	-0.037	0.039	-0.001	-5.5	-0.033	0.041	-0.004	-5.5	-0.029	0.039	-0.004	-5.5	-0.026	0.020	0.004	-5.5	-0.026	0.027	0.004	-5.5	-0.045	0.034	
-7.9	-0.048	0.044	-0.001	-7.6	-0.046	0.047	-0.006	-7.8	-0.042	0.045	-0.007	-7.6	-0.043	0.021	0.007	-7.6	-0.039	0.021	0.007	-7.6	-0.059	0.036	
-1.06	-0.068	0.059	-0.001	-1.07	-0.067	0.062	-0.006	-1.07	-0.061	0.064	-0.007	-1.07	-0.062	0.024	0.007	-1.06	-0.061	0.024	0.007	-1.06	-0.086	0.041	
-2.13	-0.129	0.128	-0.001	-2.13	-0.132	0.132	-0.002	-2.13	-0.136	0.132	-0.003	-2.13	-0.138	0.132	-0.005	-2.13	-0.137	0.132	-0.005	-2.13	-0.157	0.132	
-3.19	-0.226	0.226	-0.001	-3.13	-0.231	0.233	-0.002	-3.13	-0.236	0.234	-0.003	-3.13	-0.238	0.236	-0.005	-3.13	-0.237	0.236	-0.005	-3.13	-0.257	0.236	
-4.27	-0.322	0.329	-0.001	-4.29	-0.325	0.329	-0.001	-4.22	-0.320	0.322	-0.002	-4.22	-0.322	0.320	-0.004	-4.20	-0.323	0.320	-0.004	-4.20	-0.343	0.320	
-5.3	-0.421	0.429	-0.001	-5.3	-0.417	0.430	-0.001	-5.3	-0.412	0.431	-0.001	-5.3	-0.414	0.432	-0.001	-5.3	-0.413	0.432	-0.001	-5.3	-0.433	0.432	
-7.9	-0.520	0.529	-0.001	-7.9	-0.516	0.530	-0.001	-7.9	-0.511	0.531	-0.001	-7.9	-0.513	0.532	-0.001	-7.9	-0.512	0.532	-0.001	-7.9	-0.532	0.532	
-1.06	-0.619	0.629	-0.005	-6.67	-0.624	0.641	-0.011	-6.74	-0.629	0.646	-0.011	-6.74	-0.634	0.648	-0.011	-6.71	-0.637	0.650	-0.011	-6.71	-0.657	0.650	
-2.13	-0.718	0.729	-0.013	-7.03	-0.713	0.734	-0.016	-7.03	-0.708	0.735	-0.016	-7.03	-0.710	0.736	-0.016	-7.03	-0.711	0.736	-0.016	-7.03	-0.751	0.736	
-3.19	-0.817	0.834	-0.013	-8.08	-0.813	0.833	-0.016	-8.08	-0.808	0.834	-0.016	-8.08	-0.810	0.835	-0.016	-8.08	-0.811	0.835	-0.016	-8.08	-0.851	0.835	
-4.27	-0.916	0.934	-0.013	-9.03	-0.911	0.934	-0.016	-9.03	-0.906	0.935	-0.016	-9.03	-0.908	0.936	-0.016	-9.03	-0.909	0.936	-0.016	-9.03	-0.961	0.936	
-5.3	-1.015	1.034	-0.013	-11.07	-1.005	1.034	-0.016	-11.07	-1.000	1.034	-0.016	-11.07	-1.002	1.035	-0.016	-11.07	-1.003	1.035	-0.016	-11.07	-1.041	0.936	
-7.9	-1.114	1.134	-0.021	-11.07	-1.095	1.134	-0.022	-11.07	-1.090	1.134	-0.022	-11.07	-1.085	1.134	-0.022	-11.07	-1.080	1.134	-0.022	-11.07	-1.114	0.936	
-1.06	-1.213	1.234	-0.021	-12.21	-1.190	1.234	-0.022	-12.21	-1.185	1.234	-0.022	-12.21	-1.180	1.234	-0.022	-12.21	-1.175	1.234	-0.022	-12.21	-1.214	0.936	
-2.13	-1.312	1.334	-0.021	-13.22	-1.278	1.334	-0.022	-13.22	-1.273	1.334	-0.022	-13.22	-1.268	1.334	-0.022	-13.22	-1.263	1.334	-0.022	-13.22	-1.302	0.936	
-3.19	-1.411	1.434	-0.021	-14.23	-1.358	1.434	-0.022	-14.23	-1.353	1.434	-0.022	-14.23	-1.348	1.434	-0.022	-14.23	-1.343	1.434	-0.022	-14.23	-1.382	0.936	
-4.27	-1.509	1.529	-0.021	-15.24	-1.438	1.529	-0.022	-15.24	-1.433	1.529	-0.022	-15.24	-1.428	1.529	-0.022	-15.24	-1.423	1.529	-0.022	-15.24	-1.462	0.936	
-5.3	-1.608	1.634	-0.021	-16.25	-1.528	1.634	-0.022	-16.25	-1.523	1.634	-0.022	-16.25	-1.518	1.634	-0.022	-16.25	-1.513	1.634	-0.022	-16.25	-1.552	0.936	
-7.9	-1.707	1.734	-0.021	-17.26	-1.618	1.734	-0.022	-17.26	-1.613	1.734	-0.022	-17.26	-1.608	1.734	-0.022	-17.26	-1.603	1.734	-0.022	-17.26	-1.642	0.936	
-1.06	-1.806	1.834	-0.021	-18.27	-1.708	1.834	-0.022	-18.27	-1.703	1.834	-0.022	-18.27	-1.698	1.834	-0.022	-18.27	-1.693	1.834	-0.022	-18.27	-1.732	0.936	
-2.13	-1.905	1.934	-0.021	-19.28	-1.798	1.934	-0.022	-19.28	-1.793	1.934	-0.022	-19.28	-1.788	1.934	-0.022	-19.							

TABLE VIII.- GEOMETRIC CHARACTERISTICS AND WIND-TUNNEL DATA FOR A PLANE TRIANGULAR WING OF ASPECT RATIO 2 WITH NACA 0005-63 SECTION  
 (a) Geometric characteristics

*All dimensions shown in inches  
 unless otherwise noted*



Aspect ratio . . . . .	2
Taper ratio . . . . .	0
Airfoil section (streamwise) . . . . .	NACA 0005-63
Total area, square feet . . . . .	4.014
Mean aerodynamic chord, $\bar{c}$ , feet . . . . .	1.889
Dihedral, degrees . . . . .	0
Twist, degrees . . . . .	0
Incidence, degrees . . . . .	0
Camber . . . . .	None
Distance, wing reference plane to body axis, feet . . . . .	0



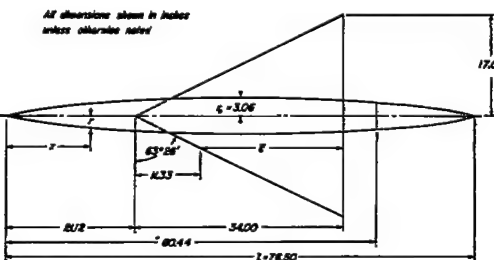
TABLE VIII.- GEOMETRIC CHARACTERISTICS AND WIND-TUNNEL DATA FOR A PLANE TRIANGULAR WING OF ASPECT RATIO 2 WITH NACA 0005-63 SECTION - Continued  
(b) Data obtained in Ames 12-foot pressure wind tunnel

$\alpha$	$C_L$	$C_D$	$C_m$	$\alpha$	$C_L$	$C_D$	$C_m$	$\alpha$	$C_L$	$C_D$	$C_m$													
$M=0.40$				$M=0.50$				$M=0.60$				$M=0.70$				$M=0.80$				$M=0.90$				
$R=1.2 \times 10^6$				$R=1.2 \times 10^6$				$R=1.2 \times 10^6$				$R=1.2 \times 10^6$				$R=1.2 \times 10^6$				$R=1.2 \times 10^6$				
$M=0.95$				$M=0.95$				$M=0.95$				$M=0.95$				$M=0.95$				$M=0.95$				
$R=1.2 \times 10^6$				$R=1.2 \times 10^6$				$R=1.2 \times 10^6$				$R=1.2 \times 10^6$				$R=1.2 \times 10^6$				$R=1.2 \times 10^6$				
0	-0.002	0.0035	0	0	-0.003	0.0053	0	0	-0.002	0.0057	0	0	-0.001	0.0063	0	0	-0.008	0.0064	0.001	0	-0.006	0.0057	0.003	
-3.03	-1.31	0.111	-0.17	0	-1.04	-0.135	0.017	0.19	-3.04	-1.14	0.182	0.023	-3.04	-1.03	0.183	-0.023	-3.04	-1.03	0.185	-0.027	-3.05	-1.15	0.170	-0.15
-8.08	-0.85	0.064	0.11	-2.02	-0.89	0.091	0.013	-2.03	-0.99	-0.995	0.016	-2.03	-0.95	0.016	-0.027	-2.03	-0.95	0.017	-0.027	-2.03	-1.13	0.125	0.024	
-1.01	-0.45	0.060	0.06	-1.01	-0.46	0.077	0.007	-1.01	-0.51	-0.974	0.009	-1.01	-0.50	0.009	-0.027	-1.01	-0.50	0.010	-0.027	-1.01	-0.61	0.053	0.002	
0	0	0.028	0	1.00	-0.003	0.007	0.007	0	-0.002	0.0058	0	0	-0.002	0.0061	0	0	-0.008	0.0061	0.001	0	-0.004	0.0057	0.002	
1.01	0.43	0.028	-0.005	-1.01	1.01	-0.040	0.009	-0.007	1.01	0.040	-0.040	0.007	1.01	0.047	0.0073	-0.009	1.01	0.048	-0.007	1.01	0.043	0.006	-0.009	
2.08	0.88	0.061	-0.11	2.08	0.79	0.077	0.034	2.08	0.86	0.087	0.014	2.08	0.90	0.090	-0.015	2.08	0.90	0.091	-0.015	2.08	0.93	0.099	0.023	
3.03	1.21	0.082	-0.11	3.03	1.25	0.111	0.013	3.03	1.20	0.114	0.020	3.04	1.16	0.112	-0.024	3.04	1.16	0.115	-0.025	3.04	1.19	0.119	0.032	
4.05	1.56	0.112	-0.22	4.05	1.70	0.148	0.023	4.05	1.77	0.148	0.023	4.05	1.64	0.149	-0.031	4.05	1.64	0.150	-0.032	4.06	1.72	0.150	-0.043	
5.06	2.12	0.126	-0.28	5.06	2.20	0.160	0.030	5.06	2.20	0.163	0.028	5.06	1.93	0.162	-0.041	5.07	1.93	0.164	-0.043	5.07	2.07	0.164	-0.058	
6.07	2.66	0.126	-0.33	6.07	2.74	0.159	0.038	6.07	2.74	0.161	0.038	6.07	2.48	0.163	-0.050	6.08	2.48	0.164	-0.054	6.09	2.70	0.164	-0.070	
8.10	3.92	0.056	-0.49	8.10	3.70	0.057	0.050	8.10	3.70	0.058	0.050	8.11	3.10	0.059	-0.070	8.11	3.10	0.060	-0.070	8.12	3.67	0.061	-0.074	
10.12	4.94	0.073	-0.62	10.12	4.72	0.068	0.068	10.12	4.72	0.069	0.068	10.12	4.06	0.070	-0.090	10.12	4.06	0.071	-0.090	10.12	4.67	0.071	-0.109	
12.15	5.46	1.037	-0.67	12.15	5.28	1.037	0.068	12.15	5.28	1.038	0.068	12.15	4.51	1.039	-0.090	12.15	4.51	1.040	-0.090	12.15	5.07	1.041	-0.111	
14.17	6.40	1.136	-0.78	14.17	6.32	1.136	0.074	14.17	6.32	1.137	0.074	14.17	5.57	1.138	-0.098	14.17	5.57	1.139	-0.098	14.17	6.15	1.140	-0.117	
16.20	7.40	1.192	-0.90	16.20	7.40	1.192	0.085	16.20	7.40	1.193	0.085	16.20	6.72	1.194	-0.107	16.21	6.72	1.195	-0.107	16.21	7.29	1.196	-0.127	
18.22	8.13	1.202	-1.06	18.22	8.23	1.204	0.093	18.22	8.23	1.205	0.093	18.22	7.54	1.207	-0.127	18.23	7.54	1.208	-0.127	18.23	8.10	1.209	-0.146	
20.24	9.34	1.212	-1.19	20.24	9.34	1.209	0.106	20.24	9.34	1.210	0.106	20.24	8.64	1.210	-0.147	20.25	8.64	1.211	-0.147	20.25	9.20	1.212	-0.166	
22.27	1.015	1.351	-1.13	22.27	1.015	1.351	0.120	22.27	1.015	1.352	0.120	22.27	9.43	1.353	-0.187	22.28	9.43	1.354	-0.187	22.28	1.018	1.354	-0.187	
24.29	1.165	1.450	-1.21	24.29	1.165	1.450	0.131	24.29	1.165	1.451	0.131	24.29	1.094	1.451	-0.207	24.30	1.094	1.452	-0.207	24.30	1.166	1.452	-0.207	
0	-0.002	0.004	0	0	-0.007	0.005	0.001	0	-0.006	0.0060	0.001	0	0	0.003	0.004	0	0	0	0.003	0.004	0	0	0	0.003
$M=0.28$				$M=0.40$				$M=0.50$				$M=0.60$				$M=0.80$				$M=0.90$				
$R=3.0 \times 10^6$				$R=3.0 \times 10^6$				$R=3.0 \times 10^6$				$R=3.0 \times 10^6$				$R=3.0 \times 10^6$				$R=3.0 \times 10^6$				
0	-0.004	0.0039	0.001	0	0.002	0.0059	0	0	-0.001	0.0077	0	0	-0.003	0.0060	0.001	0	-0.002	0.0061	0.001	0	-0.003	0.0063	0.001	
-3.03	-1.29	0.109	-0.16	-3.03	-1.29	0.109	0.017	-3.03	-1.27	0.104	0.018	-3.04	-1.12	0.116	-0.022	-3.04	-1.12	0.117	-0.022	-3.04	-1.19	0.126	-0.116	
-2.02	-0.86	0.084	0.16	-2.02	-0.87	0.077	0.011	-2.02	-0.86	0.088	0.012	-2.02	-0.86	0.089	0.014	-2.02	-0.86	0.090	0.015	-2.02	-0.93	0.096	0.016	
-1.01	-0.44	0.089	0.009	-1.01	-0.44	0.085	0.005	-1.01	-0.44	0.086	0.006	-1.01	-0.43	0.087	0.007	-1.01	-0.43	0.088	0.008	-1.01	-0.49	0.097	0.007	
0	-0.04	0.045	0.001	0	-0.01	0.054	0.002	0	0	0.052	0	0	0	0.053	0.002	0	0	0.054	0.003	0	0.055	0.002	0.001	
1.01	0.42	0.028	-0.027	1.01	0.40	0.064	-0.002	1.01	0.38	0.065	-0.002	1.01	0.38	0.066	-0.007	1.01	0.38	0.067	-0.006	1.01	0.44	0.070	-0.006	
2.02	0.61	0.070	-0.11	2.02	0.68	0.078	0.014	2.02	0.68	0.078	0.015	2.02	0.68	0.079	0.020	2.02	0.68	0.080	0.021	2.02	0.72	0.087	0.019	
3.03	1.19	0.097	-0.15	3.03	1.14	0.093	0.015	3.03	1.14	0.097	0.017	3.03	1.14	0.098	0.024	3.03	1.14	0.099	0.025	3.03	1.19	0.103	0.027	
4.04	1.82	0.131	-0.22	4.04	1.84	0.151	0.021	4.04	1.84	0.151	0.021	4.04	1.84	0.152	0.028	4.04	1.84	0.153	0.029	4.04	1.88	0.153	0.034	
5.06	2.29	0.143	-0.27	5.06	2.25	0.159	0.027	5.06	2.25	0.161	0.027	5.06	2.25	0.162	0.034	5.06	2.25	0.163	0.035	5.06	2.34	0.163	0.043	
6.07	2.47	0.143	-0.32	6.07	2.43	0.163	0.034	6.07	2.43	0.164	0.034	6.07	2.43	0.165	0.042	6.07	2.43	0.166	0.043	6.07	2.52	0.166	0.053	
8.09	3.44	0.143	-0.48	8.09	3.40	0.161	0.047	8.09	3.40	0.162	0.047	8.09	3.40	0.163	0.055	8.10	3.40	0.164	0.056	8.11	3.59	0.164	0.066	
10.11	4.46	0.149	-0.69	10.11	4.36	0.166	0.068	10.11	4.36	0.167	0.068	10.11	4.36	0.168	0.075	10.12	4.36	0.169	0.076	10.12	4.65	0.169	0.086	
12.14	5.46	0.170	-0.70	12.14	5.29	0.180	0.065	12.14	5.29	0.181	0.065	12.14	5.29	0.182	0.078	12.15	5.29	0.183	0.078	12.15	5.66	0.183	0.089	
14.16	6.20	1.239	-0.79	14.16	6.16	1.236	0.075	14.16	6.16	1.237	0.075	14.16	6.16	1.238	0.089	14.17	6.16	1.239	0.089	14.17	6.56	1.239	0.115	
16.19	7.18	1.282	-0.90	16.19	7.18	1.282	0.087	16.19	7.18	1.283	0.087	16.20	7.18	1.284	0.092	16.21	7.18	1.285	0.092	16.21	7.61	1.285	0.115	
18.21	8.08	1.294	-0.99	18.21	8.12	1.289	0.098	18.21	8.12	1.290	0.098	18.21	8.12	1.291	0.105</td									

TABLE VIII.- GEOMETRIC CHARACTERISTICS AND WIND-TUNNEL DATA FOR A PLANE TRIANGULAR WING OF ASPECT RATIO 2 WITH NACA 0005-63 SECTION - Concluded  
(c) Data obtained in Ames 6- by 6-foot supersonic wind tunnel

$a$	$c_L$	$c_D$	$c_m$	$a$	$c_L$	$c_D$	$c_m$	$a$	$c_L$	$c_D$	$c_m$	$a$	$c_L$	$c_D$	$c_m$	$a$	$c_L$	$c_D$	$c_m$	$a$	$c_L$	$c_D$	$c_m$	
$M=1.30 \quad R=1.3 \times 10^6$																								
-0.01	-0.012	0.0129	0.005	0	-0.001	0.0119	0.002	0	0.004	0.0124	0	0	0.003	0.0124	-0.001	0	0.003	0.0125	0	0	0.002	0.0068	0	
-1.02	-0.056	0.0135	0.015	-1.01	-0.046	0.0127	0.013	-1.01	-0.049	0.0129	0.011	-1.01	-0.046	0.0146	0.010	-1.02	-0.053	0.0133	0.008	-1.06	-0.043	0.0075	0.006	
-2.03	-0.108	0.0138	0.011	-2.03	-0.091	0.0120	0.024	-2.03	-0.096	0.0126	0.022	-2.03	-0.093	0.0165	0.021	-2.03	-0.075	0.0149	0.019	-2.13	-0.090	0.0090	0.013	
-3.04	-0.155	0.0139	0.013	-3.05	-0.137	0.0180	0.056	-3.04	-0.149	0.0186	0.033	-3.04	-0.148	0.0199	0.032	-3.04	-0.113	0.0178	0.028	-3.19	-0.133	0.0112	0.019	
-4.05	-0.201	0.0124	0.006	-4.06	-0.180	0.0126	0.005	-4.06	0	0.0126	0	-4.06	0.002	0.0134	0	-4.06	-0.153	0.0220	0.038	0	0	0.0070	0	
-5.06	-0.248	0.0129	0.009	-5.07	-0.221	0.0133	-0.009	-5.07	-0.241	0.013	0.034	-5.07	-0.241	0.0144	0.010	-5.07	-0.211	0.011	0.001	0	0.001	0.0078	-0.007	
-6.07	-0.293	0.0138	0.018	-6.08	-0.266	0.0136	0.023	-6.08	-0.286	0.013	0.059	-6.08	-0.286	0.0159	0.058	-6.08	-0.222	0.0119	-0.009	2.14	0.098	0.0095	-0.014	
-7.08	-0.337	0.0137	0.020	-7.09	-0.306	0.0131	0.027	-7.09	-0.326	0.013	0.065	-7.09	-0.326	0.0179	0.064	-7.09	-0.249	0.0140	-0.020	3.21	0.142	0.0123	-0.020	
-8.09	-0.377	0.0130	0.023	-8.10	-0.347	0.0129	0.043	-8.10	-0.367	0.013	0.066	-8.10	-0.367	0.0249	0.043	-8.10	-0.270	0.0160	-0.040	4.25	0.177	0.0155	-0.026	
-9.10	-0.417	0.0129	0.026	-9.11	-0.388	0.0128	0.056	-9.11	-0.408	0.013	0.067	-9.11	-0.408	0.0306	0.056	-9.11	-0.280	0.0166	-0.046	5.32	0.226	0.017	-0.034	
-10.11	-0.457	0.0129	0.028	-10.12	-0.419	0.0128	0.066	-10.11	-0.439	0.013	0.068	-10.11	-0.439	0.0308	0.068	-10.11	-0.290	0.0170	-0.048	6.40	0.287	0.0182	-0.044	
-11.12	-0.497	0.0129	0.030	-11.13	-0.450	0.0128	0.076	-11.12	-0.470	0.013	0.070	-11.12	-0.470	0.0310	0.070	-11.12	-0.300	0.0178	-0.050	7.48	0.348	0.0190	-0.046	
-12.13	-0.537	0.0129	0.032	-12.14	-0.481	0.0128	0.086	-12.13	-0.501	0.013	0.072	-12.13	-0.501	0.0312	0.072	-12.13	-0.320	0.0186	-0.052	8.52	0.408	0.0198	-0.048	
-13.14	-0.577	0.0129	0.034	-13.15	-0.512	0.0128	0.096	-13.14	-0.532	0.013	0.074	-13.14	-0.532	0.0314	0.074	-13.14	-0.340	0.0194	-0.054	9.56	0.468	0.0200	-0.050	
-14.15	-0.617	0.0129	0.036	-14.16	-0.543	0.0128	0.106	-14.15	-0.563	0.013	0.076	-14.15	-0.563	0.0316	0.076	-14.15	-0.358	0.0192	-0.056	10.60	0.528	0.0202	-0.052	
-15.16	-0.657	0.0129	0.038	-15.17	-0.574	0.0128	0.116	-15.16	-0.594	0.013	0.078	-15.16	-0.594	0.0318	0.078	-15.16	-0.378	0.0190	-0.058	11.64	0.588	0.0204	-0.054	
-16.17	-0.697	0.0129	0.040	-16.18	-0.605	0.0128	0.126	-16.17	-0.625	0.013	0.080	-16.17	-0.625	0.0320	0.080	-16.17	-0.398	0.0188	-0.060	12.70	0.648	0.0206	-0.056	
$M=0.81 \quad R=3.0 \times 10^6$																								
$M=0.91 \quad R=3.0 \times 10^6$																								
$M=1.30 \quad R=3.0 \times 10^6$																								
0	0.001	0.0069	0	0	0.001	0.0069	0	0	-0.012	0.0121	0.011	0	0	0.0124	0.001	0	0	0.002	0.0122	0	0	0.001	0.0123	0
-1.06	-0.042	0.0073	0.005	-1.07	-0.089	0.0098	0.015	-1.06	-0.058	0.0130	0.019	-1.06	-0.046	0.0133	0.012	-1.06	-0.040	0.0189	0.011	-1.08	-0.038	0.0130	0.010	
-2.13	-0.090	0.0051	0.014	-2.12	-0.150	0.0134	0.026	-2.12	-0.106	0.0158	0.031	-2.12	-0.087	0.0153	0.028	-2.12	-0.082	0.0128	0.024	-2.14	-0.078	0.0150	0.020	
-3.20	-0.138	0.0120	0.023	-3.21	-0.187	0.0134	0.043	-3.20	-0.128	0.0168	0.053	-3.20	-0.114	0.0176	0.043	-3.20	-0.097	0.0153	0.031	-3.27	-0.100	0.0154	0.031	
0	0.001	0.0065	0	0	0.001	0.0069	0	0	-0.012	0.0124	0.006	0	0	0.0124	0.001	0	0	0.002	0.0124	0	0	0.001	0.0123	0
1.08	0.043	0.0078	0.008	1.08	0.052	0.0081	0.009	1.08	0.036	0.0138	0.006	1.08	0.043	0.0133	0.001	1.08	0.044	0.013	0.011	1.03	0.043	0.0132	0.011	
2.15	0.097	0.0100	0.015	2.16	0.104	0.0104	0.020	2.15	0.058	0.0155	0.018	2.15	0.058	0.0167	0.009	2.15	0.058	0.0156	0.009	2.05	0.089	0.0154	0.026	
3.22	0.144	0.0131	0.024	3.24	0.156	0.0142	0.028	3.22	0.098	0.0189	0.031	3.22	0.098	0.0196	0.031	3.22	0.072	0.0193	0.032	3.12	0.126	0.0192	0.032	
4.30	0.198	0.0133	0.033	4.32	0.213	0.0127	0.039	4.30	0.140	0.0241	0.044	4.30	0.140	0.0249	0.044	4.30	0.110	0.0249	0.044	4.10	0.170	0.0243	0.044	
5.37	0.256	0.0251	0.043	5.42	0.275	0.0259	0.050	5.37	0.232	0.0319	0.052	5.37	0.232	0.0327	0.052	5.37	0.194	0.0326	0.052	5.13	0.214	0.0306	0.053	
6.46	0.318	0.0362	0.052	6.49	0.338	0.0405	0.061	6.46	0.286	0.0404	0.071	6.46	0.286	0.0405	0.068	6.46	0.246	0.0397	0.066	6.16	0.266	0.0396	0.065	
8.08	0.394	0.0299	0.065	8.13	0.413	0.0506	0.073	8.08	0.348	0.0574	0.085	8.08	0.348	0.0576	0.085	8.08	0.304	0.0570	0.085	7.68	0.313	0.0551	0.079	
9.70	0.464	0.0783	0.072	9.74	0.487	0.0549	0.085	9.70	0.424	0.0776	0.093	9.70	0.424	0.0794	0.093	9.70	0.383	0.0790	0.093	9.28	0.372	0.0795	0.093	
11.29	-0.217	-0.1022	-0.073	11.30	-0.237	-0.113	-0.086	11.29	-0.187	-0.202	-0.126	11.29	-0.187	-0.202	-0.126	11.29	-0.147	-0.191	-0.109	10.76	-0.229	-0.191	-0.106	
12.33	-0.263	-0.140	-0.094	12.34	-0.283	-0.133	-0.094	12.33	-0.235	-0.202	-0.126	12.33	-0.235	-0.202	-0.126	12.33	-0.192	-0.187	-0.124	12.30	-0.249	-0.184	-0.120	
14.44	-0.395	-0.178	-0.108	14.45	-0.415	-0.202	-0.126	14.44	-0.355	-0.229	-0.153	14.44	-0.355	-0.229	-0.153	14.44	-0.317	-0.228	-0.153	13.84	-0.339	-0.229	-0.152	
16.18	-0.775	-0.226	-0.123																	15.39	-0.253	-0.226	-0.152	
$M=1.70 \quad R=3.0 \times 10^6$																								
$M=0.61 \quad R=7.5 \times 10^6$																								
$M=0.79 \quad R=7.5 \times 10^6$																								
0	0.003	0.0126	0	0	-0.001	0.0087	0	-2.25	-0.109	0.0106	0.013	-2.27	-0.113	0.0108	0.017	0	0.01	0.004	0.0128	0.005	0	0.001	0.0124	0
-1.02	-0.256	-0.133	0.10	-1.11	-0.253	-0.093	0.007	-2.05	-0.082	0.008	0.012	-2.07	-0.134	0.0082	0.017	-1.02	-0.065	0.0148	0.019	-1.06	-0.045	0.0152	0.018	
-2.04	-0.075	-0.135	0.09	-2.21	-0.077	-0.112	0.014	-1.95	-0.084	0.0082	0.013	-1.97	-0.135	0.0084	0.017	-2.04	-0.052	0.0127	0.018	-2.11	-0.077	0.0151	0.020	
-3.06	-0.113	-0.187	0.09	-3.30	-0.144	-0.108	0.021	-2.91	-0.099	0.009	0.015	-2.93	-0.151	0.0092	0.019	-3.06	-0.071	0.0121	0.016	-3.21	-0.120	0.0152	0.021	
0	-0.001	0.0123	0	-0.02	-0.010	0.0086	0.001	0.																

TABLE IX.- GEOMETRIC CHARACTERISTICS AND WIND-TUNNEL  
DATA FOR A PLANE TRIANGULAR WING OF ASPECT  
RATIO 2 WITH NACA 0008-63 SECTION  
(a) Geometric characteristics



Aspect ratio . . . . .	2
Taper ratio . . . . .	0
Airfoil section (streamwise) . . . . .	NACA 0008-63
Total chord . . . . .	54.00
Mean aerodynamic chord, $C$ , feet . . . . .	1.889
Rhedral, degrees . . . . .	0
Twist, degrees . . . . .	0
Incidence, degrees . . . . .	0
Camber . . . . .	None
Distance, wing reference plane to body axis, feet . . . . .	0

(b) Data obtained in Ames 12-foot pressure wind tunnel

$\alpha$	$C_L$	$C_D$	$C_M$	$\alpha$	$C_L$	$C_D$	$C_M$	$\alpha$	$C_L$	$C_D$	$C_M$	$\alpha$	$C_L$	$C_D$	$C_M$	$\alpha$	$C_L$	$C_D$	$C_M$	$\alpha$	$C_L$	$C_D$	$C_M$
$M=0.34 \quad R=3.0 \times 10^6$																							
0	0	-0.0081	0.001	0	-0.003	0.0067	0.001	0	-0.001	0.0074	0.001	0	-0.004	0.0061	0.001	0	-0.004	0.0079	0.002	0	-0.004	0.0081	0.002
-3.04	-1.20	-0.0153	-0.001	-3.03	-1.21	-0.0152	-0.001	-3.02	-1.22	-0.0153	-0.001	-3.01	-1.21	-0.0157	-0.002	-3.00	-1.23	-0.0157	-0.002	-2.99	-1.24	-0.0158	-0.002
-6.08	-2.40	-0.0291	-0.001	-6.07	-2.41	-0.0290	-0.001	-6.06	-2.42	-0.0291	-0.001	-6.05	-2.41	-0.0292	-0.002	-6.04	-2.43	-0.0292	-0.002	-6.03	-2.44	-0.0293	-0.002
-1.01	-0.61	-0.0186	-0.006	-1.01	-0.62	-0.0185	-0.006	-1.01	-0.63	-0.0186	-0.006	-1.01	-0.62	-0.0187	-0.006	-1.00	-0.64	-0.0187	-0.006	-1.00	-0.65	-0.0188	-0.006
0	-0.02	-0.0067	-0.001	0	-0.002	-0.0063	-0.001	0	-0.002	-0.0076	-0.001	0	-0.002	-0.0073	-0.001	0	-0.003	-0.0076	-0.001	0	-0.003	-0.0076	-0.001
1.01	0.62	-0.0186	-0.006	1.01	0.62	-0.0185	-0.006	1.01	0.63	-0.0186	-0.006	1.01	0.62	-0.0187	-0.006	1.00	0.64	-0.0187	-0.006	1.00	0.65	-0.0188	-0.006
2.00	1.20	-0.0291	-0.001	2.02	1.21	-0.0290	-0.001	2.02	1.22	-0.0291	-0.001	2.02	1.21	-0.0292	-0.001	2.00	1.23	-0.0292	-0.001	2.00	1.24	-0.0293	-0.001
3.05	1.81	-0.0109	-0.015	3.05	1.82	-0.0109	-0.015	3.05	1.83	-0.0109	-0.015	3.05	1.82	-0.0117	-0.016	3.05	1.84	-0.0123	-0.019	3.04	1.81	-0.0123	-0.019
4.04	2.41	-0.0131	-0.026	4.04	2.42	-0.0130	-0.026	4.04	2.43	-0.0131	-0.026	4.04	2.42	-0.0135	-0.026	4.05	2.43	-0.0137	-0.026	4.05	2.44	-0.0137	-0.026
5.03	3.02	-0.0151	-0.036	5.03	3.03	-0.0150	-0.036	5.03	3.04	-0.0151	-0.036	5.03	3.03	-0.0158	-0.036	5.05	3.05	-0.0162	-0.033	5.06	3.03	-0.0162	-0.033
6.02	3.62	-0.0177	-0.039	6.02	3.63	-0.0176	-0.039	6.02	3.64	-0.0177	-0.039	6.02	3.63	-0.0185	-0.039	6.04	3.65	-0.0190	-0.039	6.05	3.64	-0.0190	-0.039
7.01	4.23	-0.0203	-0.042	7.01	4.24	-0.0202	-0.042	7.01	4.25	-0.0203	-0.042	7.01	4.24	-0.0211	-0.042	7.03	4.26	-0.0215	-0.042	7.04	4.25	-0.0215	-0.042
8.00	4.83	-0.0227	-0.045	8.03	4.84	-0.0226	-0.045	8.03	4.85	-0.0227	-0.045	8.03	4.84	-0.0235	-0.045	8.05	4.86	-0.0241	-0.045	8.06	4.85	-0.0241	-0.045
9.00	5.43	-0.0252	-0.048	9.00	5.44	-0.0251	-0.048	9.00	5.45	-0.0252	-0.048	9.00	5.44	-0.0260	-0.048	9.02	5.46	-0.0265	-0.048	9.03	5.45	-0.0265	-0.048
10.00	6.03	-0.0277	-0.051	10.11	6.05	-0.0276	-0.051	10.11	6.07	-0.0277	-0.051	10.11	6.05	-0.0285	-0.051	10.13	6.08	-0.0291	-0.051	10.14	6.07	-0.0291	-0.051
11.00	6.63	-0.0302	-0.054	12.11	6.75	-0.0299	-0.054	12.11	6.87	-0.0302	-0.054	12.11	6.75	-0.0310	-0.054	12.13	6.88	-0.0317	-0.054	12.14	6.87	-0.0317	-0.054
12.00	7.23	-0.0327	-0.057	13.11	7.35	-0.0324	-0.057	13.11	7.47	-0.0327	-0.057	13.11	7.35	-0.0335	-0.057	13.13	7.58	-0.0342	-0.057	13.14	7.57	-0.0342	-0.057
13.00	7.83	-0.0352	-0.060	14.16	7.95	-0.0349	-0.060	14.16	8.07	-0.0352	-0.060	14.16	7.95	-0.0360	-0.060	14.18	8.18	-0.0367	-0.060	14.19	8.17	-0.0367	-0.060
14.00	8.43	-0.0377	-0.063	15.16	8.55	-0.0374	-0.063	15.16	8.67	-0.0377	-0.063	15.16	8.55	-0.0385	-0.063	15.18	8.78	-0.0392	-0.063	15.19	8.77	-0.0392	-0.063
15.00	9.03	-0.0402	-0.066	16.18	9.15	-0.0399	-0.066	16.18	9.27	-0.0402	-0.066	16.18	9.15	-0.0410	-0.066	16.20	9.38	-0.0417	-0.066	16.21	9.37	-0.0417	-0.066
16.00	9.63	-0.0427	-0.069	17.20	9.75	-0.0424	-0.069	17.20	9.87	-0.0427	-0.069	17.20	9.75	-0.0435	-0.069	17.22	9.98	-0.0442	-0.069	17.23	9.97	-0.0442	-0.069
17.00	10.23	-0.0452	-0.072	18.21	10.35	-0.0449	-0.072	18.21	10.47	-0.0452	-0.072	18.21	10.35	-0.0463	-0.072	18.23	10.58	-0.0470	-0.072	18.24	10.57	-0.0470	-0.072
18.00	10.83	-0.0477	-0.075	19.21	10.95	-0.0474	-0.075	19.21	11.07	-0.0477	-0.075	19.21	10.95	-0.0486	-0.075	19.23	11.18	-0.0493	-0.075	19.24	11.17	-0.0493	-0.075
19.00	11.43	-0.0502	-0.078	20.21	11.55	-0.0499	-0.078	20.21	11.67	-0.0502	-0.078	20.21	11.55	-0.0513	-0.078	20.23	11.78	-0.0520	-0.078	20.24	11.77	-0.0520	-0.078
20.00	12.03	-0.0527	-0.081	21.21	12.15	-0.0524	-0.081	21.21	12.27	-0.0527	-0.081	21.21	12.15	-0.0536	-0.081	21.23	12.38	-0.0543	-0.081	21.24	12.37	-0.0543	-0.081
21.00	12.63	-0.0552	-0.084	22.21	12.75	-0.0549	-0.084	22.21	12.87	-0.0552	-0.084	22.21	12.75	-0.0563	-0.084	22.23	12.98	-0.0570	-0.084	22.24	12.97	-0.0570	-0.084
22.00	13.23	-0.0577	-0.087	23.21	13.35	-0.0574	-0.087	23.21	13.47	-0.0577	-0.087	23.21	13.35	-0.0589	-0.087	23.23	13.58	-0.0596	-0.087	23.24	13.57	-0.0596	-0.087
23.00	13.83	-0.0602	-0.090	24.21	13.95	-0.0599	-0.090	24.21	14.07	-0.0602	-0.090	24.21	13.95	-0.0613	-0.090	24.23	14.18	-0.0620	-0.090	24.24	14.17	-0.0620	-0.090
24.00	14.43	-0.0627	-0.093	25.21	14.55	-0.0624	-0.093	25.21	14.67	-0.0627	-0.093	25.21	14.55	-0.0639	-0.093	25.23	14.78	-0.0646	-0.093	25.24	14.77	-0.0646	-0.093
25.00	15.03	-0.0652	-0.096	26.21	15.15	-0.0649	-0.096	26.21	15.27	-0.0652	-0.096	26.21	15.15	-0.0666	-0.096	26.23	15.38	-0.0673	-0.096	26.24	15.37	-0.0673	-0.096
26.00	15.63	-0.0677	-0.100	27.21	15.75	-0.0674	-0.100	27.21	15.87	-0.0677	-0.100	27.21	15.75	-0.0691	-0.100	27.23	15.98	-0.0698	-0.100	27.24	15.97	-0.0698	-0.100
27.00	16.23	-0.0702	-0.103	28.21	16.35	-0.0699	-0.103	28.21	16.47	-0.0702	-0.103	28.21	16.35	-0.0719	-0.103	28.23	16.58	-0.0726	-0.103	28.24	16.57	-0.0726	-0.103
28.00	16.83	-0.0727	-0.106	29.21	16.95	-0.0724	-0.106	29.21	17.07	-0.0727	-0.106	29.21	16.95	-0.0744	-0.106	29.23	17.18	-0.0751	-0.106	29.24	17.17	-0.0751	-0.106
29.00	17.43	-0.0752	-0.109	30.21	17.55	-0.0749	-0.109	30.21	17.67	-0.0752	-0.109	30.21	17.55	-0.0770	-0.109	30.23	17.78	-0.0777	-0.109	30.24	17.77	-0.0777	-0.109
30.00	18.03	-0.0777	-0.112	31.21	18.15	-0.0774	-0.112	31.21	18.27	-0.0777	-0.112	31.21	18.15	-0.0795	-0.112	31.23	18.38	-0.0802	-0.112	31.24	18.37	-0.0802	-0.112
31.00	18.63	-0.0802	-0.115	32.21	18.75	-0.0799	-0.115	32.21	18.87	-0.0802	-0.115	32.21	18.75	-0.0823	-0.115	32.23	18.98	-0.0830	-0.115	32.24	18.97	-0.0830	-0.115
32.00	19.23	-0.0827	-0.118	33.21	19.35	-0.0824	-0.118	33.21	19.47	-0.0827	-0.118	33.21	19.35	-0.0846	-0.118	33.23	19.58	-0.0853	-0.118	33.24	19.57	-0.0853	-0.118
33.00	19.83	-0.0852	-0.121	34.21	19.95	-0.0849	-0.121	34.21	20.07	-0.0852	-0.121	34.21	19.95	-0.0870	-0.121	34.23	20.18	-0.0877	-0.121	34.24	20.17	-0.0877	-0.121
34.00	20.43	-0.0877	-0.124	35.21	20.55	-0.0874	-0.124	35.21	20.67	-0.0877	-0.124	35.21	20.55	-0.0895	-0.124	35.23	20.78	-0.0902	-0.124	35.24	20.77	-0.0902	-0.124
35.00	21.03	-0.0902	-0.127	36.21	21.15	-0.0899	-0.127	36.21	21.27	-0.0902	-0.127	36.21	21.15	-0.0920	-0.127	36.23							

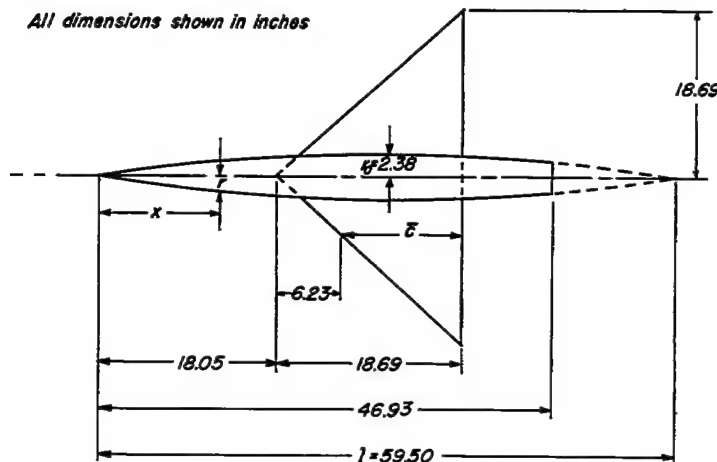
TABLE IX.- GEOMETRIC CHARACTERISTICS AND WIND-TUNNEL DATA  
FOR A PLANE TRIANGULAR WING OF ASPECT RATIO 2 WITH  
NACA 0008-63 SECTION - Concluded

(c) Data obtained in Ames 6- by 6-foot supersonic wind tunnel

$a$	$c_L$	$c_D$	$c_m$	$a$	$c_L$	$c_D$	$c_m$	$a$	$c_L$	$c_D$	$c_m$	$a$	$c_L$	$c_D$	$c_m$	$a$	$c_L$	$c_D$	$c_m$	$a$	$c_L$	$c_D$	$c_m$
$M=1.30 \quad R=1.5 \times 10^6$																							
-3.05	-0.174	0.0270	0.047	-3.05	-0.138	0.0288	0.037	-3.05	-0.131	0.0256	0.035	-3.04	-0.130	0.0281	0.032	-3.04	-0.123	0.0265	0.031	-3.09	-0.163	0.0285	0.046
-1.53	-0.098	0.0214	0.026	-1.53	-0.061	0.0215	0.021	-1.52	-0.074	0.0204	0.018	-1.52	-0.067	0.0195	0.016	-1.52	-0.062	0.0195	0.015	-1.55	-0.090	0.0231	0.027
-0.01	-0.023	0.016	0.008	0	-0.010	0.0156	0.003	0	-0.009	0.0168	0.005	0	-0.004	0.0160	0.001	0	-0.005	0.0162	0.001	0	-0.017	0.0209	0.006
1.52	-0.045	0.0205	-0.009	1.52	-0.011	0.0033	0.011	1.52	-0.026	0.0200	0.018	1.52	-0.017	0.0183	0.013	1.52	-0.026	0.0204	0.012	1.53	-0.054	0.0221	-0.010
3.04	-0.116	0.0250	-0.027	3.04	-0.118	0.0247	0.027	3.04	-0.127	0.0247	0.028	3.04	-0.115	0.0255	0.028	3.04	-0.127	0.0244	0.028	3.09	-0.125	0.0253	-0.029
4.56	-0.189	0.0320	-0.043	4.56	-0.186	0.0317	0.044	4.56	-0.197	0.0319	0.041	4.56	-0.180	0.0322	0.043	4.56	-0.170	0.0312	0.040	4.63	-0.198	0.0343	-0.047
6.09	-0.259	0.0427	-0.065	6.09	-0.248	0.0418	0.062	6.08	-0.242	0.0422	0.058	6.07	-0.238	0.0410	0.057	6.08	-0.229	0.0403	0.053	6.17	-0.266	0.0432	-0.064
7.61	-0.331	0.0579	-0.083	7.61	-0.320	0.0570	0.076	7.61	-0.301	0.0575	0.072	7.59	-0.293	0.0560	0.070	7.60	-0.274	0.0558	0.066	7.71	-0.340	0.0604	-0.083
9.14	-0.401	0.0761	-0.097	9.13	-0.384	0.0748	0.092	9.13	-0.365	0.0720	0.087	9.11	-0.355	0.0705	0.085	9.12	-0.333	0.0681	0.078	9.26	-0.407	0.0789	-0.099
10.66	-0.474	0.0983	-0.116	10.66	-0.444	0.0992	0.106	10.64	-0.429	0.0937	0.102	10.63	-0.414	0.0902	0.093	10.64	-0.393	0.0868	0.092	10.80	-0.472	0.1009	-0.116
12.18	-0.537	0.1234	-0.132	12.18	-0.506	0.1197	0.121	12.18	-0.487	0.1168	0.115	12.15	-0.469	0.1122	0.111	12.16	-0.446	0.1080	0.104	12.35	-0.538	0.1265	-0.131
$M=1.40 \quad R=3.0 \times 10^6$																							
-3.08	-0.184	0.0278	0.038	-3.08	-0.137	0.0269	0.035	-3.09	-0.132	0.0260	0.033	-3.08	-0.123	0.0255	0.031	-3.08	-0.170	0.0287	0.048	-3.17	-0.150	0.0295	0.039
-1.55	-0.077	0.0226	0.020	-1.54	-0.071	0.0222	0.018	-1.54	-0.066	0.0218	0.017	-1.53	-0.063	0.0212	0.016	-1.60	-0.099	0.0214	0.028	-1.59	-0.062	0.0206	0.007
-0.01	-0.006	0.0205	0.003	0	-0.004	0.0204	0.002	0	-0.004	0.0202	0.002	-0.003	-0.001	0.0190	0.001	0	-0.018	0.0215	0.009	0	-0.023	0.0214	0.003
1.54	-0.059	0.0213	-0.013	1.54	-0.050	0.0219	-0.014	1.54	-0.047	0.0217	-0.014	1.54	-0.047	0.0203	-0.013	1.58	-0.056	0.0226	-0.011	1.58	-0.062	0.0231	-0.013
3.08	-0.127	0.0663	-0.030	3.08	-0.126	0.0655	-0.030	3.07	-0.120	0.0656	-0.029	3.08	-0.114	0.0645	-0.027	3.16	-0.128	0.0623	-0.029	3.16	-0.130	0.0673	-0.031
4.63	-0.194	0.094	-0.046	4.62	-0.192	0.0948	-0.046	4.62	-0.182	0.0946	-0.046	4.62	-0.178	0.0937	-0.042	4.75	-0.204	0.0936	-0.048	4.75	-0.202	0.0950	-0.049
6.16	-0.260	0.044	-0.062	6.16	-0.254	0.0447	-0.062	6.15	-0.238	0.0432	-0.058	6.15	-0.229	0.0413	-0.055	6.34	-0.276	0.0449	-0.067	6.34	-0.288	0.0460	-0.069
7.71	-0.328	0.0588	-0.076	7.70	-0.317	0.0586	-0.073	7.69	-0.299	0.0567	-0.072	7.65	-0.289	0.0546	-0.069	7.93	-0.349	0.0616	-0.085	7.93	-0.339	0.0614	-0.081
9.25	-0.390	0.0767	-0.093	9.25	-0.375	0.0758	-0.093	9.24	-0.357	0.0731	-0.086	9.22	-0.341	0.0701	-0.081	9.32	-0.419	0.0811	-0.108	9.31	-0.400	0.0794	-0.095
10.80	-0.456	0.0987	-0.109	10.78	-0.432	0.0990	-0.109	10.78	-0.416	0.0929	-0.099	10.77	-0.397	0.0889	-0.093	11.11	-0.488	0.1049	-0.119	11.10	-0.469	0.1016	-0.110
12.34	-0.519	0.1236	-0.129	12.32	-0.490	0.1182	-0.113	12.32	-0.474	0.1128	-0.112	12.31	-0.452	0.1080	-0.103	12.39	-0.529	0.1269	-0.126	12.39	-0.529	0.1278	-0.126
13.89	-0.584	0.1530	-0.139	13.86	-0.547	0.1445	-0.128	13.86	-0.520	0.1388	-0.123	13.84	-0.495	0.1380	-0.115	14.2	-0.577	0.1459	-0.134	14.2	-0.577	0.1459	-0.134
$M=1.50 \quad R=3.0 \times 10^6$																							
-3.05	-0.184	0.0278	0.038	-3.05	-0.137	0.0269	0.035	-3.09	-0.132	0.0260	0.033	-3.08	-0.123	0.0255	0.031	-3.18	-0.170	0.0287	0.048	-3.17	-0.150	0.0295	0.039
-1.53	-0.077	0.0226	0.020	-1.52	-0.071	0.0222	0.018	-1.52	-0.066	0.0218	0.017	-1.52	-0.063	0.0212	0.016	-1.60	-0.099	0.0214	0.028	-1.59	-0.062	0.0206	0.007
-0.01	-0.006	0.0205	0.003	0	-0.004	0.0204	0.002	0	-0.004	0.0202	0.002	-0.003	-0.001	0.0190	0.001	0	-0.018	0.0215	0.009	0	-0.023	0.0214	0.003
1.54	-0.059	0.0213	-0.013	1.54	-0.050	0.0219	-0.014	1.54	-0.047	0.0217	-0.014	1.54	-0.047	0.0203	-0.013	1.58	-0.056	0.0226	-0.011	1.58	-0.062	0.0231	-0.013
3.08	-0.127	0.0663	-0.030	3.08	-0.126	0.0655	-0.030	3.07	-0.120	0.0656	-0.029	3.08	-0.114	0.0645	-0.027	3.16	-0.128	0.0623	-0.029	3.16	-0.130	0.0673	-0.031
4.63	-0.194	0.094	-0.046	4.62	-0.192	0.0948	-0.046	4.62	-0.182	0.0946	-0.046	4.62	-0.178	0.0937	-0.042	4.75	-0.204	0.0936	-0.048	4.75	-0.202	0.0950	-0.049
6.16	-0.260	0.044	-0.062	6.16	-0.254	0.0447	-0.062	6.15	-0.238	0.0432	-0.058	6.15	-0.229	0.0413	-0.055	6.34	-0.276	0.0449	-0.067	6.34	-0.288	0.0460	-0.069
7.71	-0.328	0.0588	-0.076	7.70	-0.317	0.0586	-0.073	7.69	-0.299	0.0567	-0.072	7.65	-0.289	0.0546	-0.069	7.93	-0.349	0.0616	-0.085	7.93	-0.339	0.0614	-0.081
9.25	-0.390	0.0767	-0.093	9.25	-0.375	0.0758	-0.093	9.24	-0.357	0.0731	-0.086	9.22	-0.341	0.0701	-0.081	9.32	-0.419	0.0811	-0.108	9.31	-0.400	0.0794	-0.095
10.80	-0.456	0.0987	-0.109	10.78	-0.432	0.0990	-0.109	10.78	-0.416	0.0929	-0.099	10.77	-0.397	0.0889	-0.093	11.11	-0.488	0.1049	-0.119	11.10	-0.469	0.1016	-0.110
12.34	-0.519	0.1236	-0.129	12.32	-0.490	0.1182	-0.113	12.32	-0.474	0.1128	-0.112	12.31	-0.452	0.1080	-0.103	12.39	-0.529	0.1269	-0.126	12.39	-0.529	0.1278	-0.126
13.89	-0.584	0.1530	-0.139	13.86	-0.547	0.1445	-0.128	13.86	-0.520	0.1388	-0.123	13.84	-0.495	0.1380	-0.115	14.2	-0.577	0.1459	-0.134	14.2	-0.577	0.1459	-0.134
$M=1.60 \quad R=6.0 \times 10^6$																							
-3.17	-0.180	0.0275	0.036	-3.16	-0.133	0.0265	0.034	-3.16	-0.123	0.0260	0.033	-3.15	-0.125	0.0263	0.031	-3.17	-0.150	0.0295	0.039	-3.17	-0.150	0.0295	0.039
-1.58	-0.071	0.0224	0.019	-1.58	-0.065	0.0215	0.018	-1.58	-0.067	0.0218	0.016	-1.58	-0.063	0.0212	0.016	-1.60	-0.099	0.0214	0.028	-1.59	-0.062	0.0206	0.007
0	-0.003	0.0204	0.005	0	-0.003	0.0201	0.002	0	-0.003	0.0201	0.002	0	-0.003	0.0201	0.002	0	-0.003	0.0202	0.001	0	-0.003	0.0201	0.001
1.58	-0.063	0.0219	-0.015	1.58	-0.056	0.0215	-0.015	1.58	-0.056	0.0218	-0.015	1.58	-0.056	0.0212	-0.013	1.58	-0.056	0.0213	-0.013	1.58	-0.062	0.0231	-0.013
3.16	-0.129	0.0667	-0.031	3.16	-0.126	0.0658	-0.031	3.16	-0.121	0.0651	-0.030	3.16	-0.116	0.0642	-0.027	3.16	-0.125	0.0623	-0.027	3.16	-0.125	0.0642	

TABLE X.- GEOMETRIC CHARACTERISTICS AND WIND-TUNNEL DATA  
FOR A PLANE TRIANGULAR WING OF ASPECT RATIO 4  
WITH 3-PERCENT-THICK BICONVEX SECTION  
(a) Geometric characteristics

*All dimensions shown in inches*



Aspect ratio . . . . .	4
Taper ratio . . . . .	0
Airfoil section (streamwise) . . . . .	3-percent-thick biconvex
Total area, square feet . . . . .	2.425
Mean aerodynamic chord, $\delta$ , feet . . . . .	1.038
Dihedral, degrees . . . . .	0
Twist, degrees . . . . .	0
Incidence, degrees . . . . .	0
Camber . . . . .	None
Distance, wing reference plane to body axis, feet . . . . .	0

(b) Data obtained in Ames 12-foot pressure wind tunnel

$\alpha$	$C_L$	$C_D$	$C_M$	$\alpha$	$C_L$	$C_D$	$C_M$	$\alpha$	$C_L$	$C_D$	$C_M$	$\alpha$	$C_L$	$C_D$	$C_M$
$M=0.25 \quad R=2.7 \times 10^6$				$M=0.60 \quad R=2.7 \times 10^6$				$M=0.25 \quad R=5.1 \times 10^6$				$M=0.25 \quad R=9.1 \times 10^6$			
0	-0.010	0.0097	0.001	0	-0.008	0.0099	0	0	-0.013	0.0093	0.001	0	-0.012	0.0087	0
-7.1	-0.049	0.0081	-0.003	-7.1	-0.052	0.0089	0.003	-7.6	-0.052	0.0085	-0.003	-7.6	-0.059	0.0089	0.004
0	-0.013	0.0097	-0.002	0	-0.007	0.0101	0	0	-0.012	0.0091	0.001	0	-0.011	0.0087	0
1.01	.029	.0100	-.003	1.01	.021	.0094	-.005	1.01	.023	.0095	-.003	1.01	.059	.0056	-.005
2.02	.109	.0107	-.007	2.02	.122	.0121	-.010	2.02	.114	.0123	-.008	2.02	.115	.0118	-.009
3.03	.171	.0156	-.011	3.03	.181	.0162	-.014	3.03	.167	.0159	-.010	3.03	.172	.0127	-.011
4.04	.220	.0205	-.012	4.04	.256	.0242	-.021	4.04	.231	.0222	-.013	4.04	.226	.0212	-.011
5.05	.288	.0293	-.013	5.05	.323	.0328	-.022	5.05	.285	.0288	-.014	5.05	.294	.0302	-.015
6.06	.346	.0401	-.013	6.06	.390	.0444	-.024	6.05	.335	.0377	-.015	6.06	.351	.0406	-.016
8.07	.453	.0694	-.012	8.08	.492	.0705	-.024	8.07	.451	.0638	-.013	8.07	.455	.0667	-.015
10.09	.540	.0946	-.008	10.09	.589	.1045	-.022	10.10	.546	.0946	-.010	10.09	.566	.0996	-.013
12.10	.629	.1321	-.007	12.11	.678	.1451	-.023	12.12	.638	.1324	-.009	12.10	.643	.1375	-.013
14.11	.714	.1760	-.009	14.12	.762	.1914	-.031	14.13	.721	.1757	-.012	13.11	.697	.1619	-.014
16.13	.790	.2246	-.018	16.13	.802	.2348	-.050	16.13	.790	.2213	-.019	0	-.013	.0088	-.001
18.13	.821	.2669	-.020	18.13	.826	.2765	-.064	18.14	.839	.2722	-.057				
20.14	.861	.3165	-.071	20.13	.848	.3186	-.096	20.14	.877	.3205	-.075				
22.14	.884	.3601	-.076	22.14	.855	.3554	-.102	22.15	.888	.3605	-.080				
24.14	.890	.3992	-.078	24.14	.891	.4081	-.111	24.15	.916	.4091	-.083				
26.15	.926	.4539	-.084	26.15	.936	.4687	-.118	26.15	.942	.4598	-.082				
28.15	.924	.4593	-.089	0	.016	.0109	-.001	28.15	.956	.5115	-.089				
0	-.013	.0097	.002					0	-.008	.0098	-.001				

~~CONFIDENTIAL~~

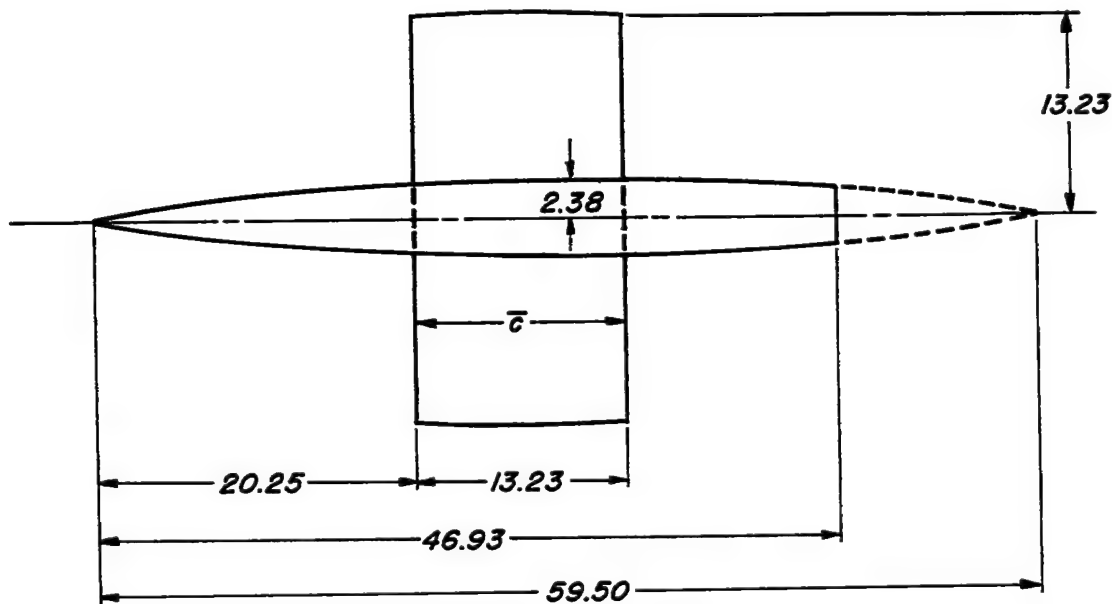
NACA

TABLE X.- GEOMETRIC CHARACTERISTICS AND WIND-TUNNEL DATA  
FOR A PLANE TRIANGULAR WING OF ASPECT RATIO 4 WITH  
3-PERCENT-THICK BICONVEX SECTION - Concluded  
(c) Data obtained Ames 6- by 6-foot supersonic wind tunnel

$a$	$c_L$	$c_D$	$c_M$	$a$	$c_L$	$c_D$	$c_M$	$a$	$c_L$	$c_D$	$c_M$	$a$	$c_L$	$c_D$	$c_M$	$a$	$c_L$	$c_D$	$c_M$	$a$	$c_L$	$c_D$	$c_M$
$M=0.61$ $R=1.7 \times 10^6$																							
-0.25	-0.035	0.0079	0.022	-0.56	-0.049	0.0090	0.004	-0.56	-0.029	0.0101	0.006	-0.57	-0.029	0.0093	0.003	-0.49	-0.048	0.0123	0.010	-0.49	-0.043	0.0130	0.008
-1.05	-0.033	0.0090	0.005	-1.11	-0.09	0.093	0.011	-1.11	-0.115	0.0111	0.019	-1.11	-0.121	0.0118	0.023	-1.02	-0.067	0.035	0.019	-1.06	-0.078	0.040	0.026
-2.18	-0.137	0.0123	0.011	-2.22	-0.18	0.0132	0.019	-2.22	-0.213	0.0123	0.024	-2.22	-0.231	0.0168	0.049	-2.09	-0.167	0.077	0.037	-2.07	-0.148	0.076	0.032
-3.26	-0.231	0.0183	0.019	-3.30	-0.254	0.0187	0.022	-3.30	-0.312	0.0183	0.047	-3.30	-0.332	0.0294	0.065	-3.12	-0.246	0.083	0.055	-3.12	-0.223	0.080	0.045
-4.33	-0.300	0.0267	0.018	-4.35	-0.340	0.0294	0.027	-4.35	-0.420	0.0307	0.074	-4.35	-0.506	0.0301	0.109	-4.16	-0.328	0.094	0.074	-4.16	-0.291	0.093	0.065
-5.35	-0.364	0.0378	0.019	-5.47	-0.409	0.0417	0.030	-5.47	-0.529	0.0395	0.095	-5.47	-0.611	0.0319	0.139	-5.20	-0.408	0.094	0.095	-5.18	-0.377	0.095	0.065
-6.43	-0.419	0.0507	0.012	-6.54	-0.492	0.056	0.011	-6.54	-0.608	0.0402	0.102	-6.54	-0.722	0.0382	0.177	-6.27	-0.516	0.099	0.23	-6.20	-0.476	0.095	0.065
-7.48	-0.476	0.0679	0.022	-7.59	-0.571	0.065	0.011	-7.59	-0.708	0.0471	0.123	-7.59	-0.834	0.0365	0.236	-7.31	-0.627	0.095	0.27	-7.24	-0.584	0.095	0.065
-8.52	-0.529	0.0869	0.022	-8.63	-0.657	0.070	0.011	-8.63	-0.799	0.0563	0.146	-8.63	-0.929	0.0472	0.310	-8.35	-0.765	0.094	0.349	-8.28	-0.726	0.093	0.065
-9.58	-0.575	0.0973	0.025	-9.69	-0.739	0.069	0.011	-9.69	-0.879	0.0653	0.166	-9.69	-1.041	0.0582	0.371	-9.41	-0.846	0.093	0.347	-9.34	-0.809	0.093	0.065
-10.65	-0.611	0.1069	0.028	-10.75	-0.819	0.065	0.011	-10.75	-0.959	0.074	0.186	-10.75	-1.122	0.0619	0.459	-10.47	-0.926	0.093	0.377	-10.40	-0.886	0.093	0.065
-12.74	-0.737	0.1732	0.032	-12.85	-0.901	0.065	0.011	-12.85	-1.049	0.0951	0.271	-12.85	-1.247	0.082	0.546	-12.56	-1.017	0.093	0.382	-12.50	-0.976	0.093	0.065
-14.81	-0.803	0.2192	0.044	-14.90	-0.981	0.065	0.011	-14.90	-1.130	0.1271	0.386	-14.90	-1.394	0.1165	0.626	-14.63	-1.103	0.127	0.392	-14.57	-1.061	0.127	0.392
-17.84	-0.897	0.2977	0.064																				
$a$	$c_L$	$c_D$	$c_M$	$a$	$c_L$	$c_D$	$c_M$	$a$	$c_L$	$c_D$	$c_M$	$a$	$c_L$	$c_D$	$c_M$	$a$	$c_L$	$c_D$	$c_M$	$a$	$c_L$	$c_D$	$c_M$
$M=1.40$ $R=1.7 \times 10^6$																							
-0.49	-0.038	0.0127	0.007	-0.49	-0.039	0.0138	0.004	-0.49	-0.030	0.0141	0.006	-0.48	-0.026	0.0143	0.005	-0.35	-0.038	0.0067	0	-0.29	-0.043	0.0086	0.001
-1.06	-0.070	0.035	0.01	-1.01	-0.063	0.0141	0.013	-1.01	-0.050	0.0144	0.012	-1.01	-0.057	0.0149	0.012	-1.16	-0.052	0.0094	0.006	-1.16	-0.052	0.0094	0.006
-2.07	-0.137	0.070	0.010	-2.06	-0.125	0.0162	0.017	-2.06	-0.118	0.0164	0.016	-2.06	-0.125	0.0164	0.016	-2.49	-0.132	0.0162	0.016	-2.49	-0.132	0.0162	0.016
-3.11	-0.222	0.1235	0.015	-3.11	-0.184	0.0205	0.016	-3.11	-0.152	0.0173	0.020	-3.11	-0.163	0.0205	0.016	-3.42	-0.175	0.0202	0.016	-3.42	-0.175	0.0202	0.016
-4.13	-0.289	0.1615	0.018	-4.13	-0.230	0.0206	0.016	-4.13	-0.208	0.0208	0.020	-4.13	-0.218	0.0206	0.016	-4.56	-0.235	0.0205	0.016	-4.56	-0.235	0.0205	0.016
-5.13	-0.344	0.1915	0.021	-5.13	-0.287	0.0206	0.016	-5.13	-0.265	0.0208	0.020	-5.13	-0.275	0.0206	0.016	-5.56	-0.292	0.0205	0.016	-5.56	-0.292	0.0205	0.016
-6.15	-0.394	0.2140	0.023	-6.15	-0.343	0.0206	0.016	-6.15	-0.321	0.0208	0.020	-6.15	-0.331	0.0206	0.016	-6.58	-0.358	0.0205	0.016	-6.58	-0.358	0.0205	0.016
-7.15	-0.434	0.2410	0.026	-7.15	-0.399	0.0206	0.016	-7.15	-0.377	0.0208	0.020	-7.15	-0.387	0.0206	0.016	-7.58	-0.404	0.0205	0.016	-7.58	-0.404	0.0205	0.016
-8.15	-0.474	0.2640	0.028	-8.15	-0.455	0.0206	0.016	-8.15	-0.433	0.0208	0.020	-8.15	-0.443	0.0206	0.016	-8.58	-0.471	0.0205	0.016	-8.58	-0.471	0.0205	0.016
-9.15	-0.514	0.2890	0.031	-9.15	-0.521	0.0206	0.016	-9.15	-0.499	0.0208	0.020	-9.15	-0.509	0.0206	0.016	-9.58	-0.527	0.0205	0.016	-9.58	-0.527	0.0205	0.016
-10.15	-0.554	0.3140	0.034	-10.15	-0.607	0.0206	0.016	-10.15	-0.585	0.0208	0.020	-10.15	-0.595	0.0206	0.016	-10.58	-0.623	0.0205	0.016	-10.58	-0.623	0.0205	0.016
-11.15	-0.594	0.3390	0.037	-11.15	-0.683	0.0206	0.016	-11.15	-0.661	0.0208	0.020	-11.15	-0.671	0.0206	0.016	-11.58	-0.699	0.0205	0.016	-11.58	-0.699	0.0205	0.016
-12.15	-0.634	0.3640	0.040	-12.15	-0.760	0.0206	0.016	-12.15	-0.738	0.0208	0.020	-12.15	-0.748	0.0206	0.016	-12.58	-0.786	0.0205	0.016	-12.58	-0.786	0.0205	0.016
-13.15	-0.674	0.3890	0.043	-13.15	-0.837	0.0206	0.016	-13.15	-0.815	0.0208	0.020	-13.15	-0.825	0.0206	0.016	-13.58	-0.853	0.0205	0.016	-13.58	-0.853	0.0205	0.016
-14.15	-0.714	0.4140	0.046	-14.15	-0.904	0.0206	0.016	-14.15	-0.882	0.0208	0.020	-14.15	-0.892	0.0206	0.016	-14.58	-0.920	0.0205	0.016	-14.58	-0.920	0.0205	0.016
-15.15	-0.754	0.4390	0.049	-15.15	-0.971	0.0206	0.016	-15.15	-0.949	0.0208	0.020	-15.15	-0.959	0.0206	0.016	-15.58	-0.979	0.0205	0.016	-15.58	-0.979	0.0205	0.016
-16.15	-0.794	0.4640	0.052	-16.15	-0.997	0.0206	0.016	-16.15	-0.975	0.0208	0.020	-16.15	-0.985	0.0206	0.016	-16.58	-0.999	0.0205	0.016	-16.58	-0.999	0.0205	0.016
-17.15	-0.834	0.4890	0.055	-17.15	-0.997	0.0206	0.016	-17.15	-0.975	0.0208	0.020	-17.15	-0.985	0.0206	0.016	-17.58	-1.000	0.0205	0.016	-17.58	-1.000	0.0205	0.016
-18.15	-0.874	0.5140	0.058	-18.15	-0.997	0.0206	0.016	-18.15	-0.975	0.0208	0.020	-18.15	-0.985	0.0206	0.016	-18.58	-1.000	0.0205	0.016	-18.58	-1.000	0.0205	0.016
-19.15	-0.914	0.5390	0.061	-19.15	-0.997	0.0206	0.016	-19.15	-0.975	0.0208	0.020	-19.15	-0.985	0.0206	0.016	-19.58	-1.000	0.0205	0.016	-19.58	-1.000	0.0205	0.016
-20.15	-0.954	0.5640	0.064	-20.15	-0.997	0.0206	0.016	-20.15	-0.975	0.0208	0.020	-20.15	-0.985	0.0206	0.016	-20.58	-1.000	0.0205	0.016	-20.58	-1.000	0.0205	0.016
-21.15	-0.994	0.5890	0.067	-21.15	-0.997	0.0206	0.016	-21.15	-0.975	0.0208	0.020	-21.15	-0.985	0.0206	0.016	-21.58	-1.000	0.0205	0.016	-21.58	-1.000	0.0205	0.016
-22.15	-0.134	0.6140	0.070	-22.15	-0.997	0.0206	0.016	-22.15	-0.975	0.0208	0.020	-22.15	-0.985	0.0206	0.016	-22.58	-1.000	0.0205	0.016	-22.58	-1.000	0.0205	0.016
-23.15	-0.169	0.6390	0.073	-23.15	-0.997	0.0206	0.016	-23.15	-0.975	0.0208	0.020	-23.15	-0.985	0.0206	0.016	-23.58	-1.000	0.0205	0.016	-23.58	-1.000	0.0205	0.016
-24.15	-0.204	0.6640	0.076	-24.15	-0.997	0.0206	0.016	-24.15	-0.975	0.0208	0.020	-24.15	-0.985	0.0206	0.016	-24.58	-1.000	0.0205	0.016	-24.58	-1.000	0.0205	0.016
-25.15	-0.239	0.6890	0.079	-25.15	-0.997	0.0206	0.016	-25.15	-0.975	0.0208	0.020	-25.15	-0.985	0.0206	0.016	-25.58	-1.000	0.0205	0.016	-25.58	-1.000	0.0205	0.016
-26.15	-0.274	0.7140	0.082	-26.15	-0.997	0.0206	0.016	-26.15	-0.975	0.0208	0.020	-26.15	-0.985	0.0206	0.016	-26.58	-1.000	0.0205	0.016	-26.58	-1.000	0.0205	0.016
-27.15	-0.309																						

TABLE XI.- GEOMETRIC CHARACTERISTICS AND WIND-TUNNEL DATA  
FOR A PLANE RECTANGULAR WING OF ASPECT RATIO 2  
WITH 3-PERCENT-THICK ROUNDED-NOSE SECTION  
(a) Geometric characteristics

*All dimensions shown in inches  
unless otherwise noted*



Aspect ratio . . . . .	2
Taper ratio . . . . .	1
Airfoil section (streamwise) . . . . .	3-percent-thick biconvex with elliptical nose
Total area, square feet . . . . .	2.430
Mean aerodynamic chord, $\bar{c}$ , feet . . . . .	1.102
Dihedral, degrees . . . . .	0
Twist, degrees . . . . .	0
Incidence, degrees . . . . .	0
Camber . . . . .	None
Distance, wing reference plane to body axis, feet . . . . .	0



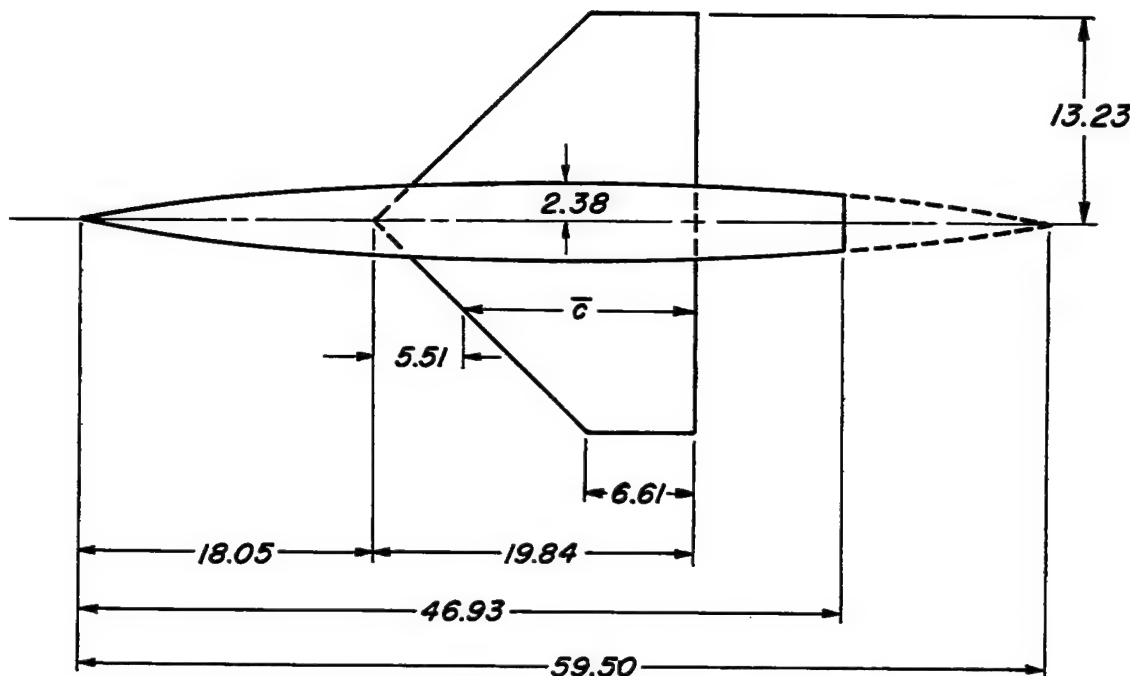
TABLE XI.- GEOMETRIC CHARACTERISTICS AND WIND-TUNNEL DATA  
FOR A PLANE RECTANGULAR WING OF ASPECT RATIO 2 WITH  
3-PERCENT-THICK ROUNDED-NOSE SECTION - Concluded  
(b) Data obtained in Ames 6- by 6-foot supersonic wind tunnel

$\alpha$	$C_L$	$C_D$	$C_M$																
$M=0.61$	$R=1.8 \times 10^{-6}$			$M=0.71$	$R=1.8 \times 10^{-6}$			$M=0.81$	$R=1.8 \times 10^{-6}$			$M=0.91$	$R=1.8 \times 10^{-6}$			$M=0.93$	$R=1.8 \times 10^{-6}$		
-0.07	-0.025	0.0072	0	-0.26	-0.027	0.0079	0	-0.30	-0.024	0.0075	0.003	-0.28	-0.023	0.0074	-0.004	-0.26	-0.022	0.0071	-0.004
-0.05	-0.010	-0.0076	-0.002	-0.16	-0.010	0.0078	-0.003	-0.16	-0.011	0.0077	-0.003	-0.16	-0.013	0.0078	-0.007	-0.26	-0.022	0.0074	-0.008
-0.04	-0.0054	0.0079	-0.003	-0.12	-0.005	0.0079	-0.004	-0.12	-0.008	0.0079	-0.004	-0.12	-0.009	0.0077	-0.011	-0.26	-0.020	0.0060	-0.013
-1.07	-0.062	-0.0053	-0.003	-1.10	-0.068	0.0050	-0.005	-1.11	-0.070	0.0080	-0.007	-1.09	-0.060	0.0056	-0.013	-1.10	-0.063	0.0055	-0.015
-2.15	-1.118	-0.068	-0.010	-2.17	-1.122	0.0096	-0.011	-2.18	-1.127	0.0139	-0.011	-2.20	-1.124	0.0107	-0.021	-2.21	-1.126	0.0107	-0.025
-1.23	-1.178	-0.073	-0.013	-1.3	-1.18	0.0100	-0.016	-1.3	-1.186	0.0121	-0.014	-1.3	-1.187	0.0120	-0.024	-1.3	-1.183	0.0117	-0.028
-1.30	-1.233	-0.0208	-0.017	-1.4	-1.33	-0.0246	-0.020	-1.4	-1.35	-0.0226	-0.021	-1.4	-1.351	-0.0226	-0.031	-1.4	-1.353	-0.0227	-0.031
-0.06	-0.006	0.0071	-0.007	-0.08	-0.006	0.0078	-0.005	-0.09	-0.007	0.0076	-0.005	-0.09	-0.007	0.0075	-0.003	-0.09	-0.007	0.0073	-0.001
-0.04	-0.010	0.0077	-0.005	-0.07	-0.009	0.0078	-0.008	-0.08	-0.008	0.0071	-0.008	-0.08	-0.008	0.0072	-0.007	-0.08	-0.008	0.0076	-0.001
-0.03	-0.023	0.0077	-0.007	-0.08	-0.009	0.0078	-0.009	-0.09	-0.008	0.0072	-0.009	-0.09	-0.008	0.0072	-0.007	-0.09	-0.008	0.0076	-0.001
1.02	-0.036	-0.0060	-0.008	1.05	-0.036	0.0079	0.010	1.05	-0.035	0.0078	0.012	1.07	-0.045	0.0065	0.013	1.07	-0.043	0.0063	0.015
-0.03	-0.023	0.0078	-0.010	-0.13	-0.023	0.0073	-0.012	-0.13	-0.021	0.0078	-0.018	-0.13	-0.021	0.0078	-0.021	-0.13	-0.021	0.0078	-0.009
-0.10	-0.023	0.0078	-0.010	-0.13	-0.023	0.0073	-0.012	-0.13	-0.021	0.0078	-0.018	-0.13	-0.021	0.0078	-0.021	-0.13	-0.021	0.0078	-0.009
-1.27	-0.008	0.0063	-0.019	-0.13	-0.019	0.0069	-0.023	-0.13	-0.019	0.0073	-0.023	-0.13	-0.019	0.0063	-0.027	-0.13	-0.019	0.0063	-0.029
-6.48	-0.008	0.012	-0.012	-6.44	-0.012	0.0125	-0.027	-6.43	-0.012	0.0121	-0.028	-6.39	-0.012	0.0123	-0.029	-6.38	-0.012	0.0121	-0.028
-8.36	-0.074	-0.014	-0.014	-8.60	-0.074	0.0126	-0.036	-8.67	-0.074	0.0127	-0.036	-8.62	-0.074	0.0126	-0.036	-8.59	-0.074	0.0126	-0.036
10.59	-0.606	-0.1180	-0.013	-10.73	-0.605	-0.1244	-0.022	-10.80	-0.605	-0.1233	-0.039	-10.86	-0.605	-0.1233	-0.039	-10.93	-0.605	-0.1233	-0.039
14.90	-0.812	-0.2247	-0.015	-14.91	-0.812	-0.2245	-0.020	-14.94	-0.812	-0.2246	-0.039	-14.98	-0.812	-0.2246	-0.039	-15.05	-0.812	-0.2246	-0.039
16.90	-0.868	-0.2760	-0.016	-16.53	-0.868	-0.2656	-0.023	-16.53	-0.868	-0.2656	-0.023	-16.53	-0.868	-0.2656	-0.023	-16.53	-0.868	-0.2656	-0.023
17.97	-0.879	-0.2974	-0.018	-18.01	-0.879	-0.2959	-0.023	-18.01	-0.879	-0.2959	-0.023	-18.01	-0.879	-0.2959	-0.023	-18.01	-0.879	-0.2959	-0.023
$M=1.30$	$R=1.8 \times 10^{-6}$			$M=1.40$	$R=1.8 \times 10^{-6}$			$M=1.50$	$R=1.8 \times 10^{-6}$			$M=1.60$	$R=1.8 \times 10^{-6}$			$M=1.70$	$R=1.8 \times 10^{-6}$		
-0.27	-0.028	0.0171	0.002	-0.27	-0.028	0.0169	0.002	-0.26	-0.028	0.0169	0.002	-0.26	-0.026	0.0153	0.002	-0.26	-0.019	0.0155	0.002
-0.24	-0.042	0.0175	0.004	-0.24	-0.042	0.0173	0.004	-0.23	-0.042	0.0173	0.004	-0.23	-0.042	0.0154	0.003	-0.23	-0.038	0.0158	0.003
-0.21	-0.071	0.0180	0.005	-0.21	-0.071	0.0173	0.005	-0.20	-0.071	0.0173	0.005	-0.20	-0.071	0.0154	0.003	-0.20	-0.069	0.0157	0.003
-1.06	-0.073	0.0187	0.006	-1.08	-0.066	0.0181	0.006	-1.05	-0.066	0.0181	0.006	-1.06	-0.066	0.0165	0.007	-1.07	-0.066	0.0165	0.007
-2.15	-1.136	-0.031	-0.013	-2.14	-1.136	-0.023	-0.013	-2.13	-1.136	-0.023	-0.013	-2.11	-1.136	-0.023	-0.013	-2.11	-1.136	-0.023	-0.013
-3.19	-2.033	-0.021	-0.013	-3.18	-2.033	-0.023	-0.013	-3.18	-2.033	-0.023	-0.013	-3.16	-2.033	-0.023	-0.013	-3.16	-2.033	-0.023	-0.013
-4.25	-2.888	-0.035	-0.026	-4.23	-2.888	-0.0350	-0.026	-4.22	-2.888	-0.0350	-0.026	-4.20	-2.888	-0.0350	-0.026	-4.18	-2.888	-0.0350	-0.026
-5.25	-0.009	0.0175	-0.007	-5.26	-0.009	0.0176	-0.007	-5.25	-0.009	0.0176	-0.007	-5.24	-0.009	0.0166	-0.006	-5.23	-0.009	0.0159	-0.004
-6.22	-0.008	0.0175	-0.007	-6.23	-0.008	0.0176	-0.007	-6.22	-0.008	0.0176	-0.007	-6.21	-0.008	0.0166	-0.006	-6.20	-0.008	0.0159	-0.004
-7.20	-0.008	0.0175	-0.007	-7.21	-0.008	0.0176	-0.007	-7.20	-0.008	0.0176	-0.007	-7.19	-0.008	0.0166	-0.006	-7.18	-0.008	0.0159	-0.004
-1.04	-0.009	0.0187	-0.006	-1.05	-0.009	0.0186	-0.006	-1.04	-0.009	0.0187	-0.006	-1.03	-0.009	0.0164	-0.007	-1.02	-0.009	0.0156	-0.008
-9.14	-1.29	-0.0229	-0.018	-2.11	-1.29	-0.0221	-0.018	-2.11	-1.29	-0.0221	-0.018	-2.11	-1.29	-0.0221	-0.018	-2.11	-1.29	-0.0221	-0.018
-3.18	-1.189	-0.0285	-0.020	-3.18	-1.175	-0.0281	-0.020	-3.16	-1.164	-0.0286	-0.020	-3.15	-1.154	-0.0281	-0.020	-3.15	-1.154	-0.0281	-0.020
-4.23	-2.023	-0.0381	-0.028	-4.22	-2.023	-0.0363	-0.028	-4.20	-2.023	-0.0363	-0.028	-4.19	-2.023	-0.0363	-0.028	-4.18	-2.023	-0.0363	-0.028
-6.13	-3.78	-0.0360	-0.046	-6.31	-3.78	-0.0354	-0.048	-6.30	-3.78	-0.0360	-0.046	-6.29	-3.78	-0.0354	-0.046	-6.28	-3.78	-0.0354	-0.046
-8.43	-5.06	-0.078	-0.061	-8.41	-5.07	-0.073	-0.061	-8.39	-5.05	-0.078	-0.060	-8.36	-5.06	-0.078	-0.060	-8.35	-5.05	-0.077	-0.060
-10.58	-6.90	-0.147	-0.062	-10.50	-6.90	-0.138	-0.064	-10.48	-6.90	-0.138	-0.064	-10.45	-6.88	-0.138	-0.064	-10.43	-6.88	-0.138	-0.064
-12.62	-7.43	-0.180	-0.060	-12.58	-7.40	-0.180	-0.060	-12.56	-7.40	-0.180	-0.060	-12.53	-7.38	-0.180	-0.060	-12.50	-7.38	-0.180	-0.060
-14.70	-8.93	-0.246	-0.120	-14.68	-8.97	-0.245	-0.120	-14.66	-8.97	-0.245	-0.120	-14.63	-8.97	-0.245	-0.120	-14.60	-8.97	-0.245	-0.120
-16.79	-9.97	-0.308	-0.140	-16.76	-9.96	-0.306	-0.140	-16.74	-9.96	-0.306	-0.140	-16.71	-9.97	-0.307	-0.140	-16.73	-9.97	-0.307	-0.140
$M=0.61$	$R=4.4 \times 10^{-6}$			$M=0.71$	$R=4.4 \times 10^{-6}$			$M=0.81$	$R=4.4 \times 10^{-6}$			$M=0.91$	$R=4.4 \times 10^{-6}$			$M=0.93$	$R=4.4 \times 10^{-6}$		
-0.30	-0.004	0.0090	-0.002	-0.30	-0.005	0.0087	-0.003	-0.30	-0.005	0.0087	-0.003	-0.29	-0.005	0.0087	-0.003	-0.28	-0.005	0.0086	-0.003
-0.20	-0.039	0.0091	-0.003	-0.61	-0.042	0.0088	-0.005	-0.61	-0.042	0.0088	-0.005	-0.60	-0.042	0.0087	-0.006	-0.59	-0.043	0.0089	-0.003
-0.18	-0.054	0.0091	-0.005	-0.91	-0.055	0.0089	-0.006	-0.91	-0.055	0.0089	-0.006	-0.90	-0.055	0.0089	-0.010	-0.89	-0.055	0.0089	-0.004
-1.17	-0.065	0.0094	-0.006	-1.19	-0.070	0.0087	-0.007	-1.19	-0.070	0.0087	-0.007	-1.18	-0.070	0.0087	-0.009	-1.17	-0.070	0.0087	-0.006
-2.29	-1.222	-0.0113	-0.011	-2.38	-1.222	-0.0116	-0.013	-2.35	-1.221	-0.0116	-0.013	-2.31	-1.220	-0.0116	-0.013	-2.29	-1.221	-0.0116	-0.013
-3.40	-1.771	-0.0224	-0.013	-3.45	-1.787	-0.0226	-0.013	-3.42	-1.787	-0.0226	-0.013	-3.39	-1.787	-0.0226	-0.013	-3.36	-1.787	-0.0226	-0.013
-4.51	-2.37	-0.0228	-0.019	-4.55	-2.38	-0.0240	-0.023	-4.51	-2.38	-0.0240	-0.023	-4.47	-2.38	-0.0240	-0.023	-4.43	-2.38	-0.0240	-0.023
-5.57	-0.020	0.0091	-0.003	-5.57	-0.021	0.0090	-0.003	-5.57	-0.021	0.0090	-0.003	-5.53	-0.021	0.0088	-0.003	-5.50	-0.021	0.0088	-0.003
-6.84	-0.039	0.0093	-0.005	-6.85	-0.037	0.0089	-0.005	-6.84	-0.037	0.0089	-0.005	-6.80	-0.037	0.0088	-0.005	-6.77	-0.037	0.0088	-0.005
-1.19	-0.049	0.0094	-0.006	-1.21	-0.050	0.0089	-0.006	-1.19	-0.050	0.0089	-0.006	-1.16	-0.050	0.0088	-0.006	-1.13	-0.050	0.0088	-0.006
-3.26	-1.56	-0.0259	-0.016	-3.24	-1.56	-0.0260	-0.016	-3.21	-1.56	-0.0260	-0.016	-3.17	-1.56	-0.0260	-0.016	-3.13	-1.56	-0.0260	-0.016
-4.47	-2.27	-0.0213	-0.011	-4.45	-2.27	-0.0217	-0.011	-4.42	-2.27	-0.0217	-0.011	-4.39	-2.27	-0.0217	-0.011	-4.35	-2.27	-0.0217	-0.011
-6.72	-3.47	-0.0438	-0.026	-6.85	-3.72	-0.0469	-0.026	-7.01	-4.12	-0.0469	-0.026	-6.98	-4.08	-0.0469	-0.026	-6.94	-4.08	-0.0469	-0.026
9.00	-1.49	-0.0807	-0.011	-8.83	-5.11	-0.0826	-0.011	-8.79	-4.05	-0.0826	-0.011	-8.75	-3.97	-0.0826	-0.011	-8.71	-3.97	-0.0826	-0.011
$M=1.30$	$R=4.4 \times 10^{-6}$			$M=1.40$	$R=4.4 \times 10^{-6}$			$M=1.50$	$R=4.4 \times 10^{-6}$			$M=1.60$	$R=4.4 \times 10^{-6}$	</td					

NACA

TABLE XIII.- GEOMETRIC CHARACTERISTICS AND WIND-TUNNEL DATA  
 FOR A PLANE 45° SWEPTBACK WING OF ASPECT RATIO 2  
 WITH 3-PERCENT-THICK ROUNDED-NOSE SECTION  
 (a) Geometric characteristics

*All dimensions shown in inches  
 unless otherwise noted*



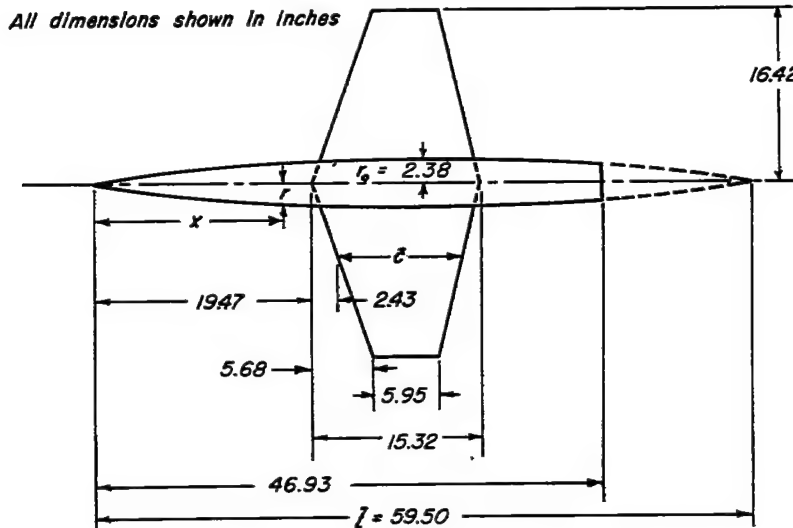
Aspect ratio . . . . .	2
Taper ratio . . . . .	.333
Airfoil section (streamwise) . . .	3-percent-thick biconvex with elliptical nose
Total area, square feet . . . . .	2.430
Mean aerodynamic chord, $\bar{c}$ , feet . . . . .	1.194
Dihedral, degrees . . . . .	0
Twist, degrees . . . . .	0
Incidence, degrees . . . . .	0
Camber . . . . .	None
Distance, wing reference plane to body axis, feet . . . . .	0



TABLE XIII.- GEOMETRIC CHARACTERISTICS AND WIND-TUNNEL DATA  
FOR A PLANE 45° SWEPTBACK WING OF ASPECT RATIO 2 WITH  
3-PERCENT-THICK ROUNDED-NOSE SECTION - Concluded  
(b) Data obtained in Ames 6- by 6-foot supersonic wind tunnel

$\alpha$	$C_L$	$C_D$	$C_m$	$\alpha$	$C_L$	$C_D$	$C_m$	$\alpha$	$C_L$	$C_D$	$C_m$	$\alpha$	$C_L$	$C_D$	$C_m$	$\alpha$	$C_L$	$C_D$	$C_m$			
$M=0.61$	$R=1.9 \times 10^6$			$M=0.71$	$R=1.9 \times 10^6$			$M=0.81$	$R=1.9 \times 10^6$			$M=0.91$	$R=1.9 \times 10^6$			$M=0.93$	$R=1.9 \times 10^6$					
-0.57	-0.023	0.072	-0.001	-0.26	-0.023	0.0071	0	-0.28	-0.023	0.0068	-0.001	-0.28	-0.023	0.0071	-0.001	-0.19	0.0079	-0.008	-0.28	-0.023	0.0105	0.004
-0.54	-0.025	0.080	-0.001	-0.24	-0.025	0.008	0	-0.25	-0.025	0.0073	-0.001	-0.25	-0.025	0.0080	-0.001	-0.17	0.0082	-0.002	-0.23	-0.025	0.0115	0.005
-0.51	-0.028	0.084	-0.002	-0.21	-0.028	0.008	0	-0.26	-0.028	0.0073	-0.001	-0.26	-0.028	0.0080	-0.001	-0.16	0.0082	-0.002	-0.22	-0.028	0.0123	0.005
-0.48	-0.028	0.084	-0.002	-0.19	-0.028	0.008	0	-0.27	-0.028	0.0073	-0.001	-0.27	-0.028	0.0080	-0.001	-0.15	0.0082	-0.002	-0.21	-0.028	0.0132	0.005
-0.45	-0.028	0.084	-0.002	-0.17	-0.028	0.008	0	-0.28	-0.028	0.0073	-0.001	-0.28	-0.028	0.0080	-0.001	-0.14	0.0082	-0.002	-0.20	-0.028	0.0141	0.005
-0.42	-0.028	0.084	-0.002	-0.15	-0.028	0.008	0	-0.29	-0.028	0.0073	-0.001	-0.29	-0.028	0.0080	-0.001	-0.13	0.0082	-0.002	-0.19	-0.028	0.0150	0.005
-0.39	-0.028	0.084	-0.002	-0.13	-0.028	0.008	0	-0.30	-0.028	0.0073	-0.001	-0.30	-0.028	0.0080	-0.001	-0.12	0.0082	-0.002	-0.18	-0.028	0.0159	0.005
-0.36	-0.028	0.084	-0.002	-0.11	-0.028	0.008	0	-0.31	-0.028	0.0073	-0.001	-0.31	-0.028	0.0080	-0.001	-0.11	0.0082	-0.002	-0.17	-0.028	0.0168	0.005
-0.33	-0.028	0.084	-0.002	-0.09	-0.028	0.008	0	-0.32	-0.028	0.0073	-0.001	-0.32	-0.028	0.0080	-0.001	-0.10	0.0082	-0.002	-0.16	-0.028	0.0177	0.005
-0.30	-0.028	0.084	-0.002	-0.07	-0.028	0.008	0	-0.33	-0.028	0.0073	-0.001	-0.33	-0.028	0.0080	-0.001	-0.09	0.0082	-0.002	-0.15	-0.028	0.0186	0.005
-0.27	-0.028	0.084	-0.002	-0.05	-0.028	0.008	0	-0.34	-0.028	0.0073	-0.001	-0.34	-0.028	0.0080	-0.001	-0.08	0.0082	-0.002	-0.14	-0.028	0.0195	0.005
-0.24	-0.028	0.084	-0.002	-0.03	-0.028	0.008	0	-0.35	-0.028	0.0073	-0.001	-0.35	-0.028	0.0080	-0.001	-0.07	0.0082	-0.002	-0.13	-0.028	0.0204	0.005
-0.21	-0.028	0.084	-0.002	-0.01	-0.028	0.008	0	-0.36	-0.028	0.0073	-0.001	-0.36	-0.028	0.0080	-0.001	-0.06	0.0082	-0.002	-0.12	-0.028	0.0213	0.005
-0.18	-0.028	0.084	-0.002	-0.01	-0.028	0.008	0	-0.37	-0.028	0.0073	-0.001	-0.37	-0.028	0.0080	-0.001	-0.05	0.0082	-0.002	-0.11	-0.028	0.0222	0.005
-0.15	-0.028	0.084	-0.002	-0.01	-0.028	0.008	0	-0.38	-0.028	0.0073	-0.001	-0.38	-0.028	0.0080	-0.001	-0.04	0.0082	-0.002	-0.10	-0.028	0.0231	0.005
-0.12	-0.028	0.084	-0.002	-0.01	-0.028	0.008	0	-0.39	-0.028	0.0073	-0.001	-0.39	-0.028	0.0080	-0.001	-0.03	0.0082	-0.002	-0.09	-0.028	0.0240	0.005
-0.09	-0.028	0.084	-0.002	-0.01	-0.028	0.008	0	-0.40	-0.028	0.0073	-0.001	-0.40	-0.028	0.0080	-0.001	-0.02	0.0082	-0.002	-0.08	-0.028	0.0249	0.005
-0.06	-0.028	0.084	-0.002	-0.01	-0.028	0.008	0	-0.41	-0.028	0.0073	-0.001	-0.41	-0.028	0.0080	-0.001	-0.01	0.0082	-0.002	-0.07	-0.028	0.0258	0.005
-0.03	-0.028	0.084	-0.002	-0.01	-0.028	0.008	0	-0.42	-0.028	0.0073	-0.001	-0.42	-0.028	0.0080	-0.001	-0.00	0.0082	-0.002	-0.06	-0.028	0.0267	0.005
0.00	-0.028	0.084	-0.002	-0.01	-0.028	0.008	0	-0.43	-0.028	0.0073	-0.001	-0.43	-0.028	0.0080	-0.001	-0.00	0.0082	-0.002	-0.05	-0.028	0.0276	0.005
0.03	-0.028	0.084	-0.002	-0.01	-0.028	0.008	0	-0.44	-0.028	0.0073	-0.001	-0.44	-0.028	0.0080	-0.001	-0.00	0.0082	-0.002	-0.04	-0.028	0.0285	0.005
0.06	-0.028	0.084	-0.002	-0.01	-0.028	0.008	0	-0.45	-0.028	0.0073	-0.001	-0.45	-0.028	0.0080	-0.001	-0.00	0.0082	-0.002	-0.03	-0.028	0.0294	0.005
0.09	-0.028	0.084	-0.002	-0.01	-0.028	0.008	0	-0.46	-0.028	0.0073	-0.001	-0.46	-0.028	0.0080	-0.001	-0.00	0.0082	-0.002	-0.02	-0.028	0.0303	0.005
0.12	-0.028	0.084	-0.002	-0.01	-0.028	0.008	0	-0.47	-0.028	0.0073	-0.001	-0.47	-0.028	0.0080	-0.001	-0.00	0.0082	-0.002	-0.01	-0.028	0.0312	0.005
0.15	-0.028	0.084	-0.002	-0.01	-0.028	0.008	0	-0.48	-0.028	0.0073	-0.001	-0.48	-0.028	0.0080	-0.001	-0.00	0.0082	-0.002	-0.00	-0.028	0.0321	0.005
0.18	-0.028	0.084	-0.002	-0.01	-0.028	0.008	0	-0.49	-0.028	0.0073	-0.001	-0.49	-0.028	0.0080	-0.001	-0.00	0.0082	-0.002	-0.00	-0.028	0.0330	0.005
0.21	-0.028	0.084	-0.002	-0.01	-0.028	0.008	0	-0.50	-0.028	0.0073	-0.001	-0.50	-0.028	0.0080	-0.001	-0.00	0.0082	-0.002	-0.00	-0.028	0.0339	0.005
0.24	-0.028	0.084	-0.002	-0.01	-0.028	0.008	0	-0.51	-0.028	0.0073	-0.001	-0.51	-0.028	0.0080	-0.001	-0.00	0.0082	-0.002	-0.00	-0.028	0.0348	0.005
0.27	-0.028	0.084	-0.002	-0.01	-0.028	0.008	0	-0.52	-0.028	0.0073	-0.001	-0.52	-0.028	0.0080	-0.001	-0.00	0.0082	-0.002	-0.00	-0.028	0.0357	0.005
0.30	-0.028	0.084	-0.002	-0.01	-0.028	0.008	0	-0.53	-0.028	0.0073	-0.001	-0.53	-0.028	0.0080	-0.001	-0.00	0.0082	-0.002	-0.00	-0.028	0.0366	0.005
0.33	-0.028	0.084	-0.002	-0.01	-0.028	0.008	0	-0.54	-0.028	0.0073	-0.001	-0.54	-0.028	0.0080	-0.001	-0.00	0.0082	-0.002	-0.00	-0.028	0.0375	0.005
0.36	-0.028	0.084	-0.002	-0.01	-0.028	0.008	0	-0.55	-0.028	0.0073	-0.001	-0.55	-0.028	0.0080	-0.001	-0.00	0.0082	-0.002	-0.00	-0.028	0.0384	0.005
0.39	-0.028	0.084	-0.002	-0.01	-0.028	0.008	0	-0.56	-0.028	0.0073	-0.001	-0.56	-0.028	0.0080	-0.001	-0.00	0.0082	-0.002	-0.00	-0.028	0.0393	0.005
0.42	-0.028	0.084	-0.002	-0.01	-0.028	0.008	0	-0.57	-0.028	0.0073	-0.001	-0.57	-0.028	0.0080	-0.001	-0.00	0.0082	-0.002	-0.00	-0.028	0.0402	0.005
0.45	-0.028	0.084	-0.002	-0.01	-0.028	0.008	0	-0.58	-0.028	0.0073	-0.001	-0.58	-0.028	0.0080	-0.001	-0.00	0.0082	-0.002	-0.00	-0.028	0.0411	0.005
0.48	-0.028	0.084	-0.002	-0.01	-0.028	0.008	0	-0.59	-0.028	0.0073	-0.001	-0.59	-0.028	0.0080	-0.001	-0.00	0.0082	-0.002	-0.00	-0.028	0.0420	0.005
0.51	-0.028	0.084	-0.002	-0.01	-0.028	0.008	0	-0.60	-0.028	0.0073	-0.001	-0.60	-0.028	0.0080	-0.001	-0.00	0.0082	-0.002	-0.00	-0.028	0.0429	0.005
0.54	-0.028	0.084	-0.002	-0.01	-0.028	0.008	0	-0.61	-0.028	0.0073	-0.001	-0.61	-0.028	0.0080	-0.001	-0.00	0.0082	-0.002	-0.00	-0.028	0.0438	0.005
0.57	-0.028	0.084	-0.002	-0.01	-0.028	0.008	0	-0.62	-0.028	0.0073	-0.001	-0.62	-0.028	0.0080	-0.001	-0.00	0.0082	-0.002	-0.00	-0.028	0.0447	0.005
0.60	-0.028	0.084	-0.002	-0.01	-0.028	0.008	0	-0.63	-0.028	0.0073	-0.001	-0.63	-0.028	0.0080	-0.001	-0.00	0.0082	-0.002	-0.00	-0.028	0.0456	0.005
0.63	-0.028	0.084	-0.002	-0.01	-0.028	0.008	0	-0.64	-0.028	0.0073	-0.001	-0.64	-0.028	0.0080	-0.001	-0.00	0.0082	-0.002	-0.00	-0.028	0.0465	0.005
0.66	-0.028	0.084	-0.002	-0.01	-0.028	0.008	0	-0.65	-0.028	0.0073	-0.001	-0.65	-0.028	0.0080	-0.001	-0.00	0.0082	-0.002	-0.00	-0.028	0.0474	0.005
0.69	-0.028	0.084	-0.002	-0.01	-0.028	0.008	0	-0.66	-0.028	0.0073	-0.001	-0.66	-0.028	0.0080	-0.001	-0.00	0.0082	-0.002	-0.00	-0.028	0.0483	0.005
0.72	-0.028	0.084	-0.002	-0.01	-0.028	0.008	0	-0.67	-0.028	0.0073	-0.001	-0.67	-0.028	0.0080	-0.001	-0.00	0.0082	-0.002	-0.00	-0.028	0.0492	0.005
0.75	-0.028	0.084	-0.002	-0.01	-0.028	0.008	0	-0.68	-0.028	0.0073	-0.001	-0.68	-0.028	0.0080	-0.001	-0.00	0.0082	-0.002	-0.00	-0.028	0.0501	0.005
0.78	-0.028	0.084	-0.002	-0.01	-0.028	0.008	0	-0.69	-0.028	0.0073	-0.001	-0.69	-0.028	0.0080	-0.001	-0.00	0.0082	-0.002	-0.00	-0.028	0.0509	0.005
0.81	-0.028	0.084	-0.002	-0.01	-0.028	0.008	0	-0.70	-0.028	0.0073	-0.001	-0.70	-									

TABLE XIII.- GEOMETRIC CHARACTERISTICS AND WIND-TUNNEL DATA  
FOR A PLANE TAPERED WING OF ASPECT RATIO 3.1  
WITH 3-PERCENT-THICK ROUNDED-NOSE SECTION  
(a) Geometric characteristics



Aspect ratio . . . . .	3.08
Taper ratio . . . . .	.388
Airfoil section (streamwise) . . . . .	3-percent-thick biconvex with elliptical nose
Total area, square feet . . . . .	2.425
Mean aerodynamic chord, $\bar{c}$ , feet . . . . .	.944
Dihedral, degrees . . . . .	0
Twist, degrees . . . . .	0
Incidence, degrees . . . . .	0
Camber . . . . .	None
Distance, wing reference plane to body axis, feet . . . . .	0

(b) Data obtained in Ames 12-foot pressure wind tunnel

$\alpha$	$C_L$	$C_D$	$C_m$	$\alpha$	$C_L$	$C_D$	$C_m$	$\alpha$	$C_L$	$C_D$	$C_m$	$\alpha$	$C_L$	$C_D$	$C_m$
M=0.25 $R=2.4 \times 10^6$				M=0.60 $R=2.4 \times 10^6$				M=0.25 $R=4.6 \times 10^6$				M=0.25 $R=8.3 \times 10^6$			
0	-0.010	0.0058	0.001	-0.01	-0.011	0.0065	-0.001	0	-0.009	0.0072	0	0	-0.013	0.0079	-0.001
-.71	-.047	.0055	-.004	-.71	-.054	.0076	-.007	-.71	-.048	.0059	-.005	-.71	-.054	.0063	-.005
0	-.007	.0055	0	-.01	-.010	.0067	-.003	0	-.009	.0069	-.002	0	-.012	.0072	-.002
1.01	.044	.0062	.006	1.01	.051	.0078	.003	1.01	.045	.0074	.004	1.01	.037	.0068	.003
2.02	.098	.0089	.010	2.02	.113	.0103	.010	2.02	.098	.0089	.008	2.01	.077	.0074	.006
3.02	.145	.0102	.014	3.03	.170	.0132	.013	3.02	.155	.0113	.012	3.02	.149	.0098	.011
4.03	.212	.0169	.019	4.04	.238	.0196	.017	4.03	.212	.0162	.017	4.03	.206	.0157	.014
5.04	.265	.0240	.025	5.05	.301	.0281	.023	5.04	.273	.0252	.021	5.04	.265	.0271	.017
6.05	.321	.0343	.031	6.06	.378	.0409	.025	6.05	.332	.0359	.026	6.05	.328	.0378	.023
8.07	.458	.0656	.033	8.08	.503	.0712	.018	8.07	.449	.0638	.030	8.07	.441	.0654	.027
10.09	.591	.1074	.014	10.10	.639	.1169	-.010	10.10	.597	.1087	.013	10.09	.583	.1063	.019
12.11	.702	.1579	-.037	12.11	.689	.1571	-.055	12.11	.708	.1590	-.036	12.12	.721	.1566	-.034
14.12	.772	.1924	-.062	14.11	.705	.1905	-.078	14.12	.732	.1954	-.073	0	-.007	.0079	-.010
16.12	.723	.2227	-.072	16.11	.692	.2166	-.079	16.11	.713	.2221	-.080				
18.11	.712	.2488	-.078	18.20	.723	.2539	-.083	18.11	.708	.2483	-.078				
20.12	.723	.2809	-.078	20.12	.727	.2849	-.079	20.12	.731	.2654	-.081				
22.12	.759	.3251	-.081	22.12	.774	.3340	-.090	22.13	.791	.3389	-.083				
24.13	.810	.3799	-.085	24.13	.831	.3915	-.103	24.13	.828	.3898	-.089				
26.14	.847	.4309	-.093	26.14	.874	.4484	-.108	26.14	.855	.4368	-.093				
28.14	.854	.4746	-.098	28.14	.900	.5015	-.115	28.14	.864	.4790	-.099				
0	-.010	.0054	0	0	-.005	.0079	-.007	0	-.007	.0052	-.002				

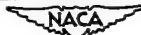


TABLE XIII.- GEOMETRIC CHARACTERISTICS AND WIND-TUNNEL DATA FOR A PLANE  
TAPERED WING OF ASPECT RATIO 3.1 WITH 3-PERCENT-THICK  
ROUNDED-NOSE SECTION - Continued

(c) Data obtained in Ames 6- by 6-foot supersonic wind tunnel

a C <sub>L</sub> C <sub>D</sub> C <sub>M</sub>				a C <sub>L</sub> C <sub>D</sub> C <sub>M</sub>				a C <sub>L</sub> C <sub>D</sub> C <sub>M</sub>				a C <sub>L</sub> C <sub>D</sub> C <sub>M</sub>				a C <sub>L</sub> C <sub>D</sub> C <sub>M</sub>							
M=0.61 Rel=1.4x10 <sup>-6</sup>				M=0.72 Rel=1.4x10 <sup>-6</sup>				M=0.76 Rel=1.4x10 <sup>-6</sup>				M=0.81 Rel=1.4x10 <sup>-6</sup>				M=0.91 Rel=1.4x10 <sup>-6</sup>							
-6.49	-0.446	0.0513	-0.019	-6.75	-0.480	0.0561	-0.016	-6.79	-0.501	0.0583	-0.022	-6.66	-0.542	0.0637	-0.033	-6.81	-0.680	0.0804	0.063	-6.79	-0.664	0.0891	0.066
-3.42	-0.375	0.0569	-0.020	-5.47	-0.400	0.0596	-0.021	-5.20	-0.416	0.0606	-0.024	-5.73	-0.441	0.0643	-0.030	-5.72	-0.605	0.0667	0.026	-5.69	-0.575	0.0765	0.064
-1.36	-0.304	0.0539	-0.017	-3.48	-0.317	0.0576	-0.018	-1.41	-0.334	0.0707	-0.021	-4.45	-0.360	0.0882	-0.024	-1.39	-0.487	0.0811	0.026	-1.36	-0.454	0.0833	0.024
-3.27	-0.334	0.0534	-0.017	-3.30	-0.347	0.0518	-0.018	-3.32	-0.353	0.0785	-0.023	-3.34	-0.295	0.0813	-0.025	-3.43	-0.332	0.0833	-0.025	-3.44	-0.347	0.0875	0.024
-4.73	-1.164	0.143	-0.008	-7.76	-0.807	0.149	-0.009	-7.77	-0.216	0.153	-0.006	-7.80	-0.234	0.150	-0.011	-7.89	-0.291	0.173	-0.010	-7.86	-0.277	0.200	-0.010
-1.56	-0.123	0.0559	-0.003	-1.22	-0.169	0.123	-0.004	-1.67	-0.153	0.030	-0.003	-1.69	-0.145	0.0301	-0.004	-1.72	-0.158	0.0404	-0.010	-1.74	-0.154	0.0405	-0.010
-1.10	-0.093	0.0563	-0.003	-1.07	-0.168	0.123	-0.003	-1.85	-0.040	0.0775	-0.001	-1.86	-0.042	0.0694	0	-1.88	-0.059	0.0808	-0.009	-1.86	-0.077	0.0975	-0.008
-0.96	-0.073	0.0561	-0.003	-0.97	-0.168	0.067	-0.003	-1.57	-0.077	0.0683	0	-1.58	-0.078	0.0671	0	-1.60	-0.088	0.074	-0.006	-1.58	-0.086	0.0704	-0.006
-0.89	-0.033	0.0528	-0.001	-0.82	-0.168	0.062	-0.001	-1.21	-0.077	0.0683	-0.001	-1.22	-0.078	0.0661	0.001	-1.24	-0.088	0.0683	-0.009	-1.22	-0.086	0.0704	-0.008
-0.86	-0.005	0.0562	0	-0.77	-0.167	0.067	-0.001	-0.91	-0.077	0.0683	-0.001	-0.92	-0.078	0.0661	0.001	-0.94	-0.088	0.0683	-0.009	-0.92	-0.086	0.0704	-0.008
-0.53	-0.027	0.0566	-0.001	-0.54	-0.168	0.068	-0.001	-0.54	-0.077	0.0683	-0.001	-0.55	-0.078	0.0661	0.001	-0.57	-0.088	0.0683	-0.009	-0.55	-0.086	0.0704	-0.008
-0.61	-0.018	0.0573	0	-0.61	-0.168	0.074	-0.001	-0.61	-0.077	0.0683	-0.001	-0.62	-0.078	0.0661	0.001	-0.63	-0.088	0.0683	-0.009	-0.62	-0.086	0.0704	-0.008
1.08	-0.067	0.0681	0.002	-1.09	-0.172	0.082	0.002	-1.10	-0.076	0.0684	0.002	-1.11	-0.077	0.0662	0.002	-1.12	-0.088	0.0684	0.009	-1.11	-0.086	0.0705	0.008
1.62	-0.103	0.100	0.003	-1.16	-0.170	0.102	0.004	-1.04	-0.113	0.103	0.005	-1.66	-0.119	0.103	0.006	-1.67	-0.120	0.103	0.005	-1.66	-0.118	0.103	0.006
2.16	-0.137	0.124	0.003	-2.18	-0.167	0.126	0.005	-2.20	-0.153	0.126	0.007	-2.21	-0.158	0.126	0.008	-2.21	-0.160	0.126	0.007	-2.21	-0.158	0.126	0.008
2.70	-0.175	0.141	0.006	-2.73	-0.168	0.150	0.008	-2.73	-0.194	0.151	0.009	-2.76	-0.202	0.151	0.010	-2.81	-0.203	0.151	0.010	-2.81	-0.202	0.151	0.010
3.23	-0.214	0.172	0.009	-3.26	-0.229	0.178	0.010	-3.27	-0.237	0.181	0.011	-3.22	-0.244	0.181	0.013	-3.28	-0.244	0.181	0.013	-3.28	-0.243	0.181	0.013
4.33	-0.286	0.253	0.014	-6.36	-0.305	0.266	0.015	-3.39	-0.324	0.273	0.018	-3.42	-0.339	0.273	0.021	-4.34	-0.340	0.273	0.021	-4.34	-0.339	0.273	0.021
5.41	-0.365	0.375	0.019	-5.45	-0.363	0.366	0.020	-5.48	-0.402	0.367	0.023	-5.53	-0.406	0.367	0.027	-5.59	-0.373	0.362	0.029	-5.57	-0.362	0.362	0.029
6.48	-0.436	0.523	0.018	-2.55	-0.476	0.584	0.026	-6.59	-0.496	0.595	0.027	-6.65	-0.537	0.637	0.030	-6.78	-0.537	0.637	0.030	-6.78	-0.536	0.637	0.030
10.73	-7.01	1.109	-0.039	-10.77	-0.597	1.150	-0.047	-10.77	-0.587	1.157	-0.047	-10.89	-0.585	1.156	-0.047	-10.89	-0.584	1.156	-0.047	-10.89	-0.583	1.156	-0.047
12.73	-7.29	1.777	-0.072	-12.80	-0.597	1.150	-0.072	-12.81	-0.573	1.158	-0.073	-12.87	-0.573	1.158	-0.073	-12.87	-0.572	1.158	-0.073	-12.87	-0.571	1.158	-0.073
14.76	-7.60	2.111	-0.087	-14.78	-0.597	1.150	-0.087	-14.85	-0.561	1.221	-0.087	-14.85	-0.561	1.221	-0.087	-14.85	-0.560	1.221	-0.087	-14.85	-0.559	1.221	-0.087
16.79	-7.65	2.483	-0.091	-16.80	-0.597	1.150	-0.091	-16.85	-0.561	1.221	-0.091	-16.85	-0.561	1.221	-0.091	-16.85	-0.560	1.221	-0.091	-16.85	-0.559	1.221	-0.091
17.87	-7.75	2.682	-0.092	-17.88	-0.597	1.150	-0.092	-17.88	-0.561	1.221	-0.092	-17.88	-0.561	1.221	-0.092	-17.88	-0.560	1.221	-0.092	-17.88	-0.559	1.221	-0.092
M=1.20 Rel=1.4x10 <sup>-6</sup>				M=1.30 Rel=1.4x10 <sup>-6</sup>				M=1.40 Rel=1.4x10 <sup>-6</sup>				M=1.50 Rel=1.4x10 <sup>-6</sup>				M=1.60 Rel=1.4x10 <sup>-6</sup>				M=1.70 Rel=1.4x10 <sup>-6</sup>			
-6.39	-0.545	0.0752	0.073	-6.34	-0.459	0.0668	0.069	-6.31	-0.404	0.0612	0.069	-6.29	-0.376	0.0563	0.069	-6.27	-0.349	0.0566	0.063	-6.27	-0.322	0.0495	0.066
-4.21	-0.366	0.0517	0.050	-4.21	-0.307	0.056	0.046	-4.22	-0.277	0.0572	0.043	-4.21	-0.252	0.0563	0.043	-4.19	-0.237	0.0523	0.042	-4.18	-0.219	0.0505	0.040
-3.21	-0.275	0.0317	0.036	-3.19	-0.333	0.0301	0.034	-3.17	-0.203	0.0287	0.032	-3.17	-0.194	0.0283	0.032	-3.16	-0.180	0.0269	0.032	-3.14	-0.165	0.0258	0.032
-2.68	-0.231	0.0267	0.031	-2.66	-0.197	0.026	0.026	-2.65	-0.174	0.0262	0.027	-2.64	-0.162	0.0231	0.027	-2.61	-0.151	0.0220	0.026	-2.63	-0.139	0.0210	0.026
-2.15	-0.185	0.0287	0.029	-2.14	-0.160	0.0229	0.023	-2.13	-0.148	0.0223	0.022	-2.12	-0.142	0.0211	0.022	-2.11	-0.122	0.0196	0.021	-2.10	-0.111	0.0188	0.021
-1.88	-0.141	0.0197	0.017	-1.81	-0.123	0.0201	0.017	-1.80	-0.108	0.0200	0.016	-1.79	-0.109	0.0183	0.017	-1.79	-0.093	0.0176	0.016	-1.78	-0.084	0.0171	0.015
-1.09	-0.099	0.0176	0.012	-1.08	-0.068	0.0182	0.011	-1.07	-0.074	0.0182	0.010	-1.06	-0.069	0.0183	0.011	-1.06	-0.064	0.0161	0.010	-1.05	-0.057	0.0158	0.010
-0.89	-0.076	0.0162	0.005	-0.76	-0.061	0.0176	0.005	-0.76	-0.077	0.0177	0.007	-0.76	-0.080	0.0165	0.009	-0.76	-0.049	0.0177	0.008	-0.75	-0.044	0.0175	0.008
-0.55	-0.032	0.0159	0.005	-0.55	-0.047	0.0178	0.005	-0.55	-0.077	0.0178	0.007	-0.55	-0.080	0.0165	0.009	-0.55	-0.036	0.0174	0.008	-0.55	-0.032	0.0173	0.008
-0.26	-0.010	0.0159	0.001	-0.26	-0.047	0.0178	0.001	-0.26	-0.077	0.0178	0.003	-0.26	-0.080	0.0165	0.003	-0.26	-0.036	0.0173	0.003	-0.26	-0.032	0.0172	0.003
-0.21	-0.014	0.0144	0.001	-0.21	-0.047	0.0178	0.001	-0.21	-0.077	0.0178	0.003	-0.21	-0.080	0.0165	0.003	-0.21	-0.036	0.0173	0.003	-0.21	-0.032	0.0172	0.003
-0.17	-0.009	0.0183	0.001	-0.17	-0.047	0.0178	0.001	-0.17	-0.077	0.0178	0.003	-0.17	-0.080	0.0165	0.003	-0.17	-0.036	0.0173	0.003	-0.17	-0.032	0.0172	0.003
-1.17	-0.077	0.0165	0.001	-1.17	-0.047	0.0178	0.001	-1.17	-0.077	0.0178	0.003	-1.17	-0.080	0.0165	0.003	-1.17	-0.036	0.0173	0.003	-1.17	-0.032	0.0172	0.003
-1.05	-0.056	0.0165	0.001	-1.05	-0.047	0.0178	0.001	-1.05	-0.077	0.0178	0.003	-1.05	-0.080	0.0165	0.003	-1.05	-0.036	0.0173	0.003	-1.05	-0.032	0.0172	0.003
-0.79	-0.039	0.0150	0.001	-0.79	-0.047	0.0177	0.001	-0.79	-0.077	0.0177	0.003	-0.79	-0.080	0.0165	0.003	-0.79	-0.036	0.0173	0.003	-0.79	-0.032	0.0172	0.003
-0.54	-0.024	0.0147	0.001	-0.54	-0.047	0.0178	0.001	-0.54	-0.077	0.0178	0.003	-0.54	-0.080	0.0165	0.003	-0.54	-0.036	0.0173	0.003	-0.54	-0.032	0.0172	0.003
-0.31	-0.014	0.0147	0.001	-0.31	-0.047	0.0178	0.001	-0.31	-0.077	0.0178	0.003	-0.31	-0.080	0.0165	0.003	-0.31	-0.036	0.0173	0.003	-0.31	-0.032	0.0172	0.003
-0.26	-0.006	0.0147	0.001	-0.26	-0.047	0.0178	0.001	-0.26	-0.077	0.0178	0.003	-0.26	-0.080	0.0165	0.003	-0.26	-0.036	0.0173	0.003	-0.26	-0.032	0.0172	0.003
-0.20	-0.005	0.0147	0.001	-0.20	-0.047	0.0178	0.001	-0.20	-0.077	0.0178	0.003	-0.20	-0.080	0.0165	0.003	-0.20	-0.036	0.0173	0.003	-0.20	-0.032	0.0172	0.003
-0.16	-0.007	0.0147	0.001	-0.16	-0.047	0.0178	0.001	-0.16	-0.077	0.0178	0.003	-0.16	-0.080	0.0165	0.003	-0.16	-0.036	0.0173	0.003	-0.16	-0.032		

## CONTINUATION

The NACA logo, which consists of the letters "NACA" in a serif font, centered within a stylized aircraft wing outline.

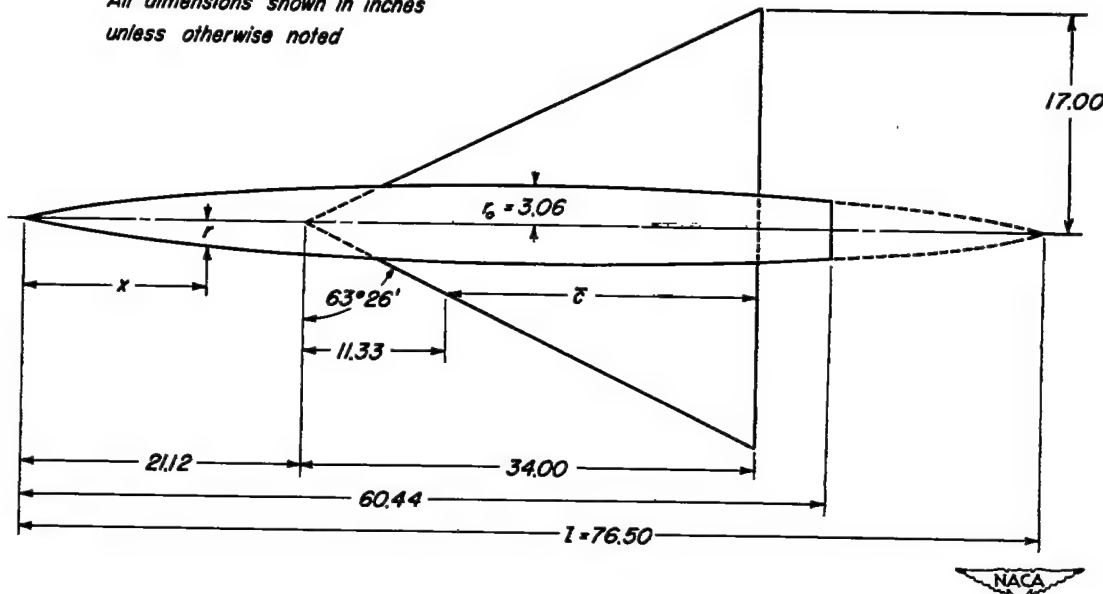
TABLE XIII.- GEOMETRIC CHARACTERISTICS AND WIND-TUNNEL DATA FOR A PLANE  
TAPERED WING OF ASPECT RATIO 3.1 WITH 3-PERCENT-THICK  
ROUNDED-NOSE SECTION - Concluded

(c) Data obtained in Ames 6- by 6-foot supersonic wind tunnel - Concluded



TABLE XIV.- GEOMETRIC CHARACTERISTICS AND WIND-TUNNEL DATA FOR  
A TRIANGULAR WING OF ASPECT RATIO 2, CAMBERED AND TWISTED  
FOR A TRAPEZOIDAL SPAN LOAD DISTRIBUTION  
(a) Geometric characteristics

*All dimensions shown in inches  
unless otherwise noted*



Aspect ratio . . . . .	2
Taper ratio . . . . .	0
Airfoil section (streamwise) . . . . .	NACA 0005-63
Total area, square feet . . . . .	4.014
Mean aerodynamic chord, $\bar{c}$ , feet . . . . .	1.889
Dihedral, degrees . . . . .	0
Twist, degrees . . . . .	see fig 1
Incidence, degrees . . . . .	0
Camber . . . . .	see fig 1
Distance, wing reference plane to body axis, feet . . . . .	0
Design lift coefficient at $M=1.53$ . . . . .	0.25

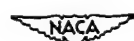
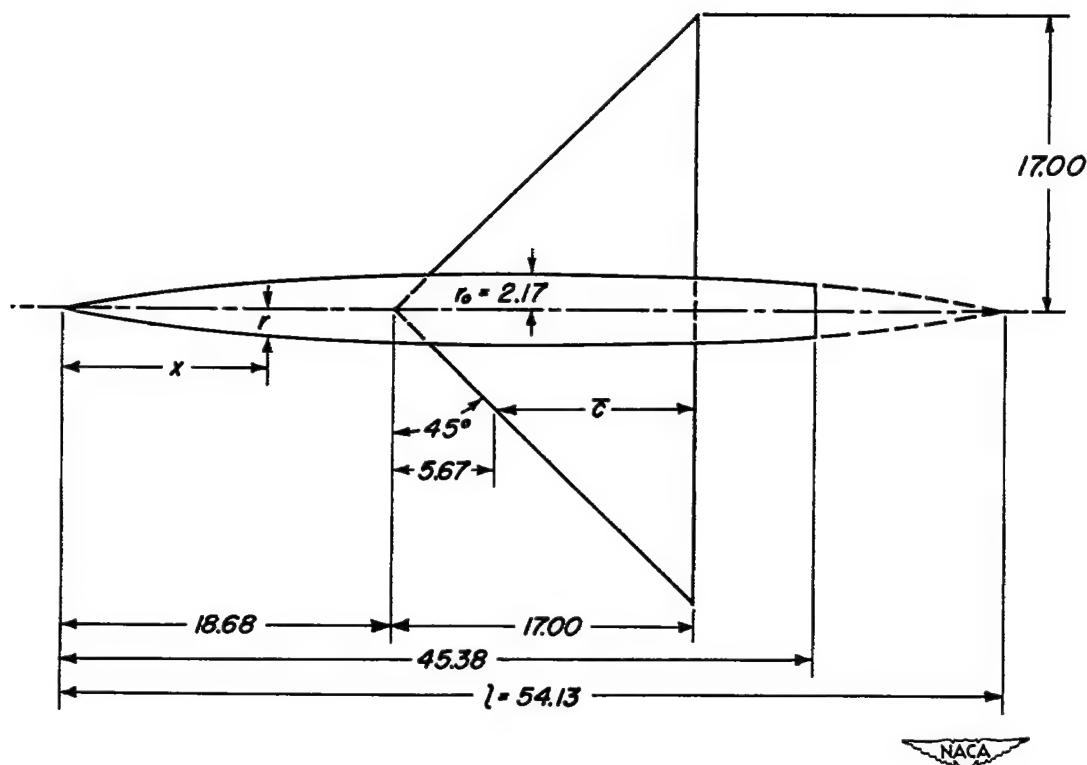
TABLE XIV. - GEOMETRIC CHARACTERISTICS AND WIND-TUNNEL DATA FOR A TRIANGULAR WING OF ASPECT RATIO 2, CAMBERED AND TWISTED FOR A TRAPEZOIDAL SPAN LOAD DISTRIBUTION - Concluded

(b) Data obtained in Ames 6- by 6-foot supersonic wind tunnel

$\alpha$	$C_L$	$C_D$	$C_m$	$\alpha$	$C_L$	$C_D$	$C_m$	$\alpha$	$C_L$	$C_D$	$C_m$	$\alpha$	$C_L$	$C_D$	$C_m$	$\alpha$	$C_L$	$C_D$	$C_m$
$M=0.62 \quad R=3 \cdot 10^{-6}$																			
0.07	0.070	0.0103	-0.010	0.07	0.056	0.0114	-0.012	0.09	0.058	0.0130	-0.015	0.02	0.040	0.0183	-0.012	0.05	0.043	0.0194	-0.014
-1.00	-0.011	-0.018	-0.002	-1.00	-0.003	-0.011	-0.005	-1.01	-0.004	-0.012	-0.005	-1.01	-0.010	-0.021	-0.002	-1.00	-0.003	-0.019	-0.002
-2.07	-0.050	-0.14	-0.006	-2.08	-0.048	-0.146	-0.005	-2.07	-0.048	-0.133	-0.005	-2.04	-0.063	-0.213	-0.015	-2.03	-0.046	-0.219	-0.009
-3.14	-0.095	0.075	-0.13	-3.16	-0.105	-0.156	-0.15	-3.17	-0.107	-0.199	-0.16	-3.06	-0.114	-0.254	-0.029	-3.06	-0.095	-0.257	-0.029
-0.7	-0.047	-0.010	-0.07	-0.7	-0.053	-0.116	-0.012	-0.9	-0.06	-0.120	-0.023	-0.1	-0.03	-0.184	-0.011	-0.04	-0.041	-0.197	-0.013
1.13	0.094	0.111	-0.17	1.15	0.108	0.129	-0.02	1.16	0.117	0.129	-0.026	1.05	0.087	0.193	-0.084	1.05	0.067	0.206	1.05
2.19	1.13	0.126	-0.023	2.23	1.16	0.143	-0.032	2.19	1.17	0.149	-0.036	2.07	1.16	0.219	-0.038	2.07	1.14	0.231	-0.037
3.26	1.19	0.151	-0.030	3.30	1.20	0.166	-0.039	3.33	1.22	0.174	-0.046	3.09	1.18	0.208	-0.050	3.09	1.17	0.205	-0.047
4.32	2.23	0.186	-0.037	4.38	2.29	0.211	-0.046	4.41	2.30	0.228	-0.054	4.12	2.23	0.233	-0.064	4.12	2.22	0.245	-0.059
5.40	2.78	0.257	-0.044	5.45	3.04	0.279	-0.053	5.49	3.27	0.310	-0.062	5.15	2.52	0.387	-0.076	5.14	2.50	0.390	-0.070
6.16	3.28	0.314	-0.051	6.52	3.49	0.342	-0.059	6.58	3.78	0.380	-0.074	6.17	3.25	0.471	-0.086	6.16	3.24	0.472	-0.077
8.05	3.91	0.465	-0.065	8.12	4.27	0.495	-0.072	8.19	4.72	0.611	-0.089	7.71	3.94	0.634	-0.107	7.70	3.65	0.624	-0.094
9.64	4.60	0.585	-0.070	9.75	5.05	0.715	-0.084	9.81	5.46	0.875	-1.03	9.24	4.28	0.936	-1.23	9.24	4.24	0.853	-1.09
11.25	5.13	0.682	-0.082	11.36	5.29	1.036	-0.099	11.43	5.62	1.269	-1.15	10.78	5.22	1.079	-1.16	10.77	5.22	1.033	-1.14
12.86	6.07	1.109	-0.092	12.99	6.69	1.110	-0.113	12.95	7.13	1.289	-1.15	12.38	5.97	1.360	-1.15	12.31	5.36	1.279	-1.12
14.17	6.93	1.663	-0.103	14.61	7.49	1.184	-0.126									13.83	5.92	1.553	-1.11
16.09	7.62	2.004	-0.113	16.26	8.40	2.375	-0.145									15.38	6.48	1.869	-1.04
17.73	8.73	2.457	-0.126	17.92	9.52	3.019	-0.169									15.37	6.09	1.766	-1.04
$M=1.40 \quad R=3 \cdot 10^{-6}$																			
0.02	0.044	0.076	-0.014	0.02	0.037	0.0185	-0.013	0.03	0.027	0.0197	-0.011	0.02	0.041	0.0186	-0.013	0.03	0.041	0.0185	-0.013
-1.01	0	-0.180	-0.004	-1.01	-0.003	-0.059	-0.005	-1.02	-0.004	-0.059	-0.005	-1.03	-0.005	-0.059	0	-1.04	-0.004	-0.058	-0.005
-2.03	-0.040	-0.096	-0.007	-2.03	-0.097	-0.137	-0.006	-2.05	-0.098	-0.137	-0.006	-2.06	-0.098	-0.213	-0.009	-2.05	-0.098	-0.213	-0.008
-3.04	-0.085	-0.182	-0.018	-3.06	-0.186	-0.231	-0.016	-3.10	-0.177	-0.268	-0.009	-3.10	-0.177	-0.289	-0.003	-3.09	-0.177	-0.289	-0.003
-0.01	-0.083	-0.181	-0.014	-0.01	-0.057	-0.031	-0.013	-0.03	-0.037	-0.029	-0.013	-0.04	-0.037	-0.029	-0.03	-0.04	-0.037	-0.029	
1.04	0.093	0.186	-0.025	1.07	0.193	0.193	-0.025	1.07	0.197	0.195	-0.026	1.06	0.197	0.195	-0.026	1.06	0.197	0.195	-0.026
2.07	1.24	0.205	-0.025	2.06	1.17	0.217	-0.031	2.12	1.37	0.220	-0.036	2.12	1.57	0.224	-0.037	2.12	1.36	0.225	-0.036
3.09	1.63	0.207	-0.036	3.08	1.59	0.234	-0.045	3.17	1.92	0.260	-0.051	3.16	1.84	0.263	-0.051	3.15	1.71	0.266	-0.047
4.11	2.06	0.311	-0.037	4.14	1.94	0.264	-0.051	4.21	2.39	0.313	-0.062	4.20	2.26	0.314	-0.061	4.19	2.17	0.316	-0.059
5.13	2.49	0.375	-0.066	5.10	2.32	0.348	-0.068	5.20	2.87	0.385	-0.078	5.20	2.71	0.391	-0.078	5.21	2.59	0.395	-0.068
6.15	2.89	0.429	-0.075	6.18	2.68	0.443	-0.077	6.30	3.36	0.477	-0.091	6.29	3.15	0.483	-0.091	6.27	2.98	0.470	-0.081
7.68	3.32	0.504	-0.099	7.68	3.20	0.507	-0.084					7.83	3.80	0.632	-0.099	7.83	3.56	0.629	-0.093
9.22	4.02	0.560	-0.108	9.21	3.71	0.524	-0.096					9.39	4.24	0.806	-0.108	7.83	3.45	0.619	-0.091
10.75	4.45	0.597	-0.115	10.79	4.20	0.594	-0.111												
12.23	4.72	0.629	-0.117	12.21	4.71	1.14	-0.120												
13.82	5.40	1.126	-0.126	13.82	5.21	1.362	-0.130												
15.36	5.88	1.700	-0.148	15.36	5.86	1.694	-0.140												
16.89	6.36	2.006	-0.158	16.88	5.99	1.902	-0.147												
18.44	6.83	2.247	-0.167	18.42	6.25	2.230	-0.153												
21.24	7.26	2.659	-0.173	19.96	6.88	2.873	-0.159												
23.07	8.12	3.466	-0.186	23.04	7.71	3.333	-0.172												
24.61	8.54	3.987	-0.193	24.58	8.03	3.773	-0.179												
$M=1.70 \quad R=5 \cdot 10^{-6}$																			
0.03	0.037	0.0384	-0.013	0.10	0.049	0.0126	-0.010	0.14	0.066	0.0117	-0.014	0.15	0.069	0.0123	-0.016	0.05	0.042	0.0165	-0.012
-1.02	-0.006	-0.187	-0.004	1.22	1.10	0.122	-0.019	-1.01	-0.005	-0.133	-0.003	-1.00	-0.007	-0.193	-0.003	-1.02	-0.010	-0.173	-0.002
-2.05	-0.041	0.026	-0.007	2.33	1.63	0.143	-0.028	-2.15	-0.079	-0.167	-0.008	-2.15	-0.061	-0.173	-0.008	-2.09	-0.065	-0.195	-0.011
-3.09	-0.084	0.026	-0.017	3.43	2.15	0.171	-0.036	-3.28	-1.21	-0.216	-0.018	-3.28	-1.20	-0.216	-0.018	-3.17	-1.21	-0.240	-0.032
-0.03	-0.037	0.187	-0.012	1.98	2.29	0.207	-0.042	-0.042	-0.059	-0.121	-0.013	2.40	1.88	0.167	-0.042	-0.05	-0.039	-0.167	-0.029
1.06	0.177	0.097	-0.023	2.02	3.07	0.327	-0.049	1.28	1.23	0.330	-0.054	3.54	2.46	0.207	-0.049	1.12	0.099	-0.176	-0.023
2.11	1.17	0.229	-0.033	6.71	3.45	0.382	-0.055	2.40	1.76	0.373	-0.054	4.87	3.05	0.259	-0.062	2.20	1.85	0.208	-0.040
3.14	1.59	0.265	-0.043	8.36	4.19	0.446	-0.065	3.55	2.22	0.381	-0.042	5.81	3.66	0.367	-0.078	3.27	1.99	0.269	-0.058
5.21	2.32	0.374	-0.062	11.70	7.71	0.564	-0.090	5.73	3.86	0.394	-0.077	8.63	5.08	0.375	-0.087	4.34	2.84	0.307	-0.067
6.29	2.66	0.449	-0.071	13.38	6.61	1.235	-0.100	6.88	3.86	0.394	-0.087								
7.81	3.21	0.586	-0.083					8.57	4.64	0.478	-0.079								
9.36	3.76	0.755	-0.096					10.23	5.45	0.608	-0.092								
$M=1.60 \quad R=5 \cdot 10^{-6}$																			
0.03	0.037	0.0184	-0.013	0.10	0.049	0.0126	-0.010	0.14	0.066	0.0117	-0.014	0.15	0.069	0.0123	-0.016	0.05	0.042	0.0165	-0.012
-1.02	-0.006	-0.187	-0.004	1.22	1.10	0.122	-0.019	-1.01	-0.005	-0.133	-0.003	-1.00	-0.007	-0.193	-0.003	-1.02	-0.010	-0.173	-0.002
-2.05	-0.048	0.027	-0.007	2.33	1.63	0.143	-0.028	-2.15	-0.079	-0.167	-0.008	-2.15	-0.061	-0.173	-0.008	-2.09	-0.065	-0.195	-0.011
-3.09	-0.096	0.023	-0.017	3.43	2.15	0.171	-0.036	-3.28	-1.21	-0.216	-0.018	-3.28	-1.20	-0.216	-0.018	-3.17	-1.21		

TABLE XV.- GEOMETRIC CHARACTERISTICS AND WIND-TUNNEL DATA FOR  
 A TRIANGULAR WING OF ASPECT RATIO 4, CAMBERED AND TWISTED  
 FOR A TRAPEZOIDAL SPAN LOAD DISTRIBUTION  
 (a) Geometric characteristics

*All dimensions shown in inches  
 unless otherwise noted*



Aspect ratio . . . . .	4
Taper ratio . . . . .	0
Airfoil section (streamwise) . . . . .	NACA 0005-63
Total area, square feet . . . . .	2.007
Mean aerodynamic chord, $\bar{c}$ , feet . . . . .	.944
Dihedral, degrees . . . . .	0
Twist, degrees . . . . .	see fig 1
Incidence, degrees . . . . .	0
Camber . . . . .	see fig 1
Distance, wing reference plane to body axis, feet . . . . .	0
Design lift coefficient at $M=1.15$ . . . . .	0.35

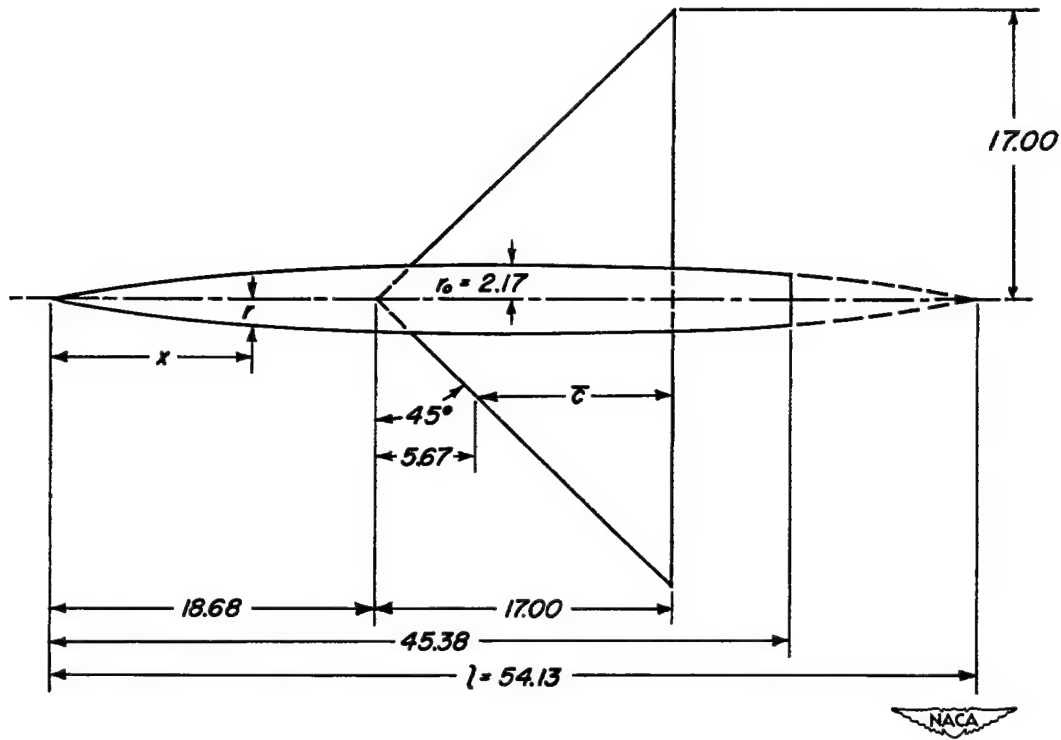
TABLE XV. - GEOMETRIC CHARACTERISTICS AND WIND-TUNNEL DATA FOR A TRIANGULAR WING OF ASPECT RATIO 4, CAMBERED AND TWISTED FOR A TRAPEZOIDAL SPAN LOAD DISTRIBUTION - Concluded  
 (b) Data obtained in Ames 12-foot pressure wind tunnel

$\alpha$	$C_L$	$C_B$	$C_K$	$\epsilon$	$C_L$	$C_B$	$C_K$	$\alpha$	$C_L$	$C_B$	$C_K$	$\epsilon$	$C_L$	$C_B$	$C_K$	$\epsilon$	$C_L$	$C_B$	$C_K$	$\epsilon$	$C_L$	$C_B$	$C_K$		
M=0.23	E=1.2e10 <sup>6</sup>				M=0.40	E=1.2e10 <sup>6</sup>			M=0.50	E=1.2e10 <sup>6</sup>			M=0.80	E=1.2e10 <sup>6</sup>			M=0.90	E=1.2e10 <sup>6</sup>			M=0.95	E=1.2e10 <sup>6</sup>			
-9.06	-0.437	0.795	0.030	-0.01	-0.057	0.0094	-0.008	-0.01	0.070	0.0111	-0.007	-0.01	-0.070	0.0111	-0.007	-0.01	-0.081	0.0110	-0.016	-0.01	-0.109	0.0110	-0.023		
-8.06	-0.437	0.656	0.031	-0.05	-0.06	-0.49	0.071	-0.015	-0.06	-0.473	-0.002	-0.05	-0.06	-0.473	-0.002	-0.05	-0.081	-0.500	-0.103	-0.08	-0.08	-0.517	-0.103	-0.073	
-5.03	-0.319	0.456	0.027	-0.03	-0.03	-0.043	0.013	-0.013	-0.03	-0.389	-0.006	-0.03	-0.06	-0.389	-0.006	-0.03	-0.046	-0.518	-0.016	-0.046	-0.046	-0.520	-0.016	0.044	
-3.05	-0.226	0.300	0.020	-0.02	-0.02	-0.027	0.007	-0.007	-0.02	-0.267	-0.007	-0.02	-0.05	-0.267	-0.007	-0.02	-0.037	-0.307	-0.007	-0.037	-0.037	-0.310	-0.007	0.040	
-1.05	-0.138	0.190	0.010	-0.01	-0.01	-0.019	0.005	-0.005	-0.01	-0.168	-0.005	-0.01	-0.03	-0.168	-0.005	-0.01	-0.017	-0.214	-0.005	-0.017	-0.017	-0.218	-0.005	0.038	
-0.01	-0.068	0.113	0.012	-0.01	-0.01	-0.009	0.004	-0.004	-0.01	-0.061	-0.004	-0.01	-0.02	-0.061	-0.004	-0.01	-0.059	-0.164	-0.004	-0.059	-0.059	-0.166	-0.004	0.036	
-1.00	-0.012	0.122	0.005	-0.01	-0.01	-0.009	0.011	-0.006	-0.01	0	0.010	-0.002	-0.01	0	0.010	-0.002	-0.01	-0.002	0.111	-0.006	-0.002	-0.002	0.114	-0.006	-0.002
0.01	-0.056	-0.007	0.005	-0.01	-0.01	-0.013	0.003	-0.003	-0.01	-0.067	-0.012	-0.003	-0.01	-0.067	-0.012	-0.003	-0.011	-0.119	-0.016	-0.003	-0.01	-0.123	-0.016	-0.003	
1.00	-0.117	-0.005	0.001	-0.01	-0.01	-0.134	-0.006	-0.013	-0.01	-0.133	-0.016	-0.013	-0.01	-0.133	-0.016	-0.013	-0.124	-0.154	-0.016	-0.013	-0.125	-0.154	-0.016	-0.007	
2.00	-0.179	-0.007	-0.005	-0.01	-0.01	-0.186	-0.013	-0.019	-0.01	-0.193	-0.018	-0.013	-0.01	-0.193	-0.018	-0.013	-0.185	-0.203	-0.018	-0.013	-0.187	-0.203	-0.018	-0.003	
3.00	-0.239	-0.015	-0.011	-0.01	-0.01	-0.268	-0.014	-0.023	-0.01	-0.266	-0.024	-0.014	-0.01	-0.266	-0.024	-0.014	-0.259	-0.281	-0.024	-0.014	-0.261	-0.281	-0.024	-0.003	
4.00	-0.297	-0.021	-0.016	-0.01	-0.01	-0.311	-0.014	-0.029	-0.01	-0.307	-0.031	-0.016	-0.01	-0.307	-0.031	-0.016	-0.301	-0.329	-0.031	-0.016	-0.303	-0.329	-0.031	-0.003	
5.00	-0.355	-0.027	-0.020	-0.01	-0.01	-0.356	-0.014	-0.035	-0.01	-0.352	-0.042	-0.020	-0.01	-0.352	-0.042	-0.020	-0.347	-0.375	-0.042	-0.020	-0.349	-0.375	-0.042	-0.003	
6.00	-0.413	-0.033	-0.025	-0.01	-0.01	-0.394	-0.014	-0.043	-0.01	-0.390	-0.060	-0.025	-0.01	-0.390	-0.060	-0.025	-0.384	-0.412	-0.060	-0.025	-0.386	-0.412	-0.060	-0.003	
7.00	-0.471	-0.039	-0.031	-0.01	-0.01	-0.431	-0.014	-0.051	-0.01	-0.427	-0.078	-0.031	-0.01	-0.427	-0.078	-0.031	-0.421	-0.449	-0.078	-0.031	-0.423	-0.449	-0.078	-0.003	
8.00	-0.529	-0.045	-0.037	-0.01	-0.01	-0.469	-0.014	-0.059	-0.01	-0.465	-0.096	-0.037	-0.01	-0.465	-0.096	-0.037	-0.459	-0.487	-0.096	-0.037	-0.461	-0.487	-0.096	-0.003	
10.00	-0.686	-0.062	-0.055	-0.01	-0.01	-0.640	-0.025	-0.086	-0.01	-0.636	-0.104	-0.055	-0.01	-0.636	-0.104	-0.055	-0.629	-0.666	-0.104	-0.055	-0.631	-0.666	-0.104	-0.003	
12.00	-1.124	-0.111	-0.112	-0.01	-0.01	-1.287	-0.155	-0.195	-0.01	-1.282	-0.174	-0.112	-0.01	-1.282	-0.174	-0.112	-1.164	-1.436	-0.174	-0.112	-1.167	-1.436	-0.174	-0.003	
14.00	-1.793	-0.231	-0.231	-0.01	-0.01	-1.862	-0.269	-0.269	-0.01	-1.858	-0.288	-0.231	-0.01	-1.858	-0.288	-0.231	-1.737	-1.998	-0.288	-0.231	-1.740	-1.998	-0.288	-0.003	
16.00	-2.644	-0.382	-0.382	-0.01	-0.01	-2.587	-0.374	-0.374	-0.01	-2.582	-0.393	-0.382	-0.01	-2.582	-0.393	-0.382	-2.465	-2.714	-0.393	-0.382	-2.468	-2.714	-0.393	-0.003	
18.00	-4.664	-0.683	-0.683	-0.01	-0.01	-4.623	-0.675	-0.675	-0.01	-4.618	-0.694	-0.683	-0.01	-4.618	-0.694	-0.683	-4.491	-4.974	-0.694	-0.683	-4.494	-4.974	-0.694	-0.003	
20.00	-8.766	-1.171	-1.171	-0.01	-0.01	-8.714	-1.163	-1.163	-0.01	-8.709	-1.153	-1.171	-0.01	-8.709	-1.153	-1.171	-8.543	-9.187	-1.153	-1.171	-8.546	-9.187	-1.153	-0.003	
22.00	-13.799	-2.121	-2.121	-0.01	-0.01	-13.757	-2.113	-2.121	-0.01	-13.752	-2.103	-2.121	-0.01	-13.752	-2.103	-2.121	-13.535	-14.468	-2.103	-2.121	-13.538	-14.468	-2.103	-0.003	
24.00	-18.865	-3.193	-2.193	-0.01	-0.01	-18.813	-3.185	-2.193	-0.01	-18.808	-3.175	-2.193	-0.01	-18.808	-3.175	-2.193	-18.581	-19.432	-3.175	-2.193	-18.584	-19.432	-3.175	-0.003	
26.00	-24.929	-4.255	-3.255	-0.01	-0.01	-24.877	-4.247	-3.255	-0.01	-24.872	-4.237	-3.255	-0.01	-24.872	-4.237	-3.255	-24.644	-25.695	-4.237	-3.255	-24.647	-25.695	-4.237	-0.003	
28.00	-31.993	-5.315	-4.315	-0.01	-0.01	-31.941	-5.305	-4.315	-0.01	-31.936	-5.295	-4.315	-0.01	-31.936	-5.295	-4.315	-31.708	-32.846	-5.295	-4.315	-31.711	-32.846	-5.295	-0.003	
30.00	-40.057	-6.375	-5.375	-0.01	-0.01	-39.995	-6.365	-5.375	-0.01	-39.990	-6.355	-5.375	-0.01	-39.990	-6.355	-5.375	-39.762	-40.903	-6.355	-5.375	-39.765	-40.903	-6.355	-0.003	

(c) Data obtained in Ames 6- by 6-foot supersonic wind tunnel

TABLE XVI.- GEOMETRIC CHARACTERISTICS AND WIND-TUNNEL DATA  
FOR A PLANE TRIANGULAR WING OF ASPECT RATIO 4  
WITH NACA 0005-63 SECTION  
(a) Geometric characteristics

*All dimensions shown in inches  
unless otherwise noted*



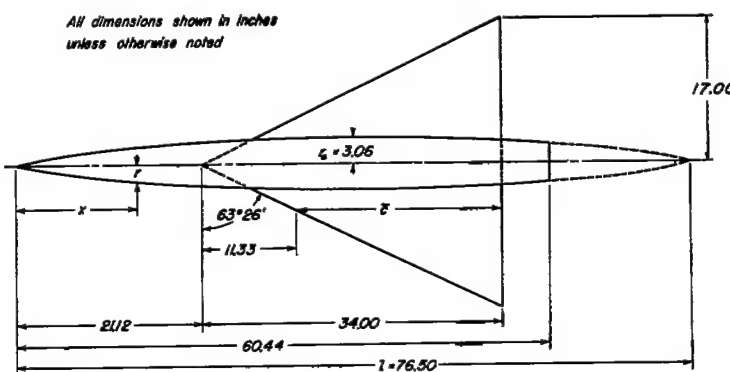
Aspect ratio . . . . .	4
Taper ratio . . . . .	0
Airfoil section (streamwise) . . . . .	NACA 0005-63
Total area, square feet . . . . .	2.007
Mean aerodynamic chord, $\bar{c}$ , feet . . . . .	.944
Dihedral, degrees . . . . .	0
Twist, degrees . . . . .	0
Incidence, degrees . . . . .	0
Camber . . . . .	None
Distance, wing reference plane to body axis, feet . . . . .	0

TABLE XVI.- GEOMETRIC CHARACTERISTICS AND WIND-TUNNEL DATA  
FOR A PLANE TRIANGULAR WING OF ASPECT RATIO 4 WITH  
NACA 0005-63 SECTION - Concluded

(b) Data obtained in Ames 12-foot pressure wind tunnel

$\alpha$	$C_L$	$C_D$	$C_H$	$\alpha$	$C_L$	$C_D$	$C_H$	$\alpha$	$C_L$	$C_D$	$C_H$	$\alpha$	$C_L$	$C_D$	$C_H$	$\alpha$	$C_L$	$C_D$	$C_H$	$\alpha$	$C_L$	$C_D$	$C_H$	
$M=0.35 \quad \alpha=1.30^{\circ}$																								
0	-0.001	0.071	-0.006	-0.07	-0.25	0.075	0.021	-0.07	-0.30	0.084	0.006	-0.07	-0.26	0.075	0.018	-0.08	-0.26	0.071	0.009	-0.08	0.02	0.029	0.009	
-1.07	-0.18	0.074	-0.08	-0.05	-0.46	0.082	0.028	-0.05	-0.50	0.084	0.02	-0.05	-0.47	0.074	0.025	-0.06	-0.48	0.070	0.023	-0.06	0.028	0.023	0.007	
-1.06	-1.07	0.073	-0.08	-0.05	-0.39	0.073	0.028	-0.05	-0.36	0.074	0.028	-0.05	-0.40	0.068	0.028	-0.06	-0.49	0.065	0.023	-0.06	0.027	0.023	0.007	
-1.05	-1.05	0.073	-0.08	-0.05	-0.39	0.070	0.028	-0.05	-0.34	0.073	0.028	-0.05	-0.37	0.064	0.027	-0.06	-0.35	0.061	0.023	-0.06	0.026	0.023	0.007	
-1.04	-1.03	0.073	-0.08	-0.05	-0.39	0.071	0.028	-0.05	-0.37	0.073	0.028	-0.05	-0.33	0.065	0.027	-0.06	-0.32	0.063	0.023	-0.06	0.025	0.023	0.007	
-1.03	-1.02	0.073	-0.08	-0.05	-0.39	0.071	0.028	-0.05	-0.38	0.073	0.028	-0.05	-0.34	0.066	0.027	-0.06	-0.31	0.062	0.023	-0.06	0.024	0.023	0.007	
-1.02	-1.01	0.073	-0.08	-0.05	-0.39	0.071	0.028	-0.05	-0.39	0.073	0.028	-0.05	-0.35	0.067	0.027	-0.06	-0.30	0.061	0.023	-0.06	0.023	0.023	0.007	
-1.01	-0.98	0.073	-0.08	-0.05	-0.39	0.072	0.028	-0.05	-0.40	0.073	0.028	-0.05	-0.36	0.068	0.027	-0.06	-0.29	0.060	0.023	-0.06	0.022	0.023	0.007	
0	0.007	0.074	-0.007	0.01	0.07	0.074	0.028	0.01	0.07	0.075	0.028	0.01	0.07	0.072	0.028	0.01	0.08	0.073	0.028	0.01	0.08	0.073	0.028	
-1.01	-0.97	0.074	-0.08	-0.05	-0.39	0.073	0.028	-0.05	-0.41	0.073	0.028	-0.05	-0.37	0.069	0.027	-0.06	-0.28	0.060	0.023	-0.06	0.022	0.023	0.007	
-1.00	-0.96	0.074	-0.08	-0.05	-0.39	0.073	0.028	-0.05	-0.42	0.073	0.028	-0.05	-0.38	0.070	0.028	-0.06	-0.27	0.059	0.023	-0.06	0.021	0.023	0.007	
-0.99	-0.95	0.074	-0.08	-0.05	-0.39	0.073	0.028	-0.05	-0.43	0.073	0.028	-0.05	-0.39	0.071	0.028	-0.06	-0.26	0.058	0.023	-0.06	0.020	0.023	0.007	
-0.98	-0.94	0.074	-0.08	-0.05	-0.39	0.073	0.028	-0.05	-0.44	0.073	0.028	-0.05	-0.40	0.072	0.028	-0.06	-0.25	0.057	0.023	-0.06	0.019	0.023	0.007	
-0.97	-0.93	0.074	-0.08	-0.05	-0.39	0.073	0.028	-0.05	-0.45	0.073	0.028	-0.05	-0.41	0.073	0.028	-0.06	-0.24	0.056	0.023	-0.06	0.018	0.023	0.007	
-0.96	-0.92	0.074	-0.08	-0.05	-0.39	0.073	0.028	-0.05	-0.46	0.073	0.028	-0.05	-0.42	0.074	0.028	-0.06	-0.23	0.055	0.023	-0.06	0.017	0.023	0.007	
-0.95	-0.91	0.074	-0.08	-0.05	-0.39	0.073	0.028	-0.05	-0.47	0.073	0.028	-0.05	-0.43	0.075	0.028	-0.06	-0.22	0.054	0.023	-0.06	0.016	0.023	0.007	
-0.94	-0.90	0.074	-0.08	-0.05	-0.39	0.073	0.028	-0.05	-0.48	0.073	0.028	-0.05	-0.44	0.076	0.028	-0.06	-0.21	0.053	0.023	-0.06	0.015	0.023	0.007	
-0.93	-0.89	0.074	-0.08	-0.05	-0.39	0.073	0.028	-0.05	-0.49	0.073	0.028	-0.05	-0.45	0.077	0.028	-0.06	-0.20	0.052	0.023	-0.06	0.014	0.023	0.007	
-0.92	-0.88	0.074	-0.08	-0.05	-0.39	0.073	0.028	-0.05	-0.50	0.073	0.028	-0.05	-0.46	0.078	0.028	-0.06	-0.19	0.051	0.023	-0.06	0.013	0.023	0.007	
-0.91	-0.87	0.074	-0.08	-0.05	-0.39	0.073	0.028	-0.05	-0.51	0.073	0.028	-0.05	-0.47	0.079	0.028	-0.06	-0.18	0.050	0.023	-0.06	0.012	0.023	0.007	
-0.90	-0.86	0.074	-0.08	-0.05	-0.39	0.073	0.028	-0.05	-0.52	0.073	0.028	-0.05	-0.48	0.080	0.028	-0.06	-0.17	0.049	0.023	-0.06	0.011	0.023	0.007	
-0.89	-0.85	0.074	-0.08	-0.05	-0.39	0.073	0.028	-0.05	-0.53	0.073	0.028	-0.05	-0.49	0.081	0.028	-0.06	-0.16	0.048	0.023	-0.06	0.010	0.023	0.007	
-0.88	-0.84	0.074	-0.08	-0.05	-0.39	0.073	0.028	-0.05	-0.54	0.073	0.028	-0.05	-0.50	0.082	0.028	-0.06	-0.15	0.047	0.023	-0.06	0.009	0.023	0.007	
-0.87	-0.83	0.074	-0.08	-0.05	-0.39	0.073	0.028	-0.05	-0.55	0.073	0.028	-0.05	-0.51	0.083	0.028	-0.06	-0.14	0.046	0.023	-0.06	0.008	0.023	0.007	
-0.86	-0.82	0.074	-0.08	-0.05	-0.39	0.073	0.028	-0.05	-0.56	0.073	0.028	-0.05	-0.52	0.084	0.028	-0.06	-0.13	0.045	0.023	-0.06	0.007	0.023	0.007	
-0.85	-0.81	0.074	-0.08	-0.05	-0.39	0.073	0.028	-0.05	-0.57	0.073	0.028	-0.05	-0.53	0.085	0.028	-0.06	-0.12	0.044	0.023	-0.06	0.006	0.023	0.007	
-0.84	-0.80	0.074	-0.08	-0.05	-0.39	0.073	0.028	-0.05	-0.58	0.073	0.028	-0.05	-0.54	0.086	0.028	-0.06	-0.11	0.043	0.023	-0.06	0.005	0.023	0.007	
-0.83	-0.79	0.074	-0.08	-0.05	-0.39	0.073	0.028	-0.05	-0.59	0.073	0.028	-0.05	-0.55	0.087	0.028	-0.06	-0.10	0.042	0.023	-0.06	0.004	0.023	0.007	
-0.82	-0.78	0.074	-0.08	-0.05	-0.39	0.073	0.028	-0.05	-0.60	0.073	0.028	-0.05	-0.56	0.088	0.028	-0.06	-0.09	0.041	0.023	-0.06	0.003	0.023	0.007	
-0.81	-0.77	0.074	-0.08	-0.05	-0.39	0.073	0.028	-0.05	-0.61	0.073	0.028	-0.05	-0.57	0.089	0.028	-0.06	-0.08	0.040	0.023	-0.06	0.002	0.023	0.007	
-0.80	-0.76	0.074	-0.08	-0.05	-0.39	0.073	0.028	-0.05	-0.62	0.073	0.028	-0.05	-0.58	0.090	0.028	-0.06	-0.07	0.039	0.023	-0.06	0.001	0.023	0.007	
-0.79	-0.75	0.074	-0.08	-0.05	-0.39	0.073	0.028	-0.05	-0.63	0.073	0.028	-0.05	-0.59	0.091	0.028	-0.06	-0.06	0.038	0.023	-0.06	0.000	0.023	0.007	
-0.78	-0.74	0.074	-0.08	-0.05	-0.39	0.073	0.028	-0.05	-0.64	0.073	0.028	-0.05	-0.60	0.092	0.028	-0.06	-0.05	0.037	0.023	-0.06	-0.001	0.023	0.007	
-0.77	-0.73	0.074	-0.08	-0.05	-0.39	0.073	0.028	-0.05	-0.65	0.073	0.028	-0.05	-0.61	0.093	0.028	-0.06	-0.04	0.036	0.023	-0.06	-0.002	0.023	0.007	
-0.76	-0.72	0.074	-0.08	-0.05	-0.39	0.073	0.028	-0.05	-0.66	0.073	0.028	-0.05	-0.62	0.094	0.028	-0.06	-0.03	0.035	0.023	-0.06	-0.003	0.023	0.007	
-0.75	-0.71	0.074	-0.08	-0.05	-0.39	0.073	0.028	-0.05	-0.67	0.073	0.028	-0.05	-0.63	0.095	0.028	-0.06	-0.02	0.034	0.023	-0.06	-0.004	0.023	0.007	
-0.74	-0.70	0.074	-0.08	-0.05	-0.39	0.073	0.028	-0.05	-0.68	0.073	0.028	-0.05	-0.64	0.096	0.028	-0.06	-0.01	0.033	0.023	-0.06	-0.005	0.023	0.007	
-0.73	-0.69	0.074	-0.08	-0.05	-0.39	0.073	0.028	-0.05	-0.69	0.073	0.028	-0.05	-0.65	0.097	0.028	-0.06	-0.00	0.032	0.023	-0.06	-0.006	0.023	0.007	
-0.72	-0.68	0.074	-0.08	-0.05	-0.39	0.073	0.028	-0.05	-0.70	0.073	0.028	-0.05	-0.66	0.098	0.028	-0.06	-0.00	0.031	0.023	-0.06	-0.007	0.023	0.007	
-0.71	-0.67	0.074	-0.08	-0.05	-0.39	0.073	0.028	-0.05	-0.71	0.073	0.028	-0.05	-0.67	0.099	0.028	-0.06	-0.00	0.030	0.023	-0.06	-0.008	0.023	0.007	
-0.70	-0.66	0.074	-0.08	-0.05	-0.39	0.073	0.028	-0.05	-0.72	0.073	0.028	-0.05	-0.68	0.100	0.028	-0.06	-0.00	0.029	0.023	-0.06	-0.009	0.023	0.007	
-0.69	-0.65	0.074	-0.08	-0.05	-0.39	0.073	0.028	-0.05	-0.73	0.073	0.028	-0.05	-0.69	0.101	0.028	-0.06	-0.00	0.028	0.023	-0.06	-0.010	0.023	0.007	
-0.68	-0.64	0.074	-0.08	-0.05	-0.39	0.073	0.028	-0.05	-0.74	0.073	0.028	-0.05	-0.70	0.102	0.028	-0.06	-0.00	0.027	0.023	-0.06	-0.011	0.023	0.007	
-0.67	-0.63	0.074	-0.08	-0.05	-0.39	0.073	0.028	-0.05	-0.75	0.073	0.028	-0.05	-0.71	0.103	0.028	-0.06	-0.00	0.026	0.023	-0.06	-0.012	0.023	0.007	
-0.66	-0.62	0.074	-0.08	-0.05	-0.39	0.073	0.028	-0.05	-0.76	0.073	0.028	-0.05	-0.72	0.104	0.028	-0.06	-0.00	0.025						

TABLE XVII.- GEOMETRIC CHARACTERISTICS AND WIND-TUNNEL DATA FOR A  
3-PERCENT-THICK TRIANGULAR WING OF ASPECT RATIO 2, CAMBERED AND  
TWISTED TO APPROXIMATE AN ELLIPTICAL SPAN LOAD DISTRIBUTION  
(a) Geometric characteristics



Aspect ratio . . . . .	2
Taper ratio . . . . .	0
Airfoil section (streamwise) . . . . .	NACA 0003-63
Total area, square feet . . . . .	4.014
Mean aerodynamic chord, $c$ , feet . . . . .	1.889
Dihedral, degrees . . . . .	0
Twist, degrees . . . . .	See Fig. 3
Incidence, degrees . . . . .	0
Camber . . . . .	See Fig. 3
Distance, wing reference plane to body axis, feet . . . . .	0
Design lift coefficient at $M = 1.53$ . . . . .	0.25

(b) Data obtained in Ames 12-foot pressure wind tunnel

$\alpha$	$C_L$	$C_D$	$C_m$	$\alpha$	$C_L$	$C_D$	$C_m$	$\alpha$	$C_L$	$C_D$	$C_m$	$\alpha$	$C_L$	$C_D$	$C_m$
$M=0.25 \quad R=4.9 \times 10^6$															
-0.01	-0.043	0.0079	0.010	-0.01	-0.044	0.0120	0.011	-0.01	-0.044	0.0111	0.010	-0.01	-0.043	0.0112	0.010
-0.72	-0.076	.0117	.014	-0.72	-0.078	0.0137	0.015	-0.72	-0.075	0.0127	0.014	-0.72	-0.078	0.0129	0.014
-0.01	-0.043	0.0099	0.010	-0.01	-0.044	0.0120	0.011	-0.01	-0.043	0.0111	0.010	-0.02	-0.046	0.0111	0.010
1.00	.006	.0080	.004	1.00	0	0.0104	0.004	1.00	0	0.0098	0.004	1.00	.001	.0099	.004
2.01	.039	.0074	-.001	2.01	.044	.0098	-.002	2.01	.040	.0092	-.001	2.01	.039	.0093	-.001
3.02	.082	.0087	-.007	3.02	.086	.0105	-.009	3.02	.080	.0096	-.007	3.02	.077	.0096	-.007
4.03	.122	.0102	-.012	4.03	.124	.0119	-.014	4.03	.119	.0109	-.012	4.03	.112	.0104	-.011
5.04	.159	.0127	-.017	5.04	.162	.0139	-.020	5.04	.156	.0130	-.017	5.04	.147	.0123	-.016
6.05	.200	.0163	-.022	6.05	.203	.0174	-.026	6.05	.191	.0158	-.021	6.05	.184	.0148	-.021
8.07	.274	.0245	-.032	8.07	.280	.0261	-.036	8.07	.264	.0229	-.031	8.07	.256	.0215	-.031
10.10	.371	.0458	-.046	10.10	.382	.0496	-.052	10.09	.357	.0419	-.045	10.09	.343	.0377	-.042
12.12	.464	.0742	-.056	12.13	.490	.0843	-.068	12.12	.458	.0721	-.056	12.12	.448	.0692	-.055
14.15	.554	.1100	-.063	14.16	.592	.1258	-.072	14.15	.536	.1105	-.064	14.14	.539	.1048	-.063
16.17	.656	.1569	-.073	16.18	.696	.1746	-.082	16.17	.660	.1567	-.075	16.17	.628	.1463	-.072
18.20	.759	.2105	-.084	18.21	.791	.2295	-.092	18.20	.758	.2103	-.084	18.19	.720	.1961	-.080
20.23	.864	.2716	-.095	20.24	.895	.2956	-.105	20.23	.861	.2735	-.094	-0.01	-.048	.0115	.010
22.25	.971	.3482	-.108	22.26	.977	.3622	-.115	22.25	.960	.3442	-.106				
24.28	1.054	.4223	-.116	24.29	1.094	.4313	-.134	24.28	1.040	.4172	-.114				
26.31	1.181	.5245	-.132	-0.01	-.045	.0125	.011	26.31	1.154	.5114	-.128				
28.33	1.253	.6111	-.139					28.32	1.225	.5978	-.132				
-0.01	-0.043	0.0090	0.010					-0.01	-0.042	0.0112	0.010				

NACA

TABLE XVII.- GEOMETRIC CHARACTERISTICS AND WIND-TUNNEL DATA  
FOR A 3-PERCENT-THICK TRIANGULAR WING OF ASPECT RATIO 2,  
CAMBERED AND TWISTED TO APPROXIMATE AN ELLIPTICAL

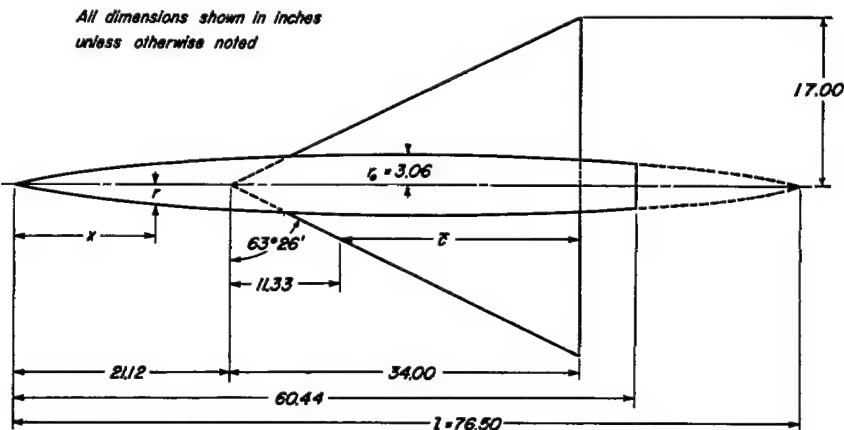
SPAN LOAD DISTRIBUTION - Concluded

(c) Data obtained in Ames 6- by 6-foot supersonic wind tunnel

M=0.61 R=7.2x10 <sup>4</sup>								M=0.81 R=3.0x10 <sup>4</sup>								M=0.91 R=3.0x10 <sup>4</sup>								M=1.30 R=3.0x10 <sup>4</sup>								M=1.53 R=3.0x10 <sup>4</sup>								M=1.70 R=3.0x10 <sup>4</sup>							
$c_L$	$c_D$	$c_m$	$c_L$	$c_D$	$c_m$	$c_L$	$c_D$	$c_m$	$c_L$	$c_D$	$c_m$	$c_L$	$c_D$	$c_m$	$c_L$	$c_D$	$c_m$	$c_L$	$c_D$	$c_m$	$c_L$	$c_D$	$c_m$	$c_L$	$c_D$	$c_m$	$c_L$	$c_D$	$c_m$	$c_L$	$c_D$	$c_m$															
-1.13	-0.090	0.0141	0.016	-1.13	-0.095	0.0142	0.019	-1.15	-0.095	0.0160	0.021	-1.05	-0.082	0.0156	0.023	-1.04	-0.073	0.0159	0.021	-1.03	-0.065	0.0177	0.019	-1.05	-0.073	0.0159	0.021	-1.06	-0.065	0.0177	0.019	-1.07	-0.071	0.0170	0.019												
-2.19	-1.140	0.087	0.023	-2.22	-1.150	0.097	0.028	-2.29	-1.162	0.0233	0.034	-2.08	-1.131	0.0216	0.036	-2.07	-1.115	0.0226	0.032	-2.06	-1.107	0.0210	0.029	-2.05	-1.107	0.0210	0.029	-2.06	-1.107	0.0210	0.029	-2.05	-1.107	0.0210	0.029												
-3.26	-1.190	0.0253	0.030	-3.31	-1.206	0.0273	0.038	-3.36	-1.222	0.0302	0.046	-3.10	-1.179	0.0273	0.044	-3.09	-1.157	0.0285	0.042	-3.08	-1.148	0.0283	0.040	-3.07	-1.148	0.0283	0.040	-3.06	-1.148	0.0283	0.040	-3.05	-1.148	0.0283	0.040												
-4.34	-1.240	0.045	0.036	-4.40	-1.254	0.047	0.047	-4.48	-1.266	0.0408	0.049	-4.13	-1.227	0.0348	0.060	-4.12	-1.201	0.0329	0.053	-4.12	-1.187	0.0315	0.049	-4.11	-1.187	0.0315	0.049	-4.10	-1.187	0.0315	0.049	-4.10	-1.187	0.0315	0.049												
-5.43	-1.289	0.044	0.046	-5.49	-1.302	0.049	0.057	-5.58	-1.303	0.0560	0.077	-5.15	-1.276	0.0442	0.073	-5.15	-1.254	0.0412	0.069	-5.14	-1.234	0.0393	0.063	-5.13	-1.234	0.0393	0.063	-5.12	-1.234	0.0393	0.063	-5.11	-1.234	0.0393	0.063												
-6.66	-1.338	0.010	0.009	-6.70	-1.341	0.011	0.009	-6.78	-1.340	0.0122	0.010	-6.32	-1.301	0.0144	0.011	-6.31	-1.281	0.0145	0.009	-6.30	-1.265	0.0145	0.009	-6.29	-1.265	0.0145	0.009	-6.28	-1.265	0.0145	0.009	-6.27	-1.265	0.0145	0.009												
-7.81	-1.387	0.0098	0.002	-7.84	-1.395	0.015	0.000	-7.91	-1.397	0.017	0.014	-7.45	-1.354	0.0114	0.010	-7.43	-1.327	0.0117	0.003	-7.41	-1.301	0.0117	0.003	-7.39	-1.281	0.0117	0.003	-7.37	-1.261	0.0117	0.003	-7.35	-1.241	0.0117	0.003												
-8.96	-1.436	0.0095	0.006	-9.10	-1.438	0.005	0.006	-9.24	-1.442	0.012	0.026	-8.84	-1.404	0.009	0.009	-8.82	-1.374	0.009	0.009	-8.80	-1.344	0.009	0.009	-8.78	-1.314	0.009	0.009	-8.76	-1.284	0.009	0.009	-8.74	-1.254	0.009	0.009												
-10.12	-1.485	0.0065	0.061	-10.75	-1.484	0.070	-0.070	-10.78	-1.484	0.070	-0.070	-10.27	-1.446	0.062	-0.111	-10.25	-1.404	0.062	-0.100	-10.23	-1.374	0.0665	-0.092	-10.21	-1.342	0.0665	-0.092	-10.19	-1.312	0.0665	-0.092	-10.17	-1.282	0.0665	-0.092												
-12.78	-1.525	1.067	-0.072	-12.90	-1.528	-0.082	-0.085	-13.03	-1.532	-0.081	-0.087	-12.33	-1.491	-0.071	-0.071	-12.31	-1.451	-0.071	-0.069	-12.29	-1.412	-0.071	-0.067	-12.27	-1.372	-0.071	-0.065	-12.25	-1.332	-0.071	-0.063	-12.23	-1.292	-0.071	-0.061	-12.21	-1.252	-0.071	-0.060								
-14.96	-1.561	1.067	-0.082	-15.11	-1.567	-0.082	-0.085	-15.24	-1.571	-0.081	-0.087	-14.64	-1.528	-0.071	-0.070	-14.62	-1.489	-0.071	-0.068	-14.59	-1.450	-0.071	-0.066	-14.56	-1.411	-0.071	-0.064	-14.53	-1.372	-0.071	-0.062	-14.50	-1.332	-0.071	-0.060												
-17.12	-1.604	1.013	-0.091	-17.25	-1.607	-0.087	-0.085	-17.37	-1.607	-0.081	-0.085	-16.61	-1.563	-0.070	-0.070	-16.59	-1.524	-0.070	-0.068	-16.56	-1.485	-0.070	-0.066	-16.53	-1.446	-0.070	-0.064	-16.50	-1.407	-0.070	-0.063	-16.47	-1.367	-0.070	-0.062												
-18.21	-1.643	-0.081	-18.37	-1.643	-0.081	-0.081	-18.50	-1.643	-0.076	-0.076	-17.84	-1.604	-0.069	-0.069	-17.81	-1.565	-0.069	-0.067	-17.78	-1.526	-0.069	-0.065	-17.75	-1.487	-0.069	-0.063	-17.72	-1.448	-0.069	-0.062	-17.69	-1.409	-0.069	-0.061													

NACA

TABLE XVIII.- GEOMETRIC CHARACTERISTICS AND WIND-TUNNEL DATA FOR A 5-PERCENT-THICK TRIANGULAR WING OF ASPECT RATIO 2, CAMBERED AND TWISTED TO APPROXIMATE AN ELLIPTICAL SPAN LOAD DISTRIBUTION  
 (a) Geometric characteristics



Aspect ratio . . . . .	2
Taper ratio . . . . .	0
Airfoil section (streamwise) . . . . .	NACA 0005-63
Total area, square feet . . . . .	4.014
Mean aerodynamic chord, $\bar{c}$ , feet . . . . .	1.889
Dihedral, degrees . . . . .	0
Twist, degrees . . . . .	see fig 3
Incidence, degrees . . . . .	0
Camber . . . . .	see fig 3
Distance, wing reference plane to body axis, feet . . . . .	0
Design lift coefficient at $M=1.53$ . . . . .	0.25

(b) Data obtained in Ames 12-foot pressure wind tunnel

$\alpha$	$C_L$	$C_D$	$C_m$	$\alpha$	$C_L$	$C_D$	$C_m$	$\alpha$	$C_L$	$C_D$	$C_m$	$\alpha$	$C_L$	$C_D$	$C_m$
$M=0.25 \quad R=4.9 \times 10^6$				$M=0.60 \quad R=4.9 \times 10^6$				$M=0.25 \quad R=9.3 \times 10^6$				$M=0.25 \quad R=16.6 \times 10^6$			
-0.01	-0.036	0.0092	0.009	-0.01	-0.039	0.0107	0.010	-0.01	-0.036	0.0102	0.009	-0.01	-0.037	0.0096	0.009
-0.68	-0.066	0.0103	0.013	-0.62	-0.072	0.0081	0.015	-0.68	-0.068	0.0119	0.014	-0.72	-0.067	0.0108	0.013
-0.01	-0.036	0.0086	0.009	-0.01	-0.039	0.0108	0.010	-0.01	-0.035	0.0104	0.009	-0.01	-0.039	0.0095	0.009
1.00	0	0.0065	0.004	1.00	0.002	0.0093	0.003	1.00	0.003	0.0095	0.003	1.00	0.002	0.0087	0.003
2.01	0.039	0.0067	-0.002	2.01	0.049	0.0091	-0.004	2.01	0.044	0.0096	-0.002	2.01	0.044	0.0090	-0.003
3.02	0.083	0.0085	-0.008	3.02	0.089	0.0096	-0.010	3.02	0.085	0.0106	-0.008	3.02	0.085	0.0100	-0.008
4.03	0.122	0.0106	-0.013	4.03	0.131	0.0113	-0.016	4.03	0.123	0.0116	-0.013	4.03	0.119	0.0111	-0.013
5.04	0.160	0.0133	-0.018	5.05	0.165	0.0132	-0.021	5.04	0.158	0.0137	-0.018	5.04	0.154	0.0130	-0.017
6.05	0.199	0.0166	-0.022	6.05	0.204	0.0166	-0.026	6.05	0.196	0.0164	-0.023	6.05	0.196	0.0154	-0.023
8.07	0.271	0.0248	-0.031	8.07	0.282	0.0246	-0.036	8.07	0.269	0.0232	-0.032	8.07	0.269	0.0223	-0.032
10.09	0.344	0.0348	-0.041	10.10	0.368	0.0371	-0.048	10.09	0.341	0.0327	-0.041	10.09	0.345	0.0317	-0.042
12.11	0.427	0.0511	-0.053	12.12	0.457	0.0591	-0.061	12.11	0.426	0.0491	-0.053	12.11	0.433	0.0482	-0.055
14.14	0.507	0.0755	-0.065	14.15	0.559	0.0959	-0.076	14.13	0.507	0.0750	-0.066	14.14	0.514	0.0724	-0.067
16.16	0.601	0.1158	-0.079	16.18	0.675	0.1472	-0.090	16.16	0.606	0.1176	-0.079	16.16	0.615	0.1155	-0.081
18.19	0.697	0.1694	-0.089	18.20	0.768	0.2077	-0.099	18.19	0.710	0.1717	-0.092	18.19	0.731	0.1762	-0.096
20.21	0.799	0.2297	-0.104	20.23	0.876	0.2758	-0.107	20.22	0.824	0.2394	-0.107	20.22	0.833	0.2359	-0.107
22.24	0.905	0.2998	-0.116	22.26	0.967	0.3460	-0.121	22.24	0.915	0.3041	-0.118	21.43	0.884	0.2725	-0.114
24.26	0.988	0.3716	-0.123	24.28	1.059	0.4248	-0.134	24.27	1.008	0.3795	-0.127	-0.01	-0.037	0.0102	0.008
26.28	1.071	0.4512	-0.132					26.29	1.089	0.4586	-0.136				
28.31	1.160	0.5415	-0.141					28.31	1.183	0.5555	-0.144				
29.62	1.199	0.5950	-0.144					30.03	1.248	0.6376	-0.151				
-0.01	-0.038	0.0094	0.010					-0.01	-0.036	0.0093	0.009				

TABLE XVIII.- GEOMETRIC CHARACTERISTICS AND WIND-TUNNEL DATA FOR A 5-PERCENT-THICK TRIANGULAR WING OF ASPECT RATIO 2, CAMBERED AND TWISTED TO APPROXIMATE AN ELLIPTICAL SPAN LOAD DISTRIBUTION - Concluded

$c$	$c_L$	$c_D$	$c_M$	$a$	$c_L$	$c_D$	$c_M$																		
M=0.61	R=3.0x10 <sup>-6</sup>	M=0.81	R=3.0x10 <sup>-6</sup>	M=0.91	R=3.0x10 <sup>-6</sup>	M=1.30	R=3.0x10 <sup>-6</sup>	M=1.53	R=3.0x10 <sup>-6</sup>	M=1.70	R=3.0x10 <sup>-6</sup>														
-0.54	-0.056	0.0114	0.0111	-0.56	-0.062	0.0122	0.013	-0.56	-0.062	0.0133	0.014	-0.51	-0.067	0.0155	0.023	-0.50	-0.068	0.0156	0.015	-0.47	-0.062	0.0159	0.011		
-1.08	-0.080	0.0311	0.0311	-1.11	-0.088	0.0311	0.018	-1.12	-0.092	0.0320	0.020	-1.03	-0.091	0.0179	0.030	-1.03	-0.070	0.0200	0.021	-1.01	-0.062	0.0157	0.0157		
-2.17	-1.32	0.076	0.072	-2.21	-1.43	0.071	0.027	-2.22	-1.52	0.0602	0.031	-2.07	-1.54	0.0229	0.043	-2.05	-1.15	0.0241	0.032	-2.05	-1.02	0.0268	0.0268		
-3.26	-1.50	0.0236	0.030	-3.29	-2.01	0.029	0.038	-3.31	-2.11	0.0278	0.034	-3.10	-1.68	0.0267	0.036	-3.10	-1.58	0.0264	0.043	-3.08	-1.41	0.0273	0.047		
-1.32	-0.82	0.0307	0.037	-1.34	-0.88	0.0229	0.047	-0.65	-4.42	0.0277	0.0381	-1.13	-0.83	0.0243	0.068	-1.13	-2.00	0.0348	0.053	-1.11	-1.79	0.0326	0.047		
-6.47	-3.31	0.0501	0.051	-6.52	-3.69	0.0572	0.053	-6.60	-3.93	0.0521	0.050	-6.20	-3.30	0.0597	0.058	-6.19	-2.82	0.0513	0.074	-6.16	-2.53	0.0475	0.053		
-55	-0.010	0.0067	0.004	-55	-0.009	0.0107	0.003	-55	-0.008	0.0059	0.004	-55	-0.018	0.0101	0.011	-50	-0.002	0.0165	0.004	-50	-0.002	0.0163	0.003		
1.08	0.013	0.0021	0	1.03	0.016	0.0097	0	1.04	0.019	0.0053	0.001	1.01	0.006	0.0157	0.004	1.03	0.017	0.0162	0.004	1.02	0.014	0.0153	0.014		
2.11	0.098	0.090	-0.007	2.07	0.094	0.005	-0.002	2.09	0.071	0.007	0.011	2.01	0.094	0.0160	0.009	2.03	0.060	0.0168	0.013	2.01	0.094	0.0168	0.014		
3.12	-1.01	0.093	0.013	3.15	-1.15	0.0102	-0.004	3.17	-1.20	0.0107	-0.019	3.05	-0.99	0.0176	-0.021	3.06	-1.04	0.0187	-0.025	3.07	-0.93	0.0189	-0.025		
4.20	-1.46	0.111	-0.019	4.24	-1.63	0.132	-0.024	4.26	-1.73	0.137	-0.028	4.09	-1.46	0.0206	-0.033	4.09	-1.46	0.0219	-0.036	4.08	-1.32	0.0219	-0.034		
6.33	-2.34	0.0203	-0.031	6.39	-2.29	0.029	-0.039	6.43	-2.78	0.028	-0.046	6.15	-2.82	0.0315	-0.029	6.16	-2.29	0.0327	-0.057	6.14	-2.09	0.0321	-0.057		
8.46	-3.80	0.0307	-0.043	8.54	-3.54	0.0363	-0.052	8.61	-3.94	0.0466	-0.070	8.21	-3.32	0.0492	-0.082	8.28	-3.10	0.0475	-0.075	8.19	-2.83	0.0474	-0.069		
10.60	-4.14	0.0756	-0.056	10.71	-4.63	0.0612	-0.069	10.86	-4.28	0.0745	-0.106	10.28	-3.59	0.0711	-0.130	10.29	-3.32	0.0723	-0.099	10.24	-3.55	0.0720	-0.080		
12.76	-5.17	0.0781	-0.073	12.89	-5.70	0.0973	-0.081			14.41	-6.03	0.1457	-0.154	14.41	-5.59	0.1341	-0.133	14.34	-1.57	0.1237	-0.103	14.34	-1.57	0.1237	-0.103
14.84	-6.61	0.1304	-0.090							16.48	-6.12	0.1734	-0.150	16.48	-5.75	0.1679	-0.164	16.48	-1.49	0.1623	-0.156	16.48	-1.49	0.1623	-0.156
17.11	-7.56	0.1484	-0.090							20.62	-7.76	0.2673	-0.176	20.62	-7.55	0.2673	-0.176	20.62	-2.84	0.265	-0.176	20.62	-2.84	0.265	-0.176
19.28	-8.66	0.2094	-0.113							22.69	-8.11	0.3236	-0.187	22.69	-8.23	0.3236	-0.187	22.69	-2.63	0.3182	-0.187	22.69	-2.63	0.3182	-0.187
M=1.50	R=3.0x10 <sup>-6</sup>	M=0.61	R=9.0x10 <sup>-6</sup>	M=0.61	R=9.0x10 <sup>-6</sup>	M=0.91	R=9.0x10 <sup>-6</sup>	M=0.91	R=9.0x10 <sup>-6</sup>	M=1.30	R=9.0x10 <sup>-6</sup>	M=1.30	R=9.0x10 <sup>-6</sup>	M=1.53	R=9.0x10 <sup>-6</sup>	M=1.53	R=9.0x10 <sup>-6</sup>	M=1.70	R=9.0x10 <sup>-6</sup>	M=1.70	R=9.0x10 <sup>-6</sup>				
-0.49	-0.040	0.0235	0.012	-0.56	-0.053	0.0124	0.013	-0.61	-0.068	0.0131	0.015	-0.62	-0.066	0.0131	0.017	-0.55	-0.070	0.0188	0.025	-0.54	-0.048	0.0172	0.015		
-1.01	-0.057	0.028	0.016	-1.14	-0.089	0.0139	0.017	-1.16	-0.094	0.0146	0.019	-1.18	-0.099	0.0153	0.022	-1.06	-0.099	0.0195	0.022	-1.04	-0.070	0.0191	0.020		
-2.05	-0.093	0.060	0.021	-2.23	-1.58	0.183	0.024	-2.27	-1.49	0.197	0.028	-2.29	-1.57	0.0204	0.033	-2.13	-1.44	0.0245	0.048	-2.12	-1.14	0.0228	0.034		
-3.07	-1.26	0.084	0.033	-3.29	-1.89	0.281	0.032	-3.36	-2.03	0.295	0.036	-3.31	-2.12	0.274	0.044	-3.19	-1.92	0.303	0.057	-3.17	-1.56	0.277	0.057		
-4.10	-1.62	0.031	0.041	-4.41	-2.39	0.313	0.039	-4.49	-2.61	0.347	0.047	-4.34	-2.70	0.373	0.071	-4.29	-2.50	0.371	0.070	-4.23	-1.95	0.370	0.070		
-6.15	-2.28	0.071	0.056	-6.56	-3.43	0.401	0.053	-6.72	-3.75	0.478	0.065	-6.50	-4.08	0.637	0.088	-6.36	-3.32	0.667	0.094	-6.33	-2.78	0.666	0.094		
-56	-0.005	0.0180	0.003	-56	-0.012	0.0103	0.005	-56	-0.011	0.0106	0.005	-56	-0.011	0.0110	0.005	-56	-0.019	0.0165	0.011	-56	-0.003	0.0160	0.011		
1.02	0.612	0.077	-0.001	1.05	0.014	0.009	0.003	1.04	0.016	0.0096	0	1.05	0.017	0.0100	0	1.03	0.007	0.0159	0.005	98	0.018	0.0159	0.005		
2.00	0.047	0.084	-0.001	2.18	0.060	0.009	-0.007	2.12	0.068	0.0093	0.009	2.14	0.067	0.0157	-0.111	2.06	0.066	0.0161	-0.023	2.06	0.060	0.0166	-0.023		
3.04	0.853	0.039	-0.018	3.18	0.107	0.007	-0.014	3.22	0.118	0.0073	0.013	3.24	0.125	0.0109	-0.020	3.11	0.113	0.0176	-0.022	3.11	0.109	0.0185	-0.022		
4.07	1.17	0.022	-0.027	4.26	0.120	0.015	-0.023	4.31	0.126	0.0165	0.020	4.35	0.117	0.0197	-0.027	4.17	0.128	0.0206	-0.035	4.17	0.114	0.0219	-0.035		
6.12	1.87	0.0320	-0.043	6.41	0.237	0.020	-0.032	6.51	0.241	0.0222	0.046	6.57	0.284	0.0383	-0.048	6.26	0.248	0.0340	-0.060	6.27	0.233	0.0349	-0.060		
8.17	2.52	0.0458	-0.058	8.57	0.243	0.0307	-0.044	8.70	0.259	0.0311	0.053	8.80	0.306	0.0449	-0.068	8.39	0.247	0.0347	-0.083	8.37	0.209	0.0451	-0.077		
10.23	3.17	0.0640	-0.073	10.73	0.249	0.049	-0.067	10.91	0.263	0.0463	0.070	11.05	0.318	0.0805	-0.096	10.47	0.268	0.0428	-0.083	10.47	0.228	0.0466	-0.083		
12.28	3.81	0.0669	-0.087	12.92	0.251	0.057	-0.073	13.13	0.263	0.0516	0.076	13.26	0.321	0.1095	-0.132	12.61	0.261	0.0428	-0.107	12.61	0.221	0.0469	-0.107		
14.34	4.49	0.116	-0.101	15.16	0.268	0.068	-0.091	15.36	0.281	0.0686	0.105	15.56	0.345	0.1506	-0.165	14.73	0.262	0.0402	-0.155	14.73	0.224	0.0454	-0.155		
15.39	5.01	0.145	-0.122	15.89	0.271	0.074	-0.103	16.28	0.286	0.0703	0.109	16.56	0.351	0.1809	-0.191	15.60	0.264	0.0407	-0.165	15.60	0.226	0.0456	-0.165		
18.45	5.60	0.1810	-0.120	19.80	0.285	0.084	-0.113	20.21	0.298	0.0803	0.116	20.56	0.367	0.2096	-0.206	19.54	0.264	0.0407	-0.174	19.54	0.226	0.0457	-0.174		
20.51	6.20	0.2275	-0.121							22.69	0.311	0.0974	-0.103	23.09	0.381	0.1606	-0.183	22.69	0.274	0.0406	-0.183	22.69	0.236	0.0458	-0.183
22.57	6.76	0.2758	-0.121							24.64	0.334	0.1393	-0.133	25.07	0.404	0.2096	-0.206	24.64	0.296	0.0406	-0.206	24.64	0.258	0.0459	-0.206
24.64	7.37	0.334	-0.133							26.70	0.372	0.1804	-0.122	27.12	0.441	0.2604	-0.206	26.70	0.334	0.0406	-0.206	26.70	0.296	0.0459	-0.206
M=1.70	R=4.0x10 <sup>-6</sup>	M=1.90	R=9.0x10 <sup>-6</sup>	M=0.61	R=7.0x10 <sup>-6</sup>	M=0.61	R=7.0x10 <sup>-6</sup>	M=0.91	R=7.0x10 <sup>-6</sup>	M=0.91	R=7.0x10 <sup>-6</sup>	M=1.30	R=7.0x10 <sup>-6</sup>	M=1.30	R=7.0x10 <sup>-6</sup>	M=1.53	R=7.0x10 <sup>-6</sup>	M=1.53	R=7.0x10 <sup>-6</sup>	M=1.70	R=7.0x10 <sup>-6</sup>	M=1.70	R=7.0x10 <sup>-6</sup>		
-0.32	-0.042	0.0168	0.013	-0.32	-0.041	0.0176	0.012	-0.32	-0.062	0.0133	0.014	-0.35	-0.067	0.0131	0.015	-0.63	-0.062	0.0131	0.015	-0.60	-0.071	0.0181	0.025		
-1.05	-0.063	0.0180	-0.019	-1.05	-0.059	0.0181	0.017	-1.05	-0.092	0.0180	0.021	-1.02	-0.097	0.0149	0.020	-1.22	-0.094	0.0156	0.022	-1.14	-0.097	0.0196	0.024		
-2.10	-1.03	0.0233	0.028	-2.10	-0.059	0.0215	0.026	-2.10	-0.092	0.0228	0.033	-2.04	-0.097	0.0159	0.030	-2.24	-0.092	0.0205	0.024	-2.14	-0.097	0.0244	0.024		
-3.16	-1.46	0.0288	0.058	-3.17	-1.09	0.0292	0.051	-3.17	-1.41	0.0281	0.063	-3.11	-1.52	0.0267	0.066	-3.16	-1.49	0.0271	0.066	-3.13	-1.56	0.0303	0.066		
-4.20	-1.80	0.0315	0.047	-4.19	-1.63	0.0304	0.041	-4.20	-1.84	0.0242	0.051	-4.04	-1.94	0.0267	0.056	-4.20	-1.74	0.0271	0.056	-4.17	-1.84	0.0302	0.066		
-5.30	-2.26	0.0470	-0.065	-5.30	-2.04	0.0416	-0.071	-5.30	-2.34	0.0285	-0.084	-5.16	-2.54	0.0359	-0.096	-5.30	-2.32	0.0366	-0.097	-5.26	-2.42	0.0358	-0.097		
-6.36	-3.07	0.0517	-0.082</																						

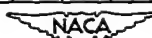
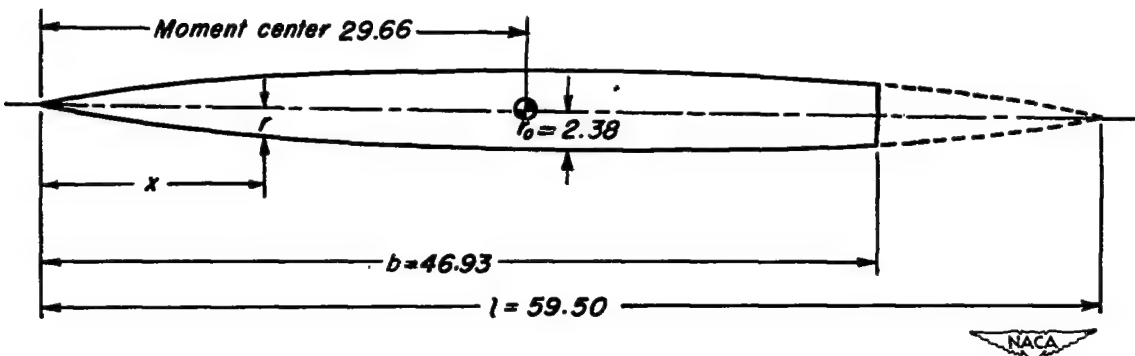


TABLE XIX.- GEOMETRIC CHARACTERISTICS AND WIND-TUNNEL  
DATA FOR THE BODY ALONE  
(a) Geometric characteristics

*All dimensions shown in inches*



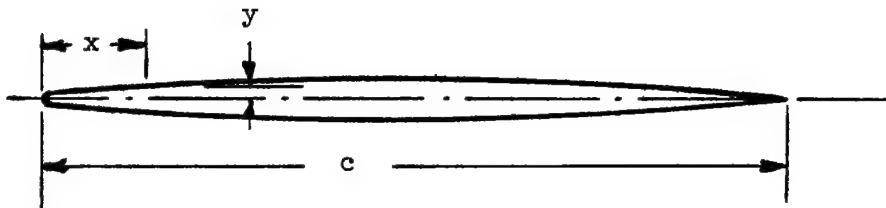
Actual fineness ratio (based on length $b$ ) . . . . .	9.86
Fineness ratio (based on length $l$ ) . . . . .	12.5
Cross-section shape . . . . .	Circular
Maximum cross-sectional area, square feet . . . . .	0.1235
Ratio at maximum cross-sectional area of body to area of wings used in conjunction with body . . . . .	0.0509
Distance to the moment center from nose, feet . . . . .	2.471

TABLE XIX.- GEOMETRIC CHARACTERISTICS AND WIND-TUNNEL  
DATA FOR THE BODY ALONE - Concluded  
(b) Data obtained in Ames 6- by 6-foot supersonic wind tunnel

NOTE: Coefficients are based on an area of 2.425 square feet and a moment arm of 3.911 feet.



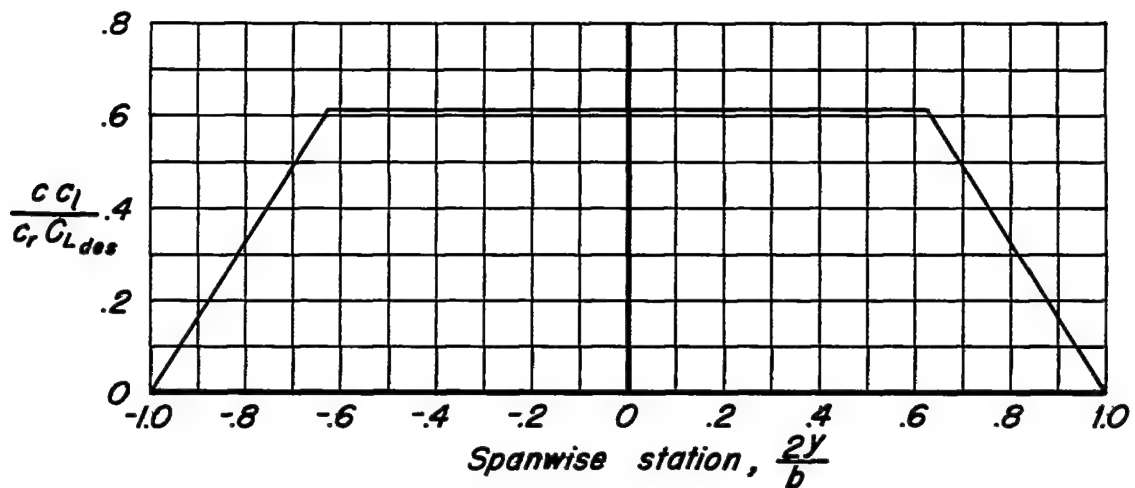
TABLE XX.- COORDINATES OF 3-PERCENT-THICK ROUND-NOSE SECTION



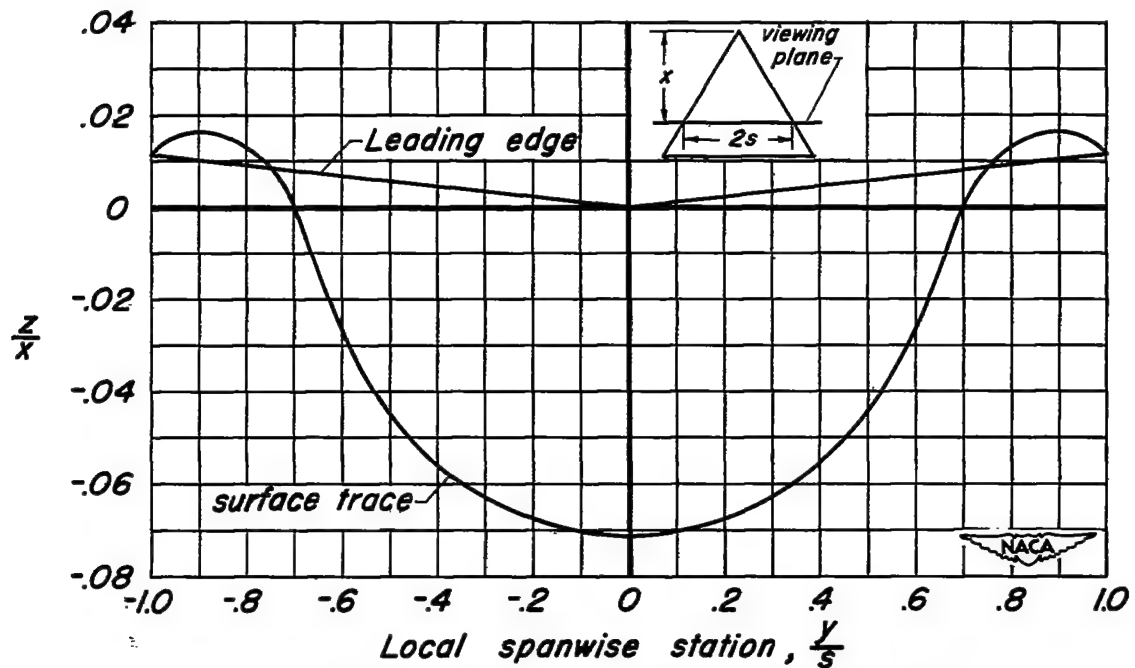
x Percent c	y Percent c
0	0
1.25	.333
2.5	.468
5	.653
7.5	.790
10	.900
15	1.071
20	1.200
30	1.375
40	1.469
50	1.500
60	1.440
70	1.260
80	.960
85	.765
90	.540
95	.285
100	0

L. E. radius: 0.045 percent c

NACA



(a) Spanwise load distribution.



(b) Shape of cambered and twisted surface.

Figure 1.—The spanwise load distribution and mean surface for the triangular wing of aspect ratio 2 cambered and twisted for a trapezoidal spanwise load distribution. Design lift coefficient, 0.25; design Mach number, 1.53.

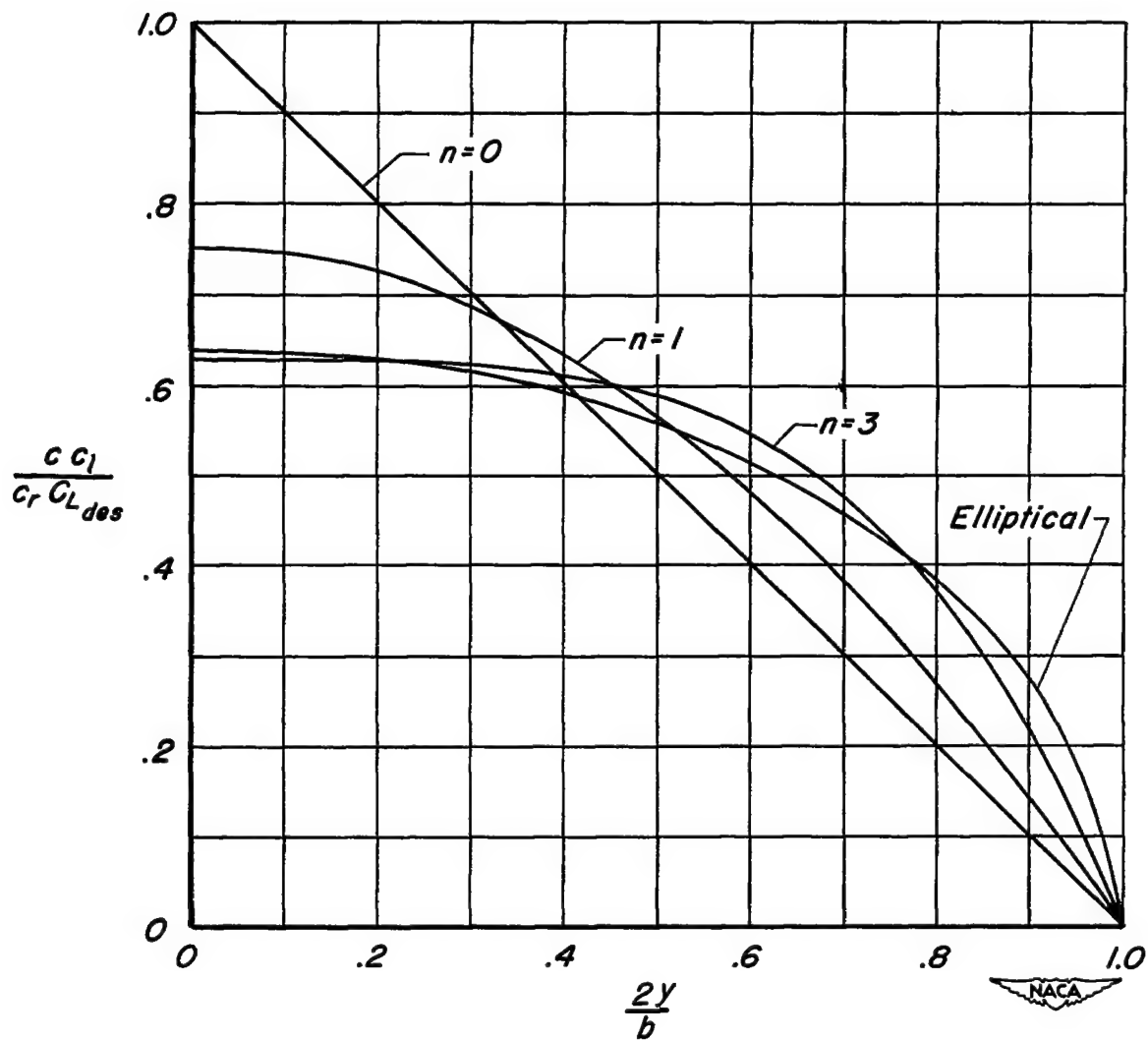
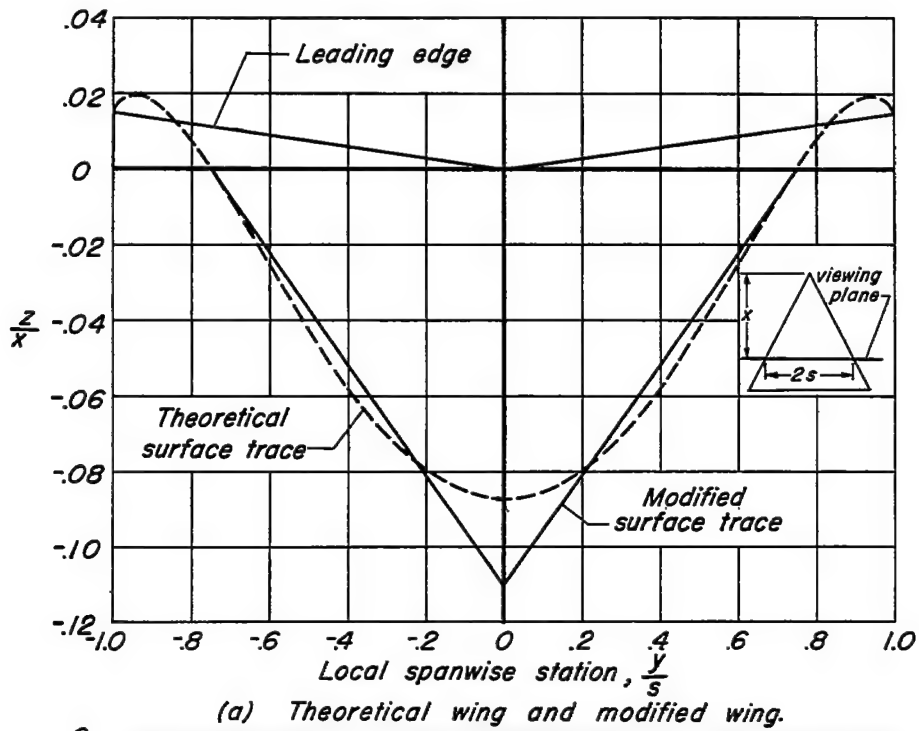
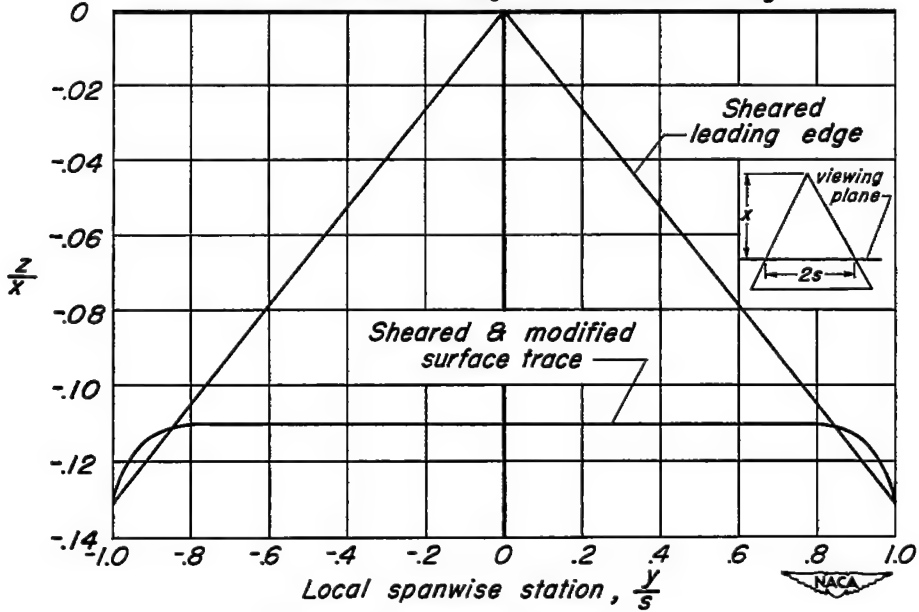


Figure 2.— The semispan load distributions corresponding to various values of  $n$  in comparison with an elliptical load distribution.

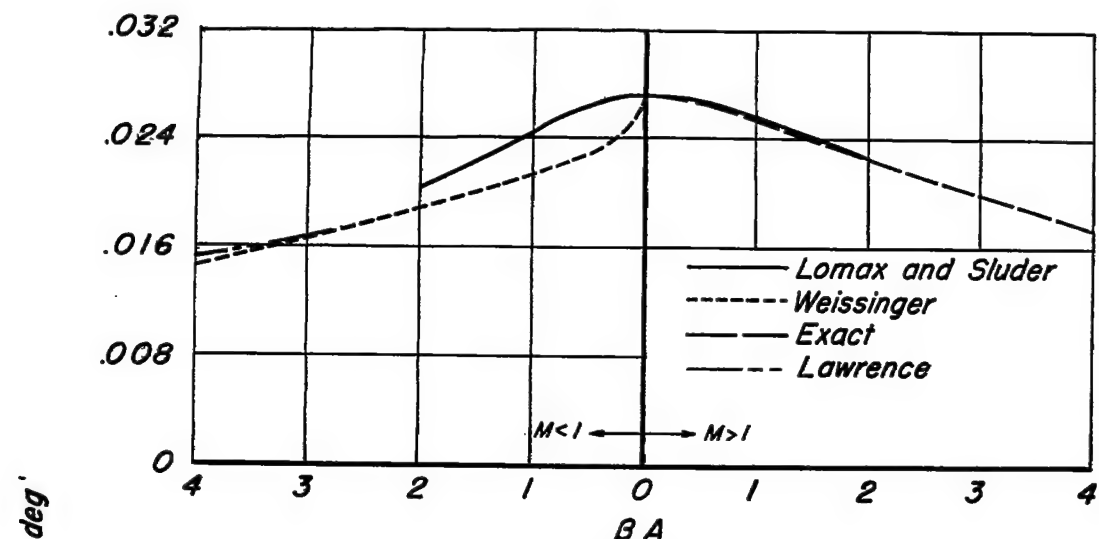


(a) Theoretical wing and modified wing.

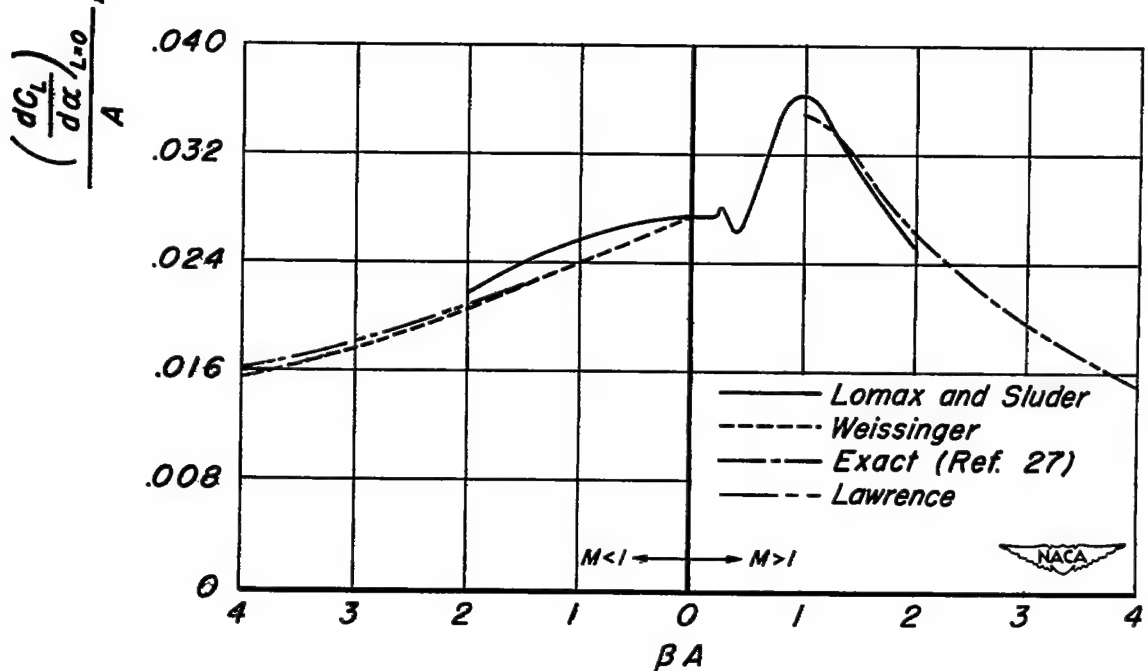


(b) Modified and sheared wing.

Figure 3.—The mean-surface shape for the triangular wing of aspect ratio 2 cambered and twisted for a nearly elliptical spanwise load distribution. Design lift coefficient, 0.25; design Mach number, 1.53.

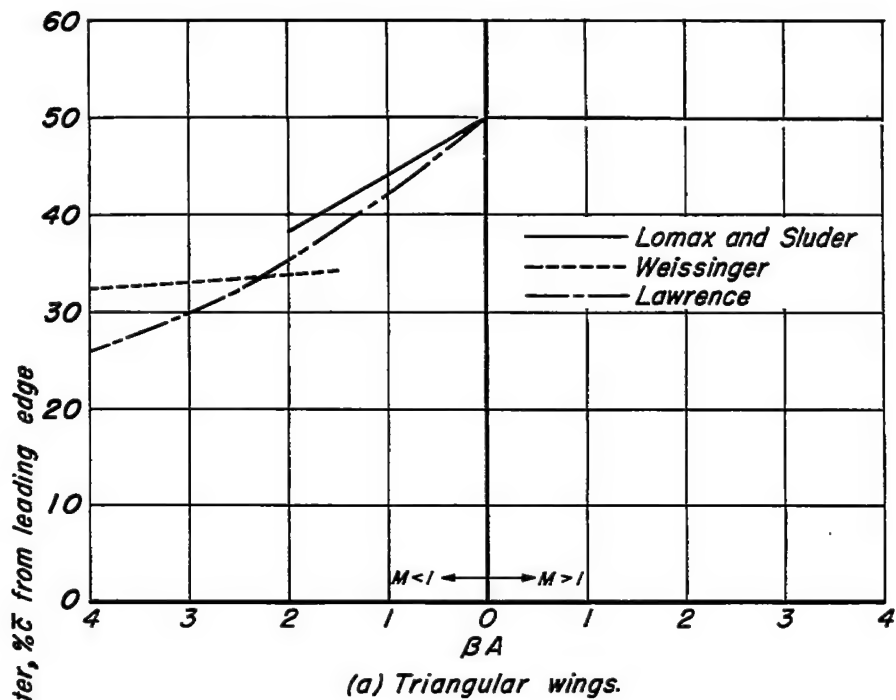


(a) Triangular wings.

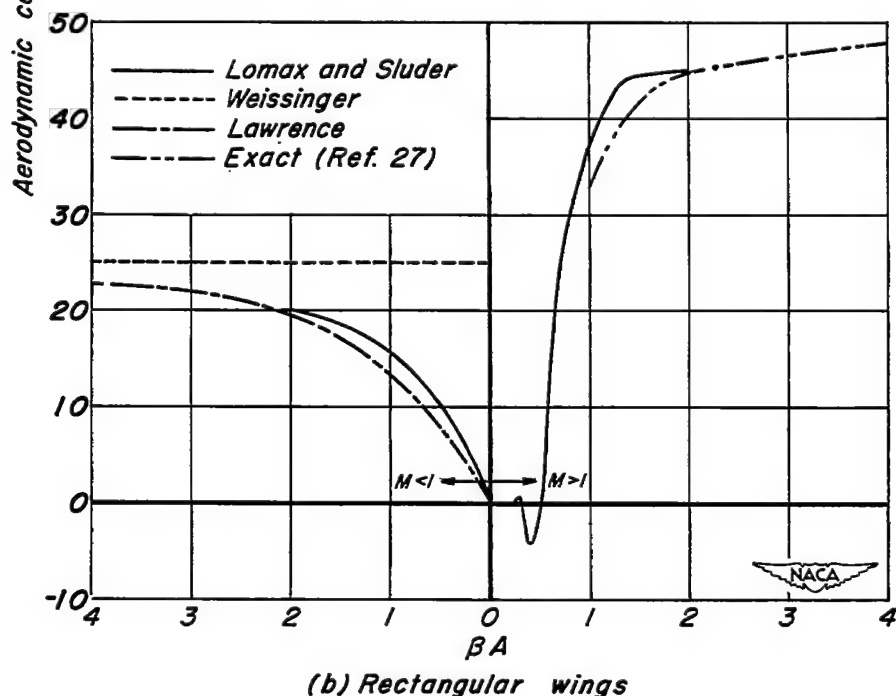


(b) Rectangular wings.

Figure 4.— The lift-curve slope for triangular and rectangular wings from several theoretical methods.

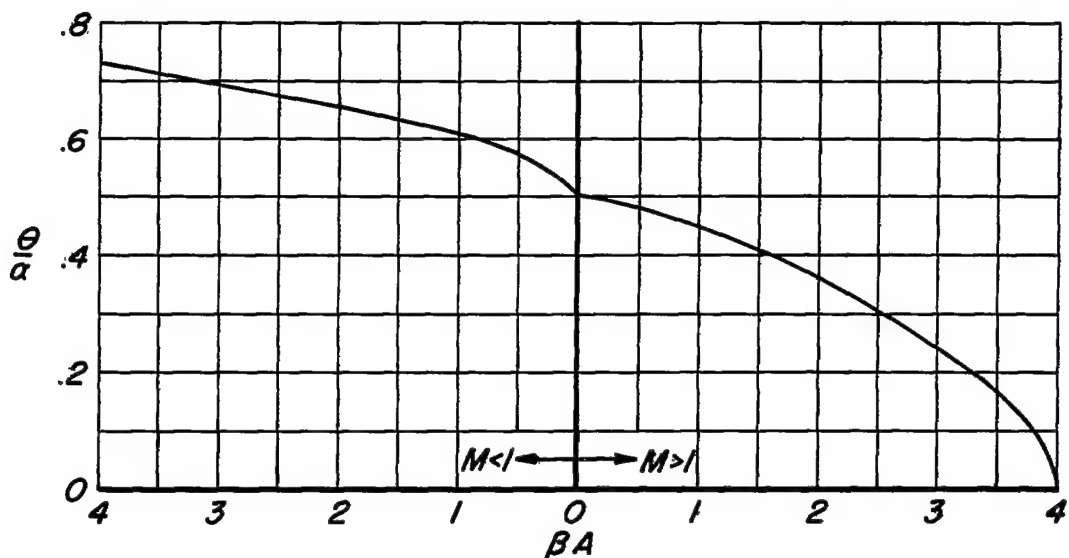


(a) Triangular wings.

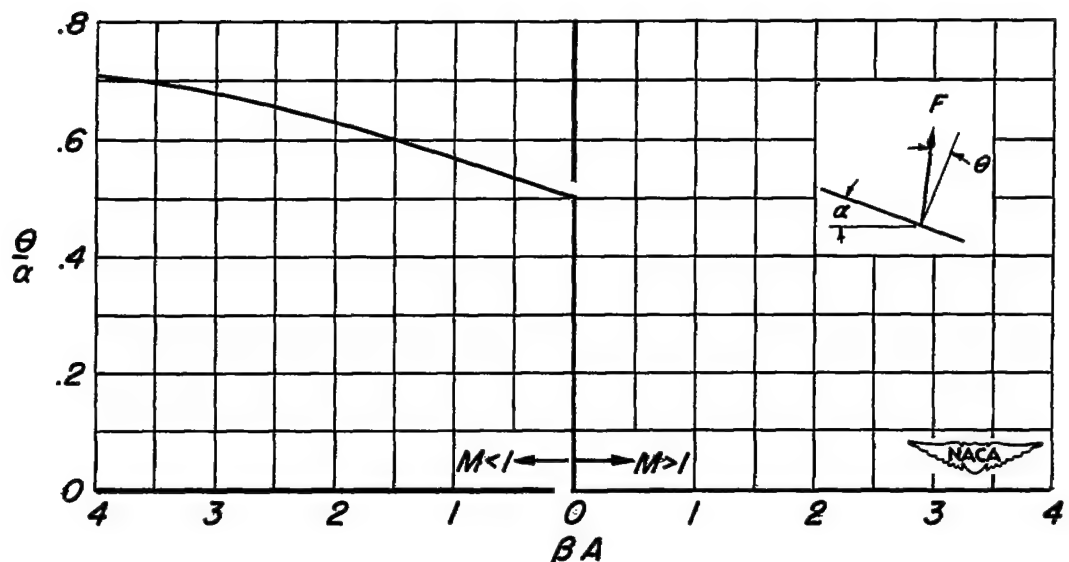


(b) Rectangular wings

Figure 5.—The center of pressure for triangular and rectangular wings from several theoretical methods.



(a) Triangular wings.



(b) Rectangular wings.

Figure 6.— The ratio of the inclination of the lift-force vector from the normal to the wing surface to the angle of attack as determined by theory.

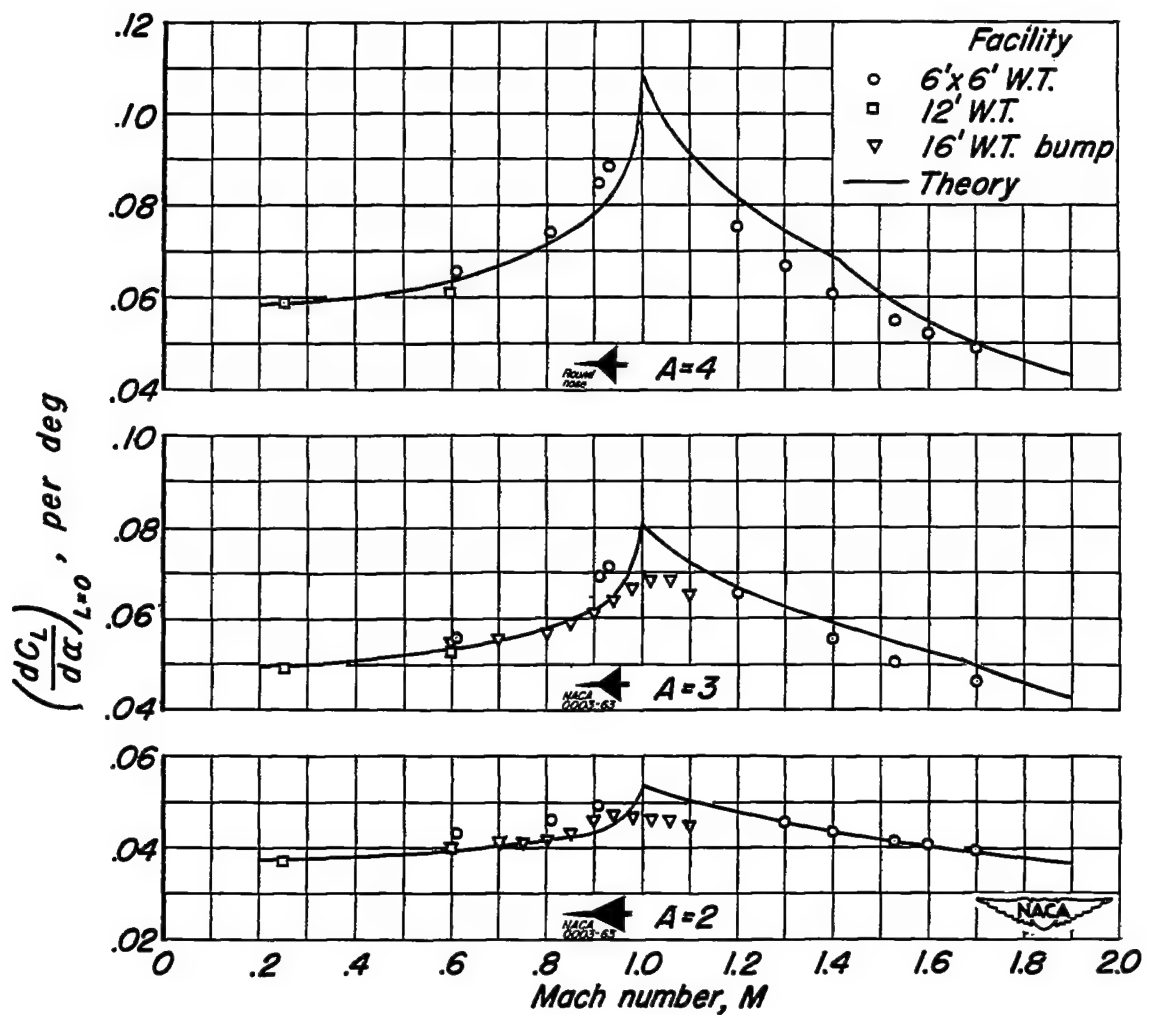


Figure 7.— The lift-curve slope of plane triangular wings 3 percent thick.

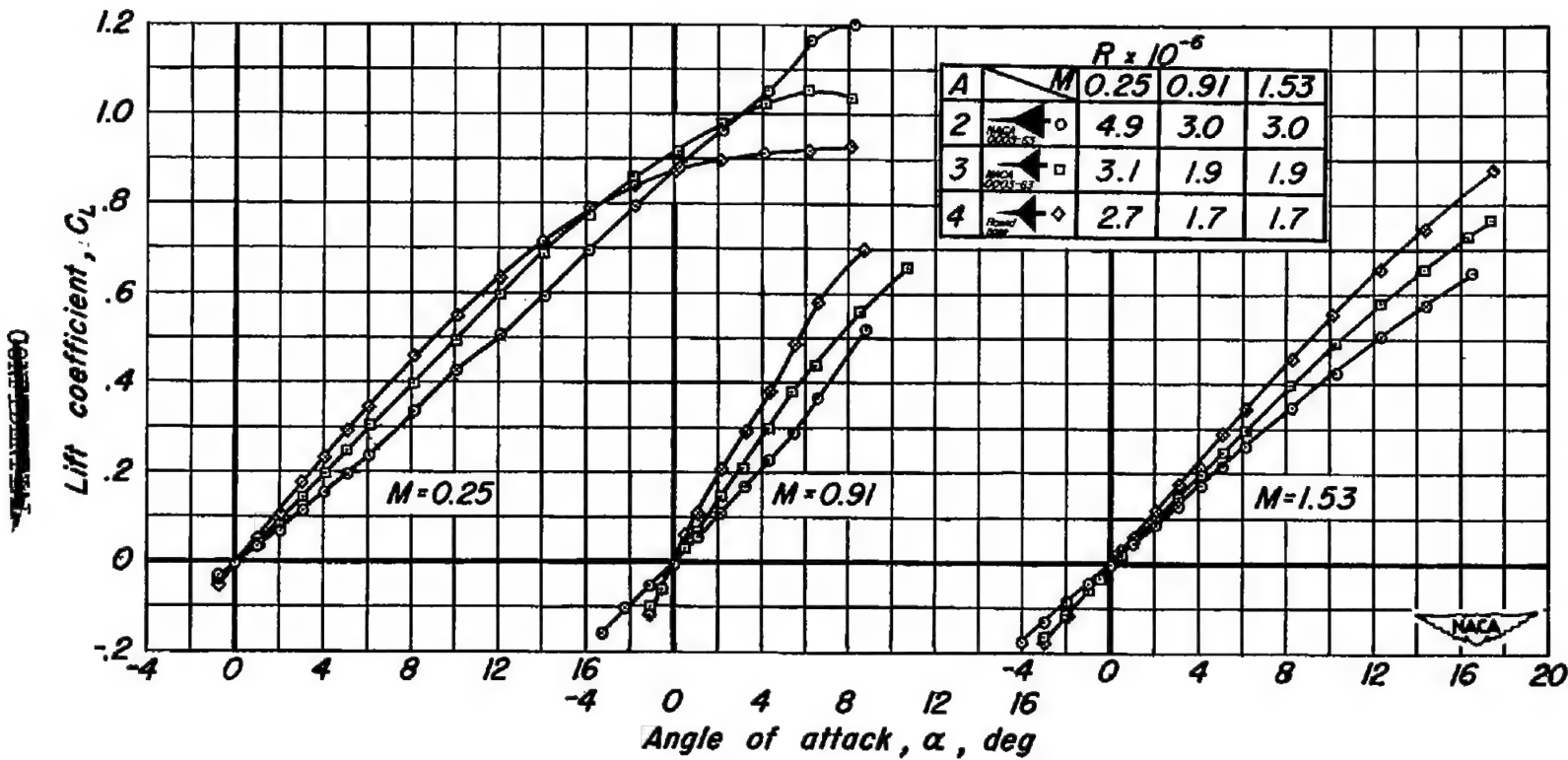


Figure 8.— The variation of lift coefficient with angle of attack for plane triangular wings 3 percent thick.

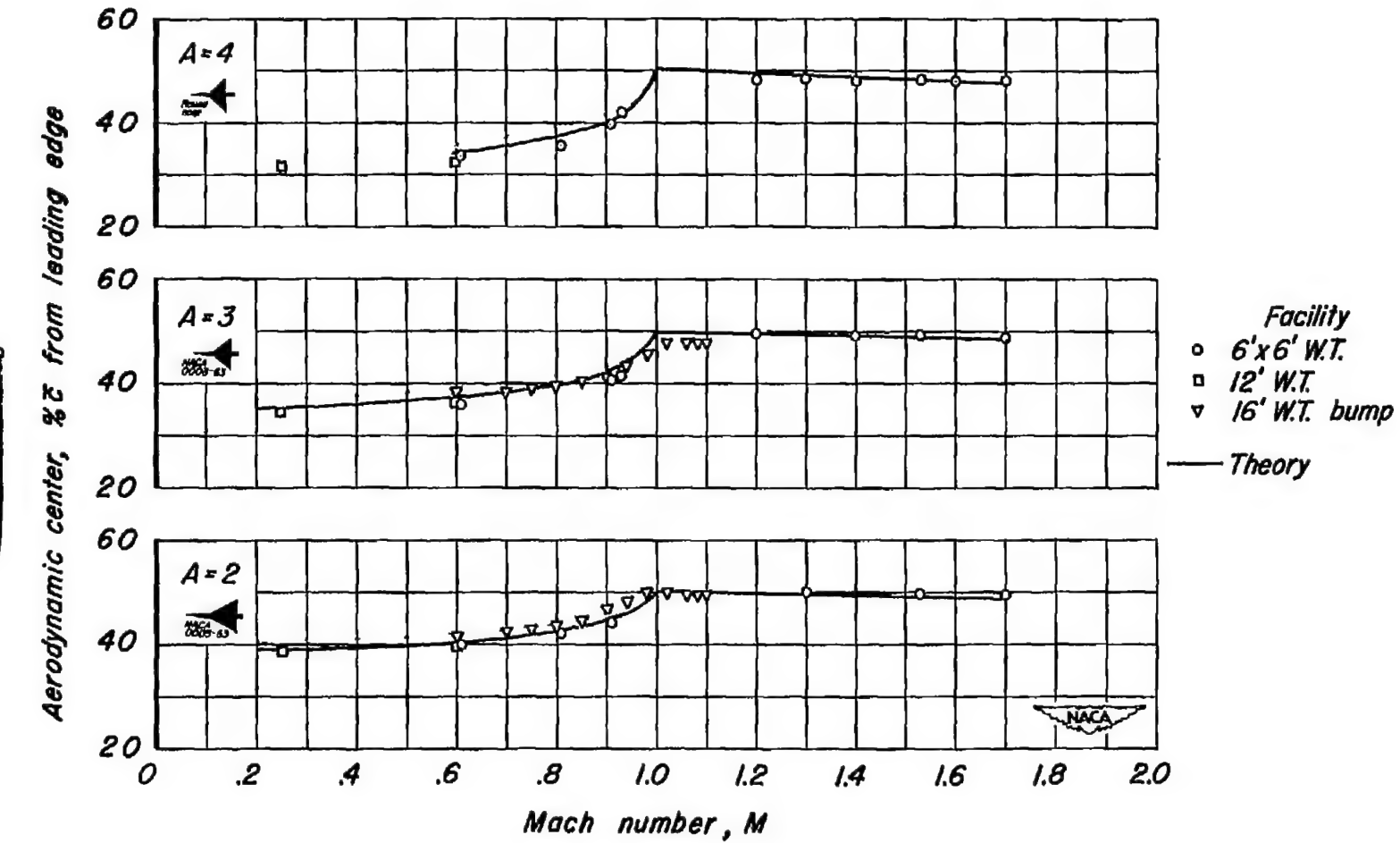


Figure 9.— The location of the aerodynamic center of plane triangular wings 3 percent thick.

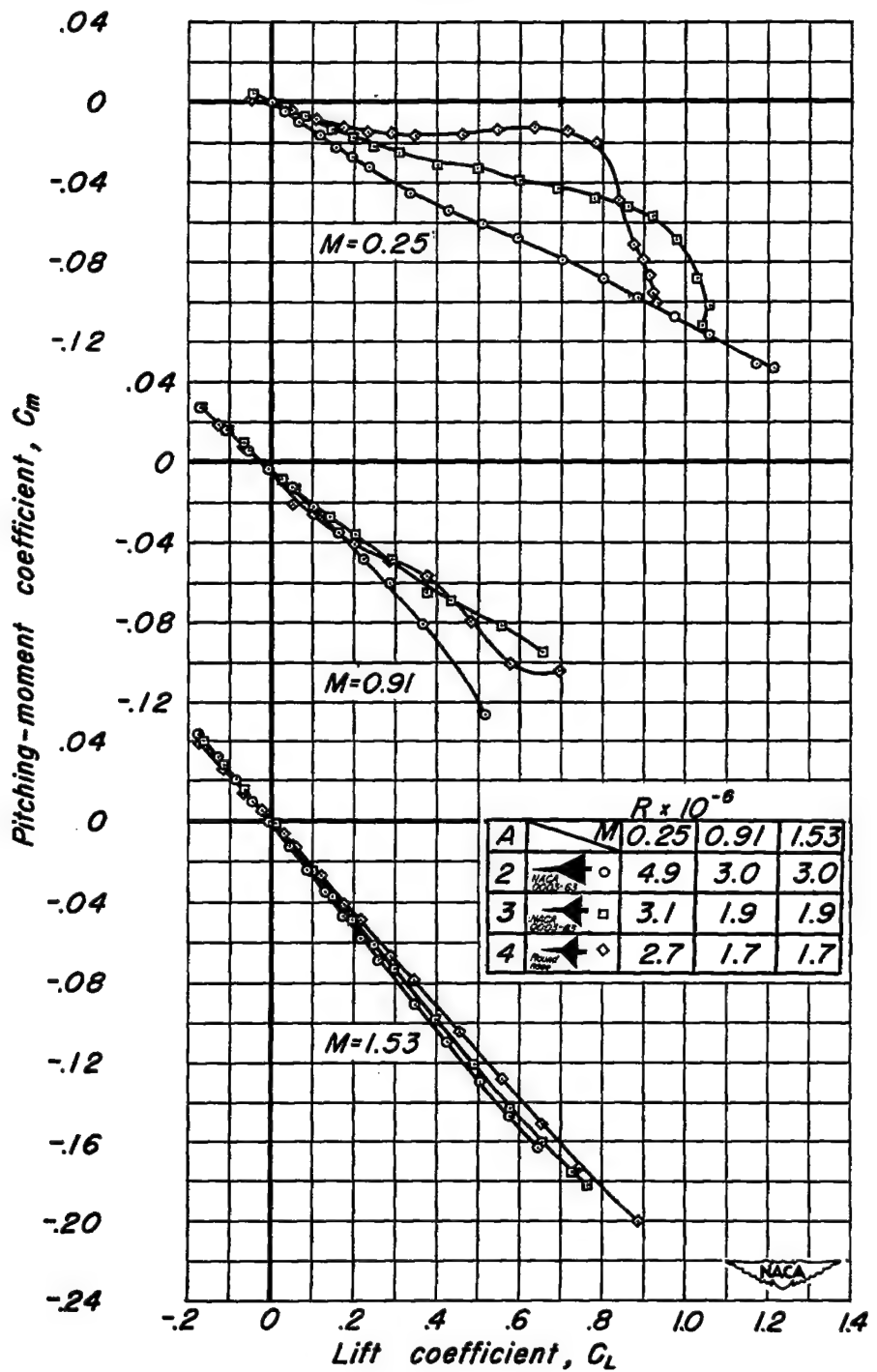


Figure 10.—The variation of pitching-moment coefficient with lift coefficient for plane triangular wings 3 percent thick.

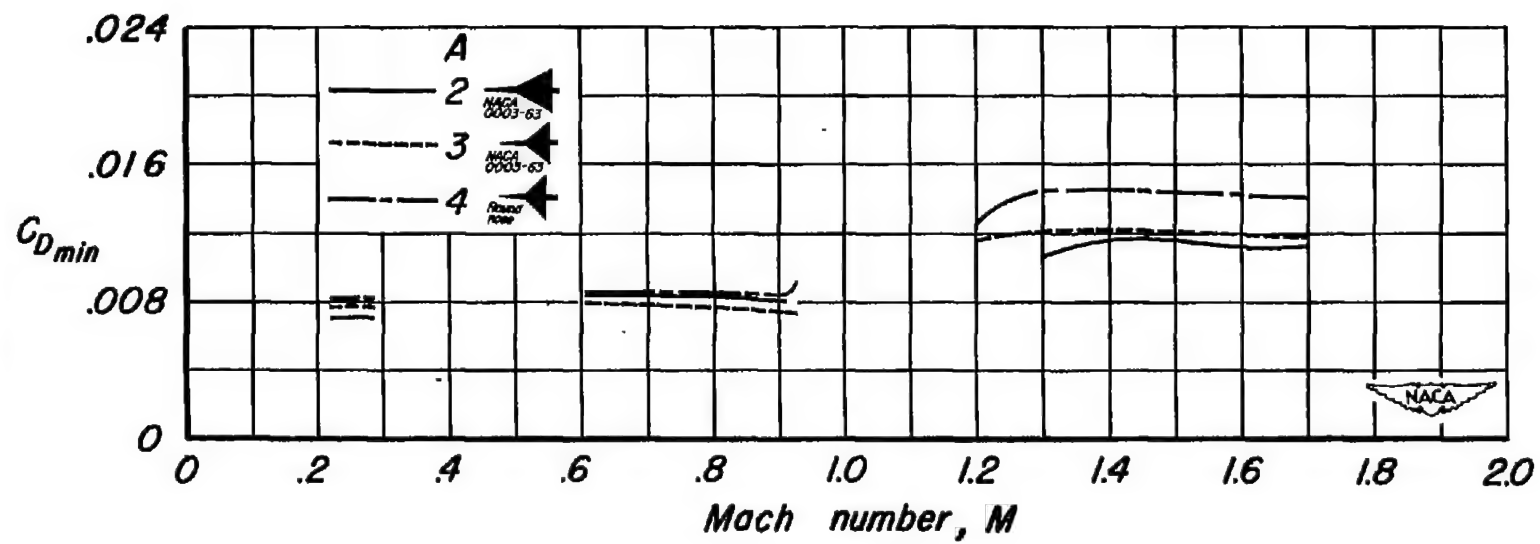


Figure 11.—The minimum drag coefficient of plane triangular wings 3 percent thick.

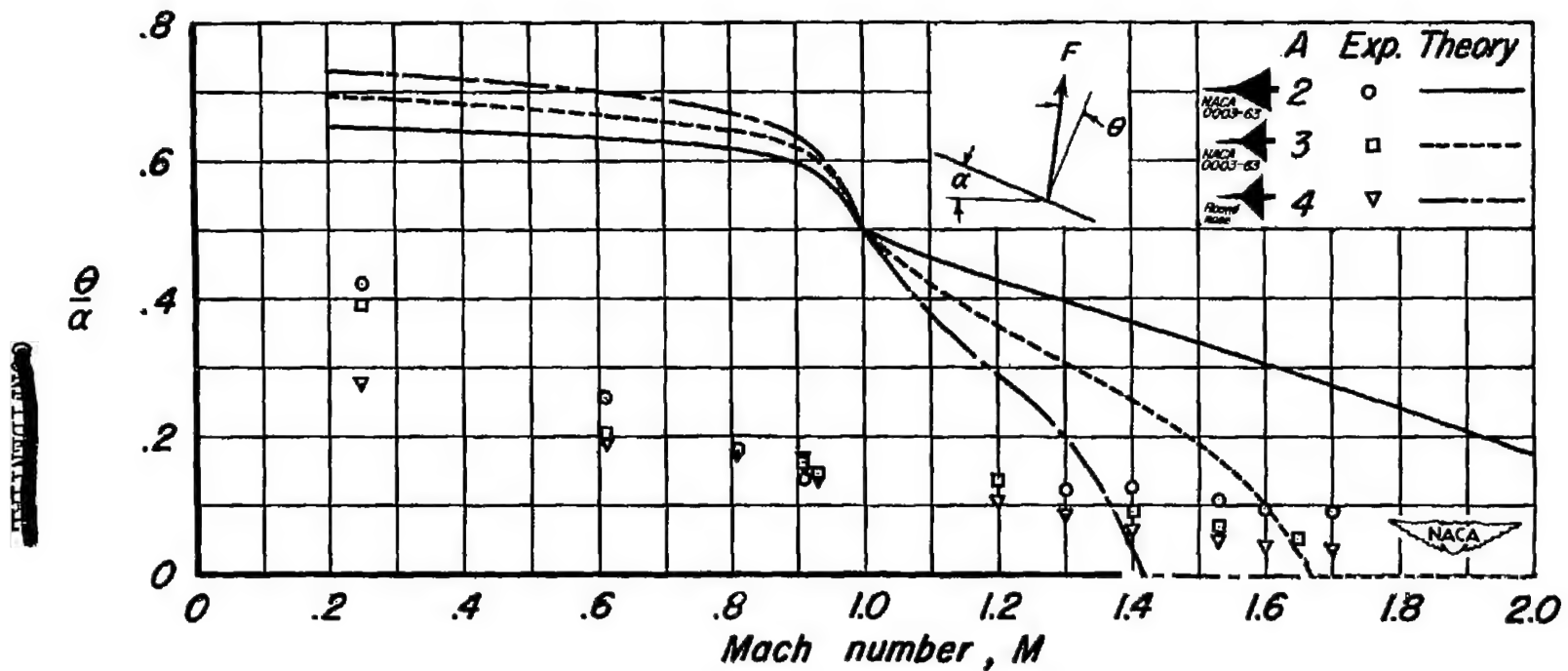


Figure 12.—The ratio of the inclination of the force vector from the normal to the angle of attack for plane triangular wings 3 percent thick.

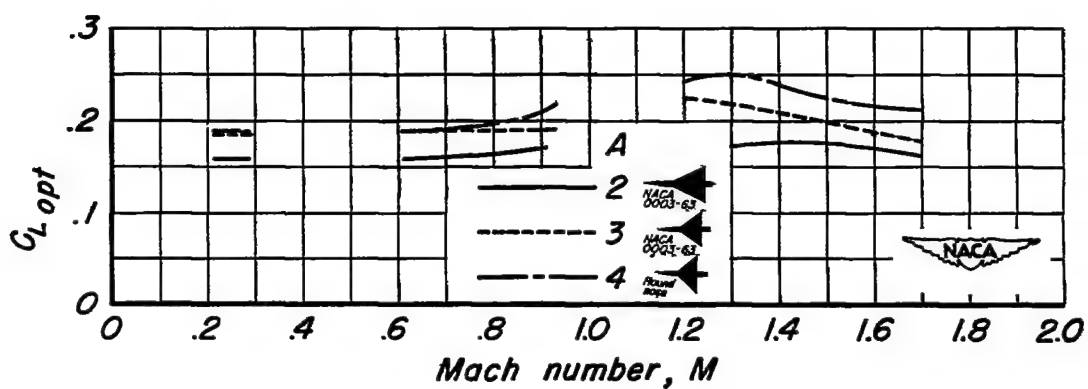
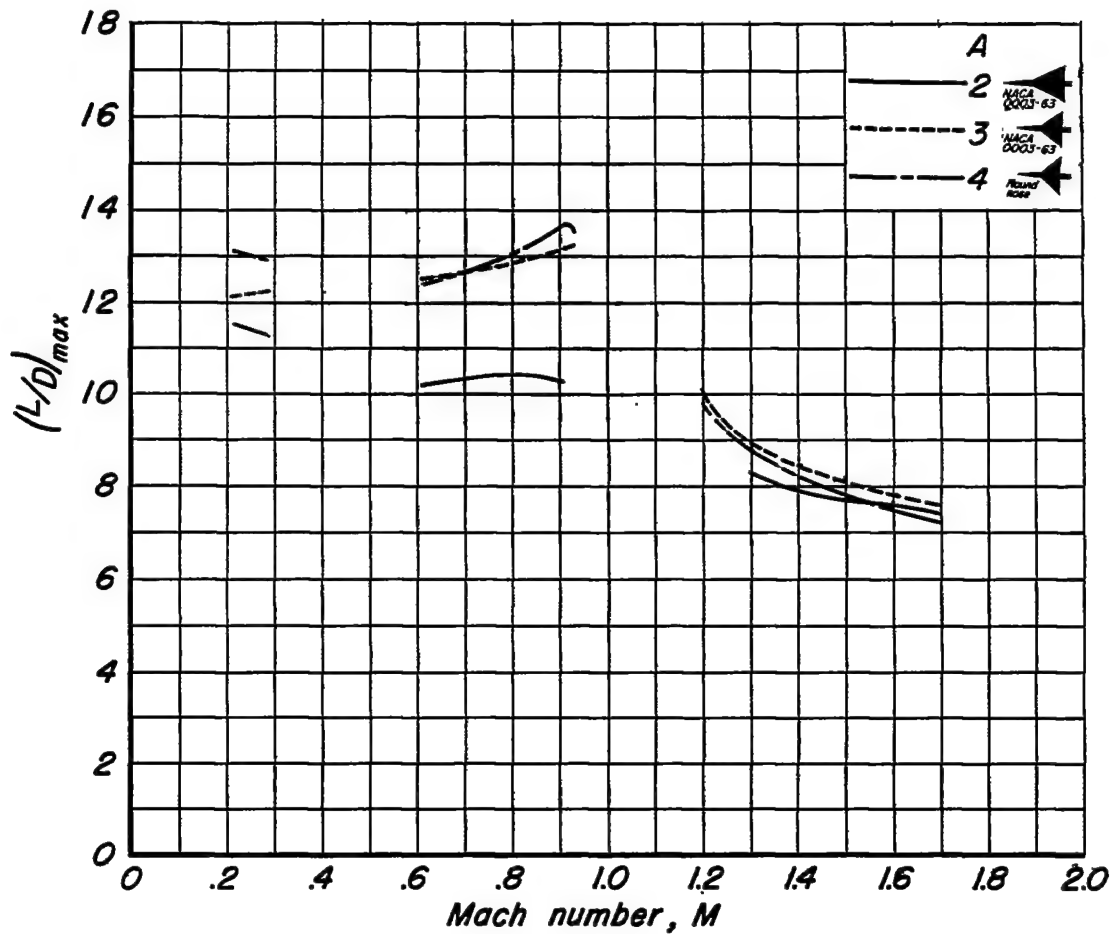


Figure 13.—The maximum lift-drag ratio and optimum lift coefficient for plane triangular wings 3 percent thick.

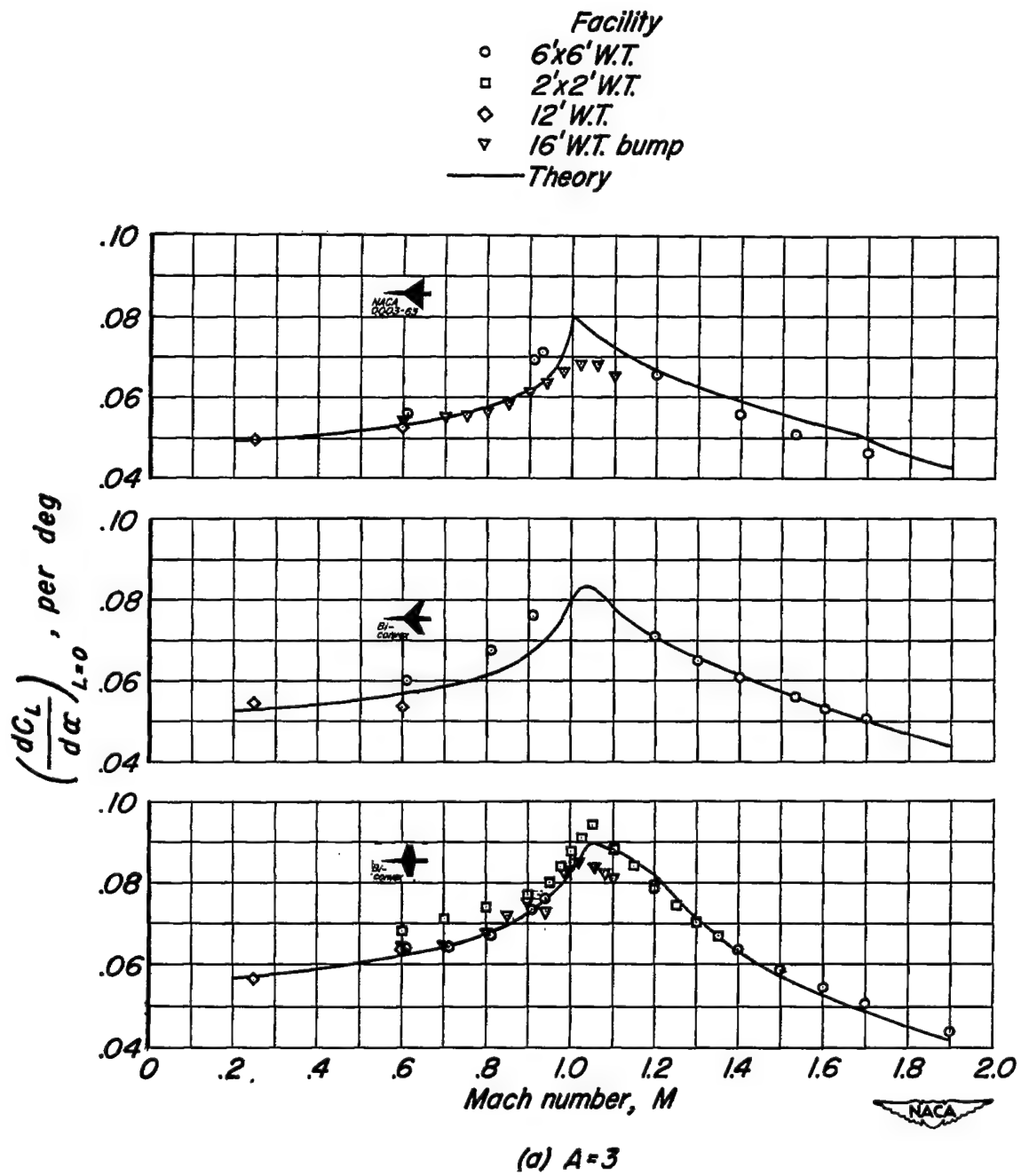


Figure 14.—The lift-curve slope for plane wings 3 percent thick and having different types of plan form.

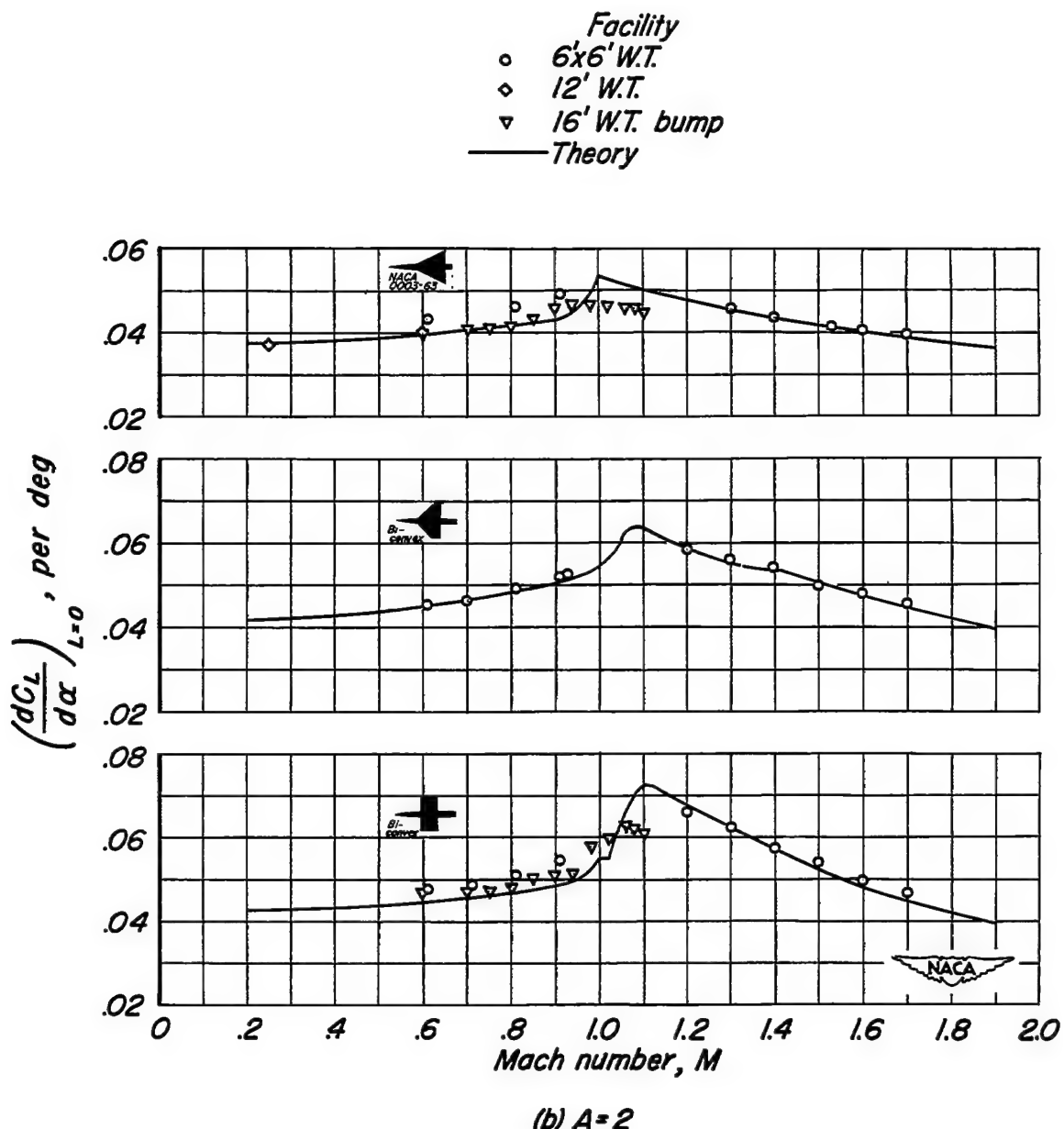


Figure 14.—Concluded.

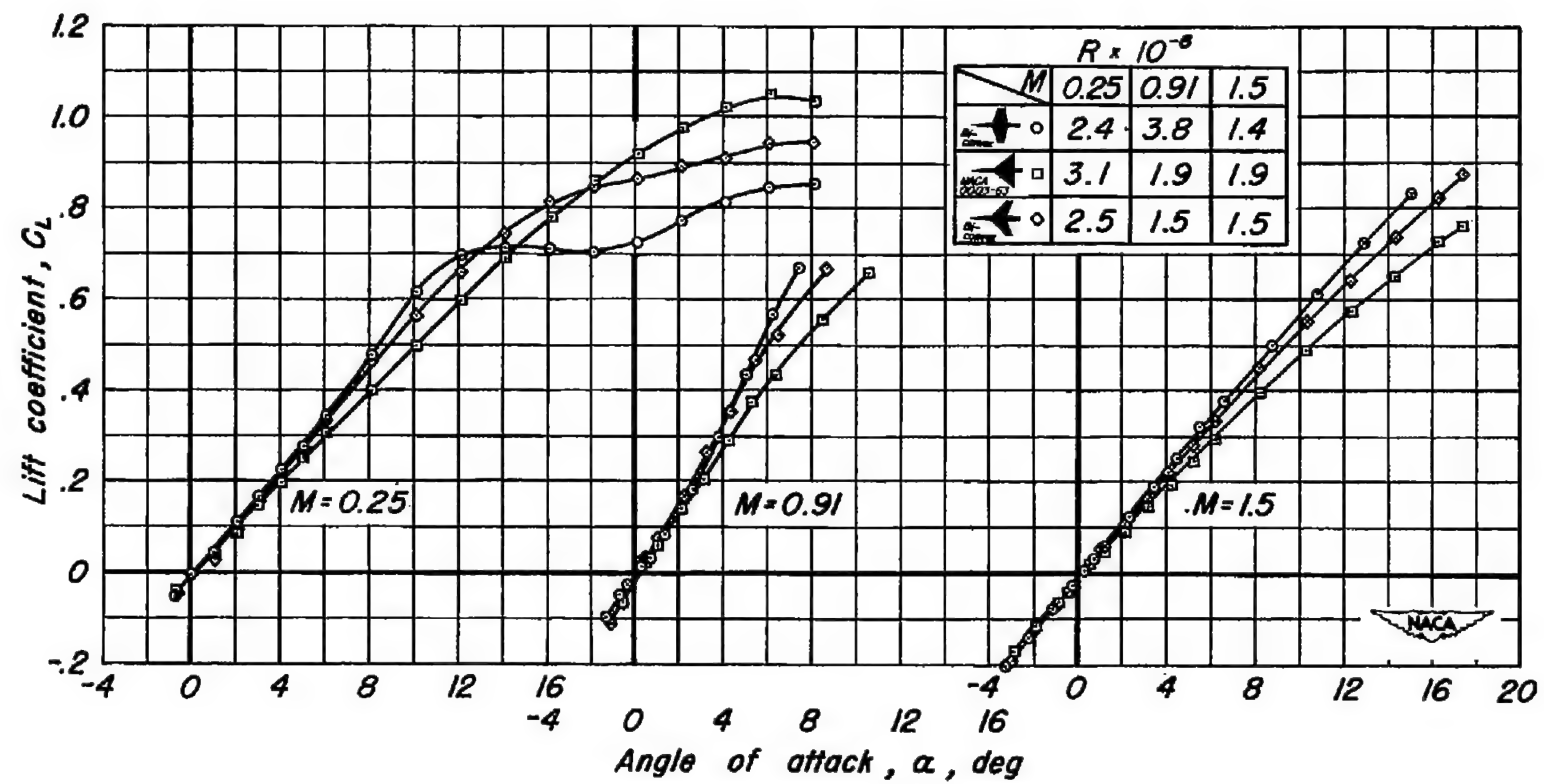


Figure 15.—The variation of lift with angle of attack for plane wings of aspect ratio 3, 3 percent thick, and having different types of plan form.

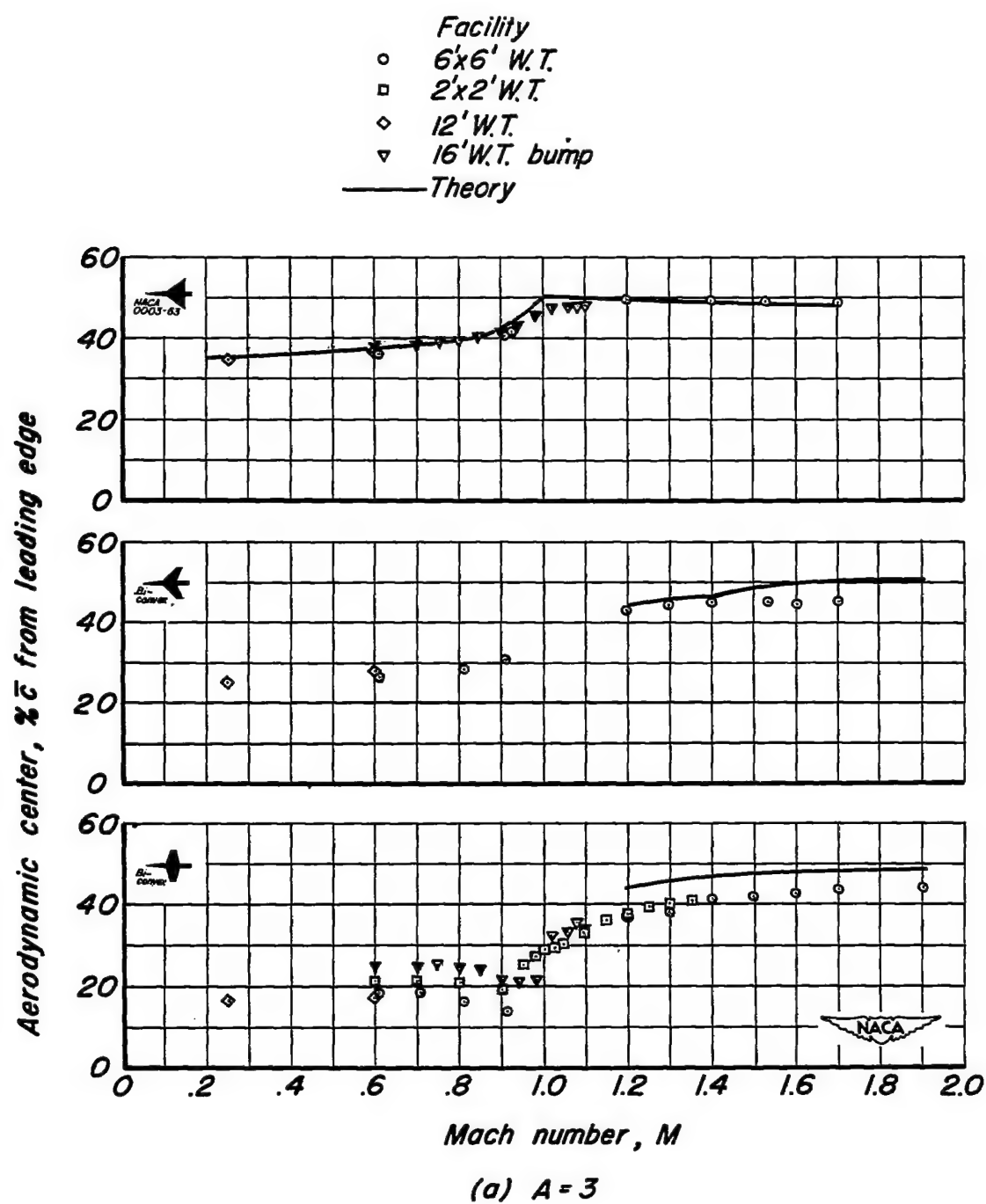


Figure 16.—The aerodynamic center for plane wings 3 percent thick and having different types of plan form.

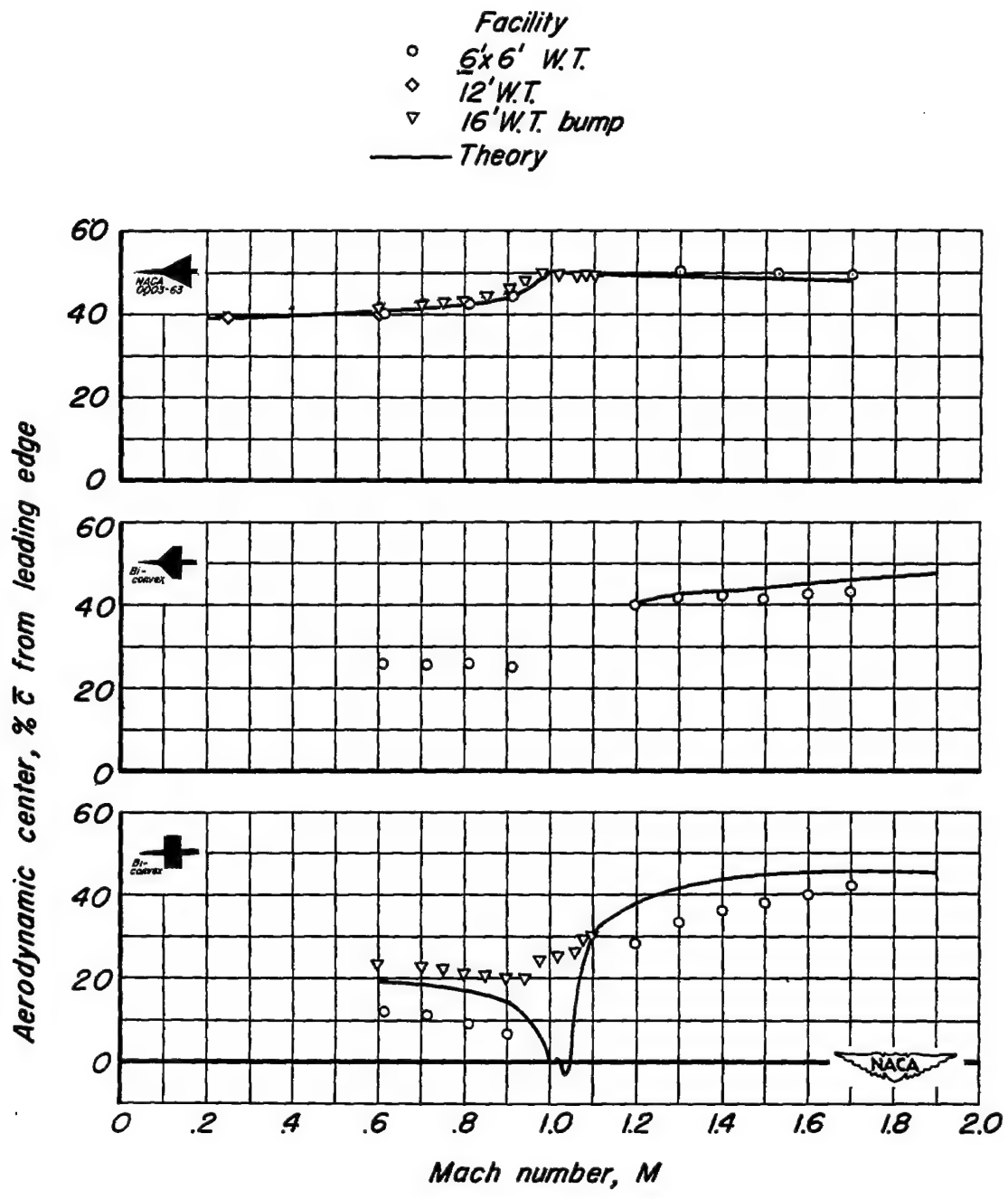
(b)  $A = 2$ 

Figure 16.—Concluded.

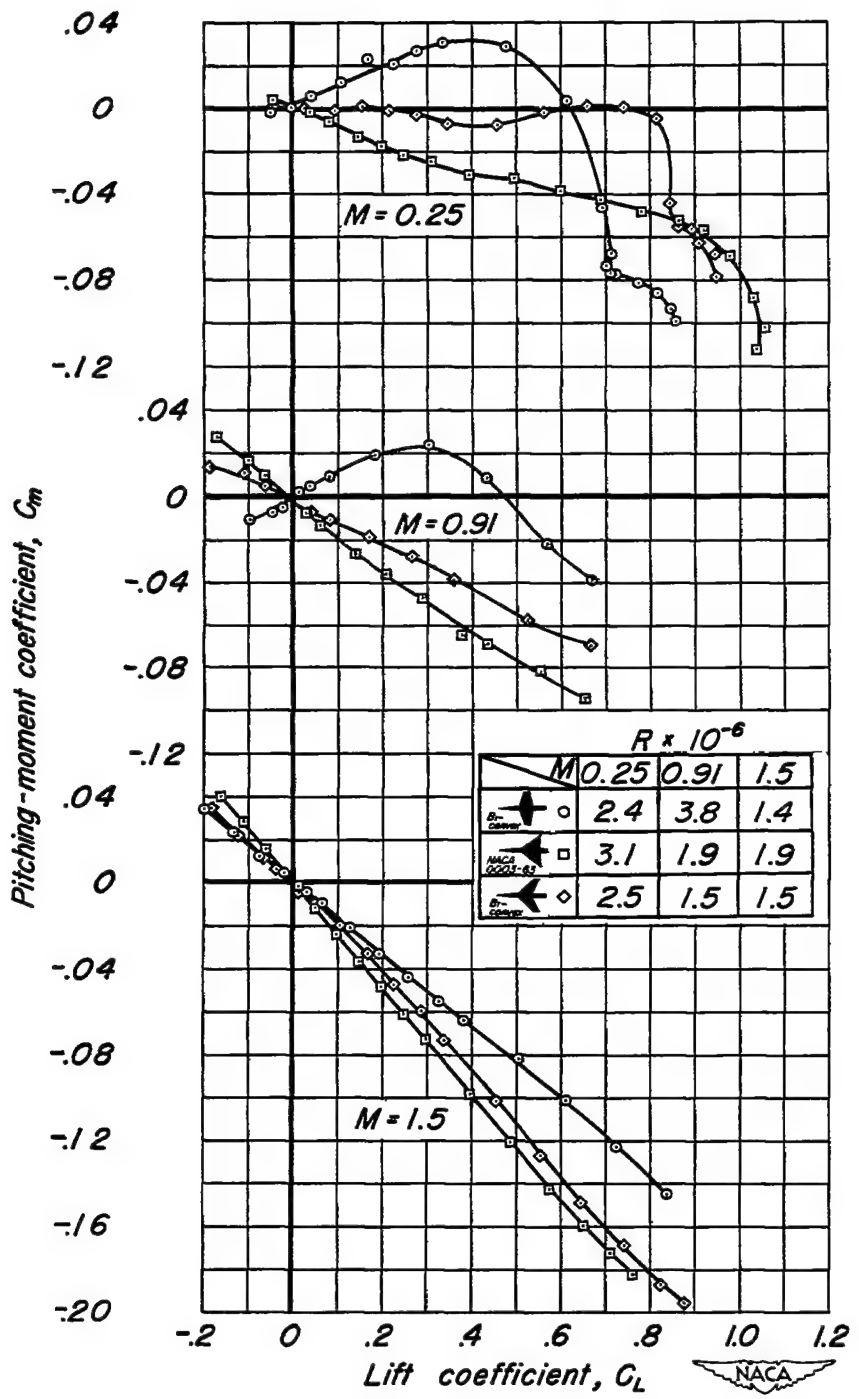


Figure 17.—The variation of pitching-moment coefficient with lift coefficient for plane wings of aspect ratio 3, 3 percent thick, and having different types of plan form.

CONFIDENTIAL

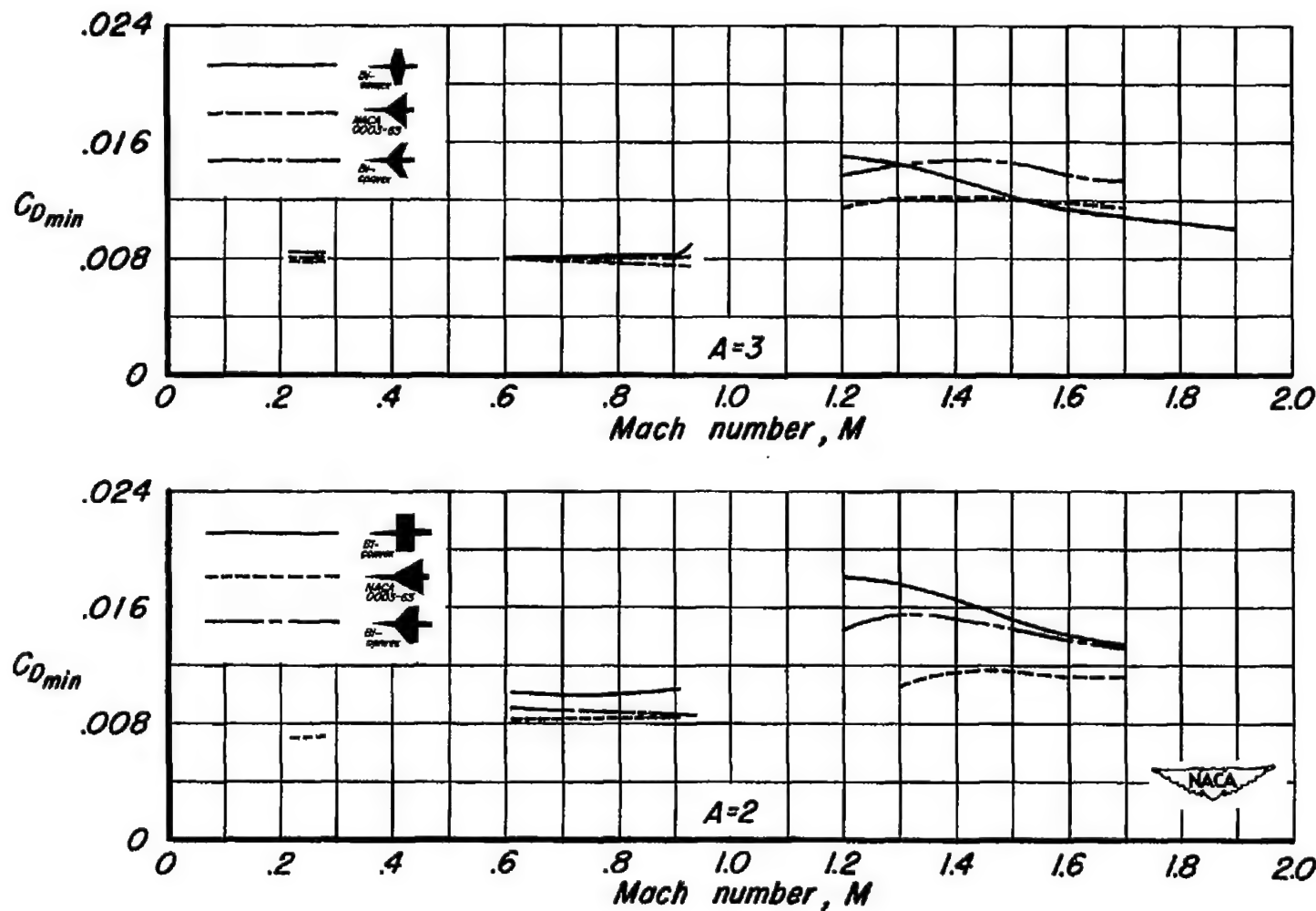


Figure 18—The minimum drag coefficient for plane wings 3 percent thick and having different types of plan form.

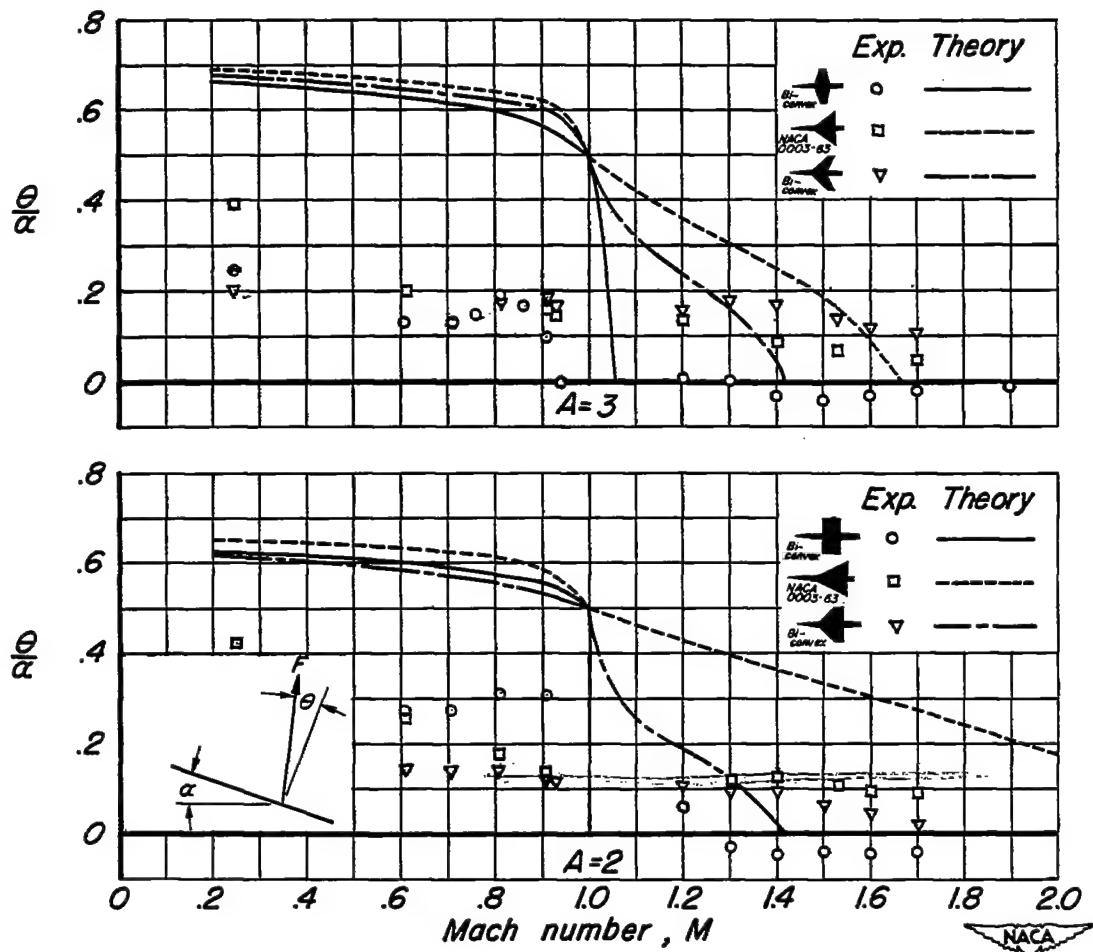


Figure 19.—The ratio of the inclination of the force vector from the normal to the wing to the angle of attack for plane wings 3 percent thick, and having different types of plan form.

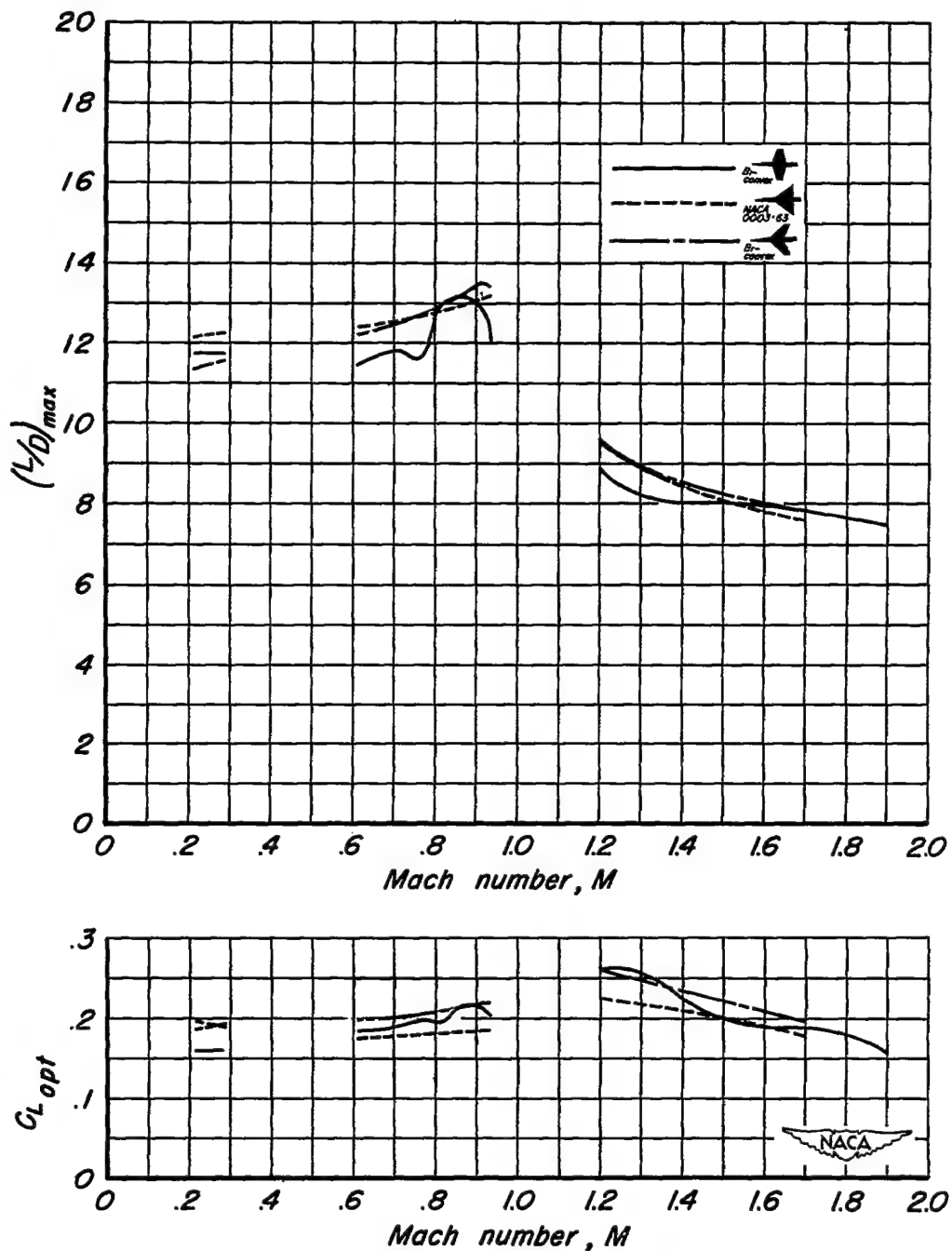
(a)  $A = 3$ 

Figure 20.—The maximum lift-drag ratio and optimum lift coefficient for plane wings 3 percent thick and having different types of plan form.

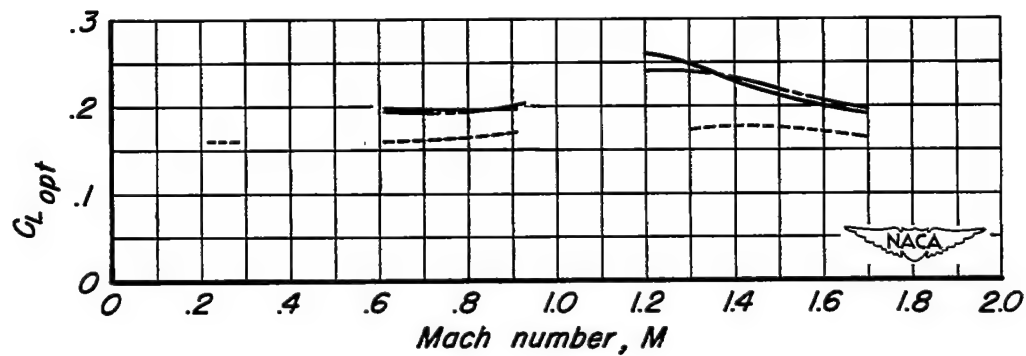
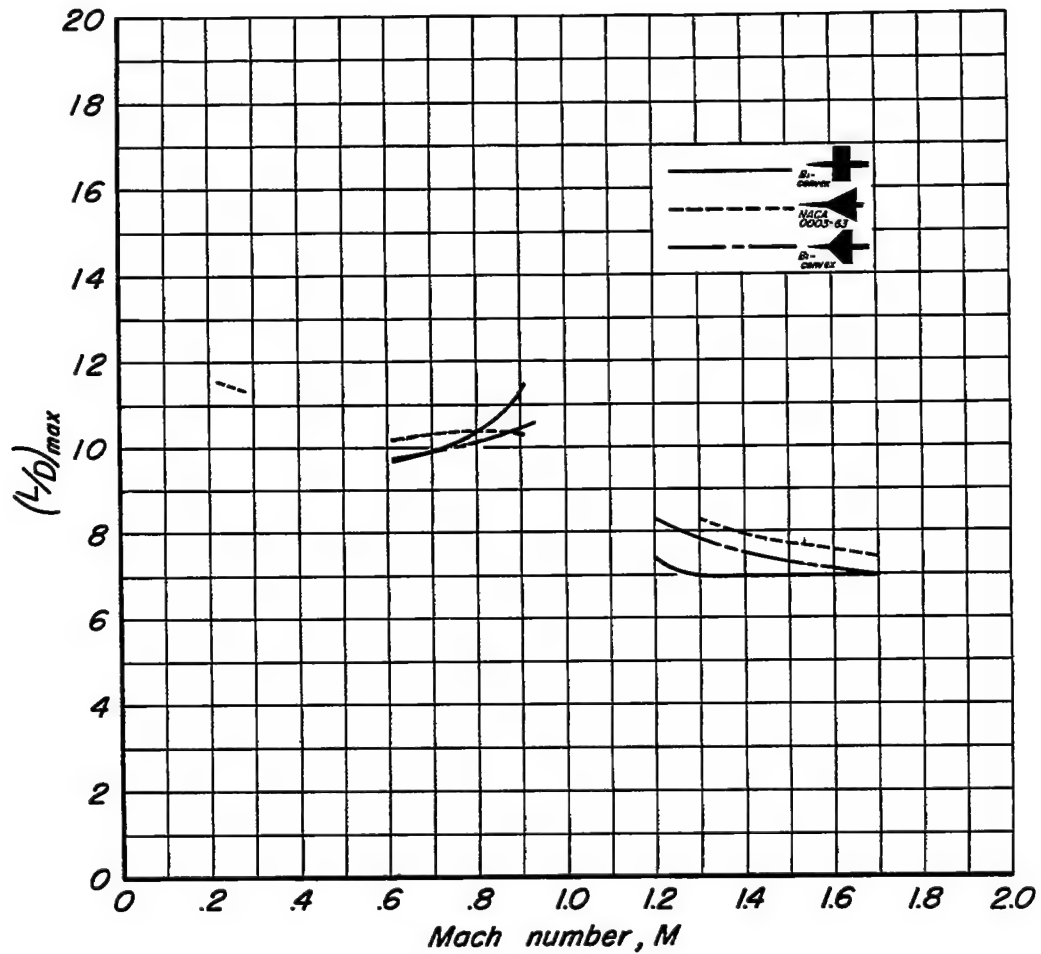
(b)  $A = 2$ 

Figure 20.—Concluded.

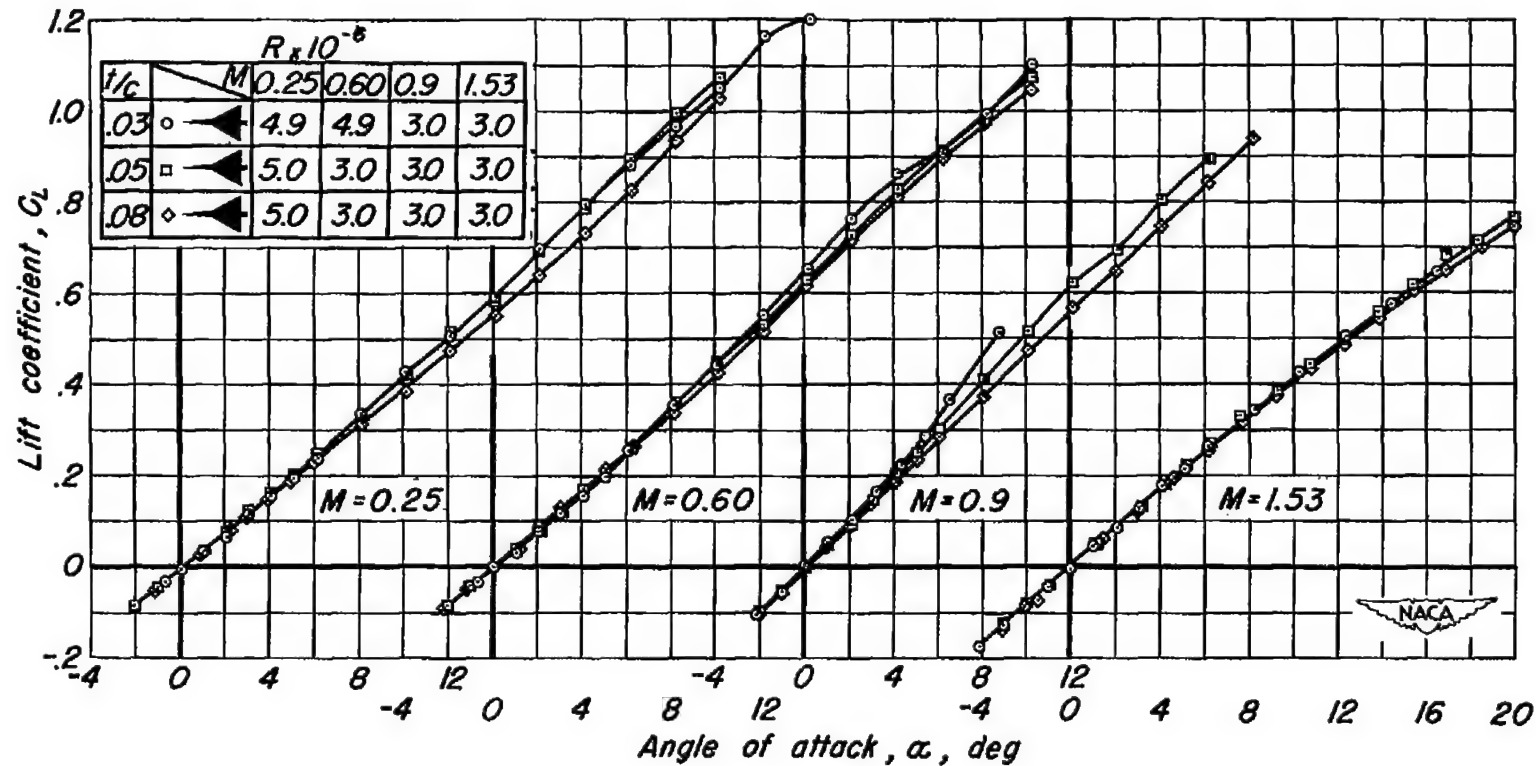


Figure 21.—The variation of lift coefficient with angle of attack for plane triangular wings of aspect ratio 2 and having NACA 000X-63 sections.

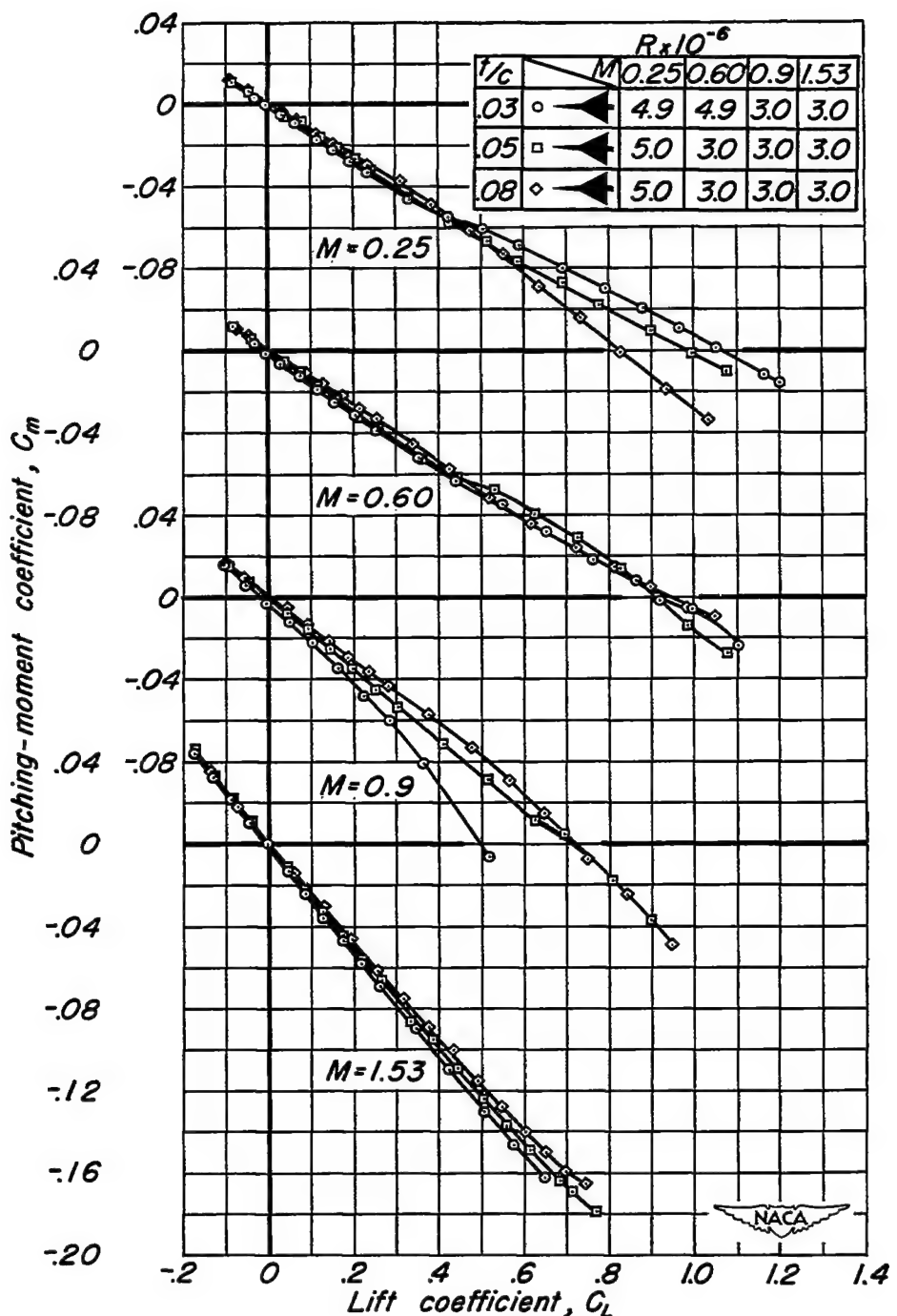


Figure 22.—The variation of pitching-moment coefficient with lift coefficient for plane triangular wings of aspect ratio 2 and having NACA 000X-63 sections.

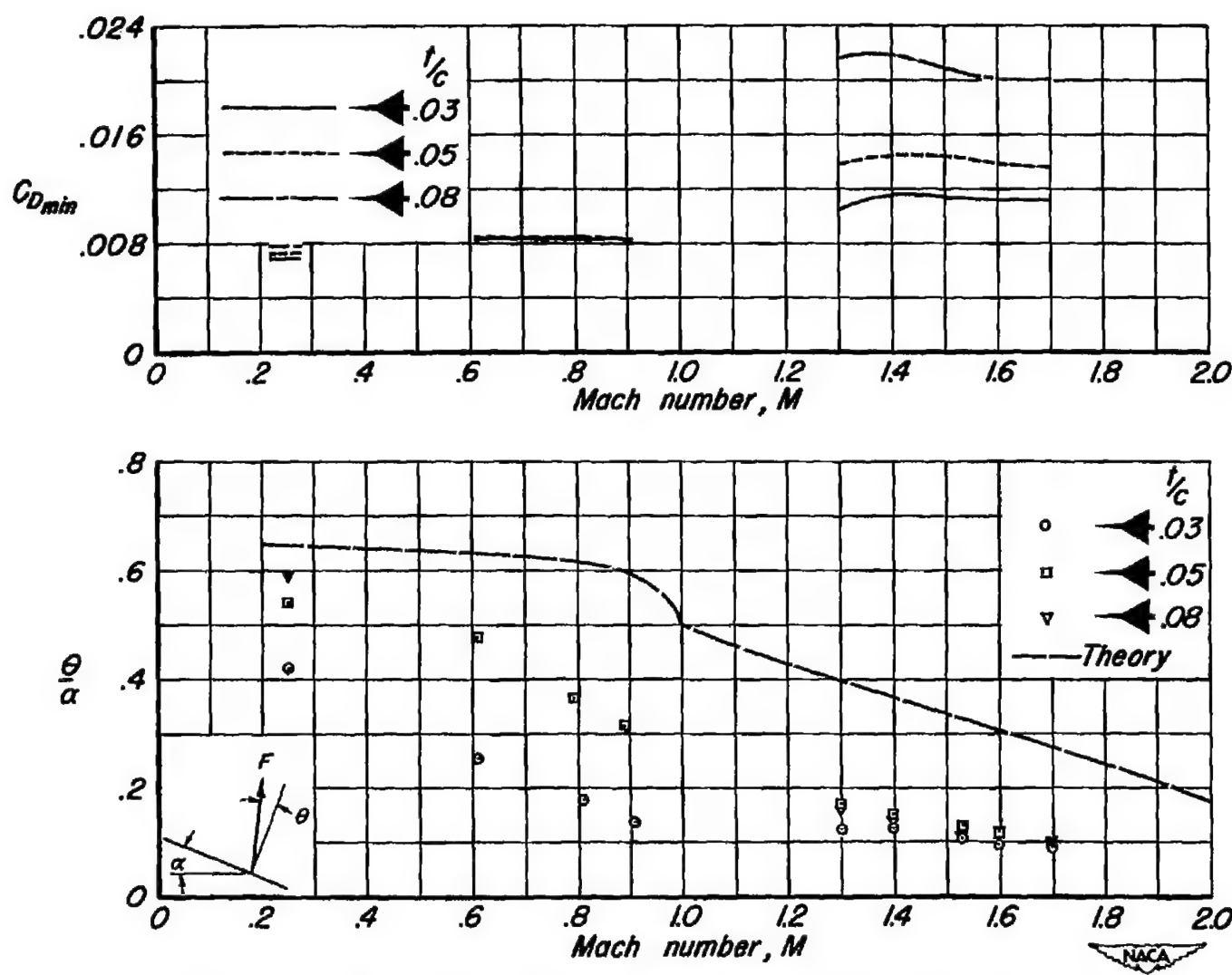
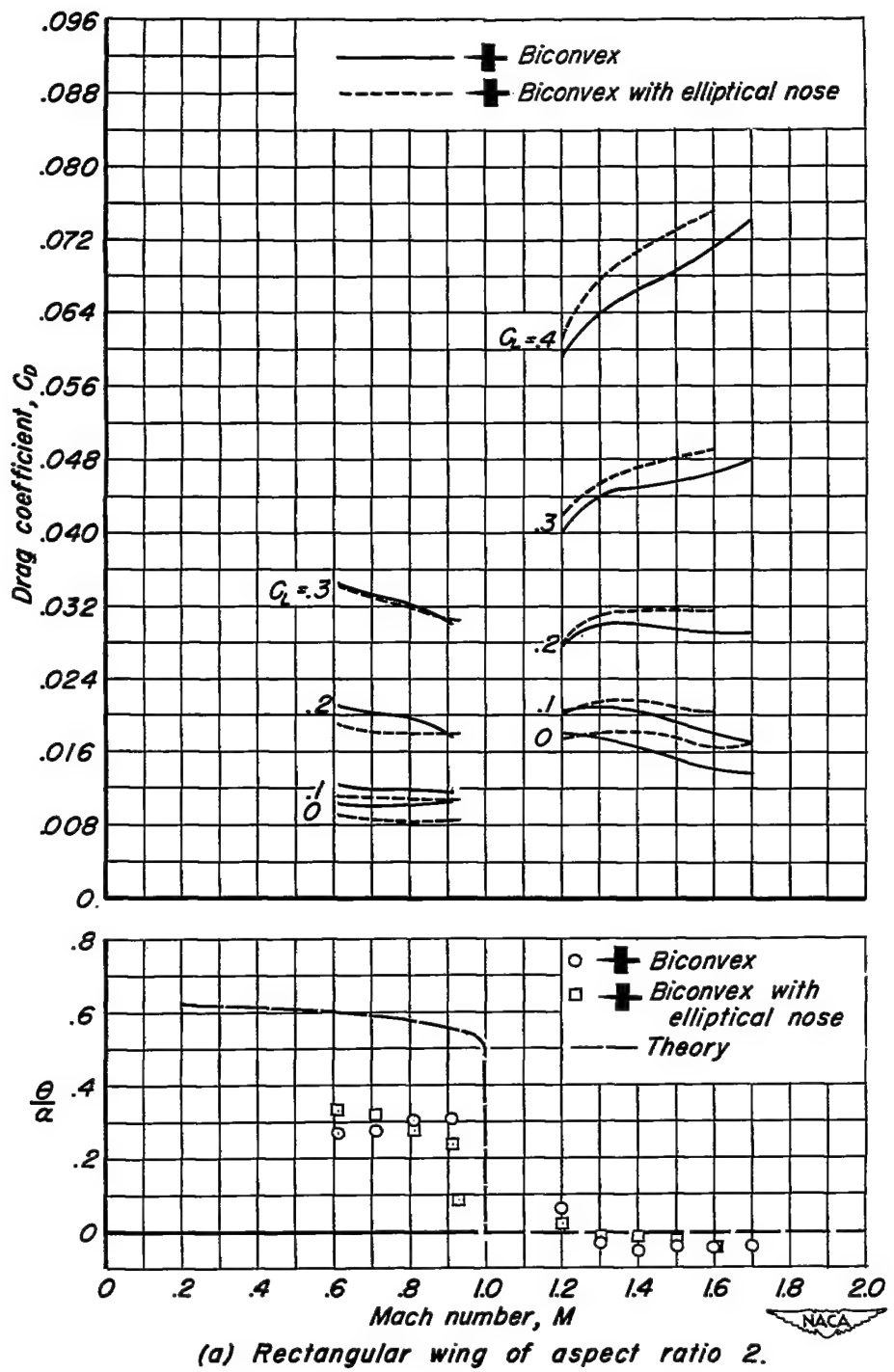
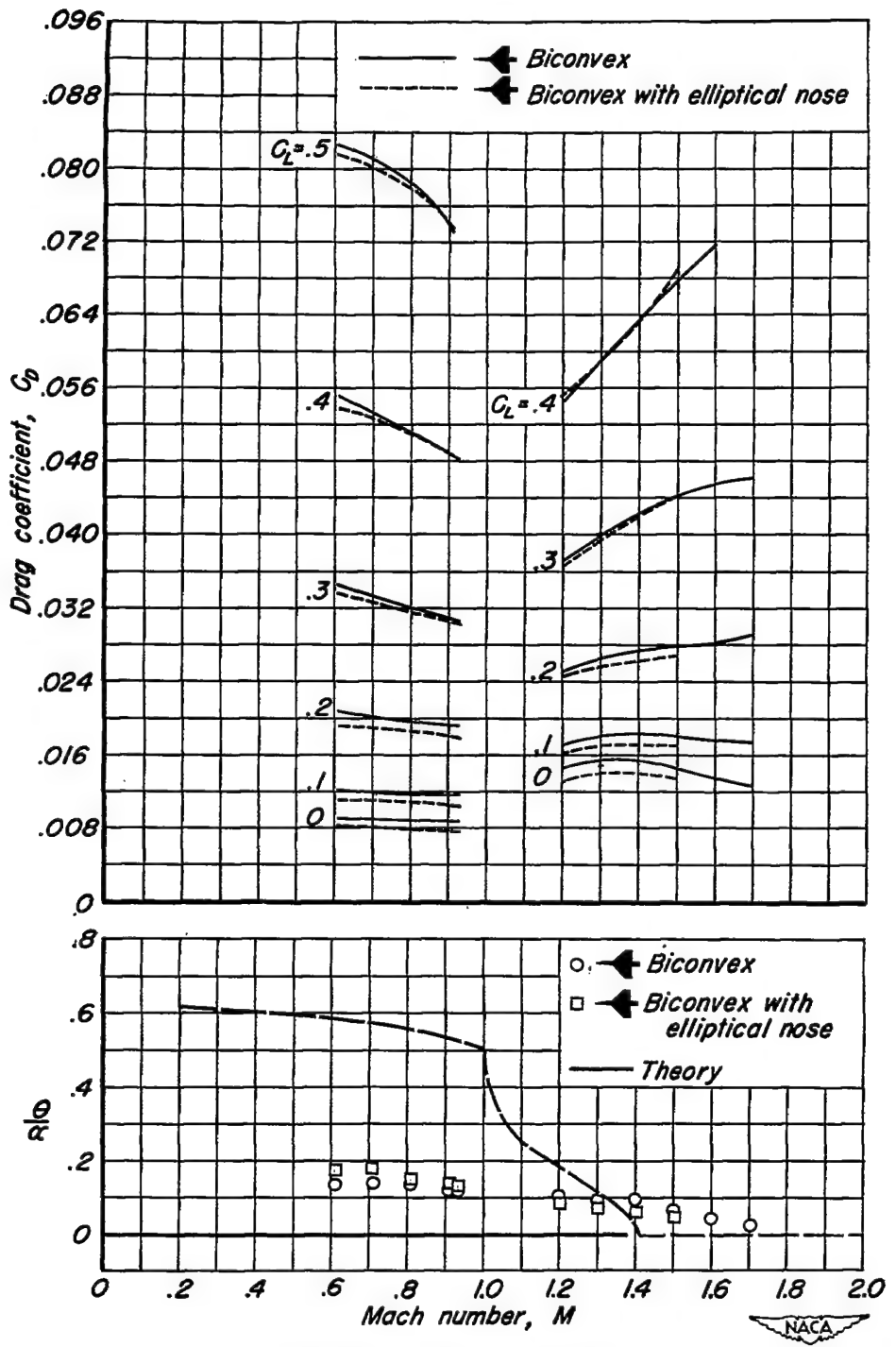


Figure 23.—The drag characteristics for plane triangular wings of aspect ratio 2 and having NACA 000X-63 sections.



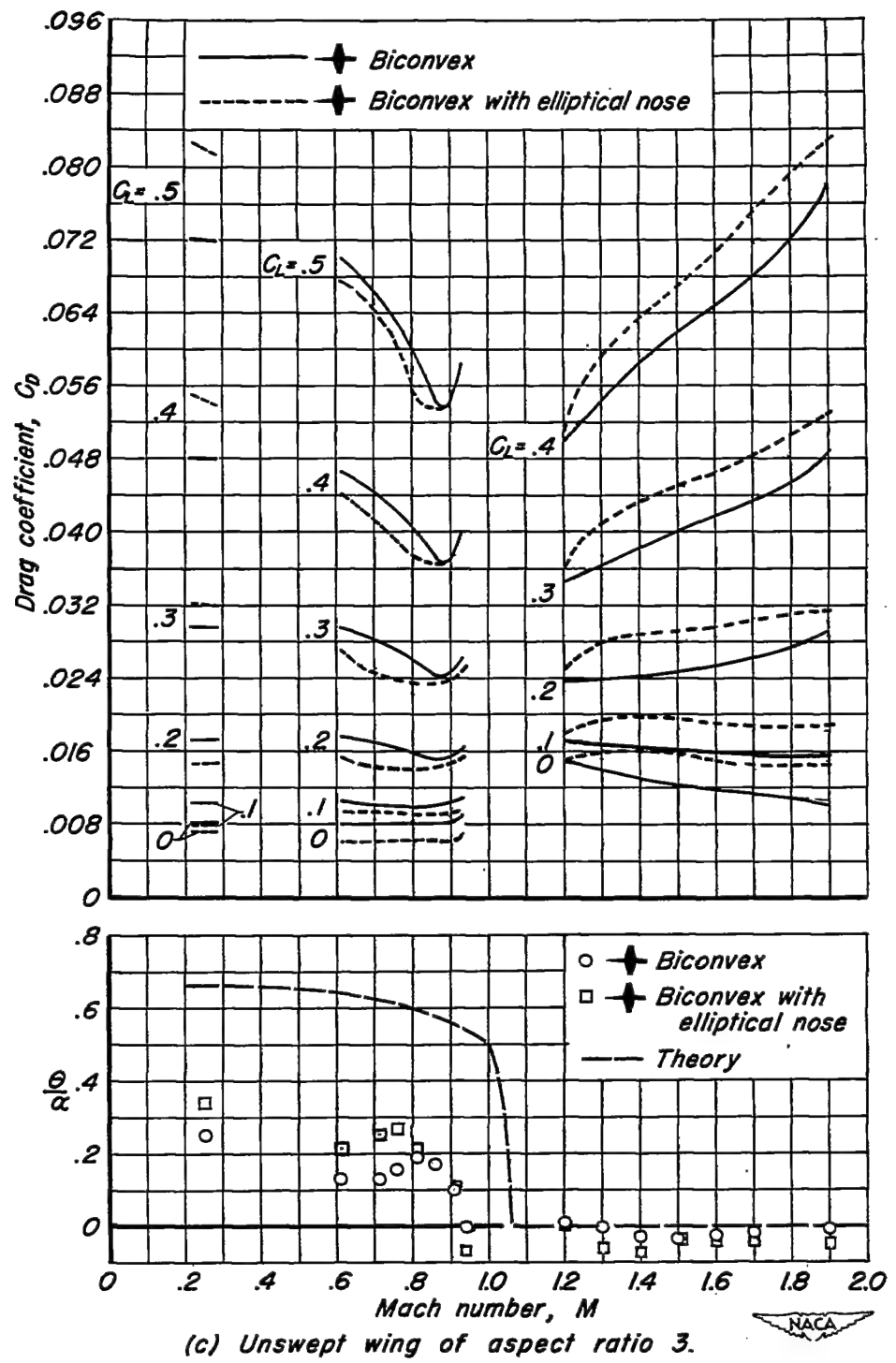
(a) Rectangular wing of aspect ratio 2.

Figure 24.—The drag coefficient for plane wings 3 percent thick and having different types of profile.



(b) Sweptback wing of aspect ratio 2

Figure 24.—Continued.



(c) Unswept wing of aspect ratio 3.

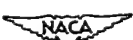
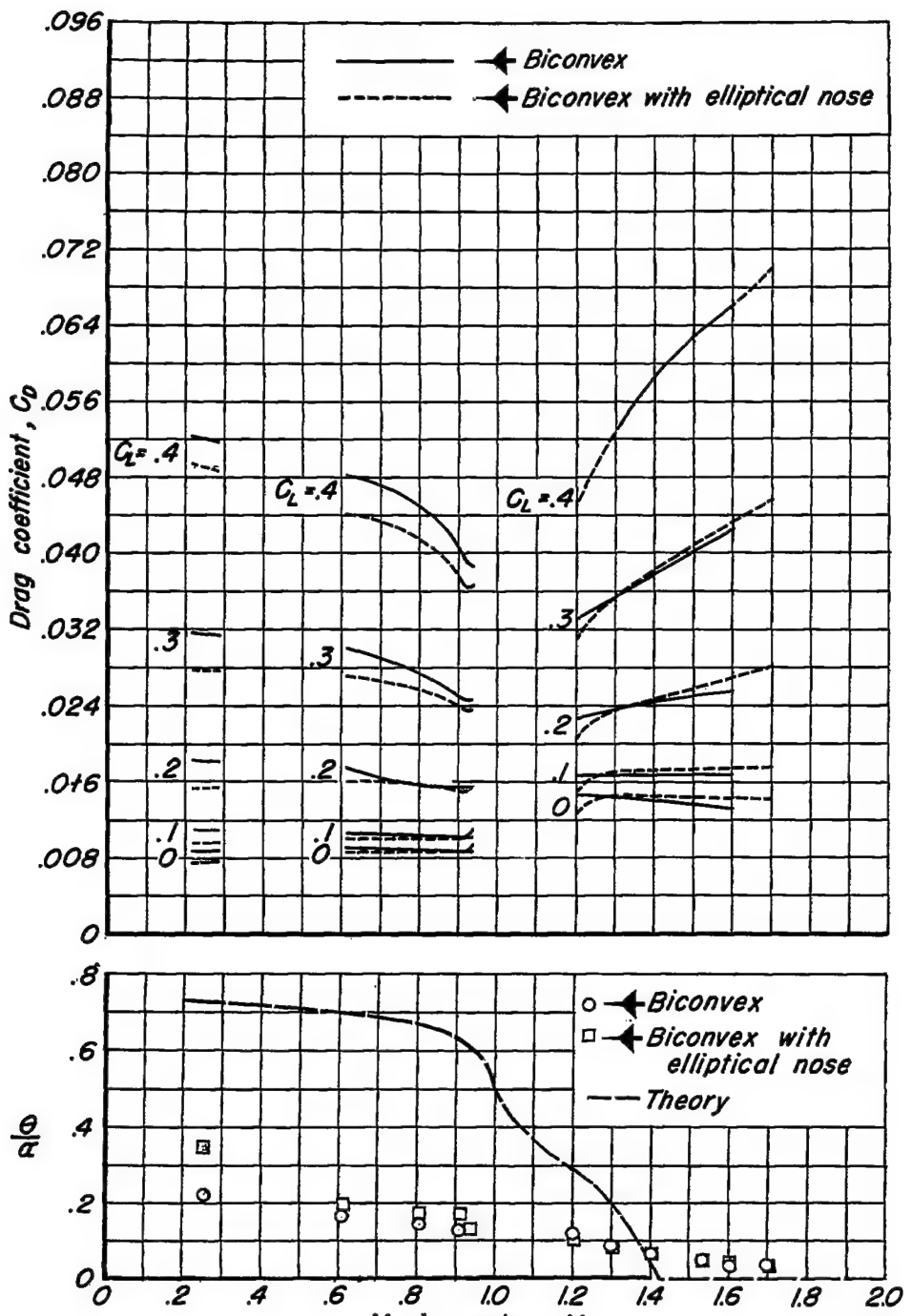


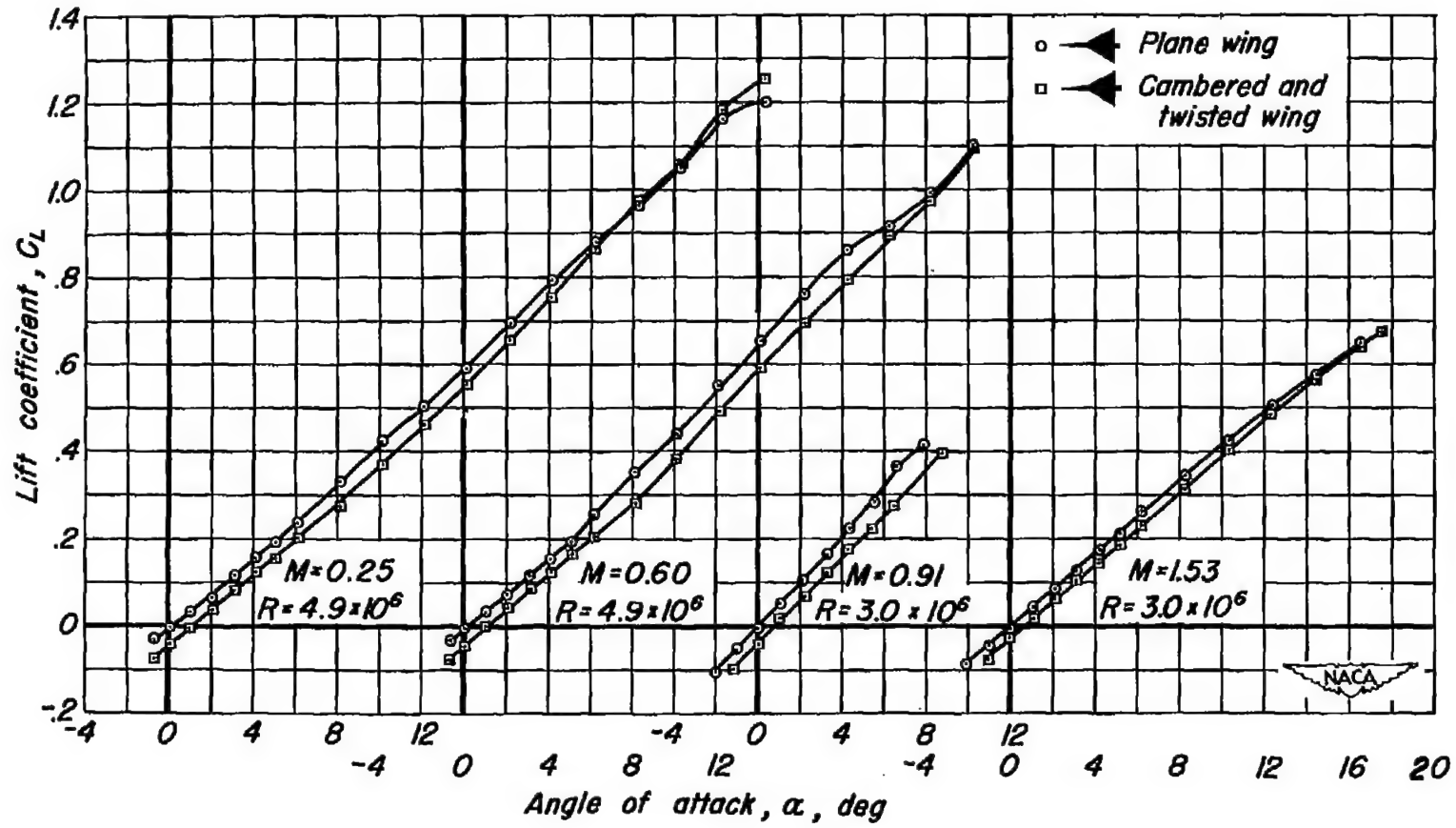
Figure 24.—Continued.



(d) Triangular wing of aspect ratio 4.

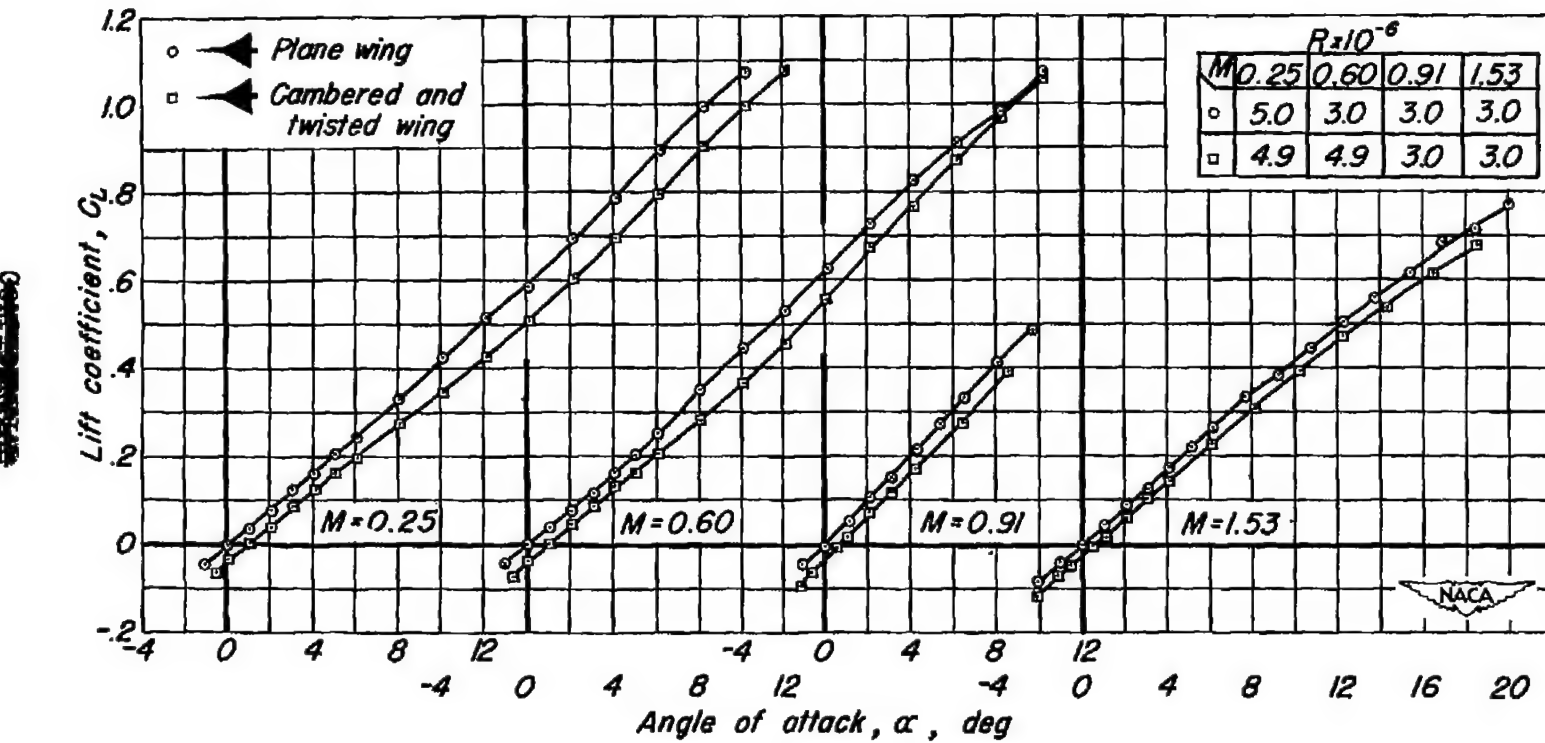
Figure 24.— Concluded.

CONTINUATION



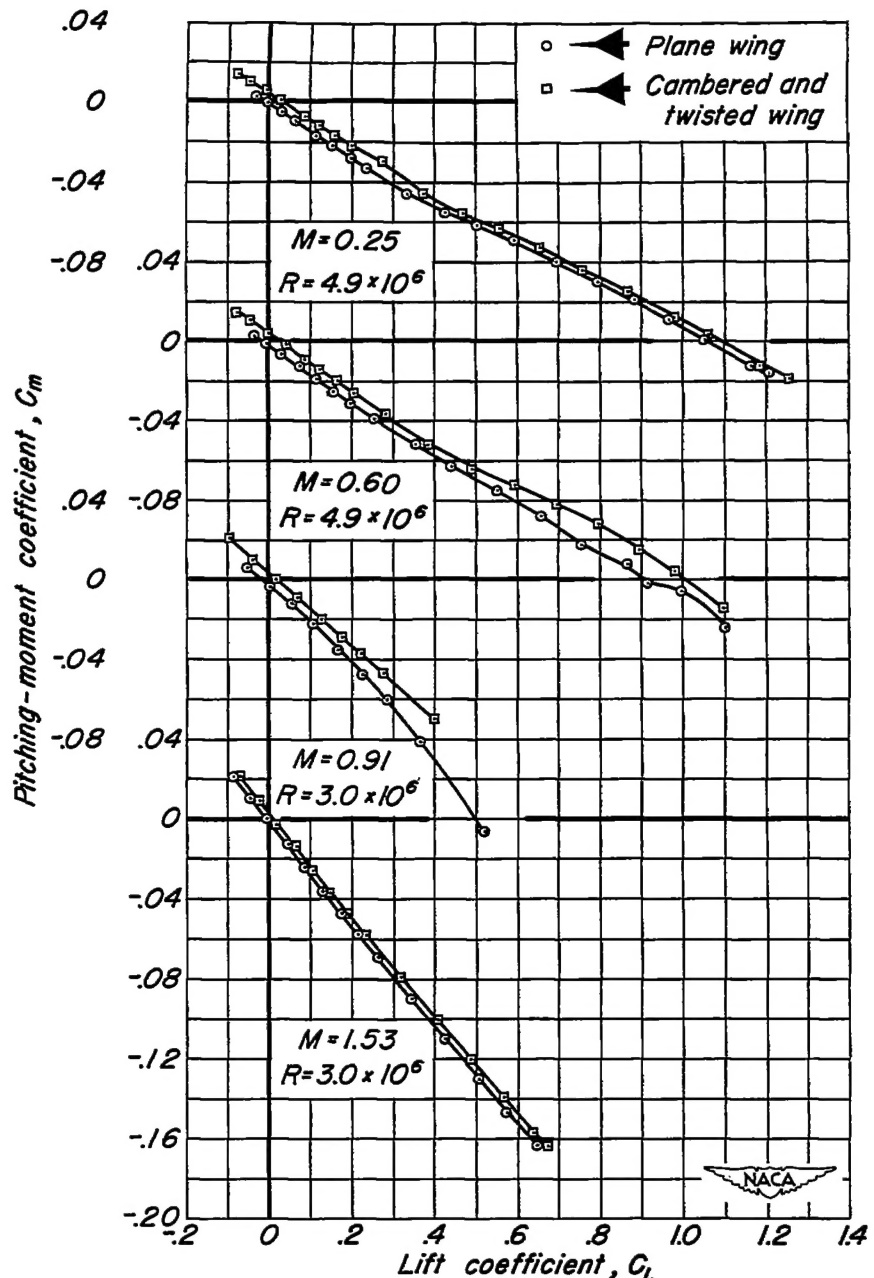
(a) Wings 3 percent thick.

Figure 25.— The variation of lift coefficient with angle of attack for triangular wings of aspect ratio 2, plane and twisted and cambered.



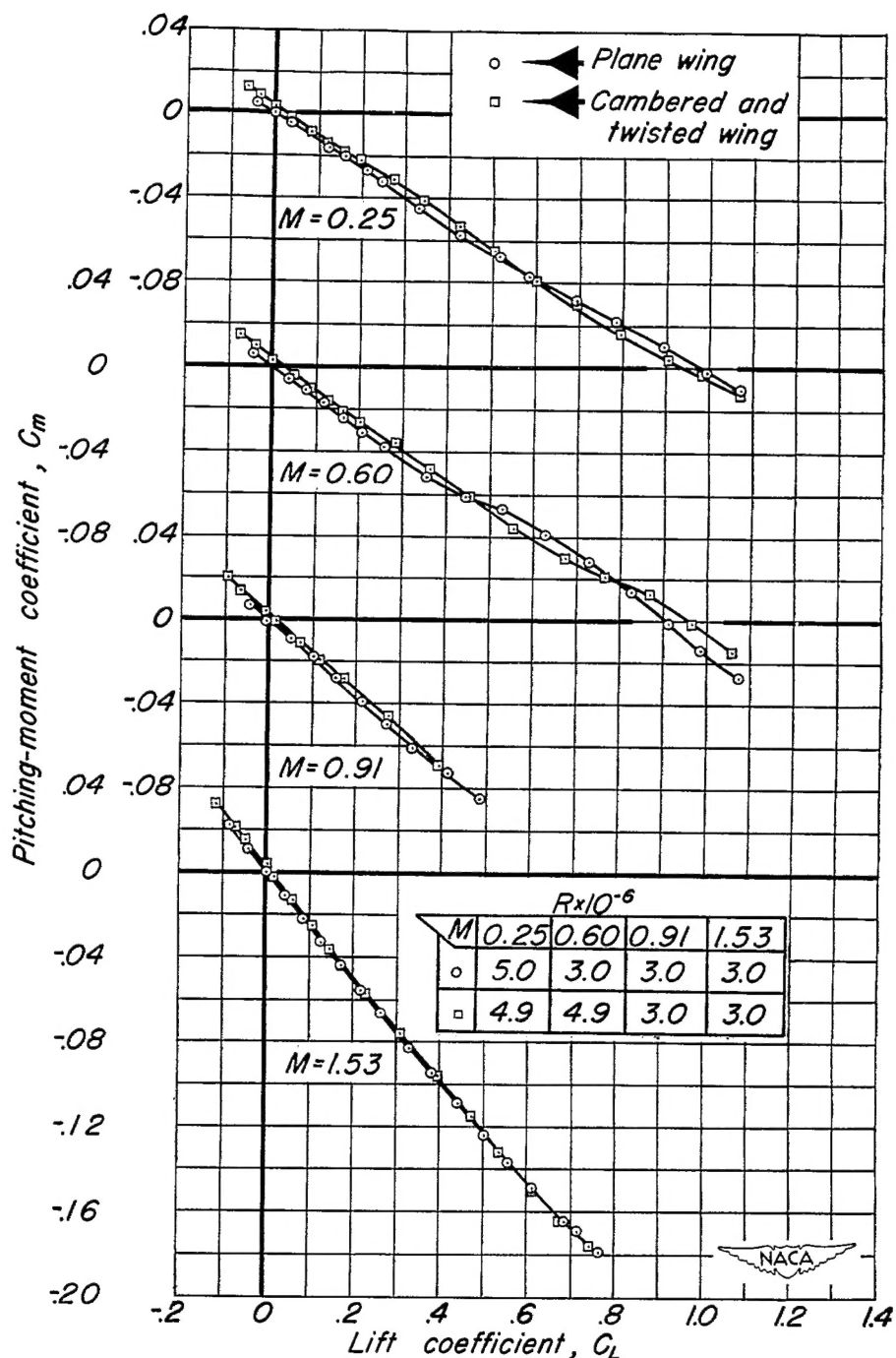
(b) Wings 5 percent thick.

Figure 25.—Concluded.



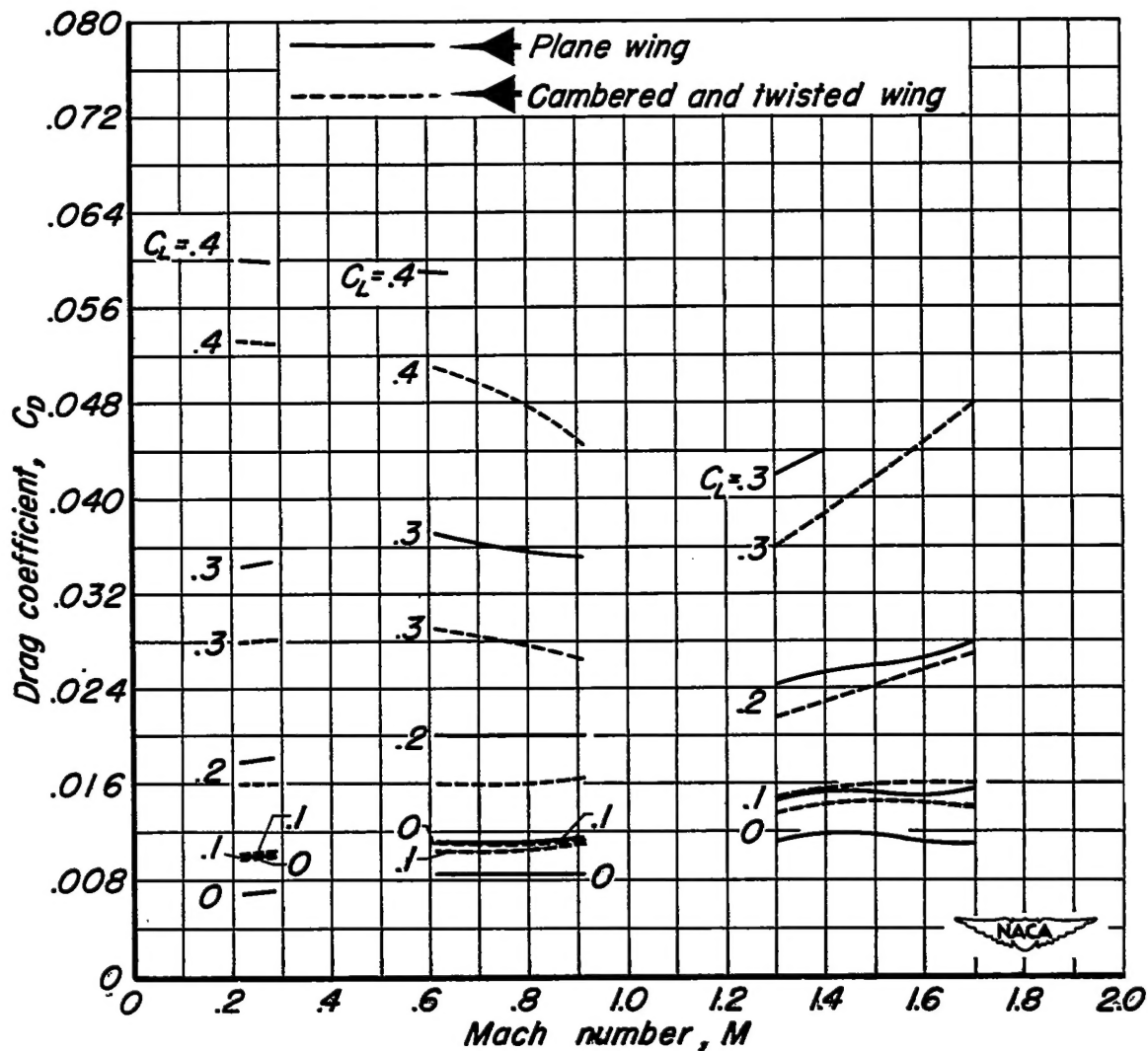
(a) Wings 3 percent thick.

Figure 26.— The variation of pitching-moment coefficient with lift coefficient for triangular wings of aspect ratio 2, plane and twisted and cambered.



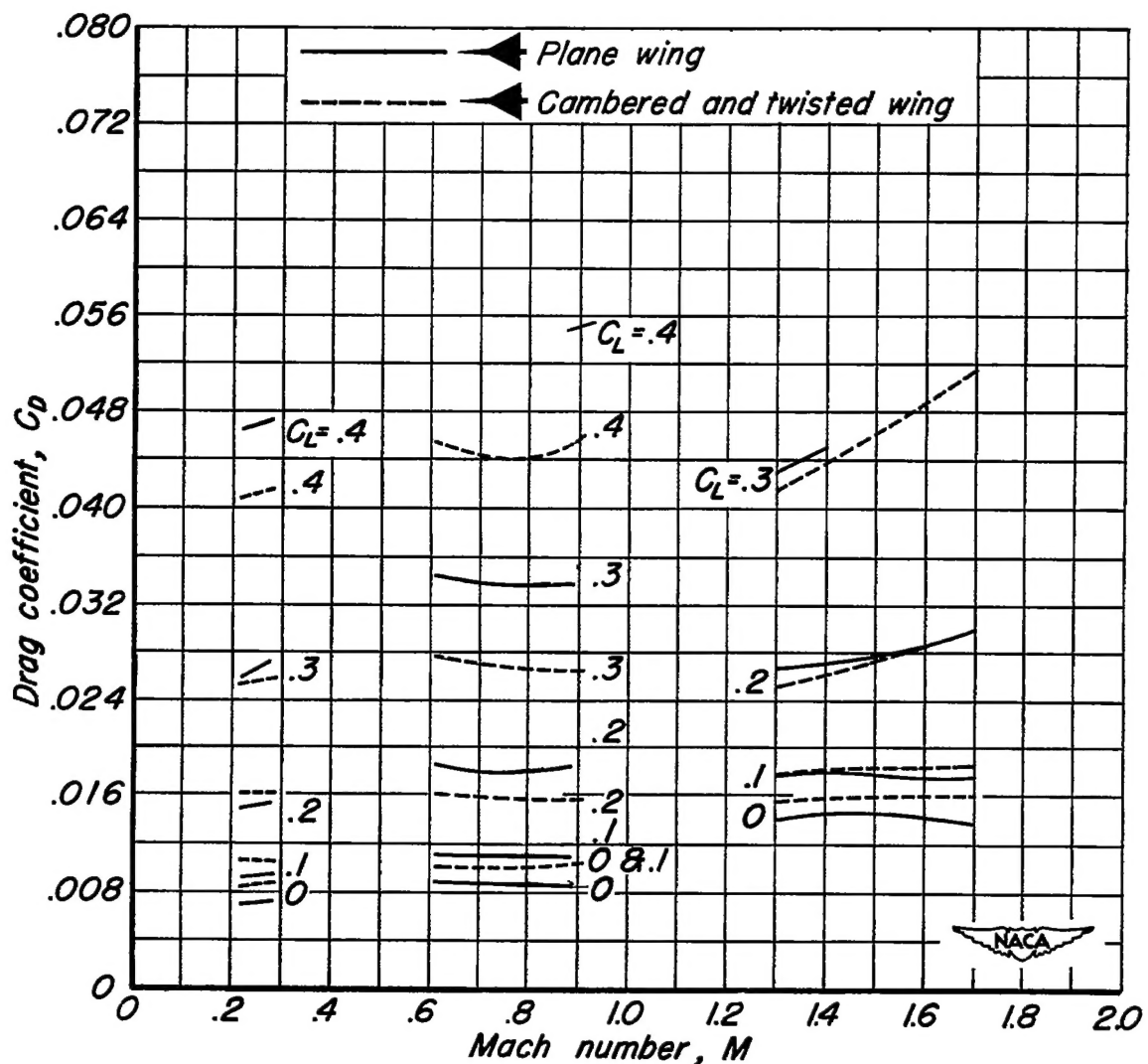
(b) Wings 5 percent thick.

Figure 26.—Concluded.



(a) Wings 3 percent thick.

Figure 27.— The drag characteristics for triangular wings of aspect ratio 2, plane and twisted and cambered.



(b) Wings 5 percent thick.

Figure 27.—Concluded.